frontiers | Research Topics

Insights in autonomic neuroscience: 2021

Edited by
Vaughan G. Macefield and Joel C. Bornstein

Published in
Frontiers in Neuroscience
Frontiers in Physiology
Frontiers in Neurology

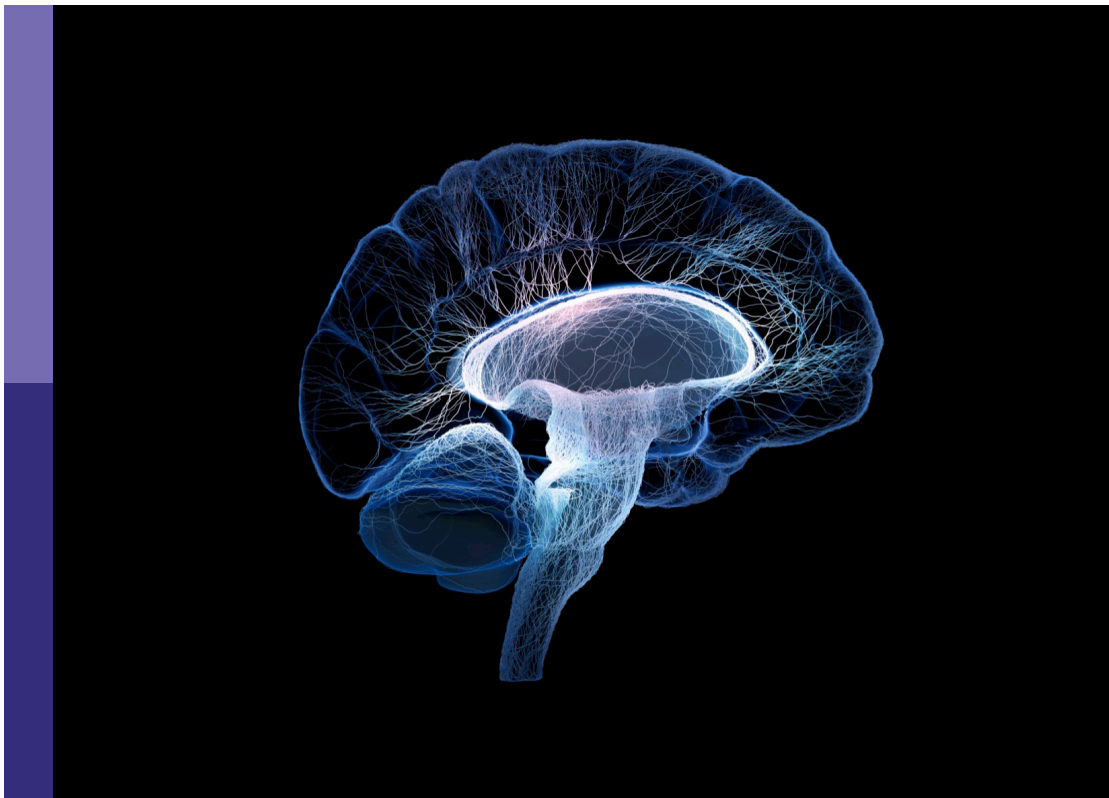

ISSN 1664-8714
ISBN 978-2-83251-681-2
DOI 10.3389/978-2-83251-681-2

About Frontiers

Frontiers is more than just an open access publisher of scholarly articles: it is a pioneering approach to the world of academia, radically improving the way scholarly research is managed. The grand vision of Frontiers is a world where all people have an equal opportunity to seek, share and generate knowledge. Frontiers provides immediate and permanent online open access to all its publications, but this alone is not enough to realize our grand goals.

Frontiers journal series

The Frontiers journal series is a multi-tier and interdisciplinary set of open-access, online journals, promising a paradigm shift from the current review, selection and dissemination processes in academic publishing. All Frontiers journals are driven by researchers for researchers; therefore, they constitute a service to the scholarly community. At the same time, the *Frontiers journal series* operates on a revolutionary invention, the tiered publishing system, initially addressing specific communities of scholars, and gradually climbing up to broader public understanding, thus serving the interests of the lay society, too.

Dedication to quality

Each Frontiers article is a landmark of the highest quality, thanks to genuinely collaborative interactions between authors and review editors, who include some of the world's best academicians. Research must be certified by peers before entering a stream of knowledge that may eventually reach the public - and shape society; therefore, Frontiers only applies the most rigorous and unbiased reviews. Frontiers revolutionizes research publishing by freely delivering the most outstanding research, evaluated with no bias from both the academic and social point of view. By applying the most advanced information technologies, Frontiers is catapulting scholarly publishing into a new generation.

What are Frontiers Research Topics?

Frontiers Research Topics are very popular trademarks of the *Frontiers journals series*: they are collections of at least ten articles, all centered on a particular subject. With their unique mix of varied contributions from Original Research to Review Articles, Frontiers Research Topics unify the most influential researchers, the latest key findings and historical advances in a hot research area.

Find out more on how to host your own Frontiers Research Topic or contribute to one as an author by contacting the Frontiers editorial office: frontiersin.org/about/contact

Insights in autonomic neuroscience: 2021

Topic editors

Vaughan G. Macefield — Baker Heart and Diabetes Institute, Australia

Joel C. Bornstein — The University of Melbourne, Australia

Citation

Macefield, V. G., Bornstein, J. C., eds. (2023). *Insights in autonomic neuroscience: 2021*. Lausanne: Frontiers Media SA.

doi:10.3389/978-2-83251-681-2

Table of contents

frontiers in Neuroscience

ORIGINAL RESEARCH
published: 17 February 2022
doi: 10.3389/fnins.2022.848079

Voluntary Exercise Prevents Hypertensive Response Sensitization Induced by Angiotensin II

Baojian Xue[1], Jun-Ling Cui[2], Fang Guo[1], Terry G. Beltz[1], Zi-Gang Zhao[3], Geng-Shen Zhang[2]* and Alan Kim Johnson[1,4,5,6]*

[1] Department of Psychological and Brain Sciences, The University of Iowa, Iowa City, IA, United States, [2] Department of Neurosurgery, Second Hospital of Hebei Medical University, Shijiazhuang, China, [3] Institute of Microcirculation, Hebei North University, Zhangjiakou, China, [4] Department of Neuroscience and Pharmacology, The University of Iowa, Iowa City, IA, United States, [5] Department of Health and Human Physiology, The University of Iowa, Iowa City, IA, United States, [6] François M. Abboud Cardiovascular Research Center, The University of Iowa, Iowa City, IA, United States

OPEN ACCESS

Edited by:
Valdir Andrade Braga, Federal University of Paraíba, Brazil

Reviewed by:
Eric Gerald Krause, University of Florida, United States
Srinivas Sriramula, The Brody School of Medicine at East Carolina University, United States
Ali Nasimi, Isfahan University of Medical Sciences, Iran

***Correspondence:**
Baojian Xue
baojian-xue@uiowa.edu
Geng-Shen Zhang
horse90325@163.com

Specialty section:
This article was submitted to Autonomic Neuroscience, a section of the journal Frontiers in Neuroscience

Received: *03 January 2022*
Accepted: *27 January 2022*
Published: *17 February 2022*

Citation:
Xue B, Cui J-L, Guo F, Beltz TG, Zhao Z-G, Zhang G-S and Johnson AK (2022) Voluntary Exercise Prevents Hypertensive Response Sensitization Induced by Angiotensin II. Front. Neurosci. 16:848079. doi: 10.3389/fnins.2022.848079

Exercise training has profound effects on the renin-angiotensin system, inflammatory cytokines and oxidative stress, all of which affect autonomic nervous system activity and regulate blood pressure (BP) in both physiological and pathophysiological states. Using the Induction-Delay-Expression paradigm, our previous studies demonstrated that various challenges (stressors) during Induction resulted in hypertensive response sensitization (HTRS) during Expression. The present study tested whether voluntary exercise would protect against subpressor angiotensin (ANG) II-induced HTRS in rats. Adult male rats were given access to either "blocked" (sedentary rats) or functional running (exercise rats) wheels for 12 weeks, and the Induction-Delay-Expression paradigm was applied for the rats during the last 4 weeks. A subpressor dose of ANG II given during Induction produced an enhanced hypertensive response to a pressor dose of ANG II given during Expression in sedentary rats in comparison to sedentary animals that received saline (vehicle control) during Induction. Voluntary exercise did not attenuate the pressor dose of ANG II-induced hypertension but prevented the expression of HTRS seen in sedentary animals. Moreover, voluntary exercise reduced body weight gain and feed efficiency, abolished the augmented BP reduction after ganglionic blockade, reversed the increased mRNA expression of pro-hypertensive components, and upregulated mRNA expression of antihypertensive components in the lamina terminalis and hypothalamic paraventricular nucleus, two key brain nuclei involved in the control of sympathetic activity and BP regulation. These results indicate that exercise training plays a beneficial role in preventing HTRS and that this is associated with shifting the balance of the brain prohypertensive and antihypertensive pathways in favor of attenuated central activity driving sympathetic outflow and reduced BP.

Keywords: voluntary exercise, blood pressure, renin-angiotensin system, inflammation, central nervous system

INTRODUCTION

Hypertension is major risk for cardiovascular disease affecting more than 31% adults worldwide. Uncontrolled hypertension is a risk factor for heart disease, renal failure, and stroke (Mills et al., 2020). The activation of the sympathetic nervous system (SNS) is a major mechanism both in human high blood pressure and in several models of hypertension in animals (DiBona, 2013; Dampney, 2016; Haspula and Clark, 2018; Johnson and Xue, 2018). In this regard, activation of renin-angiotensin system (RAS) and elevation of inflammation and oxidative stress in the central nervous system (CNS) produce a state of sympathetic overactivity that plays an essential role in the onset and development of hypertension (Peterson et al., 2006; Kalupahana and Moustaid-Moussa, 2012; Huber et al., 2017; Haspula and Clark, 2018). The brain regions involved in sympathetic activity and blood pressure (BP) regulation mainly are located in the basal forebrain including structures lying along the lamina terminalis [LT, the subfornical organ (SFO), the median preoptic nucleus (MnPO), and the vascular organ of the lamina terminalis (OVLT)] and the hypothalamic paraventricular nucleus (PVN; Johnson and Gross, 1993; Mimee et al., 2013; Sharma et al., 2021). Information reflecting the levels of blood-borne factors such as angiotensin (ANG) II, proinflammatory cytokines (PICs), reactive oxygen species (ROS), and extracellular sodium concentration sensed by the LT structures lacking a blood-brain barrier is projected through efferent pathways to the PVN. The PVN integrates this information and sends projections either to the rostral ventrolateral medulla (RVLM) or to the spinal cord intermediolateral cell column to exaggerate sympathetic outflow and elevate BP under the pathophysiological state of hypertension (Johnson and Gross, 1993; Mimee et al., 2013; Dampney, 2016; Sharma et al., 2021).

Exercise training of moderate intensity has been proven effective in preventing and managing cardiovascular diseases including heart failure and hypertension. The results of systematic reviews and meta-analysis of human participants indicate that endurance training, dynamic resistance training, and isometric resistance training significantly reduce diastolic BP. Endurance training might be most effective in reducing BP in hypertensive individuals (Cornelissen and Smart, 2013; Alpsoy, 2020). In the animal models of heart failure and hypertension, exercise training normalizes enhanced sympathetic activation and reduces elevated BP (Haack and Zucker, 2015; Michelini et al., 2015; Zucker and Musch, 2018). These beneficial effects of exercise training are associated with not only attenuation of the prohypertensive axis of the RAS [ACE1/ANG II/AT1-R; angiotensin-converting enzyme (ACE1), ANG II type 1 receptor (AT1-R)], PICs [tumor necrosis factor (TNF)-α, interleukin (IL)-1β, IL-6] and NADPH oxidase but also with improvement of the antihypertensive axis of the RAS [ACE2/ANG-(1-7)/Mas-R] and anti-inflammatory defense mechanisms (e.g., IL-10) in the brain regions including the RVLM and PVN (Agarwal et al., 2011; Zheng et al., 2012; Rossi et al., 2013; Masson et al., 2015; Zucker et al., 2015; Ferreira-Junior et al., 2019; Fragas et al., 2021).

Previous studies demonstrate that pretreatment with various challenges (stressors) resulted in hypertensive response sensitization (HTRS) to a subsequent pressor dose of ANG II (Johnson et al., 2015; Johnson and Xue, 2018; Xue et al., 2020b). The HTRS involves upregulated expression of RAS components, inflammatory markers (PICs and microglial activation) and NADPH oxidase in the LT and PVN induced by various challenges. Either central antagonism of the RAS or blockade of microglial activation or PIC production blocks the HTRS (Xue et al., 2012; Xue et al., 2016a,b; Xue et al., 2020b). Given that both the pathogenesis of cardiovascular disease and exercise training are associated with alterations in brain RAS activity, inflammation, and oxidative stress, we hypothesized that voluntary exercise training would protect against subpressor ANG II-induced HTRS *via* a similar central mechanism. To test this hypothesis, adult male rats were given access to either "blocked" (sedentary rats) or functional running (exercise rats) wheels for 12 weeks. The Induction-Delay-Expression (**I-D-E**) paradigm (Xue et al., 2012) was applied for the rats during the last 4 weeks of the sedentary vs. exercise conditions. During **I,** a low sub-pressor dose of ANG II or saline was delivered subcutaneously by osmotic minipump for 1 week. The rats then rested for 1 week (**D**), after which time, a second pump was implanted to deliver a slow-pressor dose of ANG II for 2 weeks (**E**). This experimental approach allowed assessment of the effect of voluntary exercise training on the induction of HTRS by pretreatment with a low sub-pressor dose of ANG II during **I** and expressed during **E** by administering a slow-pressor dose of ANG II. Running distances, metabolic markers and changes in BP were determined during voluntary running and **I-D-E** paradigm. Putative CNS molecular and cellular mediators including RAS components, inflammatory and oxidative stress markers in key brain structures (i.e., the LT and PVN) were also measured. The experimental results provide further evidence that exercise training blocks the sensitized hypertensive response through central mechanisms acting to alter activity in brain cardiovascular nuclei.

MATERIALS AND METHODS

Animals

All experiments were conducted in accordance with the National Institutes of Health *Guide for the Care and Use of Laboratory Animals* and were approved by the University of Iowa and the Hebei Medical University Animal Care and Use Committee (Protocol # 1012115).

Forty Sprague-Dawley male rats (10-week-old, Envigo) were used in this study. All animals were maintained in a temperature (23 ± 2°C) and light (12-h light/dark cycle) controlled facility. The rats had unlimited access to standard rat chow and water.

Voluntary Exercise and Sensitization Paradigm

Figure 1 shows the timeline of the study. Adult male rats were given access to either blocked (sedentary rats) or functional running (exercised rats) wheels equipped with activity monitors for 12 weeks, and the **I-D-E** paradigm was applied for the rats during the last 4 weeks, as described previously (Xue et al., 2012).

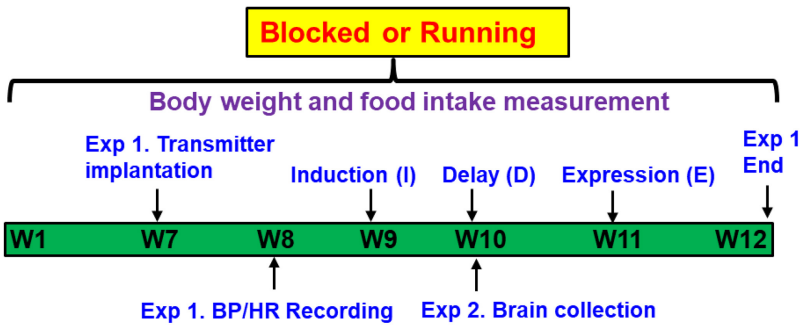

FIGURE 1 | Representative timeline of the study design. Adult male rats were given access to either "blocked" or functional running wheels for 10–12 weeks. Experiment 1 (Exp. 1): the Induction-Delay-Expression (I-D-E) paradigm was applied for the rats during the last 4 weeks. The rats were pretreated during Induction with a systemic subpressor dose of angiotensin (ANG) II (sc, 10 ng/kg/min) for 1 week. After a 1-week Delay, rats were treated during Expression with a pressor dose of ANG II (120 ng/kg/min) for 2 weeks. The hemodynamic and autonomic function were measured. Experiment 2 (Exp. 2): at the end of Delay, animals were euthanized to collect brain tissues for assessing mRNA expression of renin-angiotensin system components, NADPH oxidase and proinflammatory cytokines.

During **I,** a low sub-pressor dose of ANG II or saline (S) was delivered subcutaneously (sc, 10 ng/kg/min) by osmotic minipump (model 2001, Alzet) for 1 week. The rats then rested for 1 week (**D**), after which time, a second pump (model 2002, Alzet) was implanted to deliver a slow-pressor dose of ANG II (120 ng/kg/min) for 2 weeks (**E**) to test for HTRS.

Experiment 1. Rat transmitters (HD-S10, DSI®, St. Paul, MN, United States) were used to directly measure BP and heart rate (HR). At week 7, transmitters were implanted in both blocked and running animals. After 1-week recovery, baseline BP and HR recordings were made for 5 days, then the **I**-**D**-**E** paradigm was applied for all rats. Therefore, the experiments involved 4 groups (n = 5 rats/group): (1) Blocked **I**-S + **E**-ANG II; (2) Blocked **I**-ANG II + **E**-ANG II; (3) Running **I**-S + **E**-ANG II; and (4) Running **I**-ANG II + **E**-ANG II.

Experiment 2. Additional studies were performed to assess the effects of the sedentary or exercise conditions on mRNA expression of RAS and PIC components and NADPH oxidase in the LT and PVN. Brains (n = 5 rats/group) were collected at end of **D**, corresponding to the time at which the pressor dose of ANG II infusion was initiated in Experiment 1.

Running Distance and Metabolic Parameter Measurement

Voluntary running distance was recorded daily, and food intake and body weight were measured once a week in both sedentary and exercise rats. Running distance, food intake and body weight gain were averaged daily. Daily calorie intake was calculated: average daily food intake x diet energy density (standard rat chow, 3.85 kcal/g). Feed efficiency, the capacity to convert caloric intake into body weight, was determined by mean body weight gain (mg)/total caloric intake (kcal).

Telemetry Transmitter and Osmotic Pump Implantation

The rats were anesthetized with a ketamine-xylazine mixture (90% ketamine and 10% xylazine), and the femoral artery was accessed with a ventral incision. The right femoral artery was isolated, and the catheter of a telemetry probe was inserted into the vessel. Through the same ventral incision, a pocket along the right flank was formed. The body of the telemetry transmitter (HD-S10, DSI®, St. Paul, MN, United States) was slipped into the pocket and secured with tissue adhesive. The ventral incision was then closed with suture. Beginning 7 days after surgery, BP and HR data collection was initiated.

In separate procedures under isoflurance anesthesia (0.5–5% inhalation), osmotic pumps (model 2001 or 2002, ALZET®, Cupertino, CA, United States) containing ANG II (10 ng/kg/min or 120 ng/kg/min, Sigma) were implanted subcutaneously in the back of rats, respectively.

Evaluation of Blood Pressure Responses to Autonomic Blockade

Blood pressure was also measured in the presence of the ganglionic blocker hexamethonium (Hex, 30 mg/kg, ip). Ganglionic blockade was repeated two times in each animal once during baseline and once after 14 days of ANG II infusion. On the day of ganglionic blockade experiments, rats were allowed to stabilize for at least 60 min, after which time BP was recorded for 20 min before and after Hex injection.

Real-Time PCR Analysis

In the experiment 2, all rats were decapitated, and the brains were quickly removed and put in iced saline for 1 min. Then, the brains were cut into coronal sections of approximately 200 μm thickness, and LT and PVN tissues were punched with a 15-gauge needle stub (inner diameter: 1.5 mm). Some immediately surrounding tissue was usually included in the punch biopsies. The structures lying along the LT include the SFO, MnPO, and OVLT. Because each of the structures lying along the LT is very small, we collected these structures together and analyzed their mRNA expression as a whole. The PVN is composed of both magnocellular parvocellular components. We collected magnocellular and parvocellular regions from both sides. Total RNA was isolated from the LT or PVN using the Trizol method (Invitrogen) and treated with DNase I (Invitrogen, Carlsbad,

CA, United States) to remove any genomic DNA contamination. RNA integrity was checked by gel electrophoresis. Total RNA was reverse transcribed following the manufacturer's instructions (Applied Biosystems, Foster City, CA, United States). Real time PCR was conducted using 200–300 ng of cDNA and 500 nM of each primer in a 20 μl reaction with iQ SYBR Green Supermix (Bio-Rad, Hercules, CA, United States). Amplification cycles were conducted at 95°C for 3 min, followed by 40 cycles of 95°C for 15 s and annealing/extension at 60°C for 30 s. Reactions were performed in duplicate and analyzed using a C1000 thermocycler system (Bio-Rad). Messenger RNA levels for RAS components (ACE1, AT1-R, AT2-R, Ang-(1-7) receptor Mas-R), PICs (TNF-α, IL-1β, IL-6 and IL-10), NADPH oxidase (NOX2) and GAPDH were analyzed with SYBR Green real-time RT-PCR. The values were corrected by GAPDH, and the final concentration of mRNA was calculated using the formula $x = 2^{-\Delta\Delta Ct}$, where x = fold difference relative to control. Primers were purchased from Integrated DNA Technologies (Coralville, IA, United States). The sequences of the primers are shown in **Table 1**.

Statistical Analysis

Mean arterial pressure (MAP), HR and locomotor activity (relative animal activity movement) obtained from the telemetry recordings are presented as mean daily values averaged from daytime and nighttime measurements. Differences for MAP and HR were calculated for each animal based on the mean of a 5-day baseline subtracted from the mean of the final 5 days of ANG II treatment. For experiments of the effect of acute Hex injection, differences for BP were calculated for each animal based on the baseline subtracted from the BP after ip injection of Hex. All data were checked for the normality assumption by using Shapiro–Wilk test. One-way or Two-way ANOVAs for the experimental groups were then conducted on the means of the calculated differences for MAP and HR. After establishing a significant ANOVA, *post-hoc* analyses were performed with Tukey multiple comparison tests between pairs of mean changes (Graph-pad Prism 9.0). Running distance, body weight gain, food intake and feed efficiency are also presented as mean daily values and averaged daily values of the 12 weeks recordings. One-way ANOVAs were used to test for the differences in body weight gain, food intake, feed efficiency, and mRNA expression of the RAS and PIC components and NADPH oxidase in the LT and PVN, respectively. Running distances was analyzed by *t*-test. All data are expressed as means ± SEM. Statistical significance was set at $p < 0.05$.

RESULTS

Voluntary Exercise Intensity in Rats

The transmitter implantation surgery and I-D-E paradigm had no effects on exercise intensity in rats. The 12 weeks of running distances were comparable between two running groups [*t*-test, $P = 0.9628$] (**Figures 2A,B**).

Effect of Voluntary Exercise on Metabolic Parameters in Rats

Pretreatment with saline or the subpressor dose of ANG II and subsequent pressor dose of ANG II had no effects on body weight changes. After 12 weeks of voluntary exercise, the animals with running wheel access had significantly reduced body weight gain when compared to that of sedentary rats (One-way ANOVA analysis: $F_{(3,16)} = 7.909$, $P = 0.0019$) (**Figures 3A,B**).

There were no differences in food intake (g/d) between sedentary and exercise rats ($F_{(3,16)} = 1.710$, $P = 0.2501$). Due to the reduced body weight gain in exercise animals, feed efficiency was significantly lower in the exercise rats when compared to the sedentary rats (One-way ANOVA analysis: $F_{(3,16)} = 7.569$, $P = 0.0023$) (**Figures 3C–E**).

The Effects of Voluntary Exercise on Locomotor Activity and Sensitization of Hypertension

In sedentary rats, pretreatment with a subpressor dose of ANG II during **I** resulted in an enhanced increase in MAP induced by subsequent infusion of pressor dose of ANG II when compared with the rats pretreated with saline during **I** (Δ:36.9 ± 4.4 vs. Δ:18.4 ± 3.0 mmHg, Two-way ANOVA analysis: $F_{(1,32)} = 82.21$, $P < 0.0001$). Voluntary exercise did not alter the slow-pressor dose of ANG II-induced hypertension in rats pretreated with saline during **I** (Δ:16.6 ± 3.0 mmHg). However, exercise abolished the effect of the subpressor dose of ANG II given to induce HTRS (Δ:14.0 ± 4.4 mmHg) (Two-way ANOVA analysis: $F_{(3,32)} = 4.859$, $P = 0.0068$, **Figures 4A,B**).

TABLE 1 | Primer sequences for real time PCR.

Gene	Forward primer	Reverse primer	Product size (bp)
GAPDH	TGACTCTACCCACGGCAAGTTCAA	ACGACATACTCAGCACCAGCATCA	141
ACE	GTGTTGTGGAACGAATACGC	CCTTCTTTATGATCCGCTTGA	187
AT1-R	CTCAAGCCTGTCTACGAAAATGAG	GTGAATGGTCCTTTGGTCGT	188
NOX2	CAAGATGGAGGTGGGACAGT	GCTTATCACAGCCACAAGCA	170
TNF-α	GCCGATTTGCCACTTCATAC	AAGTAGACCTGCCCGGACTC	209
IL-6	GCCTATTGAAAATCTGCTCTGG	GGAAGTTGGGGTAGGAAGGA	160
IL-1β	AGCAACGACAAAATCCCT GT	GAAGACAAACCGCTTTTCCA	209
IL-10	GTTGCCAAGCCTTGTCAGAAA	TTTCTGGGCCATGGTTCTCT	120
AT2-R	ACCTTTTGAACATGGTGCTTTG	TTTCCTATGCCAGTGTGCAG	160
Mas-R	TGTGGGTGGCTTTCGATT	CCCGTCACATATGGAAGCAT	159

ACE, angiotensin converting enzyme 1; AT1-R, angiotensin II type 1 receptor; NOX2, NADPH oxidase 2; TNF-α, tumor necrosis factor-α; IL-6, interleukin-6; IL-1β, interleukin-1β; IL-10, interleukin-10; AT2-R, angiotensin II type 2 receptor; and Mas-R, angiotensin-(1–7) receptor.

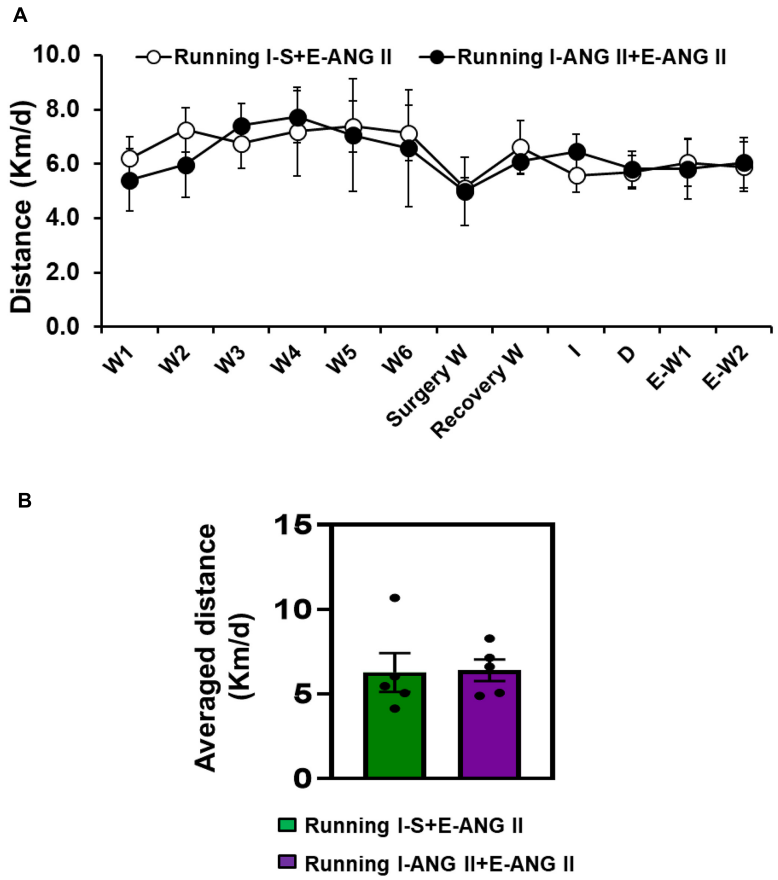

FIGURE 2 | The daily **(A)** and averaged **(B)** running distances during 12 weeks of voluntary exercise (Running) in rats with Induction-Delay-Expression (I-D-E) paradigm.

Exercise or infusion of ANG II did not produce significant changes in HR in any of the groups (Two-way ANOVA analysis: $F_{(3,12)} = 1.681$, $P = 0.2238$) (**Figures 4C,D**).

The I-D-E paradigm itself had no effect on locomotor activity in either the sedentary or exercise rats. However, the exercise rats exhibited a significant increase in locomotor activity (4.94 ± 0.34 and 5.32 ± 0.62) when compared with the sedentary rats (2.77 ± 0.26 and 2.45 ± 0.27) (One-way ANOVA analysis: $F_{(3,16)} = 13.61$, $P = 0.0001$, **Figures 4E,F**).

Effects of Autonomic Blockade on Blood Pressure

Figure 5 shows the decreases in BP with acute ganglionic blockade in all groups. The average reduction in the BP response to Hex injection before the **I-D-E** paradigm was -21.7 ± 0.7 mmHg. Following 14 days of the slow-pressor dose of ANG II, acute Hex injection resulted in a significant reduction in BP in sedentary rats pretreated with saline during **I** (Δ:-35.4 ± 1.3 mmHg, $P = 0.0023$). However, the reductions in BP after Hex injection were further augmented in sedentary rats pretreated with the subpressor dose of ANG II during **I** (Δ:-51.3 ± 3.8 mmHg, $P = 0.0006$). Voluntary exercise did not alter Hex-induced reduction in rats pretreated with saline during **I** when compared to the corresponding sedentary rats (Δ:-31.7 ± 0.8 mmHg, $P = 0.7529$). However, exercise abolished the augmented reduction in BP induced by Hex in rats pretreated with subpressor dose of ANG II during **I** (Δ:-35.2 ± 1.2 mmHg, $P = 0.0006$) (One-way ANOVA analysis: $F_{(4,29)} = 51.93$, $P < 0.0001$, **Figure 5**).

The Effects of Subpressor Dose of Angiotensin II and Voluntary Exercise on mRNA Expression of Brain Renin-Angiotensin System Components, Proinflammatory Cytokines, and NADPH Oxidase

In LT tissues of the sedentary rats collected at the end of **D**, RT-PCR analysis revealed that subpressor dose of ANG II pretreatment during **I** resulted in a significant increase in mRNA expression of all prohypertensive components including AT1-R, ACE, NOX2, TNF-α, IL-1β, and IL-6 ($P < 0.05$, **Figure 6A**), but did not alter mRNA expression of antihypertensive components such as IL-10, AT2-R, and Mas-R when compared with saline

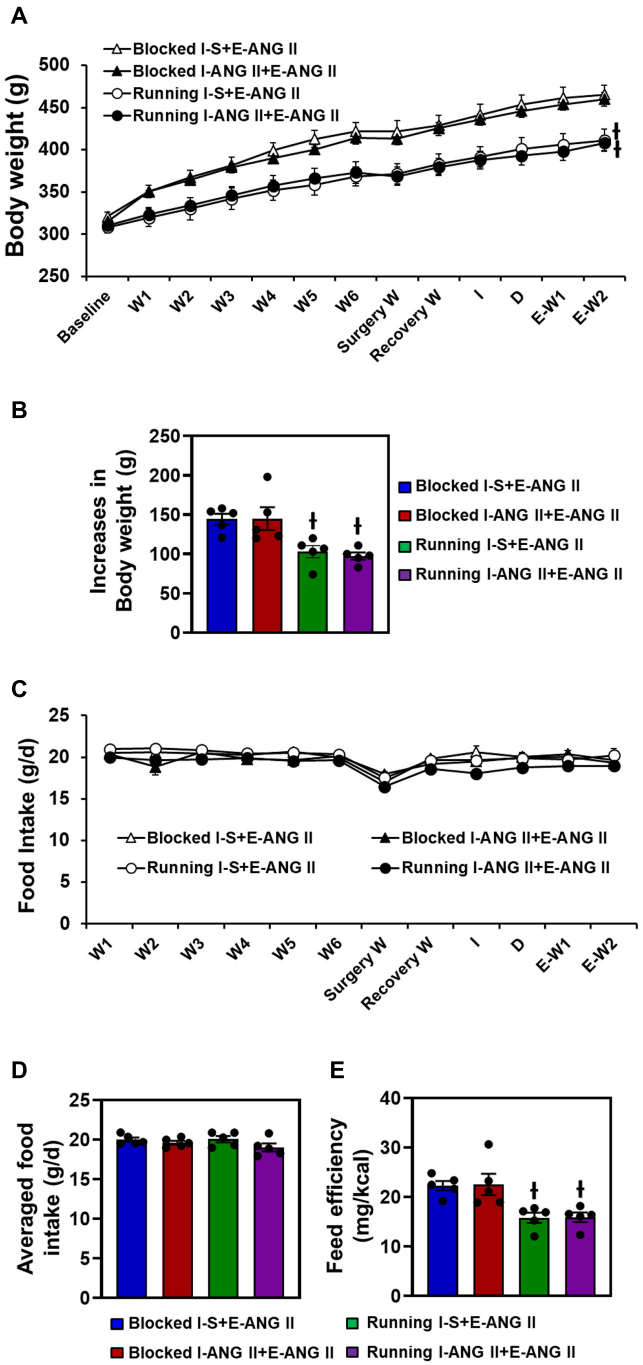

FIGURE 3 | Body weight changes **(A,B)**, daily and averaged food intakes **(C,D)** and feeding efficiency **(E)** in sedentary (Blocked) and exercise (Running) rats with Induction-Delay-Expression (I-D-E) paradigm. (n = 5/group; one-way ANOVA was used for analysis followed by Tukey's *post-hoc* tests. $p < 0.05$; ǂ vs. blocked rats).

pretreatment ($P > 0.05$, **Figure 6B**). Voluntary exercise reversed the increased mRNA expression of most of prohypertensive components except AT1-R and produced significant increase in mRNA expression of antihypertensive components ($P < 0.05$, **Figures 6A,B**). Notably, voluntary exercise in subpressor ANG II pretreated rats exhibited an augmented increase in mRNA expression of IL-10 and AT2-R when compared to the exercise rats pretreated with saline during **I** ($P < 0.05$, **Figure 6B**). (One-way ANOVA for the changes in gene expression, *P*-values from 0.0155 to less 0.0001).

In PVN tissues, the sedentary rats pretreated with the subpressor dose of ANG II during **I** exhibited upregulation of mRNA expression of the prohypertensive components (AT1-R, NOX2, TNF-α, IL-1β, $P < 0.05$) and an antihypertensive

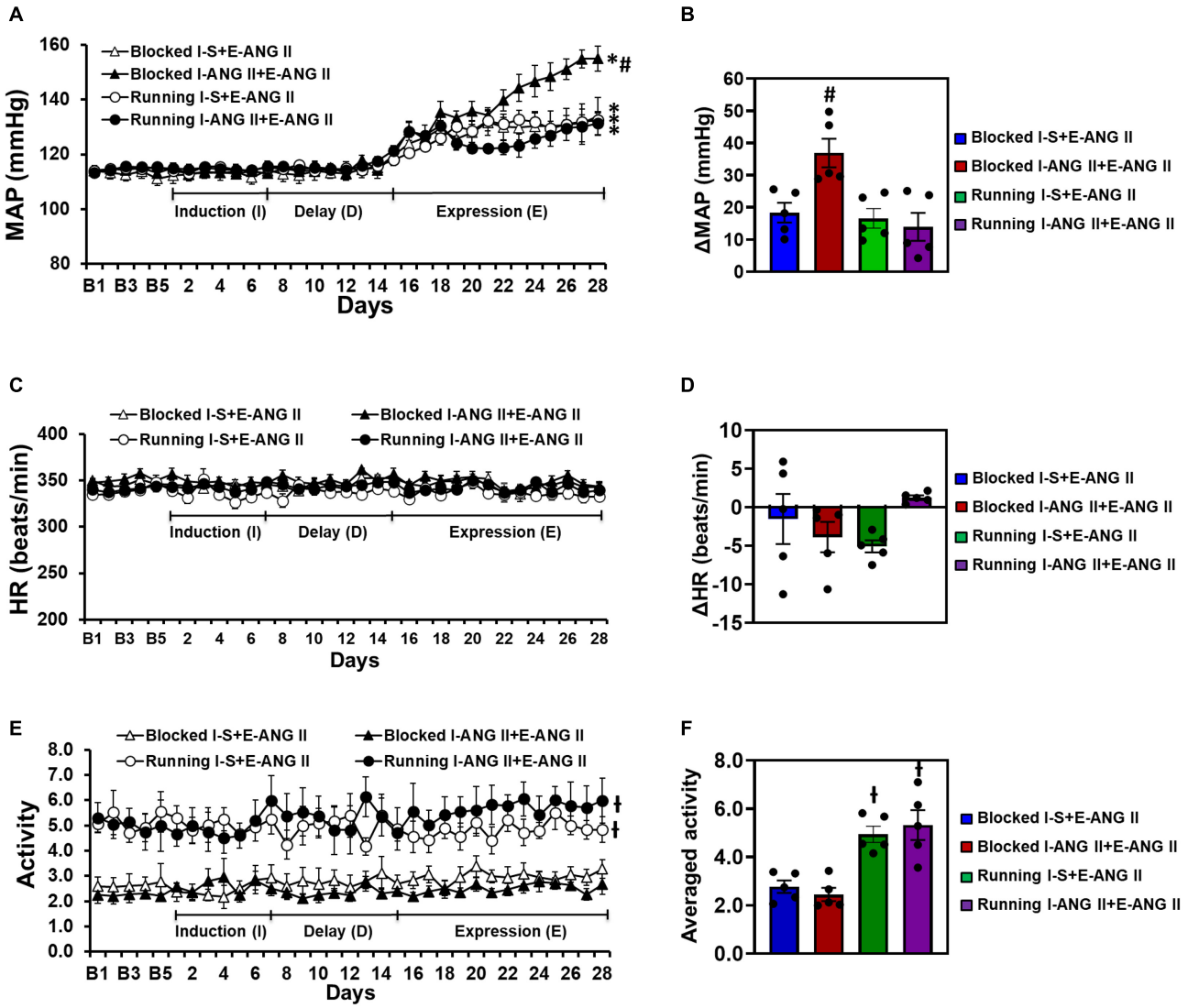

FIGURE 4 | Voluntary exercise prevented hypertensive response sensitization to angiotensin (ANG) II treatment although the locomotor activities of the rats were elevated. HRs were comparable in all groups of offspring. Daily and averaged mean arterial pressure (MAP, **A,B**), heart rate (HR, **C,D**) and locomotor activity **(E,F)** in sedentary (Blocked) or exercise (Running) rats during the Induction-Delay-Expression (I-D-E) paradigm. (n = 5/group; two-way ANOVA was used for analysis followed by Tukey's *post-hoc* tests. $p < 0.05$, * vs. baseline; # vs. blocked I-S + E-ANG II and running rats; ǂ vs. blocked rats).

component Mas-R ($P < 0.05$), but had no effects on mRNA expression of the ACE1, IL-6, IL-10, and AT2-R ($P > 0.05$, **Figures 7A,B**). The increased expression of AT1-R and TNF-α was not altered in saline pretreated rats after voluntary exercise ($P > 0.05$). However, the increased expression of AT1-R, NOX2 and TNF-α was not present in the subpressor ANG II pretreated exercise rats ($P < 0.05$). Moreover, voluntary exercise in both saline and subpressor ANG II pretreated rats upregulated mRNA expression of antihypertensive components IL-10 and AT2-R ($P < 0.05$) and did not change the increased expression of IL-1β and Mas-R induced by subpressor ANG II pretreatment in sedentary rats ($P > 0.05$) (**Figures 7A,B**). (One-way ANOVA for the changes in gene expression; ACE1, $P = 0.8126$; IL-6, $P = 0.7333$; other P-values from less 0.0008 to less 0.0001).

DISCUSSION

The goals of the current studies were to determine if voluntary exercise would attenuate the sensitized hypertensive response induced by ANG II infusion and to investigate if it was through regulating the balance between the prohypertensive and the antihypertensive pathways in the CNS. The major findings of the present study were that (1) a systemic subpressor dose of ANG II pretreatment elicited HTRS to a subsequent infusion of a slow-pressor dose of ANG II in sedentary rats, which were mediated by increased centrally driven sympathetic tone. However, this augmentation of the hypertensive response and sympathetic tone was not exhibited by the exercised rats; (2) although there were similar food intakes between the sedentary

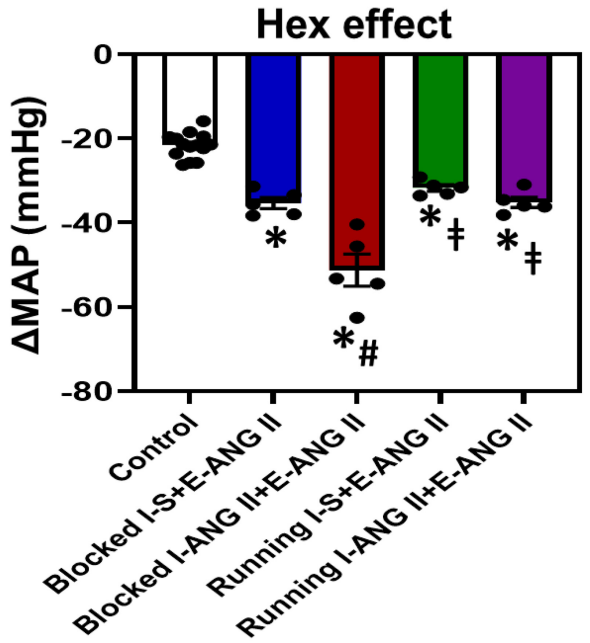

FIGURE 5 | Mean arterial pressure (MAP) in response to ganglionic blockade with hexamethonium (Hex) before starting the Induction-Delay-Expression (I-D-E) paradigm (control) and at the end of the pressor angiotensin (ANG) II infusion in all groups. (n = 5/group; one-way ANOVA was used for analysis followed by Tukey's *post-hoc* tests. $p < 0.05$, * vs. control, # vs. Blocked I-S + E-ANG II, ‡ vs. Blocked I + ANG II + E-ANG II).

and exercise rats, the exercise rats showed reduced body weight gain and feed efficiency; and (3) the subpressor dose of ANG II infusion during **I** resulted in significant increases in mRNA expression of several prohypertensive components such as AT1-R, ACE1, NOX2, TNF-α, IL-1β, and IL-6 in key brain cardiovascular nuclei when measured at the end of **D**. Exercise abolished the upregulated expression of most of the prohypertensive components, and upregulated mRNA expression of some antihypertensive components including IL-10, AT2-R, and Mas-R. The results indicate that exercise training plays a beneficial role in preventing HTRS and that this is associated with reduced expression of prohypertensive components of the RAS, PICs, and NADPH oxidase and with enhanced expression of antihypertensive components of the RAS and anti-inflammatory cytokine in the CNS. This study highlights a central mechanism by which exercise training mitigates an enhanced increase in BP and the development of hypertension when one encounters prohypertensive stressors in the lifetime.

The sympathetic nervous system (SNS) plays a pivotal role in the development and maintenance of hypertension in human and several animal models, including ANG II-induced hypertension, obesity-related hypertension, deoxycorticosterone acetate/aldosterone salt-sensitive hypertension, and spontaneously hypertensive rats (SHRs; Shi et al., 2010a; Xue et al., 2011; Cardinale et al., 2012; Chao et al., 2013; Dange et al., 2015; Hall et al., 2015; Basting and Lazartigues, 2017). In this regard, increased brain ANG II, PICs and ROS derived either from *de novo* synthesis in the brain or from the circulation and upregulated expression of their receptors or genes (i.e., AT1-R, ACE, and TNF receptors) are evident in these hypertensive animals (Young and Davisson, 2015; Nakagawa et al., 2020). Interactions between RAS, PICs and ROS activate the brain neural network containing neurons in the LT and PVN to elevate the SNS activity and increase BP (Shi et al., 2010a; Xue et al., 2011; Cardinale et al., 2012; Chao et al., 2013; Dange et al., 2015; Hall et al., 2015; Young and Davisson, 2015; Basting and Lazartigues, 2017; Nakagawa et al., 2020). Previous studies from our laboratory have also demonstrated that a wide range of stressors sensitize the hypertensive response through upregulation of these prohypertensive factors in the brain (Johnson and Xue, 2018; Xue et al., 2020b). In the present study, the subpressor dose of ANG II infusion during **I** resulted in significant increases in mRNA expression of prohypertensive components such as AT1-R, ACE1, NOX2, TNF-α, IL-1β, and IL-6 in the LT and PVN of the sedentary rats. These upregulated prohypertensive components enhancing CNS activity may provide a physiological bases for initiating and maintaining a sensitized state. As a result, the enhanced hypertensive response to the subsequent pressor dose of ANG II and augmented sympathetic tone were evident in the sedentary rats pretreated with subpressor dose of ANG II.

Exercise training is an effective strategy for maintaining health or rehabilitating subjects who are deconditioned due to cardiovascular disease (Zucker and Musch, 2018; Alpsoy, 2020). The mechanisms underlying the beneficial effects of exercise training have been investigated extensively in human and animal models of various cardiovascular diseases such as hypertension, heart failure and stroke. Central mechanisms including inhibition of RAS activity, reduction of microglial activation, inflammation and oxidative stress, and restoration of the blood-brain barrier in brain cardiovascular nuclei such as the PVN and RVLM have been demonstrated to result from exercise training. Exercise effectively reduces SNS activity and BP and improves heart failure (Agarwal et al., 2011; Zheng et al., 2012; Haack and Zucker, 2015; Masson et al., 2015; Michelini et al., 2015; Ferreira-Junior et al., 2019; Fragas et al., 2021). In the present study, we found that voluntary exercise normalized the subpressor dose of ANG II-induced upregulation of mRNA expression of several RAS components and PICs and NADPH oxidase in the LT and PVN and that these were accompanied by the abolition of HTRS and attenuation of increased sympathetic tone. Our present results confirm and extend the point that exercise training blocks the development of hypertension produced by the sensitized hypertensive response through inhibiting central prohypertensive factors and reducing sympathetic outflow.

Besides the prohypertensive components of the renin-angiotensin and immune systems, there are anti-hypertensive and anti-inflammatory components including ACE1/ANG II/AT2-R, ACE2/ANG-(1-7)/Mas-R, and IL-10 both in the CNS and in the periphery. The anti-hypertensive components oppose the actions of the prohypertensive axis of RAS (Shi et al., 2010a; Gao and Zucker, 2011; Xu et al., 2011; Sumners et al., 2015; Santos et al., 2018). Reduced AT2-R or ACE2 expression and/or enzyme activity have been found in various brain regions

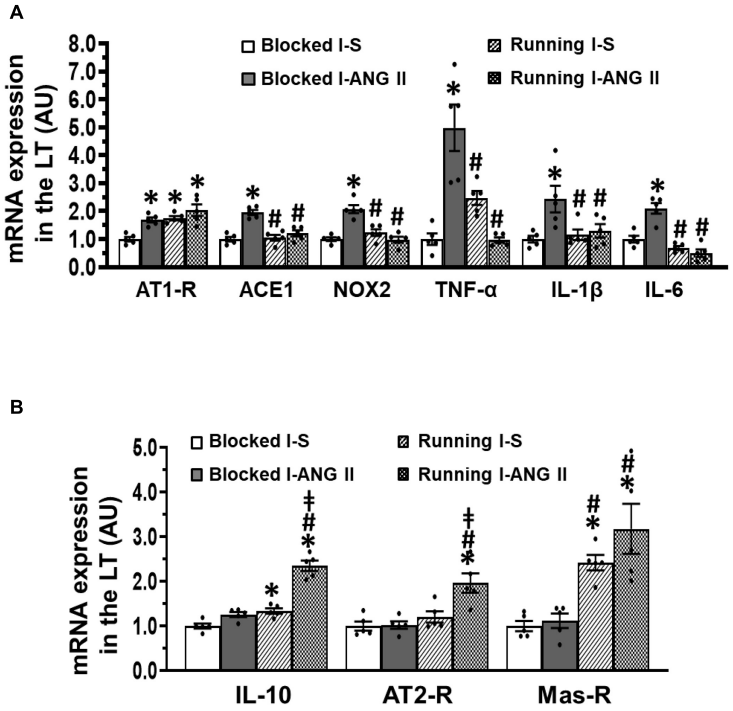

FIGURE 6 | Comparison of the mRNA expression of renin-angiotensin system components, NADPH oxidase and proinflammatory cytokines in the lamina terminalis (LT) in sedentary (Blocked) or exercise (Running) rats after Delay period of the Induction-Delay-Expression (I-D-E) paradigm. **(A)** mRNA expression of prohypertensive components; **(B)** mRNA expression of antihypertensive components (n = 5/group; one-way ANOVA was used for analysis followed by Tukey's *post-hoc* tests; $p < 0.05$; * vs. Blocked I-S; # vs Blocked I-ANG II; ǂ vs. Running I-S).

in hypertension and heart failure models. Overexpression or activation of AT2-R, ACE2, or Mas-R in the brain blunts the development of hypertension and improves heart failure (Gao et al., 2008; Feng et al., 2010; Xia et al., 2013). As an anti-inflammatory factor, IL-10 has a significant impact on sympathetic outflow, BP and cardiac remodeling in experimental models of hypertension (Shi et al., 2010b). Studies show that IL-10 can inhibit microglial activity and prevent lipopolysaccharide (LPS)-induced production and secretion of PICs through the toll-like receptor-4 (TLR4) and the nuclear factor kappa B (NF-κB) signaling cascade (Mee-Inta et al., 2019).

It has been demonstrated that long-term exercise training can upregulate IL-10, ACE2, and Mas-R expression in the brain of SHR and heart failure models (Agarwal et al., 2011; Zucker et al., 2015). Consistent with these previous studies, we also found in the present study that exercise training upregulated the mRNA expression of antihypertensive components including IL-10, AT2-R, and Mas-R in the LT and PVN of sedentary animals and induced an enhanced mRNA expression of these antihypertensive components in the LT in rats pretreated with the subpressor dose of ANG II. All these effects would tend to contribute to the attenuation of the subpressor dose of ANG II-induced increase in sympathetic tone and sensitization of hypertension. Our present results indicate that exercise training plays a protective role in the induction of HTRS not only through inhibition of prohypertensive components but also through activation of antihypertensive components of the RAS and immune system that rebalance activity of central neural network involved in regulation of BP.

Besides the effects on the autonomic nervous system, exercise training also impacts energy metabolism. In fact, the reduction of body weight and visceral adiposity, and subsequently, influence of metabolic related hormones such as leptin and insulin by exercise may interfere with the central mechanisms contributing to the development of hypertension, since high blood pressure has been associated with all these variables (Jakicic et al., 2001; Lim et al., 2013). In the present study, we found that the exercise rats showed reduced body weight gain and feed efficiency even though food intakes were similar between the sedentary and the exercise rats. Moreover, the reduced body weight and the distances run by the animals pretreated with either saline or a subpressor dose of ANG II were comparable. However, exercise did not affect the hypertensive response to a pressor dose of ANG II in saline pretreated animals, but abolished the sensitized hypertensive response induced by pretreatment with a suppressor dose of ANG II. This excludes the possibility that exercise-induced abolition of HTRS observed in this study was due to a reduction in body weight. However, the roles of exercise-induced changes in body composition, metabolic hormones (i.e., leptin and insulin) as well as their interactions with the RAS components and mediators of inflammation and oxidative stress in the sensitization of hypertension warrant further investigation. In addition, voluntary exercise has been demonstrated to induce less stress when compared with those

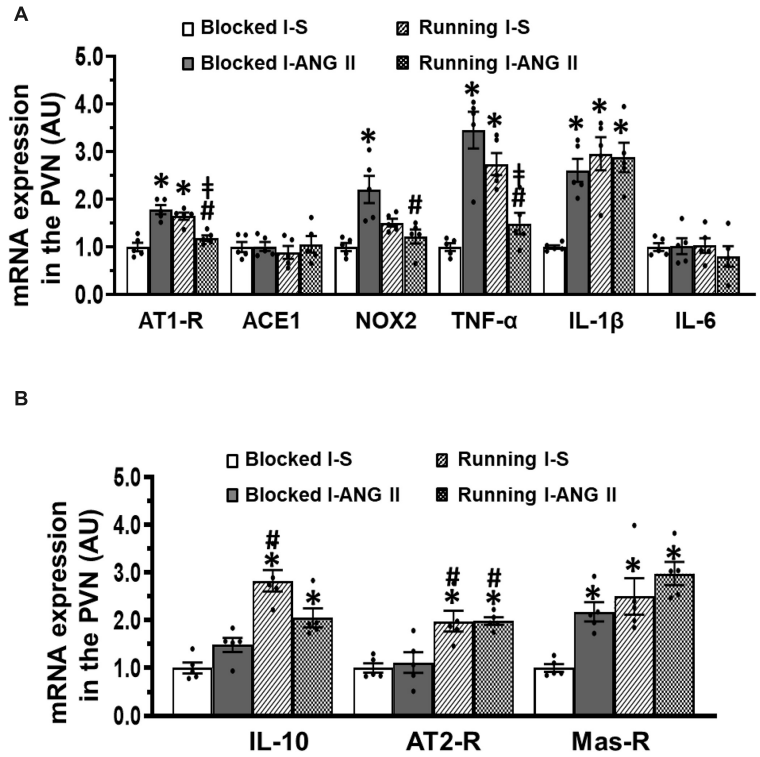

FIGURE 7 | Comparison of the mRNA expression of renin-angiotensin system components, NADPH oxidase and proinflammatory cytokines in the hypothalamic paraventricular nucleus (PVN) in sedentary (Blocked) or exercise (Running) rats after Delay period of the Induction-Delay-Expression (I-D-E) paradigm. **(A)** mRNA expression of prohypertensive components; **(B)** mRNA expression of antihypertensive components (n = 5/group; one-way ANOVA was used for analysis followed by Tukey's *post-hoc* tests; $p < 0.05$; * vs. Blocked I-S; # vs. Blocked I-ANG II; ǂ vs. Running I-S).

forced exercise such as forced treadmill running or swimming (Billman et al., 2015). Forced exercise was not chosen as the method for this study because the psychological stress has been demonstrated to induce the HTRS in our previous studies (Xue et al., 2019; Xue et al., 2020a).

There are some limitations to this study. First, besides changes in the neural network that regulates SNS and BP, the beneficial effects of exercise training in cardiovascular disease are also due to a large interplay of cellular and molecular mediators in the heart and peripheral vasculature (Zucker and Musch, 2018). It has been shown that long-term exercise plays a beneficial role in attenuating the transition from the pre- to hypertensive phase in SHRs through deactivation of the AT1-R pathway driving vascular and heart remodeling (Silva et al., 2015; da Costa et al., 2020). Based on these data, in our hypertension sensitization model, we can't rule out the possibility that exercise training also affected vascular and heart function directly to attenuate the HTRS induced by pretreatment with subpressor dose of ANG II. Second, we found that pretreatment with a subpressor dose of ANG II upregulated mRNA expression of AT1-R in both the LT and PVN. However, voluntary exercise reversed upregulated mRNA expression of AT1-R only in the PVN, but not in the LT. The results may reflect the differences in the brain location between these two structures (outside vs. inside blood–brain barrier) or in the changes in mRNA expression of related RAS component such as ACE1 (changed in the LT but not in the PVN). This difference in the mRNA expression needs to be explored by measurements of enzymatic activity or protein expression. Therefore, more studies assessing the enzymatic activity, protein levels and activation of second messenger mechanisms related to these agents in these brain nuclei are needed to confirm the functional significance of the changes in gene expression. Third, it has been shown that interplays between sex hormones and exercise have a long-term regulatory effect on BP through affecting food intake and energy balance (Gentry and Wade, 1976; Yang and Liang, 2018). In our previous study, we also found sex differences in HTRS, in which pretreatment with subpressor dose of ANG II did not elicit HTRS in intact female rats when compared to male rats and ovariectomized female rats, and females are protected from ANG II-induced sensitization through central estrogen and its regulation of brain RAS (Xue et al., 2014). Based on these results, we did not include females in the present study to explore the beneficial effect of exercise on HTRS.

CONCLUSION

This study demonstrated that in sedentary animals, pretreatment with a subpressor dose of ANG II induces HTRS probably

through shifting the balance of the prohypertensive and antihypertensive pathways in favor of enhanced central activity driving sympathetic outflow and elevated BP. The voluntary exercise-induced blockade of the prohypertensive components or activation of the antihypertensive components leads to attenuated overall activity of the RAS and reduced inflammation and oxidative stress that is effective in lowering centrally driven sympathetic activity and blocking the induction of HTRS. This study provides insight into central mechanisms that exercise training inhibits the predisposition for development of hypertension when one encounters prohypertensive stressors in the lifetime. This study also highlights voluntary exercise as a non-pharmacologic therapy and management strategy for health and hypertensive individuals.

DATA AVAILABILITY STATEMENT

The raw data supporting the conclusions of this article will be made available by the authors, without undue reservation.

ETHICS STATEMENT

The animal study was reviewed and approved by The University of Iowa and Hebei Medical University Animal Care and Use Committee.

AUTHOR CONTRIBUTIONS

BX, G-SZ, and AJ designed the experiments. BX, J-LC, FG, and TB performed the experiments and analyzed data. BX wrote the manuscript. BX, G-SZ, Z-GZ, and AJ revised the manuscript. All authors read and approved the final manuscript.

FUNDING

This work was supported by the NIH grants HL-139575 (AJ and BX), and the Funds for Prevention of Geriatric Diseases of Hebei Province (No. 303132618 to G-SZ).

REFERENCES

Agarwal, D., Welsch, M. A., Keller, J. N., and Francis, J. (2011). Chronic exercise modulates RAS components and improves balance between pro- and anti-inflammatory cytokines in the brain of SHR. *Basic Res. Cardiol.* 106, 1069–1085. doi: 10.1007/s00395-011-0231-7

Alpsoy, S. (2020). Exercise and Hypertension. *Adv. Exp. Med. Biol.* 1228, 153–167.

Basting, T., and Lazartigues, E. (2017). DOCA-Salt hypertension: an update. *Curr. Hypertens. Rep.* 19:32. doi: 10.1007/s11906-017-0731-4

Billman, G. E., Cagnoli, K. L., Csepe, T., Li, N., Wright, P., Mohler, P. J., et al. (2015). Exercise training-induced bradycardia: evidence for enhanced parasympathetic regulation without changes in intrinsic sinoatrial node function. *J. Appl. Physiol.* 118, 1344–1355. doi: 10.1152/japplphysiol.01111.2014

Cardinale, J. P., Sriramula, S., Mariappan, N., Agarwal, D., and Francis, J. (2012). Angiotensin II-induced hypertension is modulated by nuclear factor-kappabin the paraventricular nucleus. *Hypertension* 59, 113–121. doi: 10.1161/HYPERTENSIONAHA.111.182154

Chao, Y. M., Lai, M. D., and Chan, J. Y. (2013). Redox-sensitive endoplasmic reticulum stress and autophagy at rostral ventrolateral medulla contribute to hypertension in spontaneously hypertensive rats. *Hypertension* 61, 1270–1280. doi: 10.1161/HYPERTENSIONAHA.111.00469

Cornelissen, V. A., and Smart, N. A. (2013). Exercise training for blood pressure: a systematic review and meta-analysis. *J. Am. Heart Assoc.* 2:e004473.

da Costa, T. S. R., Masson, G. S., Eichler, R., Silva, J. C. S., Lacchini, S., and Michelini, L. C. (2020). Training-induced deactivation of the AT1 receptor pathway drives autonomic control and heart remodeling during the transition from the pre- to hypertensive phase in spontaneously hypertensive rats. *Circ. J.* 84, 1294–1303. doi: 10.1253/circj.CJ-19-1161

Dampney, R. A. (2016). Central neural control of the cardiovascular system: current perspectives. *Adv. Physiol. Educ.* 40, 283–296. doi: 10.1152/advan.00027.2016

Dange, R. B., Agarwal, D., Teruyama, R., and Francis, J. (2015). Toll-like receptor 4 inhibition within the paraventricular nucleus attenuates blood pressure and inflammatory response in a genetic model of hypertension. *J. Neuroinflammation* 12:31. doi: 10.1186/s12974-015-0242-7

DiBona, G. F. (2013). Sympathetic nervous system and hypertension. *Hypertension* 61, 556–560.

Feng, Y., Xia, H., Cai, Y., Halabi, C. M., Becker, L. K., Santos, R. A., et al. (2010). Brain-selective overexpression of human Angiotensin-converting enzyme type 2 attenuates neurogenic hypertension. *Circ. Res.* 106, 373–382. doi: 10.1161/CIRCRESAHA.109.208645

Ferreira-Junior, N. C., Ruggeri, A., Silva, S. D. Jr., Zampieri, T. T., Ceroni, A., and Michelini, L. C. (2019). Exercise training increases GAD65 expression, restores the depressed GABAA receptor function within the PVN and reduces sympathetic modulation in hypertension. *Physiol. Rep.* 7:e14107. doi: 10.14814/phy2.14107

Fragas, M. G., Candido, V. B., Davanzo, G. G., Rocha-Santos, C., Ceroni, A., and Michelini, L. C. (2021). Transcytosis within PVN capillaries: a mechanism determining both hypertension-induced blood-brain barrier dysfunction and exercise-induced correction. *Am. J. Physiol. Regul. Integr. Comp. Physiol.* 321, R732–R741. doi: 10.1152/ajpregu.00154.2020

Gao, L., Wang, W., Wang, W., Li, H., Sumners, C., and Zucker, I. H. (2008). Effects of angiotensin type 2 receptor overexpression in the rostral ventrolateral medulla on blood pressure and urine excretion in normal rats. *Hypertension* 51, 521–527. doi: 10.1161/HYPERTENSIONAHA.107.101717

Gao, L., and Zucker, I. H. (2011). AT2 receptor signaling and sympathetic regulation. *Curr. Opin. Pharmacol.* 11, 124–130. doi: 10.1016/j.coph.2010.11.004

Gentry, R. T., and Wade, G. N. (1976). Sex differences in sensitivity of food intake, body weight, and running-wheel activity to ovarian steroids in rats. *J. Comp. Physiol. Psychol.* 90, 747–754. doi: 10.1037/h0077246

Haack, K. K., and Zucker, I. H. (2015). Central mechanisms for exercise training-induced reduction in sympatho-excitation in chronic heart failure. *Auton. Neurosci.* 188, 44–50. doi: 10.1016/j.autneu.2014.10.015

Hall, J. E., Do Carmo, J. M., Da Silva, A. A., Wang, Z., and Hall, M. E. (2015). Obesity-induced hypertension: interaction of neurohumoral and renal mechanisms. *Circ. Res.* 116, 991–1006. doi: 10.1161/CIRCRESAHA.116.305697

Haspula, D., and Clark, M. A. (2018). Neuroinflammation and sympathetic overactivity: mechanisms and implications in hypertension. *Auton. Neurosci.* 210, 10–17. doi: 10.1016/j.autneu.2018.01.002

Huber, G., Schuster, F., and Raasch, W. (2017). Brain renin-angiotensin system in the pathophysiology of cardiovascular diseases. *Pharmacol. Res.* 125, 72–90. doi: 10.1016/j.phrs.2017.06.016

Jakicic, J. M., Clark, K., Coleman, E., Donnelly, J. E., Foreyt, J., Melanson, E., et al. (2001). American college of sports medicine position stand. appropriate intervention strategies for weight loss and prevention of weight regain for adults. *Med. Sci. Sports Exerc.* 33, 2145–2156.

Johnson, A. K., and Gross, P. M. (1993). Sensory circumventricular organs and brain homeostatic pathways. *FASEB J.* 7, 678–686. doi: 10.1096/fasebj.7.8.8500693

Johnson, A. K., and Xue, B. (2018). Central nervous system neuroplasticity and the sensitization of hypertension. *Nat. Rev. Nephrol.* 14, 750–766. doi: 10.1038/s41581-018-0068-5

Johnson, A. K., Zhang, Z., Clayton, S. C., Beltz, T. G., Hurley, S. W., Thunhorst, R. L., et al. (2015). The roles of sensitization and neuroplasticity in the long-term regulation of blood pressure and hypertension. *Am. J. Physiol. Regul. Integr. Comp. Physiol.* 309, R1309–R1325. doi: 10.1152/ajpregu.00037.2015

Kalupahana, N. S., and Moustaid-Moussa, N. (2012). The renin-angiotensin system: a link between obesity, inflammation and insulin resistance. *Obes. Rev.* 13, 136–149. doi: 10.1111/j.1467-789X.2011.00942.x

Lim, K., Burke, S. L., and Head, G. A. (2013). Obesity-related hypertension and the role of insulin and leptin in high-fat-fed rabbits. *Hypertension* 61, 628–634. doi: 10.1161/HYPERTENSIONAHA.111.00705

Masson, G. S., Nair, A. R., Silva Soares, P. P., Michelini, L. C., and Francis, J. (2015). Aerobic training normalizes autonomic dysfunction, HMGB1 content, microglia activation and inflammation in hypothalamic paraventricular nucleus of SHR. *Am. J. Physiol. Heart Circ. Physiol.* 309, H1115–H1122. doi: 10.1152/ajpheart.00349.2015

Mee-Inta, O., Zhao, Z. W., and Kuo, Y. M. (2019). Physical exercise inhibits inflammation and microglial activation. *Cells* 8:691. doi: 10.3390/cells8070691

Michelini, L. C., O'leary, D. S., Raven, P. B., and Nobrega, A. C. (2015). Neural control of circulation and exercise: a translational approach disclosing interactions between central command, arterial baroreflex, and muscle metaboreflex. *Am. J. Physiol. Heart Circ. Physiol.* 309, H381–H392. doi: 10.1152/ajpheart.00077.2015

Mills, K. T., Stefanescu, A., and He, J. (2020). The global epidemiology of hypertension. *Nat. Rev. Nephrol.* 16, 223–237.

Mimee, A., Smith, P. M., and Ferguson, A. V. (2013). Circumventricular organs: targets for integration of circulating fluid and energy balance signals? *Physiol. Behav.* 121, 96–102. doi: 10.1016/j.physbeh.2013.02.012

Nakagawa, P., Gomez, J., Grobe, J. L., and Sigmund, C. D. (2020). The renin-angiotensin system in the central nervous system and its role in blood pressure regulation. *Curr. Hypertens. Rep.* 22:7. doi: 10.1007/s11906-019-1011-2

Peterson, J. R., Sharma, R. V., and Davisson, R. L. (2006). Reactive oxygen species in the neuropathogenesis of hypertension. *Curr. Hypertens. Rep.* 8, 232–241. doi: 10.1007/s11906-006-0056-1

Rossi, N. F., Chen, H., and Maliszewska-Scislo, M. (2013). Paraventricular nucleus control of blood pressure in two-kidney, one-clip rats: effects of exercise training and resting blood pressure. *Am. J. Physiol. Regul. Integr. Comp. Physiol.* 305, R1390–R1400. doi: 10.1152/ajpregu.00546.2012

Santos, R. A. S., Sampaio, W. O., Alzamora, A. C., Motta-Santos, D., Alenina, N., Bader, M., et al. (2018). The ACE2/Angiotensin-(1-7)/MAS axis of the renin-angiotensin system: focus on angiotensin-(1-7). *Physiol. Rev.* 98, 505–553. doi: 10.1152/physrev.00023.2016

Sharma, N. M., Haibara, A. S., Katsurada, K., Nandi, S. S., Liu, X., Zheng, H., et al. (2021). Central ang ii (angiotensin ii)-mediated sympathoexcitation: role for hif-1alpha (hypoxia-inducible factor-1alpha) facilitated glutamatergic tone in the paraventricular nucleus of the hypothalamus. *Hypertension* 77, 147–157. doi: 10.1161/HYPERTENSIONAHA.120.16002

Shi, P., Diez-Freire, C., Jun, J. Y., Qi, Y., Katovich, M. J., Li, Q., et al. (2010a). Brain microglial cytokines in neurogenic hypertension. *Hypertension* 56, 297–303. doi: 10.1161/HYPERTENSIONAHA.110.150409

Shi, P., Raizada, M. K., and Sumners, C. (2010b). Brain cytokines as neuromodulators in cardiovascular control. *Clin. Exp. Pharmacol. Physiol.* 37, e52–e57. doi: 10.1111/j.1440-1681.2009.05234.x

Silva, S. D. Jr., Zampieri, T. T., Ruggeri, A., Ceroni, A., Aragao, D. S., Fernandes, F. B., et al. (2015). Downregulation of the vascular renin-angiotensin system by aerobic training - focus on the balance between vasoconstrictor and vasodilator axes. *Circ. J.* 79, 1372–1380. doi: 10.1253/circj.CJ-14-1179

Sumners, C., De Kloet, A. D., Krause, E. G., Unger, T., and Steckelings, U. M. (2015). Angiotensin type 2 receptors: blood pressure regulation and end organ damage. *Curr. Opin. Pharmacol.* 21, 115–121. doi: 10.1016/j.coph.2015.01.004

Xia, H., Sriramula, S., Chhabra, K. H., and Lazartigues, E. (2013). Brain angiotensin-converting enzyme type 2 shedding contributes to the development of neurogenic hypertension. *Circ. Res.* 113, 1087–1096. doi: 10.1161/CIRCRESAHA.113.301811

Xu, P., Sriramula, S., and Lazartigues, E. (2011). ACE2/ANG-(1-7)/Mas pathway in the brain: the axis of good. *Am. J. Physiol. Regul. Integr. Comp. Physiol.* 300, R804–R817. doi: 10.1152/ajpregu.00222.2010

Xue, B., Beltz, T. G., Yu, Y., Guo, F., Gomez-Sanchez, C. E., Hay, M., et al. (2011). Central interactions of aldosterone and angiotensin II in aldosterone- and angiotensin II-induced hypertension. *Am. J. Physiol. Heart Circ. Physiol.* 300, H555–H564. doi: 10.1152/ajpheart.00847.2010

Xue, B., Thunhorst, R. L., Yu, Y., Guo, F., Beltz, T. G., Felder, R. B., et al. (2016a). Central renin-angiotensin system activation and inflammation induced by high-fat diet sensitize angiotensin ii-elicited hypertension. *Hypertension* 67, 163–170. doi: 10.1161/HYPERTENSIONAHA.115.06263

Xue, B., Yu, Y., Zhang, Z., Guo, F., Beltz, T. G., Thunhorst, R. L., et al. (2016b). Leptin mediates high-fat diet sensitization of angiotensin ii-elicited hypertension by upregulating the brain renin-angiotensin system and inflammation. *Hypertension* 67, 970–976. doi: 10.1161/HYPERTENSIONAHA.115.06736

Xue, B., Zhang, Y., and Johnson, A. K. (2020b). Interactions of the brain renin-angiotensin-system (ras) and inflammation in the sensitization of hypertension. *Front. Neurosci.* 14:650. doi: 10.3389/fnins.2020.00650

Xue, B., Xue, J., Yu, Y., Wei, S. G., Beltz, T. G., Felder, R. B., et al. (2020a). Predator scent-induced sensitization of hypertension and anxiety-like behaviors. *Cell. Mol. Neurobiol.* [Epub ahead of print]. doi: 10.1007/s10571-020-01005-y

Xue, B., Yu, Y., Wei, S. G., Beltz, T. G., Guo, F., Felder, R. B., et al. (2019). Stress-induced sensitization of angiotensin ii hypertension is reversed by blockade of angiotensin-converting enzyme or tumor necrosis factor-alpha. *Am. J. Hypertens.* 32, 909–917. doi: 10.1093/ajh/hpz075

Xue, B., Zhang, Z., Beltz, T. G., Guo, F., Hay, M., and Johnson, A. K. (2014). Estrogen regulation of the brain renin-angiotensin system in protection against angiotensin II-induced sensitization of hypertension. *Am. J. Physiol. Heart Circ. Physiol.* 307, H191–H198. doi: 10.1152/ajpheart.01012.2013

Xue, B., Zhang, Z., Johnson, R. F., and Johnson, A. K. (2012). Sensitization of slow pressor angiotensin II (Ang II)-initiated hypertension: induction of sensitization by prior ang II treatment. *Hypertension* 59, 459–466. doi: 10.1161/HYPERTENSIONAHA.111.185116

Yang, T. Y., and Liang, N. C. (2018). Ovarian hormones mediate running-induced changes in high fat diet choice patterns in female rats. *Horm. Behav.* 100, 81–93. doi: 10.1016/j.yhbeh.2018.02.010

Young, C. N., and Davisson, R. L. (2015). Angiotensin-II, the brain, and hypertension: an update. *Hypertension* 66, 920–926. doi: 10.1161/HYPERTENSIONAHA.115.03624

Zheng, H., Sharma, N. M., Liu, X., and Patel, K. P. (2012). Exercise training normalizes enhanced sympathetic activation from the paraventricular nucleus in chronic heart failure: role of angiotensin II. *Am. J. Physiol. Regul. Integr. Comp. Physiol.* 303, R387–R394. doi: 10.1152/ajpregu.00046.2012

Zucker, I. H., and Musch, T. I. (2018). Benefits of exercise training on cardiovascular dysfunction: molecular and integrative. *Am. J. Physiol. Heart Circ. Physiol.* 315, H1027–H1031. doi: 10.1152/ajpheart.00516.2018

Zucker, I. H., Schultz, H. D., Patel, K. P., and Wang, H. (2015). Modulation of angiotensin II signaling following exercise training in heart failure. *Am. J. Physiol. Heart Circ. Physiol.* 308, H781–H791. doi: 10.1152/ajpheart.00026.2015

Conflict of Interest: The authors declare that the research was conducted in the absence of any commercial or financial relationships that could be construed as a potential conflict of interest.

Publisher's Note: All claims expressed in this article are solely those of the authors and do not necessarily represent those of their affiliated organizations, or those of the publisher, the editors and the reviewers. Any product that may be evaluated in this article, or claim that may be made by its manufacturer, is not guaranteed or endorsed by the publisher.

frontiers in Neuroscience

ORIGINAL RESEARCH
published: 17 March 2022
doi: 10.3389/fnins.2022.863662

Sympathetic Pathways Target Cholinergic Neurons in the Human Colonic Myenteric Plexus

*Dominic R. Parker[1,2], Lukasz Wiklendt[1], Adam Humenick[1], Bao Nan Chen[1], Tiong Cheng Sia[2], David A. Wattchow[1,2], Phil G. Dinning[1] and Simon J. H. Brookes[1]**

[1] Laboratory of Neurogastroenterology, College of Medicine and Public Health, Flinders University, Adelaide, SA, Australia, [2] Colorectal Surgical Unit, Division of Surgery, Flinders Medical Centre, Bedford Park, SA, Australia

Background: The sympathetic nervous system inhibits human colonic motility largely by effects on enteric neurons. Noradrenergic axons, which branch extensively in the myenteric plexus, are integral to this modulatory role, but whether they contact specific types of enteric neurons is unknown. The purpose of this study was to determine the association of noradrenergic varicosities with types of enteric neurons.

Methods: Human colonic tissue from seven patients was fixed and dissected prior to multi-layer immunohistochemistry for human RNA binding proteins C and D (HuC/D) (pan-neuronal cell body labelling), tyrosine hydroxylase (TH, catecholaminergic labelling), Enkephalin (ENK), choline acetyltransferase (ChAT, cholinergic labelling) and/or nitric oxide synthase (NOS, nitrergic labelling) and imaged using confocal microscopy. TH-immunoreactive varicose nerve endings and myenteric cell bodies were reconstructed as three dimensional digital images. Data was exported to a purpose-built software package which quantified the density of varicosities close to the surface of each myenteric cell body.

Results: TH-immunoreactive varicosities had a greater mean density within 1 μm of the surface of ChAT +/NOS− nerve cell bodies compared with ChAT−/NOS + cell bodies. Similarly, ENK-immunoreactive varicosities also had a greater mean density close to ChAT +/NOS− cell bodies compared with ChAT−/NOS + cells.

Conclusion: A method for quantifying close associations between varicosities and nerve cell bodies was developed. Sympathetic axons in the myenteric plexus preferentially target cholinergic excitatory cells compared to nitrergic neurons (which are largely inhibitory). This connectivity is likely to be involved in inhibitory modulation of human colonic motility by the sympathetic nervous system.

Keywords: enteric nervous system, myenteric plexus, sympathetic nervous system, colon, human, gastrointestinal motility

OPEN ACCESS

Edited by:
Jan D. Huizinga, McMaster University, Canada

Reviewed by:
Winfried Neuhuber, University of Erlangen Nuremberg, Germany
Peter Neckel, University of Tübingen, Germany

***Correspondence:**
Simon J. H. Brookes
simon.brookes@flinders.edu.au

Specialty section:
This article was submitted to Autonomic Neuroscience, a section of the journal Frontiers in Neuroscience

Received: *27 January 2022*
Accepted: *21 February 2022*
Published: *17 March 2022*

Citation:
Parker DR, Wiklendt L, Humenick A, Chen BN, Sia TC, Wattchow DA, Dinning PG and Brookes SJH (2022) Sympathetic Pathways Target Cholinergic Neurons in the Human Colonic Myenteric Plexus. Front. Neurosci. 16:863662. doi: 10.3389/fnins.2022.863662

INTRODUCTION

The sympathetic nervous system modulates the functions of the gastrointestinal tract (GIT) (Lomax et al., 2010). In addition to causing vasoconstriction and reduced secretomotor function, sympathetic activity inhibits gut motility. Post-ganglionic sympathetic neurons to the GIT are noradrenergic, with cell bodies in the prevertebral and paravertebral ganglia, which project through the extrinsic mesenteric nerves to enter the intestinal wall (Wood, 1999).

In animal and humans, sympathetic activity inhibits motility by two mechanisms. Sphincteric smooth muscle receives a direct noradrenergic innervation and contracts in response to sympathetic activation, slowing the progression of content through the GIT (Costa and Gabella, 1971; Gillespie and Maxwell, 1971). In contrast, sympathetic axons are generally sparse in non-sphincteric smooth muscle. The myenteric plexus is also a major target of sympathetic axons (Norberg, 1964; Jacobowitz, 1965). Functional studies demonstrated that noradrenergic nerve activity inhibits the release of acetylcholine from enteric nerve terminals (Kewenter, 1965; Jansson and Martinson, 1966; Beani et al., 1969; Hulten, 1969; Jansson et al., 1969; Del Tacca et al., 1970) *via* presynaptic inhibition (Nishi and North, 1973; Hirst and McKirdy, 1974) mediated primarily by alpha 2a adrenergic receptors (Drew, 1978; Stebbing et al., 2001; Scheibner et al., 2002). However, noradrenaline and agonists also cause membrane hyperpolarisation of some myenteric neurons (Galligan and North, 1991) which may contribute to rare inhibitory post-synaptic potentials recorded in myenteric neurons.

The association between noradrenergic terminals (axon varicosities) and intrinsic cells of the myenteric ganglia remains poorly characterised. Using electron microscopy, several studies have reported synaptic contacts between sympathetic endings and myenteric nerve cell bodies (Manber and Gershon, 1979; Gershon and Sherman, 1982, 1987; Llewellyn-Smith et al., 1984).

The specific details of these connections may be important in helping us to understand the causes of functional colonic disorders in humans. For instance, post-operative ileus, the temporary cessation of GIT motility following surgery, has a significant sympathetic component (Behm and Stollman, 2003; Bauer and Boeckxstaens, 2004; Wattchow et al., 2020). Slow transit constipation is a debilitating disorder with a largely unknown aetiology, however, extrinsic sympathetic inputs running in the extrinsic nerves have been implicated (Dinning et al., 2016). Gaining insight into the specific types of myenteric neurons targetted by varicose neurotransmitter released from sympathetic axons is therefore of clinical relevance.

In this study our aim was to determine if noradrenergic (post-ganglionic sympathetic) nerve terminals target specific neurons in the myenteric plexus of the human colon and compare this to enkephalin-immunoreactive axons which arise primarily from enteric ascending interneuronal pathways and thus provide a comparison group from a different source (Brookes et al., 2020; Humenick et al., 2020).

MATERIALS AND METHODS

Colonic Tissue Collection

Specimens from eight patients were collected for this study. Due to high background labelling, one of these was discarded. For the seven specimens analysed, the median age was 66 years (range 37–90), five patients were female, and there were two specimens for each of the ascending, transverse and descending colon, with one specimen from the sigmoid colon.

Human colonic tissue was acquired from the patients undergoing surgical colonic resection for cancer. Ethics approval for this project was obtained from the Southern Adelaide Clinical Human Research Ethics Committee, approval number 207.17. All patients had the process of tissue donation explained to them and signed a written consent form, and all specimens were de-identified. Only non-cancerous regions were examined.

Colonic Tissue Collection and Preparation

At the time of resection, a 2 cm ring of tissue was cut from the uninvolved healthy margin of the colonic specimen. The colonic tissue was transported in oxygenated Krebs solution (pH; 7.4, NaCl; 118 mM, KCl; 4.8 mM, $CaCl_2$; 2.5 mM, $MgSO_4$; 1.2 mM, $NaHCO_3$; 25 mM, NaH_2PO_4; 1.0 mM, glucose; 11 mM, bubbled with 95% O_2 and 5% CO_2) from the operating theatre to a laboratory in the same building. The colonic tissue was pinned out in a Sylgard-lined petri dish (Dow Corning, Midland, MI, United States) under a dissecting microscope. Oxygenated Krebs solution was regularly changed. The mucosa, submucosa and some of the serosa were removed by microdissection. The tissue was then stretched maximally in both longitudinal and circular axes and fixed with 4% paraformaldehyde (pH 7.2, 4% paraformaldehyde in 0.1 M phosphate buffer) overnight at 4°C. It was then further fixed in 4% paraformaldehyde on an orbital mixer at room temperature, for a total of 24 h, thus ensuring penetration of the fixative. Subsequently the tissue was further dissected in 1× phosphate buffered saline (PBS) to remove most of the circular muscle and any remaining submucosa and serosa. This produced a wholemount of longitudinal muscle and myenteric plexus, from which a 10 mm × 15 mm specimen was cut from a region between the taenia coli.

Multiple Layer Immunohistochemistry, Confocal Microscopy, and Antibody Elution

Antisera to human RNA binding proteins C and D (HuC/D), a pan-neuronal marker, tyrosine hydroxylase (TH), an enzyme integral to catecholamine biosynthesis and leu-Enkephalin (ENK), a neuropeptide expressed by some classes of enteric neurons were applied to specimens for 2–4 days at room temperature. The primary and secondary antibodies used are shown in **Table 1**. The HuC/D antibody was incubated with a biotinylated secondary antibody for a 6-h period, followed by Streptavidin AMCA (aminomethylcoumarin) overnight, producing intense blue immunofluorescence. The tissue preparations were mounted in 100% buffered glycerol on a glass slide and cover-slipped.

A confocal microscope (Zeiss LSM880) was used to image 6–7 individual ganglia from each preparation. Ganglia with good quality immunohistochemistry, low background noise, consistent labelling by antisera, with few artefacts and without damage were chosen. Images were captured with 20× magnification and other parameters (exposure times) were kept uniform throughout. Each ganglion was imaged using the Z-stack function with 1 μm "Z-steps" between individual

TABLE 1 | First and second layers of immunohistochemistry, primary and secondary antibodies.

	Species	Manufacturer	Ref number	Concentration used	Duration
First layer, primary antibodies					
HuC/D	Mouse	Molecular probes	1986151	1:200	3 days
Leu-ENK	Rabbit	ImmunoStar	20066	1:1,000	3 days
TH	Sheep	Millipore	AB1542	1:1,000	3 days
First layer, secondary antibodies					
Biotin	Donkey anti-mouse	Jackson	62976	1:100	6 h
Streptavidin AMCA		Jackson	54773	1:100	Overnight (16–18 h)
AF488	Donkey anti-rabbit	Invitrogen	Ref A21206Lot 1480470	1:1,000	Overnight (16–18 h)
CY5	Donkey anti-sheep	Jackson	87481	1:200	Overnight (16–18 h)
Second layer, primary antibodies					
ChAT	Rabbit	Schemann	P3YEB	1:1,000	3 days
NOS	Sheep	Emson	K205	1:5,000	3 days
Second layer, secondary antibodies					
CY3	Donkey anti-rabbit	Jackson	711-165-152	1:200	Overnight (16–18 h)
AF488	Donkey anti-sheep	Jackson	713-545-147	1:1,000	Overnight (16–18 h)

Leu-ENK, Leu-Enkephalin; TH, Tyrosine Hydroxylase; AMCA, aminomethylcoumarin; AF488, Alexa Fluor 488; CY5, cyanine dye 5; ChAT, choline acetyltransferase; NOS, nitric oxide synthase; CY3, cyanine dye 3.

slices, care was taken to include all varicosities associated with the HuC/D cell bodies. This produced a 3-dimensional image of each ganglion.

After visualisation, preparations were then treated with 50 mls of 2-mercaptoethanol/SDS buffer (2-ME/SDS) (Gendusa et al., 2014) in a pre-heated waterbath (56°C) and allowed incubate for 1 h with agitation at 60 rpm. Afterward, the colonic tissue was removed and washed in PBS-Tween (Sigma Aldrich, North Ryde, NSW, Australia) three times for 10 min, before being washed in standard 1% PBS. This eluted the primary and secondary antisera, with the exception of the HuC/D labelling. Due to the high-affinity of the biotin-streptavidin bond, staining for HuC/D was not affected by the 2-ME/SDS solution. Specimens were then re-mounted in buffered glycerol, and viewed and photographed using standard exposures on an epi-fluorescence microscope to check that the TH and ENK immunoreactivity had been effectively eluted.

After unmounting, washing with PBS, clearing with 0.5% Triton^{TM} X-100 in PBS overnight and a further wash with PBS, the preparations were immersed in antisera to choline acetyltransferase (ChAT), a marker of cholinergic cell bodies, and nitric oxide synthase (NOS), a marker of nitrergic cell bodies, followed by appropriate secondary antisera (see **Table 1**). Specimens were remounted in 100% buffered glycerol and the same ganglia were imaged on the confocal microscope. This protocol made it possible to identify whether each HuC/D-labelled nerve cell body was immunoreactive for ChAT and/or NOS. An example of confocal images from a single ganglion in the myenteric plexus put through multilayer immunohistochemistry is shown in **Figure 1**.

Imaris 3 Dimensions Reconstruction of Cells and Varicosities

Two ganglia from each preparation were reconstructed in 3D using confocal Z-stack images and were uploaded to the software package Imaris (Bitplane AG, Imaris x64, version 8.4.1). Ganglia were reconstructed individually for HuC/D, TH and ENK immunoreactivity.

HuC/D cell bodies were reconstructed using the "surface" function in Imaris. Each individual cell body was rendered as a surface, then numbered in a micrograph of the ganglion. TH and ENK varicosities were reconstructed using the "spots" function, where each individual varicosity was represented as a single point. Parameters for rendering cell body surfaces and varicosity spots were kept uniform for the two ganglia of each preparation, but were changed between preparations due to variations in staining

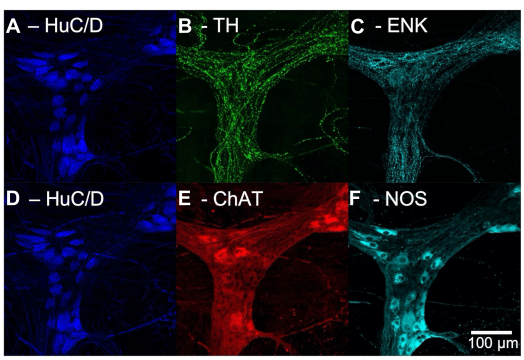

FIGURE 1 | Confocal images of multi-layer immunohistochemistry of a single ganglion in the myenteric plexus of human colon. Panels **(A–C)** show the first layer of immunohistochemistry. **(A)** Human RNA binding proteins C and D (HuC/D), a marker for neuronal cell bodies, shown in blue. **(B)** Tyrosine Hydroxylase (TH) a marker for noradrenergic varicosities, in green. **(C)** Enkephalin (ENK) varicosities, in cyan. Panels **(D–F)** show the second layer of immunohistochemistry. **(D)** HuC/D labelling is retained after elution due to the high affinity Biotin-Streptavidin bond. **(E)** Choline acetyltransferase (ChAT), a marker for cholinergic neurons, shown in red. **(F)** Nitric oxide synthase (NOS), a marker for nitrergic neurons, shown in cyan.

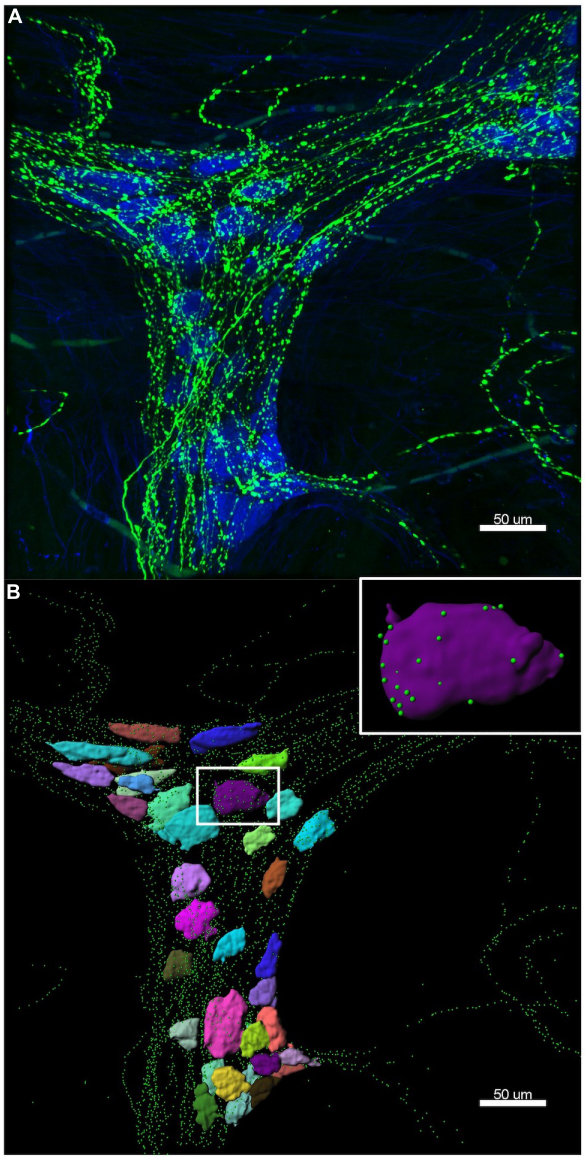

FIGURE 2 | Example of a 3D reconstruction. **(A)** Confocal image of the same ganglion shown in **Figure 1**, with HuC/D cell bodies in blue and tyrosine hydroxylase (TH) varicosities in green. **(B)** The Imaris 3D reconstruction of HuC/D cell bodies is shown as multi-coloured surfaces to demonstrate individual cells, and TH varicosities are rendered as green spots. The colours assigned to the cells have no significance. Inset is a single HuC/D reconstructed cell body, with only the TH varicosities within 1 μm of the cell surface shown. Imaris allows accurate measurement of distances between varicosities and cell body surfaces. Data extracted from these 3D reconstructions was used to calculate the density of TH varicosities close to each myenteric cell body.

intensity. **Figure 2** shows an example of a 3D reconstruction of a myenteric ganglion.

For each numbered cell "surface", data was exported for its position (in coordinates x, y, and z), 3D shape, surface area (μm^2) and volume (μm^3), while the coordinates for each varicosity "spot" were also collected. At this stage, visually defined "baskets" of varicosities surrounding the numbered cell bodies were identified using the raw confocal images.

Identification of Cell Type

Next, each numbered cell was classified, based on ChAT and NOS immunoreactivity in the second layer of immunohistochemical staining (ChAT +/NOS−, ChAT−/NOS +, ChAT +/NOS + or ChAT−/NOS−). Cell "surfaces" were excluded if they were incomplete (e.g., on the edge of the image), or if a single "surface" represented two or more apposed cells which could not be visually separated. It was not possible to classify cells on the basis of enkephalin immunoreactivity (i.e., ENK +/ENK−) because this neuropeptide is not reliably detected in nerve cell bodies without pre-incubation in colchicine (Furness et al., 1983; Brehmer et al., 2005).

Varicosity Density Analysis

A novel analysis algorithm was developed by one of the authors (LW) to measure the density of varicosities close to cell surfaces, using data exported from Imaris. Density measurement requires calculating the number of varicosities within a given space and the volume of that space (μm^3). It is independent of the size of the targetted neuron. The algorithm was programmed to determine the outlines of a 2 μm "shell," incorporating the 3D space from 1 μm inside the cell surface to 1 μm outside the cell surface. Varicosities within this "shell" were counted and divided by the volume of the shell to derive an absolute density. The distance of 1 μm either side of the rendered cell body "surface" was chosen to measure nearby varicosities whose transmitter release is likely to have the largest effect on the cell or its synaptic inputs from other enteric neurons. The inclusion of varicosities up to 1 μm inside the cell accounted for varicosities located within clefts and allowed a margin of error of the rendered cell surface (cell "surface" detail was set to 1 μm). Varicosities were attributed only to the one cell they were closest to, in order to avoid double-counting. This process was carried out for both TH (sympathetic) and ENK (enteric) varicosities.

Statistical Analysis of Varicosity Density

Only ChAT +/NOS−, ChAT−/NOS +, and ChAT +/NOS + cells were analysed and compared. ChAT−/NOS− were excluded as there were too few of these cells for meaningful analysis (Murphy et al., 2007).

To compare the densities of varicosities between the three remaining cell types (ChAT +/NOS−, ChAT−/NOS +, and ChAT +/NOS +), a generalised linear mixed-effects model of a negative-binomial family with log-link was used. A negative-binomial distribution model better accounts for the potential overdispersion of varicosities within the 2 μm thick shell, compared to a Poisson model. The 2 μm-thick shell volume was used as a multiplicative offset for each cell, which allows the regression coefficients to be effectively converted to varicosity densities. The brms R package was used to fit the model (Bürkner, 2017). The formulae below were used:

$$Count \sim cell\_type \times varic\_type + (cell\_type \times varic\_type \mid subj/gang) + offset[log(volume)]$$
$$Shape \sim cell\_type \times varic\_type$$

where Count is an integer variable for the number of varicosities in a cell; cell_type is a categorical variable encoding the cell as one of the three combinations (ChAT +/NOS−, ChAT−/NOS +, or ChAT + /NOS +); varic_type is a categorical variable encoding varicosities for the count as either Enkephalin or TH; volume is a continuous offset equal to the volume of the 2 μm-thick shell surrounding the cell over which the count was taken, which induces units of density in the coefficients for cell_type and varic_type. The random-effect/multi-level variables subj and gang indicate the subject from which the tissue was obtained and the ganglion in which the cell was imaged, so that cells in the same subject and ganglion can share potential random variations in varicosity density. A prior of normal (0, 1) for coefficients, and LKJ(2) for correlations was used. Four chains were sampled, retaining 1,000 samples per chain, following 1,000 warmup samples. Diagnostics did not show any divergences and showed an Rhat close to 1.

To then compare the relative distributions of varicosity density close to cell types, a density ratio was calculated with 95% credible intervals (density of varicosities close to one cell type divided by the density of varicosities close to a different cell type). This method of statistical analysis was used to compare varicosity densities between ChAT +/NOS−, ChAT−/NOS +, and ChAT +/NOS + cells in three combinations:

(i) ChAT +/NOS− vs. ChAT−/NOS +
(ii) ChAT +/NOS− vs. ChAT +/NOS +
(iii) ChAT−/NOS + vs. ChAT +/NOS +

Statistical Analysis of Cell Surface Area and Volume

Cell body surface area and volume were determined by Imaris and then presented as a mean ± standard error of the mean (SEM) for each cell type. A one-way analysis of variance (ANOVA) statistical test followed by Tukey's *post-hoc* test was used to determine a difference in mean surface area and volume between cell types. Statistical analysis was performed using Prism version 8.4.1 for Mac (GraphPad Software, La Jolla, CA, United States). Statistical values <0.05 were considered statistically significant.

Tyrosine Hydroxylase Immunoreactive Nerve Cell Bodies

Tyrosine hydroxylase-immunoreactive cell bodies from all ganglia in all seven preparations were manually counted using the raw confocal images. These were presented as a proportion of the total number of HuC/D cells counted in the imaged ganglia.

RESULTS

A total of 673 HuC/D-immunoreactive cell bodies were reconstructed from 14 ganglia from the seven patients. One hundred eighty-seven reconstructed cells were excluded because they were incomplete (cut-off by the edges of the imaged area), or unable to be separated from neighbouring cells. This left 486 cells for density analysis. As mentioned above, ChAT−/NOS− cell types (33 cells) were excluded from the varicosity density analysis due to their small numbers (Murphy et al., 2007).

Tyrosine Hydroxylase Varicosity Density

The TH varicosity density was greatest close to ChAT +/NOS− cells with a median (of the mean distribution) of 7.43 varicosities per 1,000 μm^3 (190 cells), measured within ± 1 μm of the cell surface. This was followed by ChAT +/NOS + cells (6.02 TH varicosities per 1,000 μm^3, 58 cells) then ChAT−/NOS + cells (5.59 varicosities per 1,000 μm^3, 205 cells). The posterior median of the mean TH varicosity density and distribution of TH varicosities close to cells is shown in **Figure 3**.

Mean densities of TH-immunoreactive varicosities close to cell types differentiated by ChAT and NOS immunoreactivities were compared. There was a significantly greater density of TH varicosities close to ChAT +/NOS− compared with ChAT−/NOS + cells, with a median density ratio of 1.35 (95% credible interval 1.04–1.69, see **Figure 4**). There was a trend toward a greater density of TH varicosities close to ChAT +/NOS− cells vs. ChAT +/NOS + cells.

Enkephalin-Immunoreactive Varicosities

The density of ENK-immunoreactive varicosities around myenteric nerve cell bodies was calculated using the same method. Overall, ENK varicosities had a higher density than TH + varicosities. However, a notable feature of ENK varicosities is that they formed dense baskets around about 10% of myenteric nerve cell bodies; such baskets were very rare for TH varicosities. Disregarding the presence of baskets, the density of ENK varicosities was also greatest close to ChAT +/NOS− cells, with a posterior median of the mean distribution of 19.52 varicosities per 1,000 μm^3, with lower densities for ChAT−/NOS + cells (12.99 varicosities per 1,000 μm^3) and ChAT +/NOS + cells (13.22 varicosities per 1,000 μm^3), see **Figure 5**.

Comparing the different myenteric neuron types, the density of ENK varicosities close to ChAT +/NOS− was greater than vs. ChAT−/NOS + cells, with a median density ratio of 1.51 (95% credible interval 1.23–1.83, see **Figure 6**). The same is true of ChAT +/NOS− vs. ChAT +/NOS + cells, which had a median density ratio of 1.49 (95% credible interval 1.19–1.88). There were no differences between the ChAT−/NOS + cells and the ChAT +/NOS + cells.

Visually Defined Baskets

Of the nerve cells used for density analysis, 10 TH-immunoreactive "baskets" of varicosities were identified and these all surrounded HuC/D-immunoreactive nerve cell bodies (10/486 cells, 2.10%). Of these 10 baskets, all 10 surrounded myenteric neurons which were subsequently shown to be ChAT +/NOS−. There were 61 cells in the 7 specimens that were surrounded by ENK baskets (61/486, 12.6%), of which 53 were ChAT +/NOS− (87%); a highly significant association ($\chi^2 = 75.0$, $df = 3$, $p < 0.01$). There were no ChAT−/NOS +

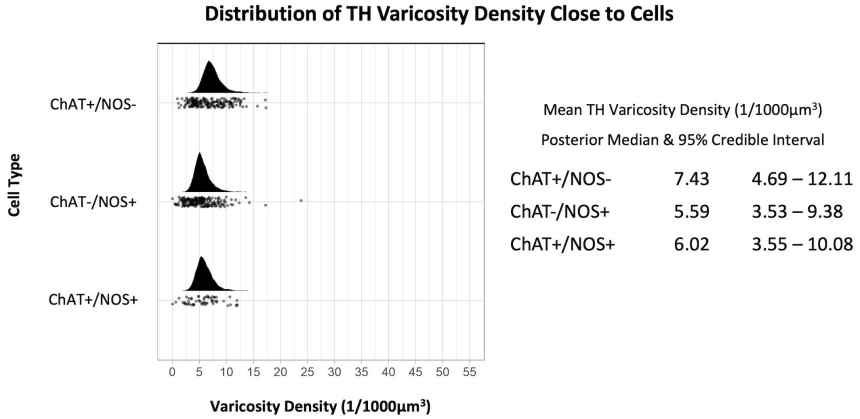

FIGURE 3 | Graph of the distribution of tyrosine hydroxylase varicosities close to cells. The upright curve in each graph is the distribution of the mean density for each cell type. Every small black dot beneath represents the density of TH varicosities close to an individual cell. The posterior median of the mean varicosity density is greatest for the ChAT +/NOS– cell type at 7.43 varicosities per 1,000 μm^3. The posterior median of the mean TH varicosity density for each cell type is presented with the 95% credible intervals on the right. ChAT, choline acetyltransferase; NOS, nitric oxide synthase; TH, tyrosine hydroxylase.

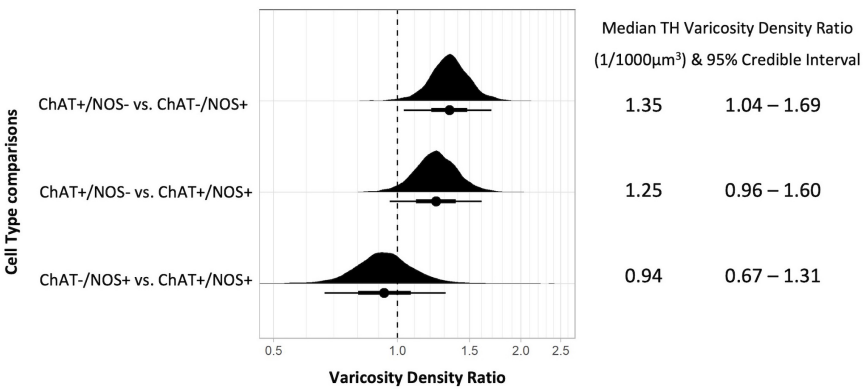

FIGURE 4 | Graph of tyrosine hydroxylase varicosity density ratios comparing cell types. Density ratio is plotted on a logarithmic scale. The filled black curves indicate the ratio between the distributions of the mean of density (mean varicosity density of cell type divided by another). The bars beneath indicate the median (dot), the 66th percentiles and the 95th percentiles of the mean. A ratio of 1.0 indicates that the densities for the two types of cells compared are identical. In this graph, ChAT +/NOS– cells compared to the ChAT–/NOS + cells have a median density ratio of 1.35 and the 95% percentile bar is to the right of 1.0. This shows there is a significantly greater varicosity density close to ChAT +/NOS– cells compared to ChAT–/NOS + cells. The median TH varicosity density ratios are presented with the 95% credible intervals on the right. ChAT, choline acetyltransferase; NOS, nitric oxide synthase; TH, tyrosine hydroxylase.

cells surrounded by ENK + baskets (see **Table 2**). Examples of HuC/D cells with TH and ENK baskets surrounding them are shown in **Figure 7**.

Human RNA Binding Proteins C and D (HuC/D) Cell Characteristics

From the 486 reconstructed myenteric cell bodies, 190 (38%) were ChAT +/NOS−, 205 (42%) were ChAT−/NOS +, 58 (12%) were ChAT +/NOS +, and 33 (8%) were ChAT−/NOS−. HuC/D cell characteristics are presented in **Table 3**.

ChAT +/NOS + cells had the largest surface area and the largest mean cell volume, followed by ChAT +/NOS−, ChAT−/NOS +, and ChAT−/NOS− cells. There was a statistically significant difference in surface area between cell types using a one-way ANOVA test [$F_{(3,8)} = 24.61$, $p < 0.0001$), and using Tukey's *post-hoc* test, ChAT +/NOS + cells were larger than ChAT−/NOS− cells (mean difference 2,261 μm^2, 95% CI 1,243–3,279, $p = 0.001$) and ChAT−/NOS + cells (mean difference 1,572 μm^2, 95% CI 833–2,311, $p = 0.0013$). ChAT +/NOS− cells were larger than ChAT−/NOS− cells (mean difference 1,517 μm^2, 95% CI 618–2,415, $p = 0.0045$).

There was also a statistically significant difference in cell volumes [one-way ANOVA test, $F_{(3,18)} = 47.09$, $p < 0.0001$]. ChAT +/NOS + cells had a larger volume than all other cell types using *post-hoc* analysis: vs. ChAT−/NOS− (mean difference 3,922 μm^3, 95% CI 2,841–5,002, $p < 0.0001$); vs. ChAT−/NOS + (mean difference 2,900 μm^3, 95% CI 2,097–3,704, $p < 0.0001$); vs. ChAT +/NOS− (mean difference 1,512 μm^3, 95% CI

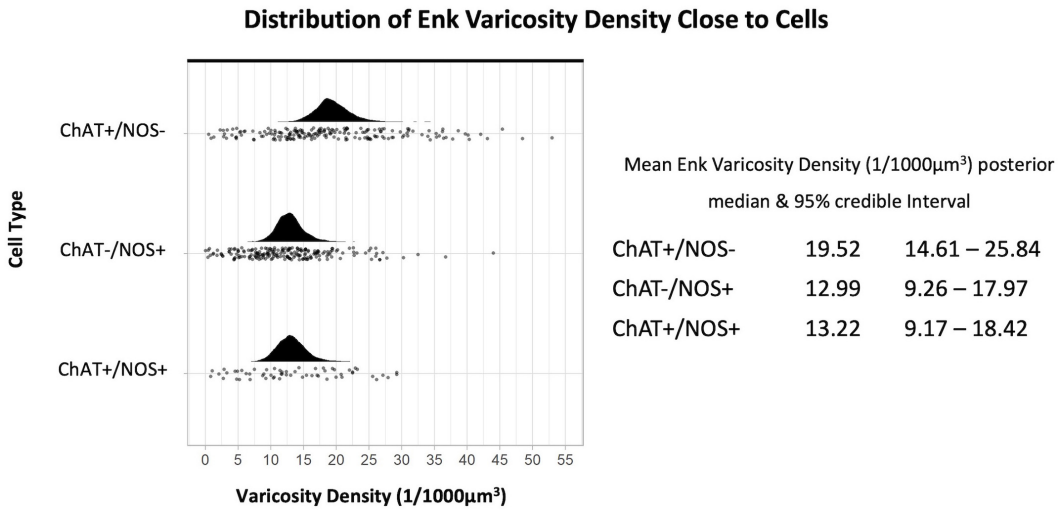

FIGURE 5 | Graph of the distribution of enkephalin varicosities close to cells. The upright curve in each graph is the distribution of the mean density for each cell type. Each small black dot beneath represents the density of ENK varicosities close to an individual cell. The posterior median of the mean varicosity density is greatest for the ChAT +/NOS– cell type, at 19.52 varicosities per 1,000 μm^3. The posterior median of the mean ENK varicosity density for each cell type is presented with the 95% credible intervals on the right. ChAT, choline acetyltransferase; NOS, nitric oxide synthase; ENK, enkephalin.

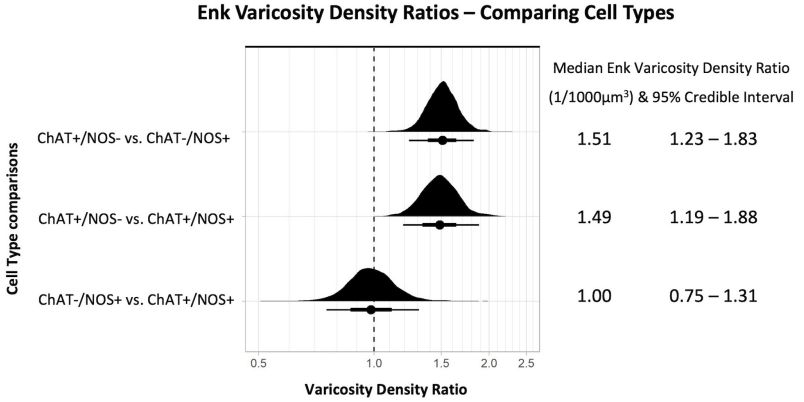

FIGURE 6 | Graph of enkephalin (ENK) varicosity density ratios comparing cell types. Density ratio is on a logarithmic scale. The filled black curves indicate the ratio between the distributions of the mean of density (mean varicosity density of cell type divided by another). The bars beneath indicate the median (dot), the 66th percentiles and the 95th percentiles of the mean. A ratio of 1.0 indicates that the densities for the two types of cells compared are identical. In this graph, ChAT +/NOS– cells compared to the ChAT–/NOS + cells and also compared to the ChAT +/NOS + cells have a median density ratio and 95% percentile bar to the right of 1.0. This shows there is a significantly greater density of ENK varicosities close to ChAT +/NOS– cells compared to both ChAT–/NOS + and ChAT +/NOS + cells. The median ENK varicosity density ratios are presented with the 95% credible intervals on the right. ChAT, choline acetyltransferase; NOS, nitric oxide synthase; ENK, enkephalin.

174–2,850, $p = 0.03$). ChAT +/NOS− cells were larger than ChAT−/NOS− cells (mean difference 2,409 μm^3, 95% CI 1,308–3,511, $p < 0.0011$).

Intrinsic Tyrosine Hydroxylase-Immunoreactive Myenteric Nerve Cell Bodies

Forty-four ganglia from seven patients were included in the analysis of intrinsic TH positive cell bodies. An example of a TH -immunoreactive cell body is shown in **Figure 8**. This analysis did not require 3D reconstruction. Of 2,252 HuC/D cell bodies in 44 ganglia, 22 (1%) were TH positive. After elution of TH and relabelling with NOS and ChAT antisera, 21 of these 22 cell bodies were ChAT +/NOS−, while one was ChAT−/NOS−. None contained NOS immunoreactivity.

DISCUSSION

The sympathetic nervous system has a net inhibitory effect on intestinal motility. Sympathetic axons release noradrenaline, which binds to alpha 2a adrenergic receptors to cause

TABLE 2 | Visually defined TH and ENK baskets surrounding myenteric plexus human RNA binding proteins C and D (HuC/D) cells.

	ChAT +/NOS−	ChAT−/NOS +	ChAT +/NOS +	ChAT−/NOS−	Total
TH Baskets	10 (100%)	0 (0%)	0 (0%)	0 (0%)	10
ENK Baskets	53 (87%)	0 (0%)	5 (8%)	3 (5%)	61

TH, tyrosine hydroxylase; ENK, Enkephalin; ChAT, choline acetyltransferase; NOS, nitric oxide synthase.

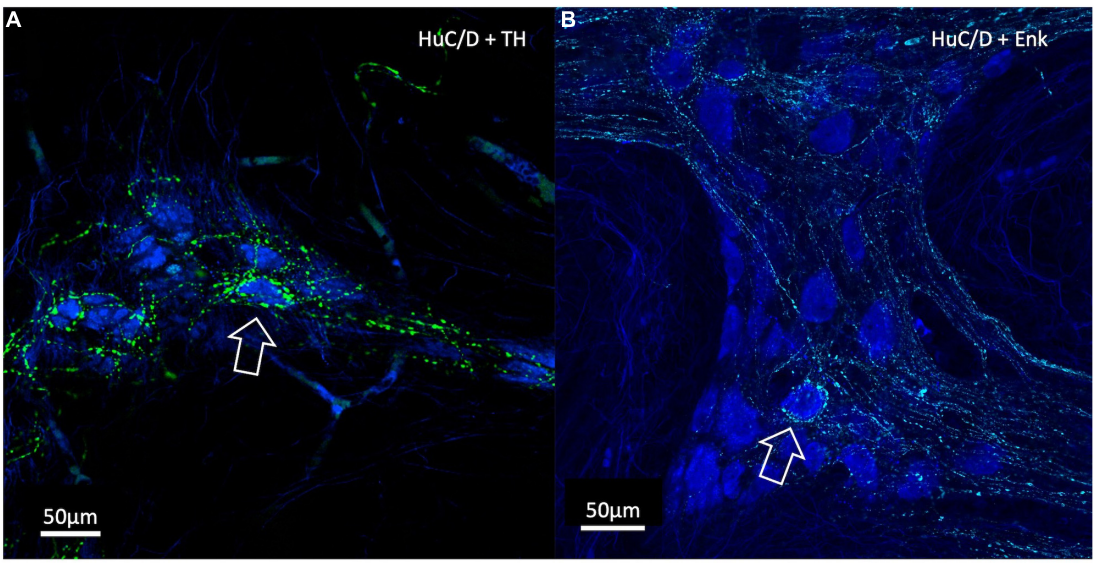

FIGURE 7 | Confocal Images of HuC/D cells with surrounding varicosity baskets. TH varicosities are in green, ENK varicosities are in cyan and HuC/D myenteric cell bodies are in blue. **(A)** A TH-immunoreactive basket of varicosities surrounding an individual HuC/D cell (open arrow). **(B)** An ENK varicosity basket surrounding an individual HuC/D cell (open arrow). In both cases, these myenteric cells were ChAT +. Baskets represent a high density of varicosities with close appositions encircling a myenteric cell body and are likely to indicate targetted neural connectivity. ChAT, Choline Acetyltransferase; NOS, Nitric Oxide Synthase; TH, Tyrosine Hydroxylase; ENK, Enkephalin.

presynaptic inhibition of the release of acetylcholine, thus inhibiting interneuronal pathways and reducing smooth muscle excitation and contraction (Nishi and North, 1973; Hirst and McKirdy, 1974). Theoretically, if noradrenaline also inhibited excitatory cholinergic synaptic drive to inhibitory motor neurons, sympathetic activation could lead to net excitation. Using 3D reconstruction and novel density analysis, our study demonstrated that noradrenergic varicosities have a significantly greater density close to ChAT +/NOS− cells compared to ChAT−/NOS + cells in the myenteric plexus. This arrangement suggests that extrinsic post-ganglionic sympathetic inputs to the myenteric plexus act via cholinergic cell bodies in human colonic myenteric ganglia. It should be noted that myenteric nerve cell bodies may not be the primary target of sympathetic axons. Rather, the adjacent cholinergic synaptic terminals are likely to be a major site of action via presynaptic inhibition (Hirst and McKirdy, 1974). However, enteric neurons generally have very restricted dendritic fields (Dogiel, 1899), so measuring the distance of varicosities to HuC/D immunoreactive nerve cell bodies is likely to be a reasonable approximation of proximity to presynaptic terminals.

Enkephalin varicosities similarly had a greater density close to ChAT +/NOS− cell types compared to nitrergic neurons. Previous studies have shown that ENK-immunoreactive interneurons, which give rise to varicose endings in myenteric ganglia, belong to several populations of cholinergic ascending interneurons (Brookes et al., 2020; Humenick et al., 2020). Baskets indicate "targetted wiring" where there is a concentration of close contacts between varicosities and neuron cell bodies. In our present study, most visually defined ENK baskets surrounded ChAT +/NOS− cells. TH varicosity baskets are much less abundant but also targetted specific cells; all 10 nerve cell

TABLE 3 | HuC/D myenteric cell body proportions, surface area and volume.

Cell type	Number and percentage (mean% ± SEM)	Surface area (μm^2, mean ± SEM)	Volume (μm^3, mean ± SEM)
ChAT +/NOS−	190 38% ± 2.0	3,127 ± 428	4,566 ± 404
ChAT−/NOS +	205 42% ± 2.3	2,299 ± 371	3,177 ± 389
ChAT +/NOS +	58 12% ± 2.1	3,871 ± 494	6,078 ± 391
ChAT−/NOS−	33 8% ± 1.7	1,610 ± 238	2,156 ± 265

SEM, standard error of the mean; ChAT, choline acetyltransferase; NOS, nitric oxide synthase.

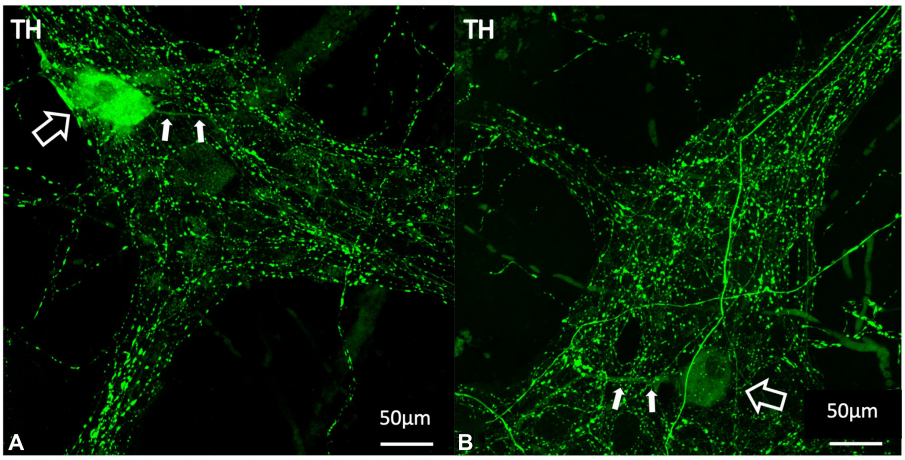

FIGURE 8 | Examples of TH positive myenteric cell bodies **(A,B)**. TH labelling is shown in green. The larger open white arrows show TH immunoreactive cell bodies and the smaller filled arrows demonstrate single long axonal projections from each of these cells, seen in 10 of the 22 identified TH positive cell bodies. TH immunoreactive cell bodies make up 1% of the total population of myenteric cells and are likely to indicate intrinsic catecholaminergic cells in the myenteric plexus, some of which may be dopaminergic in nature. TH, tyrosine hydroxylase.

bodies surrounded by TH baskets were ChAT +/NOS−. The 3D reconstruction and density analysis provides a quantifiable method of demonstrating targetted connectivity onto enteric neurons for both identifiable baskets and the distribution of varicosities that were not part of baskets.

Relative proportions of cell types defined by ChAT and NOS immunoreactivities in our study are similar to those reported previously in human colon (Murphy et al., 2007; Wattchow et al., 2008; Beck et al., 2009; Ng et al., 2018). The four cell types differed in both cell body surface area and volume. This suggests they are distinct and may form different functional types. HuC/D labelling is a pan-neuronal marker in the ENS, and the vast majority HuC/D cells are immunoreactive for either ChAT and/or NOS (Murphy et al., 2007). ChAT +/NOS− cells are likely to represent several different functional types of neurons in the myenteric plexus, including excitatory motor neurons to the longitudinal and circular muscle, ascending interneurons, some descending interneurons, primary afferent neurons, some vasomotor neurons and some secretomotor neurons (Porter et al., 2002; Murphy et al., 2007). Based on the results of our study, noradrenergic inputs innervate one or several of these functional cell types in a targetted manner.

Electron microscopy is considered the gold standard in identifying synaptic connections morphologically. Previous research using both electron microscopy and light microscopy has shown that varicosities arranged in dense pericellular baskets often form synaptic connections onto the encircled cell bodies (Pompolo and Furness, 1995). In a study by Mann et al. (1997) numerous direct appositions between varicosities and neurons identified by confocal microscopy, corresponded to numerous synaptic connections confirmed by electron microscopy. In our study, reconstructed varicosities at a distance of 1 µm from the reconstructed HuC/D cell body surface (within or outside the reconstructed surface) were counted as close appositions. Therefore, it is possible that the targetted innervation of ChAT +/NOS− neurons by noradrenergic varicosities may be synaptic in nature, however, this cannot be definitively concluded from our study without directly observing ultrastructural features of synapses by electron microscopy. Llewellyn-Smith et al. (1984) previously demonstrated ultrastructural synapses using electron microscopy between noradrenergic neurons and unspecified myenteric neurons in human small intestine, and several animal studies have also identified noradrenergic synaptic connections in the myenteric plexus of the GIT (Manber and Gershon, 1979; Gershon and Sherman, 1982, 1987; Hayakawa et al., 2008). Additionally, volume transmission *via* the diffuse release of noradrenaline within a ganglion to act on distant cells which express appropriate receptors, cannot be ruled out (Vanhatalo and Soinila, 1998).

The novel method in our study, including 3D reconstruction and density analysis has several benefits. Reconstruction of TH-immunoreactive varicosities and myenteric cell bodies from confocal images enabled precise measurement of distances between the two objects in 3 dimensions. Importantly, the reconstruction of varicosities and myenteric cell bodies was done only with reference to the first layer of immunohistochemistry, i.e., TH, ENK, and HuC/D immunoreactivity. Thus the investigator was blinded to the cell type defined by ChAT and NOS antisera, which were applied in the second layer. Density of varicosities in a shell volume within ± 1 µm of the cell surface was chosen as this value is independent of the size of cells. The surface areas and volumes of ChAT and NOS–immunoreactive neurons differed; close packing within the ganglia would predict larger absolute numbers of varicosities close to larger cells; density measurement avoids this.

It should be noted that our study contained specimens from only seven patients. All ganglia studied were from the myenteric plexus between the taenia. It has

been shown that the plexus is denser under the taenia than between taenia and we cannot exclude that there may be differences at the cellular level too (Hanani et al., 2012). During the 3D-reconstruction process, many reconstructed cells had to be removed because the rendering was imperfect, or because they lay partially outside the boundaries of the image. Some cells had to be cut to separate them from a closely apposed cell. In addition, the images had lower resolution in the *z*-axis than in *x* and *y*-axes. In theory this could increase errors for points located above cell surfaces, although it appears unlikely that this could explain the differences between NOS + and ChAT + cells. The tissue was all maximally stretched in both axes prior to fixation and it is possible that this affected the absolute distances of varicosities from cell surfaces due to distortion of the ganglia (Gabella and Trigg, 1984). In addition, distances were measured at the moment of fixation; we cannot rule out the possibility that varicosities may be capable of some movement over time. In addition, we have assumed that a higher density of varicosities close to a nerve cell body will, on average, have a larger effect than a lower density of varicosities. No attempt was made to quantify this or to assess the tortuosity of diffusion pathways within myenteric ganglia. Lastly, it is possible that some of the TH varicosities may arise from the rare intrinsic TH-immunoreactive myenteric nerve cell bodies. However, only 1% of myenteric neurons were found to be TH positive, therefore it is likely that intrinsic catecholaminergic varicosities made up a very minor contribution to the total number of TH varicosities. Some intrinsic TH-immunoreactive cell bodies are likely to be dopaminergic and may play a role in modulating gastrointestinal motility (Wakabayashi et al., 1989; Anlauf et al., 2003). In our study we found these intrinsic catecholaminergic cells almost exclusively belonged to the ChAT +/NOS− type.

In this research we have verified a novel method for quantifying the density of innervation of neurons by different types of varicose nerve terminals. Our findings suggest that post-ganglionic sympathetic (noradrenergic) inputs preferentially target a subset of cholinergic neurons in the human colon myenteric plexus, and are likely to cause presynaptic inhibition to those cells involved in excitatory pathways. The connectivity demonstrated here may represent an important pathway in the modulation of colonic motility by the sympathetic nervous system.

DATA AVAILABILITY STATEMENT

The datasets presented in this study can be found in online repositories. The names of the repository/repositories and accession number(s) can be found below: Pennsieve, University of Pennsylvania: SPARC Consortium, Accession Number 1509, DOI: 10.26275/aqri-vyb4.

ETHICS STATEMENT

The studies involving human participants were reviewed and approved by the Southern Adelaide Clinical Human Research Ethics Committee, Approval number 207.17. The patients/participants provided their written informed consent to participate in this study.

AUTHOR CONTRIBUTIONS

DP conducted the research as the lead and wrote the manuscript. DP, SB, PD, and DW developed the study concept and design. LW developed the software and statistical methods to analysed data. AH and BC contributed to the laboratory experiments. DP, SB, PD, DW, LW, AH, BC, and TS reviewed the final manuscript and images. All authors contributed to the article and approved the submitted version.

FUNDING

Funding was provided in part by a grant from the National Institute of Health (NIH) Stimulating Peripheral Activity to Relieve Conditions (SPARC) initiative (OT2OD24899 "Comprehensive Structural and Functional Mapping of Mammalian Colonic Nervous System" to Y. Tache, UCLA).

ACKNOWLEDGMENTS

The authors would like to acknowledge the Flinders Medical Centre Colorectal Unit for assistance in providing human colonic tissue.

REFERENCES

Anlauf, M., Schafer, M. K., Eiden, L., and Weihe, E. (2003). Chemical coding of the human gastrointestinal nervous system: cholinergic, VIPergic, and catecholaminergic phenotypes. *J. Comp. Neurol.* 459, 90–111. doi: 10.1002/cne.10599

Bauer, A. J., and Boeckxstaens, G. E. (2004). Mechanisms of postoperative ileus. *Neurogastroenterol. Motil.* 16, 54–60. doi: 10.1111/j.1743-3150.2004.00558.x

Beani, L., Bianchi, C., and Crema, A. (1969). The effect of catecholamines and sympathetic stimulation on the release of acetylcholine from the guinea-pig colon. *Br. J. Pharmacol.* 36, 1–17. doi: 10.1111/j.1476-5381.1969.tb08298.x

Beck, M., Schlabrakowski, A., Schrodl, F., Neuhuber, W., and Brehmer, A. (2009). ChAT and NOS in human myenteric neurons: co-existence and co-absence. *Cell Tissue Res.* 338, 37–51. doi: 10.1007/s00441-009-0852-4

Behm, B., and Stollman, N. (2003). Postoperative ileus: etiologies and interventions. *Clin. Gastroenterol. Hepatol.* 1, 71–80. doi: 10.1053/cgh.2003.50012

Brehmer, A., Lindig, T. M., Schrodl, F., Neuhuber, W., Ditterich, D., Rexer, M., et al. (2005). Morphology of enkephalin-immunoreactive myenteric neurons in the human gut. *Histochem. Cell Biol.* 123, 131–138. doi: 10.1007/s00418-005-0757-6

Brookes, S. J., Humenick, A., Chen, B. N., Dinning, P. G., Costa, M., and Wattchow, D. (2020). Multiplexed Immunohistochemistry to Identify Systematically Classes of Human Colonic Myenteric Neurons. *FASEB J.* 34:1. doi: 10.1096/fasebj.2020.34.s1.09525

Bürkner, P.-C. (2017). brms: an R Package for Bayesian Multilevel Models Using Stan. *2017. J. Stat. Softw.* 80, 1–28. doi: 10.18637/jss.v080.i01

Costa, M., and Gabella, G. (1971). Adrenergic innervation of the alimentary canal. *Z Zellforsch. Mikrosk. Anat.* 122, 357–377. doi: 10.1007/BF00935995

Del Tacca, M., Soldani, G., Selli, M., and Crema, A. (1970). Action of catecholamines on release of acetylcholine from human taenia coli. *Eur. J. Pharmacol.* 9, 80–84. doi: 10.1016/0014-2999(70)90323-7

Dinning, P. G., Sia, T. C., Kumar, R., Mohd Rosli, R., Kyloh, M., Wattchow, D. A., et al. (2016). High-resolution colonic motility recordings in vivo compared with ex vivo recordings after colectomy, in patients with slow transit constipation. *Neurogastroenterol. Motil.* 28, 1824–1835. doi: 10.1111/nmo.12884

Dogiel, A. S. (1899). Über den Bau der Ganglien in den Geflechten des Darmes und der Gallenblase des Menschen und der Säugetiere. *Arch. Anat. Physiol. Leipzig Anat. Abt Jg* 1899, 130–158.

Drew, G. M. (1978). Pharmacological characterization of the presynaptic alpha-adrenoceptors regulating cholinergic activity in the guinea-pig ileum. *Br. J. Pharmacol.* 64, 293–300. doi: 10.1111/j.1476-5381.1978.tb17303.x

Furness, J. B., Costa, M., and Miller, R. J. (1983). Distribution and projections of nerves with enkephalin-like immunoreactivity in the guinea-pig small intestine. *Neurosci.* 8, 653–664. doi: 10.1016/0306-4522(83)90001-5

Gabella, G., and Trigg, P. (1984). Size of neurons and glial cells in the enteric ganglia of mice, guinea-pigs, rabbits and sheep. *J. Neurocytol.* 13, 49–71. doi: 10.1007/BF01148318

Galligan, J. J., and North, R. A. (1991). Opioid, 5-HT1A and alpha 2 receptors localized to subsets of guinea-pig myenteric neurons. *J. Auton. Nerv. Syst.* 32, 1–11. doi: 10.1016/0165-1838(91)90229-v

Gendusa, R., Scalia, C. R., Buscone, S., and Cattoretti, G. (2014). Elution of High-affinity (>10-9 KD) Antibodies from Tissue Sections: clues to the Molecular Mechanism and Use in Sequential Immunostaining. *J. Histochem. Cytochem.* 62, 519–531. doi: 10.1369/0022155414536732

Gershon, M. D., and Sherman, D. L. (1982). Identification of and interactions between noradrenergic and serotonergic neurites in the myenteric plexus. *J. Comp. Neurol.* 204, 407–421. doi: 10.1002/cne.902040411

Gershon, M. D., and Sherman, D. L. (1987). Noradrenergic innervation of serotoninergic neurons in the myenteric plexus. *J. Comp. Neurol.* 259, 193–210. doi: 10.1002/cne.902590203

Gillespie, J. S., and Maxwell, J. D. (1971). Adrenergic innervation of sphincteric and nonsphincteric smooth muscle in the rat intestine. *J. Histochem. Cytochem.* 19, 676–681. doi: 10.1177/19.11.676

Hanani, M., Grossman, S., Nissan, A., and Eid, A. (2012). Morphological and quantitative study of the myenteric plexus in the human tenia coli. *Anat. Rec.* 295, 1321–1326. doi: 10.1002/ar.22511

Hayakawa, T., Kuwahara, S., Maeda, S., Tanaka, K., and Seki, M. (2008). Fine structural survey of tyrosine hydroxylase immunoreactive terminals in the myenteric ganglion of the rat duodenum. *J. Chem. Neuroanat.* 36, 191–196. doi: 10.1016/j.jchemneu.2008.04.005

Hirst, G. D., and McKirdy, H. C. (1974). Presynaptic inhibition at mammalian peripheral synapse? *Nature* 250, 430–431.

Hulten, L. (1969). Extrinsic nervous control of colonic motility and blood flow. *Acta Physiol. Scand. Suppl.* 335, 1–116.

Humenick, A., Chen, B. N., Wattchow, D. A., Zagorodnyuk, V. P., Dinning, P. G., Spencer, N. J., et al. (2020). Characterization of putative interneurons in the myenteric plexus of human colon. *Neurogastroenterol. Motil.* 33:e13964. doi: 10.1111/nmo.13964

Jacobowitz, D. (1965). Histochemical studies of the autonomic innervation of the gut. *J. Pharmacol. Exp. Ther.* 149, 358–364.

Jansson, G., Lisander, B., and Martinson, J. (1969). Hypothalamic control of adrenergic outflow to the stomach in the cat. *Acta Physiol. Scand.* 75, 176–186. doi: 10.1111/j.1748-1716.1969.tb04370.x

Jansson, G., and Martinson, J. (1966). Studies on the Ganglionic Site of Action of Sympathetic Outflow to the Stomach. *Acta Physiol. Scand.* 68, 184–192.

Kewenter, J. (1965). The vagal control of the jejunal and ileal motility and blood flow. *Acta Physiol. Scand.* 257, 1–68.

Llewellyn-Smith, I. J., Furness, J. B., O'Brien, P. E., and Costa, M. (1984). Noradrenergic nerves in human small intestine. *Distr. Ultrastruct. Gastroenterol.* 87, 513–529.

Lomax, A. E., Sharkey, K. A., and Furness, J. B. (2010). The participation of the sympathetic innervation of the gastrointestinal tract in disease states. *Neurogastroenterol. Motil.* 22, 7–18. doi: 10.1111/j.1365-2982.2009.01381.x

Manber, L., and Gershon, M. D. (1979). A reciprocal adrenergic-cholinergic axoaxonic synapse in the mammalian gut. *Am. J. Physiol.* 236, E738–E745. doi: 10.1152/ajpendo.1979.236.6.E738

Mann, P. T., Southwell, B. R., Young, H. M., and Furness, J. B. (1997). Appositions made by axons of descending interneurons in the guinea-pig small intestine, investigated by confocal microscopy. *J. Chem. Neuroanat.* 12, 151–164. doi: 10.1016/s0891-0618(96)00189-5

Murphy, E. M., Defontgalland, D., Costa, M., Brookes, S. J., and Wattchow, D. A. (2007). Quantification of subclasses of human colonic myenteric neurons by immunoreactivity to Hu, choline acetyltransferase and nitric oxide synthase. *Neurogastroenterol. Motil.* 19, 126–134. doi: 10.1111/j.1365-2982.2006.00843.x

Ng, K. S., Montes-Adrian, N. A., Mahns, D. A., and Gladman, M. A. (2018). Quantification and neurochemical coding of the myenteric plexus in humans: no regional variation between the distal colon and rectum. *Neurogastroenterol. Motil.* 30:e13193. doi: 10.1111/nmo.13193

Nishi, S., and North, R. A. (1973). Presynaptic action of noradrenaline in the myenteric plexus. *J. Physiol.* 231, 29–30.

Norberg, K. A. (1964). Adrenergic Innervation of the Intestinal Wall Studied by Fluorescence Microscopy. *Int. J. Neuropharmacol.* 3, 379–382. doi: 10.1016/0028-3908(64)90067-x

Pompolo, S., and Furness, J. B. (1995). Sources of inputs to longitudinal muscle motor neurons and ascending interneurons in the guinea-pig small intestine. *Cell Tissue Res.* 280, 549–560. doi: 10.1007/BF00318359

Porter, A. J., Wattchow, D. A., Brookes, S. J., and Costa, M. (2002). Cholinergic and nitrergic interneurones in the myenteric plexus of the human colon. *Gut* 51, 70–75. doi: 10.1136/gut.51.1.70

Scheibner, J., Trendelenburg, A. U., Hein, L., Starke, K., and Blandizzi, C. (2002). Alpha 2-adrenoceptors in the enteric nervous system: a study in alpha 2A-adrenoceptor-deficient mice. *Br. J. Pharmacol.* 135, 697–704. doi: 10.1038/sj.bjp.0704512

Stebbing, M., Johnson, P., Vremec, M., and Bornstein, J. (2001). Role of alpha(2)-adrenoceptors in the sympathetic inhibition of motility reflexes of guinea-pig ileum. *J. Physiol.* 534, 465–478. doi: 10.1111/j.1469-7793.2001.00465.x

Vanhatalo, S., and Soinila, S. (1998). The concept of chemical neurotransmission–variations on the theme. *Ann. Med.* 30, 151–158. doi: 10.3109/07853899808999398

Wakabayashi, K., Takahashi, H., Ohama, E., and Ikuta, F. (1989). Tyrosine hydroxylase-immunoreactive intrinsic neurons in the Auerbach's and Meissner's plexuses of humans. *Neurosci. Lett.* 96, 259–263. doi: 10.1016/0304-3940(89)90388-1

Wattchow, D., Brookes, S., Murphy, E., Carbone, S., de Fontgalland, D., and Costa, M. (2008). Regional variation in the neurochemical coding of the myenteric plexus of the human colon and changes in patients with slow transit constipation. *Neurogastroenterol. Motil.* 20, 1298–1305. doi: 10.1111/j.1365-2982.2008.01165.x

Wattchow, D., Heitmann, P., Smolilo, D., Spencer, N. J., Parker, D., Hibberd, T., et al. (2020). Postoperative ileus-An ongoing conundrum. *Neurogastroenterol. Motil.* 33:e14046. doi: 10.1111/nmo.14046

Wood, J. D. (1999). Neurotransmission at the interface of sympathetic and enteric divisions of the autonomic nervous system. *Chin. J. Physiol.* 42, 201–210.

Conflict of Interest: The authors declare that the research was conducted in the absence of any commercial or financial relationships that could be construed as a potential conflict of interest.

Publisher's Note: All claims expressed in this article are solely those of the authors and do not necessarily represent those of their affiliated organizations, or those of the publisher, the editors and the reviewers. Any product that may be evaluated in this article, or claim that may be made by its manufacturer, is not guaranteed or endorsed by the publisher.

frontiers | Frontiers in Neuroscience

ORIGINAL RESEARCH
published: 10 May 2022
doi: 10.3389/fnins.2022.878927

Site-Specific Regulation of Stress Responses Along the Rostrocaudal Axis of the Insular Cortex in Rats

*Rodrigo A. Tomeo†, Lucas Gomes-de-Souza†, Ricardo Benini, Lilian L. Reis-Silva and Carlos C. Crestani**

Laboratory of Pharmacology, School of Pharmaceutical Sciences, São Paulo State University (UNESP), Araraquara, Brazil

The insular cortex (IC) has been described as a part of the central network implicated in the integration and processing of limbic information, being related to the behavioral and physiological responses to stressful events. Besides, a site-specific control of physiological functions has been reported along the rostrocaudal axis of the IC. However, a functional topography of the IC in the regulation of stress responses has never been reported. Therefore, this study aimed to investigate the impact of acute restraint stress in neuronal activation at different sites along the rostrocaudal axis of the IC. Furthermore, we evaluated the involvement of IC rostrocaudal subregions in the cardiovascular responses to acute restraint stress. We observed that an acute session of restraint stress increased the number of Fos-immunoreactive cells in the rostral posterior region of the IC, while fewer activated cells were identified in the anterior and caudal posterior regions. Bilateral injection of the non-selective synaptic inhibitor $CoCl_2$ into the anterior region of the IC did not affect the blood pressure and heart rate increases and the sympathetically mediated cutaneous vasoconstriction to acute restraint stress. However, synaptic ablation of the rostral posterior IC decreased the restraint-evoked arterial pressure increase, whereas tachycardia was reduced in animals in which the caudal posterior IC was inhibited. Taken together, these pieces of evidence indicate a site-specific regulation of cardiovascular stress response along the rostrocaudal axis of the IC.

Keywords: cardiovascular function, Fos, topography, prefrontal cortex, restraint stress, sympathetic activity

OPEN ACCESS

Edited by:
Christopher J. Madden, Oregon Health and Science University, United States

Reviewed by:
László Ákos Kovács, University of Pécs, Hungary
Naoya Kataoka, Nagoya University, Japan

***Correspondence:**
Carlos C. Crestani
carlos.crestani@unesp.br

†These authors have contributed equally to this work and share first authorship

Specialty section:
This article was submitted to Autonomic Neuroscience, a section of the journal Frontiers in Neuroscience

Received: *18 February 2022*
Accepted: *14 March 2022*
Published: *10 May 2022*

Citation:
Tomeo RA, Gomes-de-Souza L, Benini R, Reis-Silva LL and Crestani CC (2022) Site-Specific Regulation of Stress Responses Along the Rostrocaudal Axis of the Insular Cortex in Rats. Front. Neurosci. 16:878927. doi: 10.3389/fnins.2022.878927

INTRODUCTION

The responses evoked by stressful stimuli are mediated by limbic networks in the central nervous system involving cortical, subcortical, hypothalamic, and brainstem structures (Dampney, 2015; Myers, 2017; Schaeuble and Myers, 2022). In this sense, the insular cortex (IC) has been described as a part of the brain network implicated in the integration and processing of limbic information in humans subjects and animals (Augustine, 1996; Nieuwenhuys, 2012; Uddin, 2014; Gogolla, 2017). The IC has been proposed to integrate limbic information from several cortical and subcortical areas and, in turn, to control physiological and behavioral responses during aversive situations through connections with hypothalamic and brainstem structures (Augustine, 1996; Nieuwenhuys, 2012; Uddin, 2014; Gogolla, 2017). Previous studies showed an involvement of the

IC in the cardiovascular responses to aversive threats. For instance, it was identified that non-selective synaptic inhibition of the IC of rats caused by local microinjection of $CoCl_2$ reduced the cardiovascular responses caused by both conditioned (i.e., contextual conditioned response) and unconditioned (i.e., restraint stress) aversive stimuli (Alves et al., 2010, 2013).

A site-specific control of the cardiovascular function under basal conditions (i.e., non-stressed) along the rostrocaudal axis of the IC has been described in rodents (Verberne and Owens, 1998; Marins et al., 2016, 2021). Indeed, stimulation of the IC (electrical or chemical with excitatory amino acids) evidenced that activation of anterior regions evoked mainly decreases in arterial pressure (Hardy and Holmes, 1988; Hardy and Mack, 1990; Sun, 1992). Conversely, stimulation of posterior IC caused either a pressor response accompanied by tachycardia or a reduction of both blood pressure and heart rate (HR) (Verberne and Owens, 1998). It was identified that the sites in the posterior IC causing pressor and tachycardiac responses were located more rostrally than those evoking arterial pressure and HR decreases (Verberne and Owens, 1998). Recent results have confirmed a site-specific control of cardiovascular function under basal conditions in the posterior region of the IC (Marins et al., 2016, 2021).

Despite these pieces of evidence, a rostrocaudal organization in the control of stress responses by the IC has never been investigated. Thus, even though previous studies in humans and animals have identified that several stressful stimuli (including restraint stress in rats) caused neuronal activation in the IC (Cullinan et al., 1995; Yokoyama and Sasaki, 1999; Gianaros et al., 2007; Cechetto, 2014), we did not identify studies that have systematically evaluated stress-induced changes on the number of activated cells along the rostrocaudal axis of the IC. Furthermore, despite evidence of a rostrocaudal organization in cardiovascular control by the IC at rest, evaluation of a functional topography of the IC in the regulation of cardiovascular and autonomic changes to stressful stimuli was never performed. Therefore, in this study we investigated the effect of acute restraint stress on neuronal activation of anterior, rostral posterior, and caudal posterior subregions of the IC. Besides, we evaluated the role of these specific sites along the rostrocaudal axis of the IC in the cardiovascular changes caused by acute restraint stress.

MATERIALS AND METHODS

Animals

This study used 76 male Wistar rats (230–250 g; 60 days old) provided by the Central Animal Facility of the UNESP (Botucatu, SP, Brazil). All rats had free access to standard laboratory food and water and were kept in acclimatized rooms (temperature at 24 ± 2°C and humidity at 50 ± 5%) with lights on between 7:00 and 19:00 h. Experimental procedures were approved by the Institutional Ethical Committee for Use of Animals (approval # 38/2018).

Experimental Design

Animals were brought to the trial room in their own home-cages and were allowed to adapt to the experimental room conditions (at least 60 min) before beginning the tests. The trial room was temperature-controlled (24°C) and isolated from the other rooms.

Effect of Acute Restraint Stress on the Number of Fos-Positive Cells Along the Rostrocaudal Axis of the Insular Cortex

Different sets of rats were subjected to either a 60-min session of restraint stress (restraint group) or kept at rest in the home-cage (control group). Thirty minutes following the termination of the stress session (i.e., 90 min after the beginning of the restraint session), the animals of control and restraint groups were anesthetized [urethane, 1.2 g/kg, intraperitoneally (i.p.)], perfused, and the brain was removed for assessment of the number of Fos-positive cells in the anterior, rostral posterior, and caudal posterior subregions of the IC. The definitions of the subregions were based on previous studies (Saper, 1982; Oppenheimer and Cechetto, 1990, Oppenheimer and Cechetto, 2016; Marins et al., 2016, 2020).

Effect of Non-selective Synaptic Inhibition Along the Rostrocaudal Axis of the Insular Cortex on Cardiovascular and Tail Skin Temperature Responses to Acute Restraint Stress

Each animal was connected to the cardiovascular recording system in its respective home-cage. Then, baseline arterial pressure and HR recording was performed for a period of at least 20 min. Later, different sets of animals received bilateral microinjection of the non-selective synaptic inhibitor $CoCl_2$ (1 mM/100 nl) or vehicle (saline, 100 nl) (Alves et al., 2010) into either the anterior, rostral posterior, or caudal posterior subregions of the IC. Ten min after IC treatment, rats underwent a 60-min session of restraint stress (restraint period) (Alves et al., 2010, 2014). Following restraint termination, the animals returned to the respective home-cage and the cardiovascular parameters were recorded for a 60-min period (recovery period).

Cardiovascular recordings (i.e., arterial pressure and HR) started at least 20 min before the restraint stress session and were performed throughout the restraint and recovery periods. Sympathetically mediated vasoconstriction of cutaneous beds during aversive threats reduces skin temperature (Blessing, 2003; Vianna and Carrive, 2005). Therefore, the drop in tail skin temperature during restraint was measured as an indirect measure of the sympathetic response to cutaneous beds (Oliveira et al., 2015; Gomes-de-Souza et al., 2021). Measurements of tail skin temperature were performed at 5 and 0 min before restraint for basal values; 5, 10, 20, 40, and 60 min during restraint, as well as 10, 20, 30, 40, 50, and 60 min during the recovery phase (Benini et al., 2019; Barretto-de-souza et al., 2021).

Acute Restraint Stress

For restraint stress, animals were kept for 60 min into a cylindrical plastic tube, as previously described (Alves et al., 2010, 2014). Animals were subjected to only one restraint session to

avoid the habituation process (Benini et al., 2019; Santos et al., 2020).

Immunohistochemistry

The procedures for the assessment of Fos-positive cells were as previously described (Gomes-de-Souza et al., 2021). Briefly, 90 min after the onset of the restraint stress (i.e., 30 min following the termination of the restraint stress session), the rats were anesthetized (urethane, 1.2 g/kg, i.p.) and subjected to perfusion. Later, the brain was obtained and fixed [paraformaldehyde and 30% sucrose solution in phosphate-buffered saline (PBS)]. Then, the brains were sectioned into 35-μm frontal cuts (CM1900, Leica, Wetzlar, Germany) and the slices containing the anterior, rostral posterior, and caudal posterior subregions of the IC were obtained. The IC subregions were determined according to Paxinos and Watson (1997). The slices were washed (PBS) and incubated for 1 h at room temperature in a blocking solution (0.25% Triton X-100 and 3% goat serum in PBS). Next, the slices were incubated for 24 h at 4°C with an anti-Fos primary antibody produced in rabbits (cat.# 5348; dilution 1:2,000; Cell Signaling, Danvers, MA, United States). Later, the slices were washed (PBS) and incubated for 2 h at room temperature with biotinylated antirabbit secondary antibody (cat.# BA-1000; dilution 1:600; Vector Laboratories, Burlingame, CA, United States). The slices were then washed (PBS) and incubated for 1 h in avidin–biotin–peroxidase solution [cat.# PK-6100; Vectastain Elite ABC-HRP Kit, Peroxidase (Standard); Vector Laboratories, Burlingame, CA, United States]. Then, the slices were washed and incubated for 7 min in 3, 3'-diaminobenzidine tetrahydrochloride hydrate (cat.# D5637, Sigma-Aldrich, St Louis, MO, United States). Finally, the slices were washed and mounted on gelatinized slides.

Images of the right and left hemispheres were captured in each slice, and the analysis was performed in at least two slices per animal. The number of Fos-immunoreactive cells was calculated from a fixed area of each IC subregion using the ImageJ software. The results are presented as the number of Fos-immunoreactive neurons/mm^2.

Stereotaxic Surgery

Five days before the experiments, rats were anesthetized with tribomoethanol at a dose of 250 mg/kg i.p. The animal's head was shaved and then fixed to a stereotaxic apparatus (Stoelting, Wood Dale, IL, United States), and the surgical field was cleaned with 70% alcohol and iodine. A solution of lidocaine with vasoconstrictor (2% lidocaine + 3% phenylephrine, Harvey Química Farmacêutica, Catanduva, SP, Brazil) was administrated for scalp anesthesia and bleeding reduction. Then, the skull was exposed, and the region was cleaned with saline and hydrogen peroxide (10%). Bilateral cannulas were then directed to either the anterior, rostral posterior, or caudal posterior subregions of the IC. The coordinates used for implanting the guide cannulas were anteroposterior, +11.7 mm (anterior IC); +9.1 mm (rostral posterior IC) or +7.0 mm (caudal posterior IC) in relation to the interaural; lateral, +4 mm (anterior IC), +5 mm (rostral posterior IC), or +6.2 mm (caudal posterior IC) from the middle suture; vertical, −4.5 mm (anterior IC), −5.0 mm (rostral posterior IC), or −6.0 mm (caudal posterior IC) in relation to the skull (Paxinos and Watson, 1997). Cannulas were implanted without lateral angulation, and incisor bar was set at −3.2 mm. Two holes were made in the skull using a dental drill through which the bilateral cannulas (26 G, 12 mm) were introduced. The cannulas were fixed to the skull with a self-curing acrylic resin (Simples, DFL, Ind. Com., Rio de Janeiro, RJ, Brazil) and stainless-steel screws were previously implanted in the skull to fix the resin. A 0.2-mm-diameter mandrel was introduced into the cannula to prevent it from clogging. At the end of the surgery, the rats were treated with a veterinary antibiotic intramuscularly (560 mg/ml/kg) and the non-steroidal anti-inflammatory flunixin meglumine by the subcutaneous route (0.5 mg/ml/kg).

Cannulation of Femoral Artery

Twenty-four hours before the trial, the rats were again anesthetized (tribromoethanol, 250 mg/kg, i.p.) and a polyethylene catheter was implanted into the femoral artery for arterial pressure and HR recording. The cannula consisted of a PE-10 polyethylene segment (4–5 cm) welded to a PE-50 polyethylene segment (12–13 cm) (Clay Adams, Parsippany, NJ, United States). The cannulas were filled with a saline solution containing anticoagulant (50 IU/ml of heparin; Hepamax-S, Blausiegel, Cotia, SP, Brazil) and occluded with a metal pin before the implantation. The catheter was exteriorized in the animal's dorsal region and fixed to the skin by surgical suture.

Animals were individually housed during the postoperative period and trials. At the end of the surgery, the animals were treated with the non-steroidal anti-inflammatory flunixin meglumine by the subcutaneous route (0.5 mg/ml/kg).

Arterial Pressure and Heart Rate Recording

Cardiovascular parameters (i.e., arterial pressure and HR) were recorded as previously described (Almeida et al., 2015; Oliveira et al., 2015). Briefly, the arterial catheter (implanted into the femoral artery) was connected to a pressure transducer and pulsatile arterial pressure (PAP) was recorded using an amplifier connected to an acquisition system (ADInstruments, Australia). The mean arterial pressure (MAP) and HR were calculated from the PAP signal.

Tail Skin Temperature Recording

Tail skin temperature recording was performed as previously described (Oliveira et al., 2015; Gomes-de-Souza et al., 2021). Briefly, the recordings were performed using a thermal camera (IRI4010, InfraRed Integrated Systems Ltd., Northampton, United Kingdom) and the temperature was obtained at five sites along the tail, and then the mean was obtained for each record (Oliveira et al., 2015; Gomes-de-Souza et al., 2021).

Drugs and Solutions

$CoCl_2$ (non-selective synaptic inhibitor) (cat. # 232696; Sigma-Aldrich, St Louis, Missouri, United States), tribromoethanol (cat. # T48402, Sigma-Aldrich), and urethane (cat. # U2500, Sigma-Aldrich) were dissolved in saline solution (0.9% NaCl). The antibiotic (Pentabiotico, Fort-Dodge, Campinas, SP, Brazil) and the non-steroidal anti-inflammatory flunixin meglumine

(Banamine, Schering Plough, Cotia, SP, Brazil) were used as supplied by the manufacturers.

Intra-Brain Microinjection

The injection needles (33 G, Small Parts, Miami Lakes, FL, United States) used for intra-brain pharmacological treatment (1 mm longer than the guide-cannulas) were connected to a microsyringe (7002-KH, Hamilton Co., Reno, NV, United States) using a polyethylene tube (PE-10). Vehicle and $CoCl_2$ were microinjected in a final volume of 100 nl/side (Alves et al., 2010; Marins et al., 2016).

Determination of Intra-Brain Microinjection Sites

Following the termination of each experiment, the rats subjected to intra-brain pharmacological treatment were anesthetized (urethane, 1.2 g/kg, i.p.) and 1% Evan's blue dye was bilaterally microinjected (100 nl/side) in the brain to determine the injection sites. Then, the brain was removed, fixed in 10% formalin, and subsequently sectioned into 50-μm frontal cuts (CM1900, Leica, Wetzlar, Germany). Microinjection sites were determined in a microscope (Zeiss Axioskop 2) based on Paxinos and Watson (1997).

Statistical Analysis

Data were expressed as mean ± standard error of the mean (SEM). Baseline parameters of MAP, HR, and tail skin temperature, as well as the number of Fos-immunoreactive cells, were analyzed using Student's *t*-test. Two-way analysis of variance (ANOVA), with treatment as an independent factor and time as a repeated measure, was used to analyze the time-course curves. The mean of cardiovascular and tail skin temperature responses during the restraint and recovery periods was also obtained and analyzed using the two-way ANOVA (treatment as an independent factor and time as a repeated measure). $P < 0.05$ was assumed to be significant.

RESULTS

Diagrammatic representations of coronal sections (Paxinos and Watson, 1997) as well as photomicrographs of coronal brain sections showing microinjection sites of representative animals in the anterior, rostral posterior, and caudal posterior subregions of the IC are presented in **Figure 1**. **Figure 1** also presents the representation of a sagittal section of the rat brain (Paxinos and Watson, 1997), indicating the rostrocaudal position of the IC subregions along the rat brain.

Effect of Restraint Stress on the Number of Fos-Positive Cells Along the Rostrocaudal Axis of the Insular Cortex

Figures 2A,B also presents coronal brain sections of representative animals showing Fos-immunoreactive cells in the anterior, rostral posterior, and caudal posterior subregions of the IC of control animals and rats subjected to restraint stress, as well as an indication of the IC locations where the analysis was performed. Analysis indicated that exposure to a

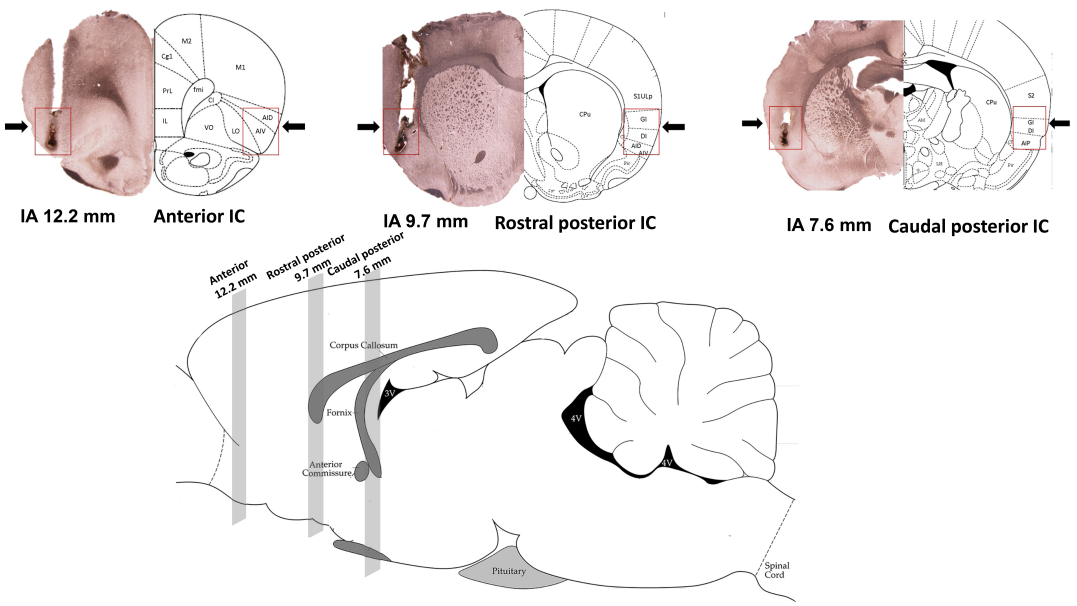

FIGURE 1 | Location of the subregions along the rostrocaudal axis of the insular cortex (IC). (Top) Photomicrograph of coronal brain sections depicting the microinjection sites of representative animals (left hemisphere) and diagrammatic representations modified from the rat brain atlas of Paxinos and Watson (1997) (right hemisphere) indicating the anterior [interaural (IA) 12.7 mm], rostral posterior (IA 9.7 mm), and caudal posterior (IA 7.6 mm) subregions of the IC. Arrows and red squares indicate the microinjection site and IC region. (Bottom) Representation of a sagittal section of the rat brain modified from the rat brain atlas of Paxinos and Watson (1997) indicating the position of the anterior (12.7 mm), rostral posterior (9.7 mm), and caudal posterior (7.6 mm) subregions of the IC along the rat brain. The numbers indicate the IA distance.

TABLE 1 | Basal parameters (i.e., pre-stress values) of mean arterial pressure (MAP), heart rate (HR), and tail skin temperature (T) after pharmacological treatment of either the anterior, rostral posterior, or caudal posterior regions of the insular cortex (IC) with the non-selective synaptic inhibitor $CoCl_2$ or vehicle.

Groups	n	MAP (mmHg)	HR (bpm)	T (°C)
Anterior IC				
Vehicle	8	98 ± 1	370 ± 12	29.3 ± 0.4
$CoCl_2$	9	100 ± 2	344 ± 7	31.5 ± 0.6*
		t = 1.2, df = 15	t = 1.9, df = 15	t = 2.9, df = 15
		P = 0.2373	P = 0.0668	P = 0.0096
Rostral posterior IC				
Vehicle	11	102 ± 2	351 ± 5	29.6 ± 0.6
$CoCl_2$	12	106 ± 2	355 ± 12	30.2 ± 0.5
		t = 1.2, df = 21	t = 0.3, df = 21	t = 0.8, df = 21
		P = 0.2439	P = 0.7458	P = 0.4481
Caudal posterior IC				
Vehicle	10	101 ± 2	354 ± 5	28.9 ± 0.1
$CoCl_2$	9	102 ± 3	378 ± 12	30.2 ± 0.4
		t = 0.4, df = 17	t = 2.0, df = 17	t = 0.9, df = 17
		P = 0.6942	P = 0.0542	P = 0.4559

Values are mean ± SEM, Student's t-test.
**$p < 0.05$.*

60-min session of restraint stress ($n = 9$) decreased the number of Fos-positive cells in the anterior ($t = 2.44$, $df = 15$, $p = 0.0276$) (**Figure 2C**) and caudal posterior ($t = 2.27$, $df = 15$, $p = 0.0388$) (**Figure 2E**) subregions of the IC (**Figure 2**) when compared with control animals ($n = 8$). Conversely, increased number of Fos-immunoreactive cells was found in the rostral posterior IC following acute restraint stress ($t = 2.95$, $df = 15$, $p = 0.0106$) (**Figure 2D**).

Effect of Non-selective Synaptic Inhibition Along the Rostrocaudal Axis of the Insular Cortex on Basal Parameters of Mean Arterial Pressure, Heart Rate, and Tail Skin Temperature

Analysis of the basal parameters indicated that bilateral microinjection of the non-selective synaptic inhibitor $CoCl_2$ (1 mM/100 nl) into either the rostral posterior or caudal posterior subregions of the IC did not affect the baseline values of MAP, HR, and tail skin temperature (**Table 1**). However, analysis of basal parameters in animals that received $CoCl_2$ into the anterior IC indicated enhanced tail skin temperature values when compared with vehicle-treated animals, without changes of MAP and HR (**Table 1**).

Effect of Non-selective Synaptic Inhibition Along the Rostrocaudal Axis of the Insular Cortex on Cardiovascular and Tail Skin Temperature Changes Evoked by Acute Restraint Stress Anterior Insular Cortex

Analysis of the time-course curves indicated that an acute 60-min session of restraint stress increased MAP [time factor: $F_{(65, 975)} = 14.52$; $p < 0.0001$] and HR [time factor: $F_{(65, 975)} = 11.06$; $p < 0.0001$], and decreased tail skin temperature [time factor: $F_{(13, 195)} = 16.79$; $p < 0.001$] (**Figures 3A–C**). Treatment of the anterior subregion of the IC with the non-selective synaptic inhibitor $CoCl_2$ (1 mM/100 nl, $n = 9$) did not affect the restraint-evoked increase in MAP [$F_{(1, 15)} = 0.90$, $p = 0.3633$] and HR [$F_{(1, 15)} = 0.3$, $p = 0.5691$], as well as the drop in tail skin temperature [$F_{(1, 15)} = 2.23$, $p = 0.1608$] when compared with animals treated locally with vehicle (100 nl, $n = 8$) (**Figures 3A–C**). We identified an interaction between time and treatment for MAP [$F_{(65, 975)} = 1.82$, $p = 0.0004$], but not for HR [$F_{(65, 975)} = 0.68$, $p = 0.9786$] and tail skin temperature [$F_{(13, 195)} = 1.75$, $p = 0.0624$] values.

Analysis of mean responses during the restraint and recovery periods indicated differences in the values during restraint and recovery periods for MAP [time factor: $F_{(1, 15)} = 13.21$, $p = 0.0025$), HR [time factor: $F_{(1, 15)} = 25.40$, $p = 0.0002$], and tail skin temperature [time factor: $F_{(1, 15)} = 5.33$, $p = 0.0363$] (**Figures 3D–F**). However, two-way ANOVA did not indicate neither effect of the bilateral microinjection of $CoCl_2$ into the anterior IC [MAP: $F_{(1, 15)} = 0.80$, $p = 0.3879$; HR: $F_{(1, 15)} = 0.69$, $p = 0.4865$; and skin temperature: $F_{(1, 15)} = 2.38$, $p = 0.1213$]nor treatment × time interaction [MAP: $F_{(1, 15)} = 0.47$, $p = 0.5041$; HR: $F_{(1, 15)} = 0.01$, $p = 0.9206$; and skin temperature: $F_{(1, 15)} = 0.59$, $p = 0.6354$] for all measurements (**Figures 3D–F**).

Rostral Posterior Insular Cortex

Analysis of the time-course curves indicated that acute restraint stress increased MAP [time factor: $F_{(65, 1, 365)} = 9.5$, $p < 0.0001$] and HR [time factor: $F_{(65, 1, 365)} = 12.3$, $p < 0.0001$] and decreased the tail skin temperature values [time factor: $F_{(13, 273)} = 15.8$, $p < 0.0001$] (**Figures 4A–C**). Treatment of the rostral posterior subregion of the IC with $CoCl_2$ (1 mM/100 nl, $n = 12$) decreased the restraint-evoked MAP increase [$F_{(1, 21)} = 5.3$, $p = 0.0313$], without affecting the tachycardia [$F_{(1, 21)} = 4.1$, $p = 0.0561$] and the reduction in tail skin temperature [$F_{(1, 21)} = 0.05$, $p = 0.8411$]; when compared with animals treated locally with vehicle (100 nl, $n = 11$) (**Figures 4A–C**). Analysis also indicated an interaction between time and treatment for MAP [$F_{(65, 1, 365)} = 1.63$, $p = 0.0013$], but not for HR [$F_{(65, 1, 365)} = 0.6$, $p = 0.9827$] and tail skin temperature [$F_{(13, 273)} = 0.4$, $p = 0.9708$].

Analysis of the mean Δ MAP during the restraint and recovery periods indicated effect of the $CoCl_2$ microinjection into the rostral posterior IC [$F_{(1, 21)} = 8.47$, $p = 0.0081$], but without significant differences in values during restraint and recovery periods [time factor: $F_{(1, 21)} = 2.62$, $p = 0.1216$] and interaction between treatment and time [$F_{(1, 21)} = 2.35$, $p = 0.1414$] (**Figure 4D**). Bonferroni *post-hoc* analysis revealed that MAP values during the restraint ($p = 0.0045$), but not during the recovery period ($p = 0.0603$), were reduced in animals treated with $CoCl_2$ in the rostral posterior IC (**Figure 4D**). Analysis of HR values indicated effect of time [$F_{(1, 21)} = 18.12$, $p = 0.0004$], but without influence of $CoCl_2$ treatment [$F_{(1, 21)} = 4.20$, $p = 0.0531$] and interaction between the factors [$F_{(1, 21)} = 0.005$, $p = 0.9481$] (**Figure 4E**). Analysis of tail skin temperature

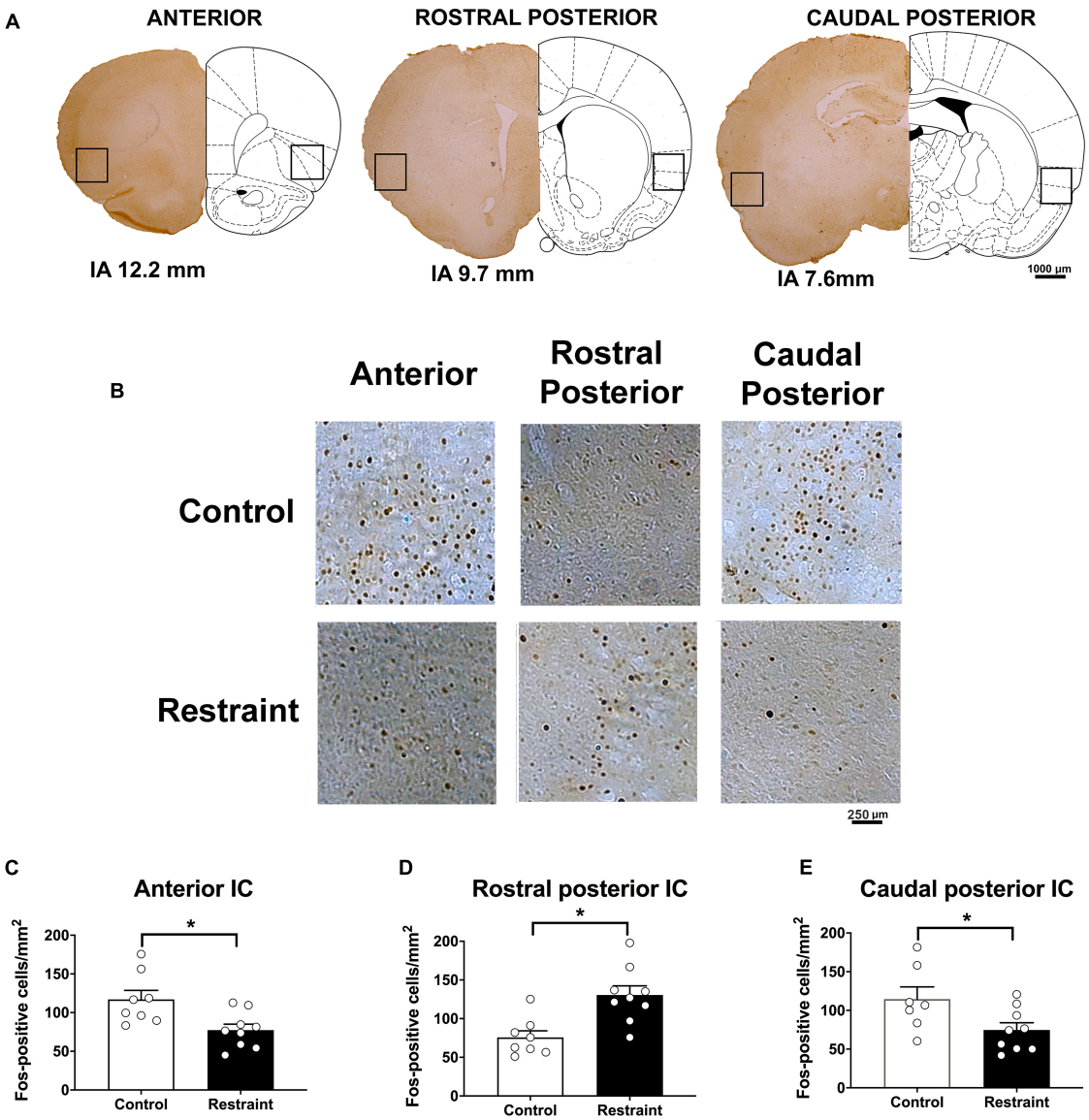

FIGURE 2 | Effect of restraint stress on the number of Fos-positive cells along the rostrocaudal axis of the insular cortex (IC) **(A)**. Representative coronal sections indicating the IC locations where the Fos-positive cells were quantified **(B)**. Representative coronal sections showing Fos-positive cells of representative animals in the anterior (left), rostral posterior (middle), and caudal posterior (right) subregions of the IC in control animals (top) and rats subjected to an acute 60-min session of restraint stress (bottom). **(C–E)** Number of Fos-positive cells in the anterior **(C)**, rostral posterior **(D)**, and caudal posterior **(E)** regions of the IC in control animals (white bars, $n = 8$) and rats subjected to an acute 60-min session of restraint stress (black bars, $n = 9$). The bars represent the mean ± SEM. *$p < 0.05$, Student's *t*-test.

did not indicate effect of either time [$F_{(1,\ 21)} = 1.29$, $p = 0.2707$] or treatment [$F_{(1,\ 21)} = 0.03$, $p = 0.8557$], or interaction between the factors [$F_{(1,\ 21)} = 0.002$, $p = 0.9653$] (**Figure 4F**).

Caudal Posterior Insular Cortex

Analysis of the time-course curves indicated that acute restraint stress caused an increase on MAP [time factor: $F_{(65,\ 1,105)} = 11.6$, $p < 0.0001$] and HR [time factor: $F_{(65,\ 1,105)} = 6.3$, $p < 0.0001$] and decreased the values of tail skin temperature [time factor: $F_{(13,\ 221)} = 13.5$, $p < 0.0001$] (**Figures 5A–C**). Bilateral microinjection of $CoCl_2$ (1 mM/100 nl, $n = 9$) into the caudal posterior IC decreased the tachycardia to restraint stress [$F_{(1,\ 17)} = 11.3$, $p = 0.0036$], without affecting the MAP [$F_{(1,\ 17)} = 0.11$, $p = 0.7462$] and tail skin temperature [$F_{(1,\ 17)} = 1.4$, $p = 0.2640$] responses when compared to vehicle-treated animals (100 nl, $n = 10$) (**Figures 5A–C**). Analysis did not indicate a time × treatment interaction for either MAP [$F_{(65,\ 1,105)} = 1.4$, $p = 0.0686$], HR [$F_{(65,\ 1,105)} = 1.1$, $p = 0.2151$], or tail skin temperature [$F_{(13,\ 221)} = 0.9$, $p = 0.5022$].

Analysis of the mean Δ HR during the restraint and recovery periods indicated effect of the microinjection of $CoCl_2$ into

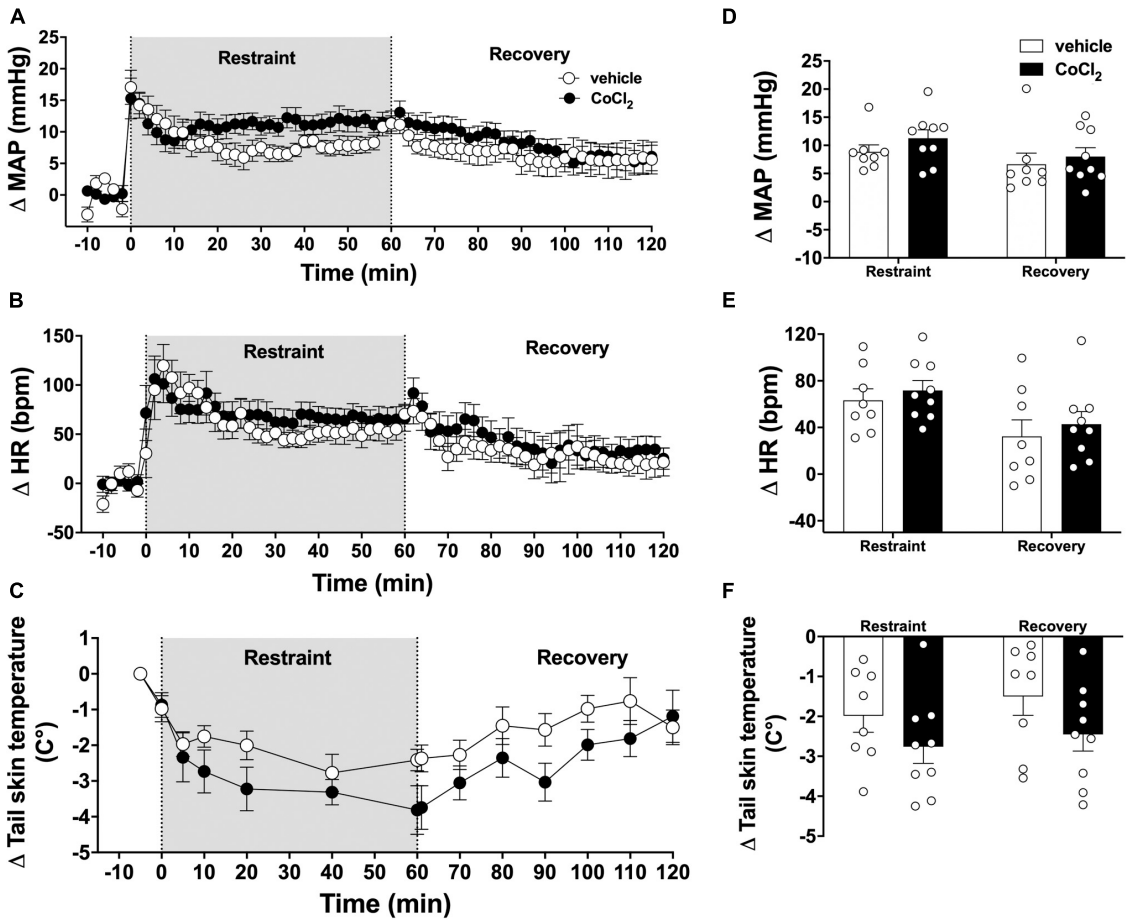

FIGURE 3 | Effect of bilateral microinjection of the non-selective synaptic inhibitor $CoCl_2$ into the anterior subregion of the insular cortex (IC) on mean arterial pressure (MAP), heart rate (HR), and tail skin temperature responses evoked by an acute 60-min session of restraint stress. **(A–C)** Time-course curves of changes on MAP (Δ MAP), HR (Δ HR), and tail skin temperature (Δ tail skin temperature) evoked by acute restraint stress in animals treated bilaterally into the anterior subregion of the IC with vehicle (saline, 100 nl, $n = 8$) or the non-selective synaptic inhibitor $CoCl_2$ (1 mM/100 nl, $n = 9$). Shaded area indicates the restraint stress period. Circles represent the mean ± SEM. Two-way ANOVA. **(D–F)** Mean of Δ MAP, Δ HR, and Δ tail skin temperature during the restraint and recovery periods in animals treated bilaterally into the anterior IC with vehicle ($n = 8$) or $CoCl_2$ ($n = 9$). Bars represent the mean ± SEM. Two-way ANOVA.

the caudal posterior IC [$F_{(1,\ 17)} = 11.85$, $p = 0.0029$], without differences in values during restraint and recovery periods [time factor: $F_{(1,\ 17)} = 3.85$, $p = 0.0602$] and interaction between treatment and time [$F_{(1,\ 17)} = 0.23$, $p = 0.4569$] (**Figure 5E**). Bonferroni *post-hoc* analysis revealed that HR values during restraint ($p = 0.0076$) and recovery ($p = 0.0294$) periods were reduced in animals treated with $CoCl_2$ into the caudal posterior IC (**Figure 5E**). Analysis of MAP values indicated effect of time [$F_{(1,\ 17)} = 8.63$, $p = 0.0092$], without treatment influence [$F_{(1,\ 17)} = 0.12$, $p = 0.7243$] and interaction between the factors [$F_{(1,\ 17)} = 0.75$, $p = 0.3964$] (**Figure 5D**). Analysis of tail skin temperature did not indicate effect of either time [$F_{(1,\ 17)} = 3.57$, $p = 0.0763$] or treatment [$F_{(1,\ 17)} = 1.32$, $p = 0.2683$], or interaction between the factors [$F_{(1,\ 17)} = 0.35$, $p = 0.5648$] (**Figure 5F**).

DISCUSSION

This study reports the effect of restraint stress in neuronal activation along the rostrocaudal axis of the IC. We also document the role of the anterior, rostral posterior, and caudal posterior subregions of the IC in cardiovascular and tail skin temperature changes to acute restraint stress. We identified that acute restraint stress exposure decreased the number of Fos-positive cells in the anterior and caudal posterior regions of the IC, whereas enhanced neuronal activation was observed in the rostral posterior subregion. Analysis of the cardiovascular responses indicated a role of the rostral posterior IC in the pressor response to restraint stress, whereas the caudal posterior region seems to be involved in tachycardia. Non-selective synaptic inhibition in the anterior IC did not affect

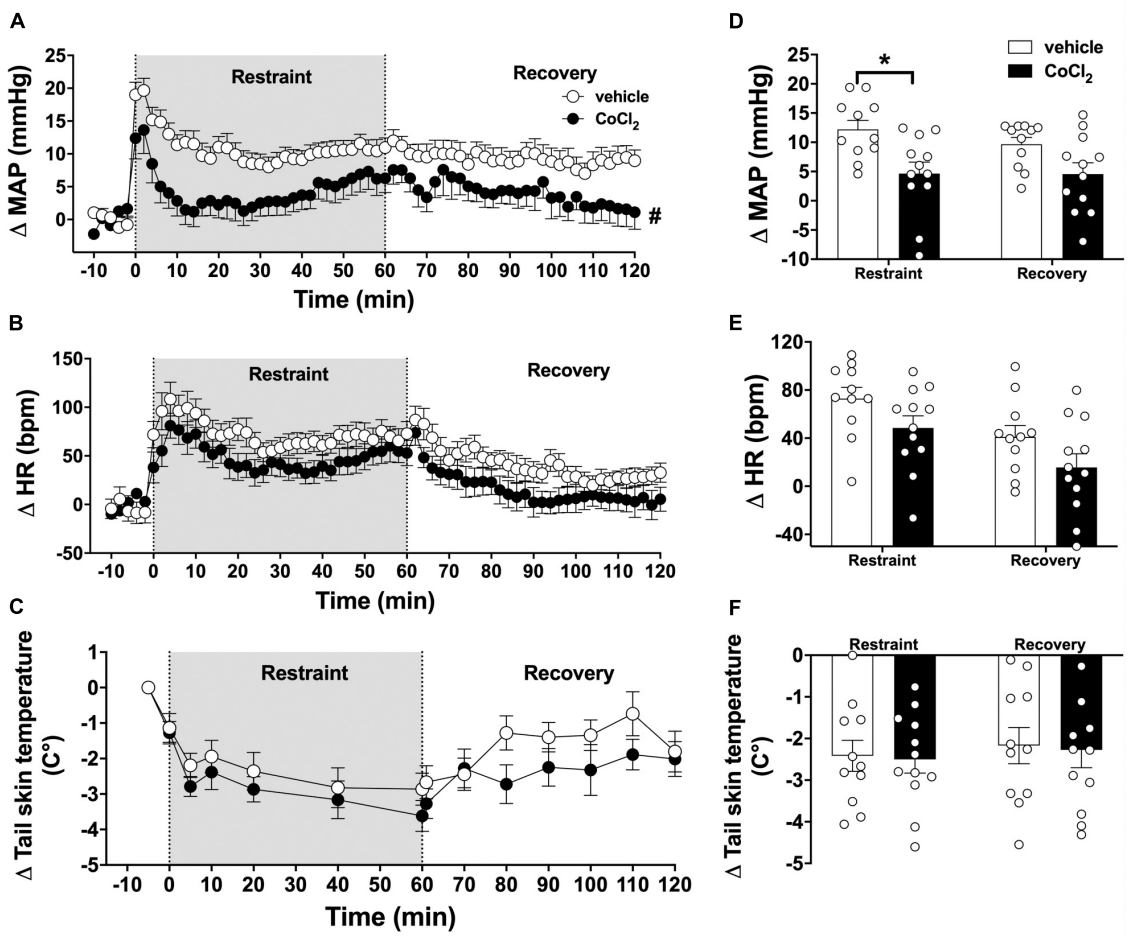

FIGURE 4 | Effect of bilateral microinjection of the non-selective synaptic inhibitor $CoCl_2$ into the rostral posterior subregion of the insular cortex (IC) on mean arterial pressure (MAP), heart rate (HR), and tail skin temperature responses evoked by an acute 60-min session of restraint stress. **(A–C)** Time-course curves of changes on MAP (Δ MAP), HR (Δ HR), and tail skin temperature (Δ tail skin temperature) evoked by acute restraint stress in animals treated bilaterally into the rostral posterior IC with vehicle (saline, 100 nl, $n = 11$) or the non-selective synaptic inhibitor $CoCl_2$ (1 mM/100 nl, $n = 12$). Circles represent the mean ± SEM. $^{\#}p < 0.05$ over the entire restraint and recovery period compared to vehicle group. Two-way ANOVA. **(D–F)** Mean of Δ MAP, Δ HR, and Δ tail skin temperature during the entire restraint and recovery periods in animals treated bilaterally into the rostral posterior IC with vehicle ($n = 11$) or $CoCl_2$ ($n = 12$). Bars represent the mean ± SEM. $^{*}p < 0.05$ compared to vehicle group. Two-way ANOVA followed by Bonferroni *post-hoc* test.

any parameter analyzed. **Table 2** summarizes the main findings reported in this study.

Alves et al. (2010) first documented an involvement of the IC in the cardiovascular changes to restraint stress. They observed that bilateral injection of the non-selective synaptic inhibitor $CoCl_2$ into sites located in the anterior region of the IC decreased both the MAP and HR increases observed during restraint stress. Conversely, the results obtained by us did not indicate a role of the anterior subregion of the IC in restraint-evoked cardiovascular changes. However, the microinjection sites in the study by Alves et al. (2010) reached slightly more caudal regions of the anterior IC (11.7–12.7 mm from interaural) when compared to those in this study (12.2–12.7 mm from interaural). Thus, an explanation for the discrepancy might be the existence of a site-specific control along the rostrocaudal axis of the anterior portion of the IC, so that control of cardiovascular changes to stress occurs in caudal regions of the anterior IC. However, a possible characterization in this sense using intra-brain microinjection approach is difficult since the extent of the anterior region of the IC is short, which would entail very close microinjections for a rostrocaudal analysis. Thus, although our findings do not indicate an involvement of the anterior IC in the cardiovascular responses to restraint stress, we cannot completely exclude its participation. Besides, the evidence documented here that restraint stress decreased the neuronal activity in anterior IC indicates that the sites of the anterior region explored in this study might be involved in responses to aversive threats.

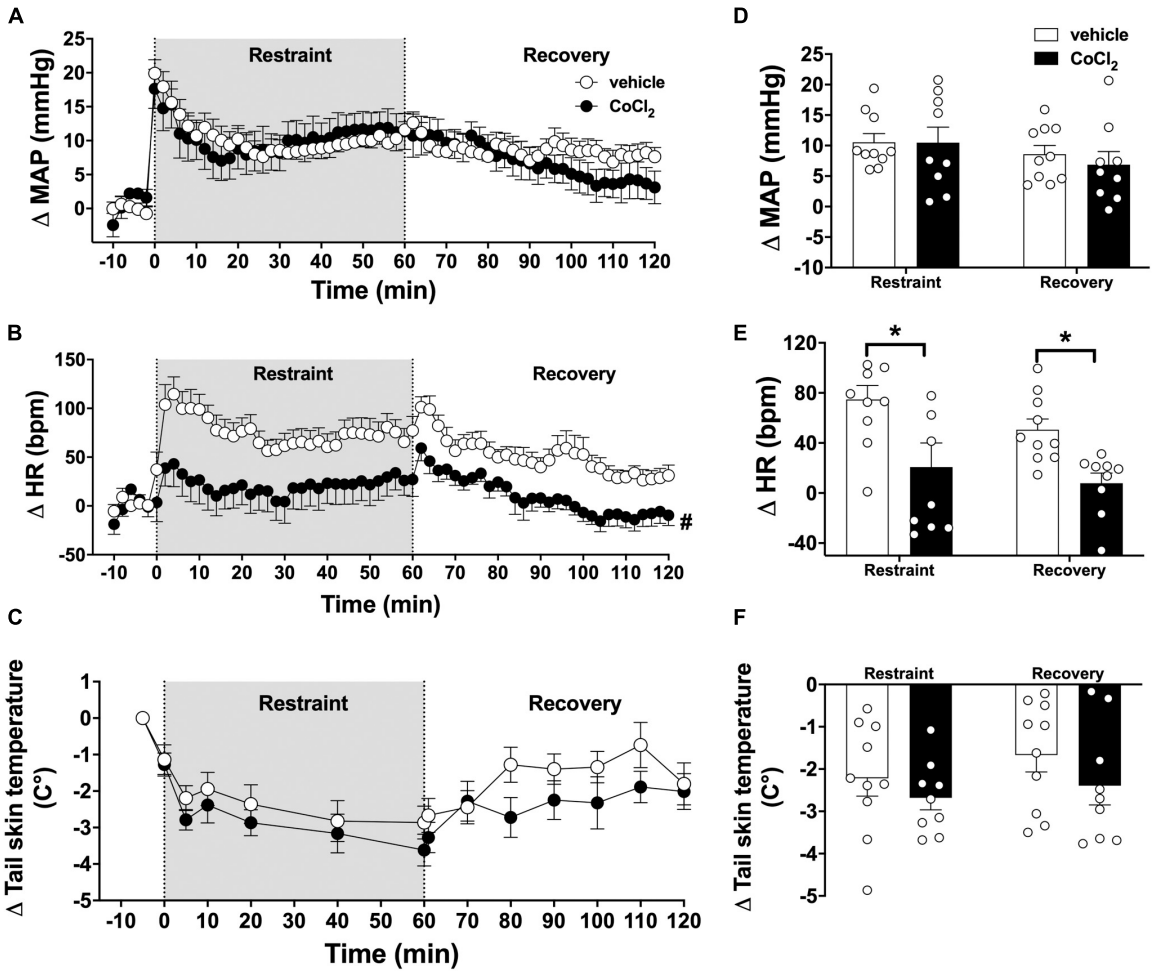

FIGURE 5 | Effect of bilateral microinjection of the non-selective synaptic inhibitor $CoCl_2$ into the caudal posterior subregion of the insular cortex (IC) on mean arterial pressure (MAP), heart rate (HR), and tail skin temperature responses evoked by an acute session of restraint stress. **(A–C)** Time-course curves of changes on MAP (Δ MAP), HR (Δ HR), and tail skin temperature (Δ tail skin temperature) evoked by acute restraint stress in animals treated bilaterally into the caudal posterior IC with vehicle (saline, 100 nl, $n = 10$) or the non-selective synaptic inhibitor $CoCl_2$ (1 mM/100 nl, $n = 9$). Shaded area indicates the restraint stress period. Circles represent the mean ± SEM. $^{\#}p < 0.05$ over the entire restraint and recovery period compared to vehicle group. Two-way ANOVA. **(D–F)** Mean of Δ MAP, Δ HR, and Δ tail skin temperature during the entire restraint and recovery periods in animals treated bilaterally into the caudal posterior IC with vehicle ($n = 10$) or $CoCl_2$ (1 nmol/100 nl, $n = 9$). Bars represent the mean ± SEM. $^{*}p < 0.05$ compared to vehicle group. Two-way ANOVA followed by Bonferroni *post-hoc* test.

Our data evidenced a site-specific control of MAP and HR responses during restraint stress in the posterior portion of the IC. Indeed, while inhibition of the rostral posterior region decreased specifically the pressor response to restraint stress, the caudal posterior IC was implicated in the tachycardia. Analysis of Fos-immunoreactive neurons indicated that involvement of rostral posterior region in the restraint-evoked pressor response is mediated by neuronal activation of this region, as evidenced by the enhanced number of Fos-positive cells in animals subjected to restraint stress. Previous studies indicated that the arterial pressure increase caused by restraint stress is mainly due to vasomotor sympathoexcitation (Dos Reis et al., 2014). In this sense, our findings are supported by previous evidence from studies in animals at rest (i.e., non-stressed) in which vasomotor sympathoexcitatory responses were evoked by stimulation of rostral regions of the posterior IC (Verberne and Owens, 1998; Marins et al., 2016). Thus, restraint stress seems to activate excitatory output in the rostral posterior IC to centers in the medulla regulating the sympathetic activity to blood vessels.

The control of pressor response by rostral posterior IC seems to occur *via* indirect connections with autonomic centers in the medulla controlling the sympathetic activity. Indeed, a recent study identified neurons in the rostral posterior region projecting to the caudal ventrolateral medulla (CVLM), but not to rostral ventrolateral medulla (RVLM) (Marins et al., 2016). The site in rostral posterior region in which the projections to

TABLE 2 | Summary of the main findings obtained in this study.

	Insular Cortex (IC)		
	Anterior	**Rostral posterior**	**Caudal posterior**
Effect of restraint stress			
Fos-positive cells	↓	↑	↓
Effect of local $CoCl_2$ microinjection			
Pressor effect	=	↓	=
Tachycardia	=	=	↓
Cutaneous vasoconstriction	=	=	=

↓, decrease; ↑, increase; =, no effect.

CVLM were identified (IA 10.5 mm) is slightly more rostral in relation to that in which we identified an involvement in pressor response to restraint stress (IA 9.7 mm) (Marins et al., 2016). However, stimulation of both regions in rostral posterior IC evoked the same pattern of cardiovascular response (i.e., pressor response) in rats under resting conditions (Yasui et al., 1991; Marins et al., 2016), thus indicating that the sites explored in the present study might also project to CVLM. GABAergic neurons in the CVLM inhibit premotor sympathetic neurons located in the RVLM. In this sense, projections to infralimbic cortex, basolateral and central amygdala, bed nucleus of the stria terminalis (BNST), and lateral hypothalamus (LH) were identified from sites in the rostral posterior IC in which stimulation evoked pressor response in animals at rest (Yasui et al., 1991; Verberne and Owens, 1998). More recent evidence indicated that these projections are mainly glutamatergic (Centanni et al., 2019; McGinnis et al., 2020; Girven et al., 2021), and some of these structures (e.g., LH) have already been implicated in cardiovascular regulation by IC under resting conditions (Cechetto and Chen, 1990; Oppenheimer et al., 1992). Furthermore, all these limbic structures are involved in the regulation of stress-evoked cardiovascular changes (Tavares et al., 2009; Deolindo et al., 2013; Oscar et al., 2015; Barretto-de-Souza et al., 2018; Gomes-de-Souza et al., 2019; Silva et al., 2020). Therefore, these regions might constitute intermediate sites connecting the rostral posterior IC to autonomic centers in the medulla for control of the pressor response during aversive threats.

The decreased number of Fos-positive cells in the caudal posterior region of the IC following restraint stress exposure indicates that the control of restraint-evoked tachycardia by this region is mediated by a reduction in local neuronal activity. Previous studies provided evidence that stimulation of caudal regions of the posterior IC evoked bradycardia in rats at rest *via* inhibition of cardiac sympathetic activity (Oppenheimer and Cechetto, 1990, Oppenheimer and Cechetto, 2016). Therefore, the role of the caudal posterior IC in restraint-evoked tachycardia seems to be mediated by a decrease in the activity of neuronal output inhibiting cardiac sympathetic activity. This idea is supported by the evidence obtained in animals subjected to lesion of the posterior IC, including the caudal regions, of a tonic inhibitory influence on sympathetic activity regulating the cardiovascular function (Butcher and Cechetto, 1995a,b; Marins et al., 2020). Moreover, removal of this sympathetic inhibitory influence obtained by neuronal lesion of the posterior IC (including caudal regions) enhanced the HR response to air-jet stress (Cheung et al., 1997).

Regarding the neural network involved in the control of restraint tachycardia by caudal posterior IC, previous evidence indicated a similar projection pattern of the subregions along the posterior IC (Yasui et al., 1991; Verberne and Owens, 1998). Therefore, although Marins et al. (2016) have not explored the connections of caudal posterior IC, regulation of tachycardia during restraint might be mediated by a decrease in the activity of neurons in the caudal posterior region projecting to CVLM. Besides, such as discussed for the control by rostral posterior region, regulation by caudal posterior IC might also be mediated by connection with limbic intermediate sites, which in turn projects to autonomic centers in the medulla controlling the cardiac sympathetic activity. Considering the evidence that projections from the IC are mainly glutamatergic (Centanni et al., 2019; McGinnis et al., 2020; Girven et al., 2021), the involvement in HR response to restraint *via* a decrease in local neuronal activation indicates that this control is mediated by connection with limbic structures playing an inhibitory role in restraint-evoked tachycardia. Thus, the decrease in the activity of IC glutamatergic neurons projecting to limbic regions inhibiting the HR response to stress would decrease the neuronal activity in these regions, which in turn would contribute to the HR increase during restraint stress. In this sense, the LH and BNST might constitute prominent limbic intermediate centers since previous studies demonstrated that activation of neurons in these regions inhibits restraint-evoked HR increase (Crestani et al., 2009; Deolindo et al., 2013; Gomes-de-Souza et al., 2019).

In summary, the findings documented in this study suggest a site-specific regulation of cardiovascular changes to restraint stress along the rostrocaudal axis of the posterior IC. Our data indicate that neuronal activation in the rostral region of the posterior IC seems to be involved in the arterial pressure increase during aversive threats. Besides, the present findings provide evidence that a decrease in neuronal activity in the caudal region of the posterior IC contributes to tachycardiac response during restraint stress. Finally, decreased neuronal activity in the anterior IC seems to be important in the control of responses other than cardiovascular adjustments during aversive threats.

DATA AVAILABILITY STATEMENT

The original contributions presented in the study are included in the article/supplementary material, further inquiries can be directed to the corresponding author/s.

ETHICS STATEMENT

The animal study was reviewed and approved by Ethical Committee for Use of Animals of the School of Pharmaceutical Sciences—UNESP.

AUTHOR CONTRIBUTIONS

RT and LG-d-S: conceptualization, methodology, formal analysis, investigation, writing—original draft, and visualization. LR-S: formal analysis, investigation, writing—review and editing. CC: conceptualization, methodology, resources, data curation, writing—review and editing, visualization, supervision, project administration, and funding acquisition. All authors contributed to the article and approved the submitted version.

FUNDING

This work was supported by grants from FAPESP (grants # 2017/19249-0 and 2019/24478-3), CNPq (grant # 431339/2018-0), and Scientific Support and Development Program of School of Pharmaceutical Sciences (UNESP). This study was financed in part by the Coordenação de Aperfeiçoamento de Pessoal de Nível Superior—Brazil (CAPES)—Finance Code 001. CC was a CNPq Research Fellow (process # 304108/2018-9).

REFERENCES

Almeida, J., Duarte, J. O., Oliveira, L. A., and Crestani, C. C. (2015). Effects of nitric oxide synthesis inhibitor or fluoxetine treatment on depression-like state and cardiovascular changes induced by chronic variable stress in rats. *Stress* 18, 462–474. doi: 10.3109/10253890.2015.1038993

Alves, F. H. F., Crestani, C. C., and Corrêa, F. M. A. (2010). The insular cortex modulates cardiovascular responses to acute restraint stress in rats. *Brain Res.* 1333, 57–63. doi: 10.1016/j.brainres.2010.03.077

Alves, F. H. F., Crestani, C. C., Resstel, L. B. M., and Corrêa, F. M. A. (2014). Both α1- and α2-adrenoceptors in the insular cortex are involved in the cardiovascular responses to acute restraint stress in rats. *PLoS One* 9:e83900. doi: 10.1371/journal.pone.0083900

Alves, F. H. F., Gomes, F. V., Reis, D. G., Crestani, C. C., Corrêa, F. M. A., Guimarães, F. S., et al. (2013). Involvement of the insular cortex in the consolidation and expression of contextual fear conditioning. *Eur. J. Neurosci.* 38, 2300–2307. doi: 10.1111/ejn.12210

Augustine, J. (1996). Circuitry and functional aspects of the insular lobe in primates including humans. *Brain Res. Brain Res. Rev.* 22, 229–244. doi: 10.1016/S0165-0173(96)00011-2

Barretto-de-Souza, L., Adami, M. B., Benini, R., and Crestani, C. C. (2018). Dual role of nitrergic neurotransmission in the bed nucleus of the stria terminalis in controlling cardiovascular responses to emotional stress in rats. *Br. J. Pharmacol.* 175, 3773–3783. doi: 10.1111/bph.14447

Barretto-de-souza, L., Benini, R., Reis-silva, L. L., and Crestani, C. C. (2021). Corticotropin-releasing factor neurotransmission in the lateral hypothalamus modulates the tachycardiac response during acute emotional stress in rats. *Brain Res. Bull.* 166, 102–109. doi: 10.1016/j.brainresbull.2020.11.010

Benini, R., Oliveira, L. A., Gomes-de-Souza, L., and Crestani, C. C. (2019). Habituation of the cardiovascular responses to restraint stress in male rats: influence of length, frequency and number of aversive sessions. *Stress* 22, 151–161. doi: 10.1080/10253890.2018.1532992

Blessing, W. W. (2003). Lower brainstem pathways regulating sympathetically mediated changes in cutaneous blood flow. *Cell. Mol. Neurobiol.* 23, 527–538. doi: 10.1023/A:1025020029037

Butcher, K. S., and Cechetto, D. F. (1995a). Autonomic responses of the insular cortex in hypertensive and normotensive rats. *Am. J. Physiol. Integr. Comp. Physiol.* 268, R214–R222. doi: 10.1152/ajpregu.1995.268.1.R214

Butcher, K. S., and Cechetto, D. F. (1995b). Insular lesion evokes autonomic effects of stroke in normotensive and hypertensive rats. *Stroke* 26, 459–465. doi: 10.1161/01.STR.26.3.459

Cechetto, D. F. (2014). Cortical control of the autonomic nervous system. *Exp. Physiol.* 99, 326–331. doi: 10.1113/expphysiol.2013.075192

Cechetto, D. F., and Chen, S. J. (1990). Subcortical sites mediating sympathetic responses from insular cortex in rats. *Am. J. Physiol. Integr. Comp. Physiol.* 258, R245–R255. doi: 10.1152/ajpregu.1990.258.1.R245

Centanni, S. W., Morris, B. D., Luchsinger, J. R., Bedse, G., Fetterly, T. L., Patel, S., et al. (2019). Endocannabinoid control of the insular-bed nucleus of the stria terminalis circuit regulates negative affective behavior associated with alcohol abstinence. *Neuropsychopharmacology* 44, 526–537. doi: 10.1038/s41386-018-0257-8

Cheung, R. T. F., Hachinski, V. C., and Cechetto, D. F. (1997). Cardiovascular response to stress after middle cerebral artery occlusion in rats. *Brain Res.* 747, 181–188. doi: 10.1016/S0006-8993(96)01137-7

Crestani, C. C., Alves, F. H. F., Tavares, R. F., and Corrêa, F. M. A. (2009). Role of the bed nucleus of the stria terminalis in the cardiovascular responses to acute restraint stress in rats. *Stress* 12, 268–278. doi: 10.1080/10253890802331477

Cullinan, W. E., Herman, J. P., Battaglia, D. F., Akil, H., and Watson, S. J. (1995). Pattern and time course of immediate early gene expression in rat brain following acute stress. *Neuroscience* 64, 477–505. doi: 10.1016/0306-4522(94)00355-9

Dampney, R. A. L. (2015). Central mechanisms regulating coordinated cardiovascular and respiratory function during stress and arousal. *Am. J. Physiol. Regul. Integr. Comp. Physiol.* 309, R429–R443. doi: 10.1152/ajpregu.00051.2015

Deolindo, M. V., Reis, D. G., Crestani, C. C., Tavares, R. F., Resstel, L. B. M., and Corrêa, F. M. A. (2013). NMDA receptors in the lateral hypothalamus have an inhibitory influence on the tachycardiac response to acute restraint stress in rats. *Eur. J. Neurosci.* 38, 2374–2381. doi: 10.1111/ejn.12246

Dos Reis, D. G., Fortaleza, E. A. T., Tavares, R. F., and Corrêa, F. M. A. (2014). Role of the autonomic nervous system and baroreflex in stress-evoked cardiovascular responses in rats. *Stress* 17, 362–372. doi: 10.3109/10253890.2014.930429

Gianaros, P. J., Jennings, J. R., Sheu, L. K., Derbyshire, S. W. G., and Matthews, K. A. (2007). Heightened functional neural activation to psychological stress covaries with exaggerated blood pressure reactivity. *Hypertension* 49, 134–140. doi: 10.1161/01.HYP.0000250984.14992.64

Girven, K. S., Aroni, S., Navarrete, J., Marino, R. A. M., McKeon, P. N., Cheer, J. F., et al. (2021). Glutamatergic input from the insula to the ventral bed nucleus of the stria terminalis controls reward-related behavior. *Addict. Biol.* 26:e12961. doi: 10.1111/ADB.12961

Gogolla, N. (2017). The insular cortex. *Curr. Biol.* 27, R580–R586. doi: 10.1016/J.CUB.2017.05.010

Gomes-de-Souza, L., Benini, R., Costa-Ferreira, W., and Crestani, C. C. (2019). GABAA but not GABAB receptors in the lateral hypothalamus modulate the tachycardic response to emotional stress in rats. *Eur. Neuropsychopharmacol.* 29, 672–680. doi: 10.1016/j.euroneuro.2019.03.001

Gomes-de-Souza, L., Costa-Ferreira, W., Mendonça, M. M., Xavier, C. H., and Crestani, C. C. (2021). Lateral hypothalamus involvement in control of stress response by bed nucleus of the stria terminalis endocannabinoid neurotransmission in male rats. *Sci. Rep.* 11:16133. doi: 10.1038/s41598-021-95401-z

Hardy, S., and Holmes, D. (1988). Prefrontal stimulus-produced hypotension in rat. *Exp. Brain Res.* 73, 249–255. doi: 10.1007/BF00248217

Hardy, S., and Mack, S. (1990). Brainstem mediation of prefrontal stimulus-produced hypotension. *Exp. Brain Res.* 79, 393–399. doi: 10.1007/BF00608250

Marins, F. R., Limborço-Filho, M., D'Abreu, B. F., Machado de Almeida , P. W., Gavioli, M., Xavier, C. H., et al. (2020). Autonomic and cardiovascular consequences resulting from experimental hemorrhagic stroke in the left or right intermediate insular cortex in rats. *Auton. Neurosci.* 227:102695. doi: 10.1016/J.AUTNEU.2020.102695

Marins, F. R., Limborço-Filho, M., Xavier, C. H., Biancardi, V. C., Vaz, G. C., Stern, J. E., et al. (2016). Functional topography of cardiovascular regulation along the rostrocaudal axis of the rat posterior insular cortex. *Clin. Exp. Pharmacol. Physiol.* 43, 484–493. doi: 10.1111/1440-1681.12542

Marins, F. R., Oliveira, A. C., Qadri, F., Motta-Santos, D., Alenina, N., Bader, M., et al. (2021). Alamandine but not angiotensin-(1-7) produces cardiovascular effects at the rostral insular cortex. *Am. J. Physiol. Integr. Comp. Physiol.* 321, R513–R521. doi: 10.1152/ajpregu.00308.2020

McGinnis, M. M., Parrish, B. C., and McCool, B. A. (2020). Withdrawal from chronic ethanol exposure increases postsynaptic glutamate function of insular cortex projections to the rat basolateral amygdala. *Neuropharmacology* 172:108129. doi: 10.1016/J.NEUROPHARM.2020.108129

Myers, B. (2017). Corticolimbic regulation of cardiovascular responses to stress. *Physiol. Behav.* 172, 49–59. doi: 10.1016/j.physbeh.2016.10.015

Nieuwenhuys, R. (2012). The insular cortex: a review. *Prog. Brain Res.* 195, 123–163. doi: 10.1016/B978-0-444-53860-4.00007-6

Oliveira, L. A., Almeida, J., Benini, R., and Crestani, C. C. (2015). CRF 1 and CRF 2 receptors in the bed nucleus of the stria terminalis modulate the cardiovascular responses to acute restraint stress in rats. *Pharmacol. Res.* 9, 53–62. doi: 10.1016/j.phrs.2015.03.012

Oppenheimer, S., and Cechetto, D. (2016). The insular cortex and the regulation of cardiac function. *Compr. Physiol.* 6, 1081–1133. doi: 10.1002/cphy.c140076

Oppenheimer, S. M., and Cechetto, D. F. (1990). Cardiac chronotropic organization of the rat insular cortex. *Brain Res.* 533, 66–72. doi: 10.1016/0006-8993(90)91796-J

Oppenheimer, S. M., Saleh, T., and Cechetto, D. F. (1992). Lateral hypothalamic area neurotransmission and neuromodulation of the specific cardiac effects of insular cortex stimulation. *Brain Res.* 581, 133–142. doi: 10.1016/0006-8993(92)90352-A

Oscar, C. G., Müller-Ribeiro, F. C. D. F., de Castro, L. G., Martins Lima, A., Campagnole-Santos, M. J., Santos, R. A. S., et al. (2015). Angiotensin-(1–7) in the basolateral amygdala attenuates the cardiovascular response evoked by acute emotional stress. *Brain Res.* 1594, 183–189. doi: 10.1016/j.brainres.2014.11.006

Paxinos, G., and Watson, C. (1997). *The Rat Brain in Stereotaxic Coordinates*, 3rd Edn. San Diego: Academic Press.

Santos, C. E., Benini, R., and Crestani, C. C. (2020). Spontaneous recovery, time course, and circadian influence on habituation of the cardiovascular responses to repeated restraint stress in rats. *Pflugers Arch.* 472, 1495–1506. doi: 10.1007/s00424-020-02451-9

Saper, C. B. (1982). Convergence of autonomic and limbic connections in the insular cortex of the rat. *J. Comp. Neurol.* 210, 163–173. doi: 10.1002/CNE.902100207

Schaeuble, D., and Myers, B. (2022). Cortical–hypothalamic integration of autonomic and endocrine stress responses. *Front. Physiol.* 13:151. doi: 10.3389/FPHYS.2022.820398/BIBTEX

Silva, C. C., Correa, A. M. B., Kushmerick, C., Sharma, N. M., Patel, K. P., de Almeida, J. F. Q., et al. (2020). Angiotensin-converting enzyme 2 activator, DIZE in the basolateral amygdala attenuates the tachycardic response to acute stress by modulating glutamatergic tone. *Neuropeptides* 83:102076. doi: 10.1016/j.npep.2020.102076

Sun, M. K. (1992). Medullospinal vasomotor neurones mediate hypotension from stimulation of prefrontal cortex. *J. Auton. Nerv. Syst.* 38, 209–217. doi: 10.1016/0165-1838(92)90032-C

Tavares, R. F., Corrêa, F. M. A., and Resstel, L. B. M. (2009). Opposite role of infralimbic and prelimbic cortex in the tachycardiac response evoked by acute restraint stress in rats. *J. Neurosci. Res.* 87, 2601–2607. doi: 10.1002/jnr.22070

Uddin, L. (2014). Salience processing and insular cortical function and dysfunction. *Nat. Rev. Neurosci.* 161, 55–61. doi: 10.1038/nrn3857

Verberne, A., and Owens, N. C. (1998). Cortical modulation of thecardiovascular system. *Prog. Neurobiol.* 54, 149–168. doi: 10.1016/S0301-0082(97)00056-7

Vianna, D. M. L., and Carrive, P. (2005). Changes in cutaneous and body temperature during and after conditioned fear to context in the rat. *Eur. J. Neurosci.* 21, 2505–2512. doi: 10.1111/j.1460-9568.2005.04073.x

Yasui, Y., Breder, C. D., Safer, C. B., and Cechetto, D. F. (1991). Autonomic responses and efferent pathways from the insular cortex in the rat. *J. Comp. Neurol.* 303, 355–374. doi: 10.1002/cne.903030303

Yokoyama, C., and Sasaki, K. (1999). Regional expressions of Fos-like immunoreactivity in rat cerebral cortex after stress; restraint and intraperitoneal lipopolysaccharide. *Brain Res.* 816, 267–275. doi: 10.1016/S0006-8993(98)00927-5

Conflict of Interest: The authors declare that the research was conducted in the absence of any commercial or financial relationships that could be construed as a potential conflict of interest.

Publisher's Note: All claims expressed in this article are solely those of the authors and do not necessarily represent those of their affiliated organizations, or those of the publisher, the editors and the reviewers. Any product that may be evaluated in this article, or claim that may be made by its manufacturer, is not guaranteed or endorsed by the publisher.

frontiers | Frontiers in Physiology

MINI REVIEW
published: 23 June 2022
doi: 10.3389/fphys.2022.919422

Sympathetic and Vagal Nerve Activity in COPD: Pathophysiology, Presumed Determinants and Underappreciated Therapeutic Potential

Jens Spiesshoefer[1,2†], Binaya Regmi[1†], Matteo Maria Ottaviani[2], Florian Kahles[3], Alberto Giannoni[2], Chiara Borrelli[2], Claudio Passino[2], Vaughan Macefield[4,5‡] and Michael Dreher[1‡]*

[1]Department of Pneumology and Intensive Care Medicine, University Hospital RWTH Aachen, Aachen, Germany, [2]Institute of Life Sciences, Scuola Superiore Sant'Anna, Pisa, Italy, [3]Department of Cardiology and Vascular Medicine, University Hospital RWTH Aachen, Aachen, Germany, [4]Human Autonomic Neurophysiology Laboratory, Baker Heart and Diabetes Institute, Melbourne, VIC, Australia, [5]Department of Anatomy and Physiology, University of Melbourne, Melbourne, VIC, Australia

OPEN ACCESS

Edited by:
Alberto Porta,
University of Milan, Italy

Reviewed by:
Beatrice Cairo,
University of Milan, Italy
Antonio Roberto Zamunér,
Catholic University of Maule, Chile
Franca Barbic,
Humanitas University Department of Biomedical Sciences, Italy

***Correspondence:**
Jens Spiesshoefer
jspiesshoefer@ukaachen.de
orcid.org/0000-0001-8205-1749

†These authors have contributed equally to this work and share first authorship

‡These authors have contributed equally to this work and share senior authorship

Specialty section:
This article was submitted to Autonomic Neuroscience, a section of the journal Frontiers in Physiology

Received: 13 April 2022
Accepted: 02 June 2022
Published: 23 June 2022

Citation:
Spiesshoefer J, Regmi B, Ottaviani MM, Kahles F, Giannoni A, Borrelli C, Passino C, Macefield V and Dreher M (2022) Sympathetic and Vagal Nerve Activity in COPD: Pathophysiology, Presumed Determinants and Underappreciated Therapeutic Potential. Front. Physiol. 13:919422. doi: 10.3389/fphys.2022.919422

This article explains the comprehensive state of the art assessment of sympathetic (SNA) and vagal nerve activity recordings in humans and highlights the precise mechanisms mediating increased SNA and its corresponding presumed clinical determinants and therapeutic potential in the context of chronic obstructive pulmonary disease (COPD). It is known that patients with COPD exhibit increased muscle sympathetic nerve activity (MSNA), as measured directly using intraneural microelectrodes—the gold standard for evaluation of sympathetic outflow. However, the underlying physiological mechanisms responsible for the sympathoexcitation in COPD and its clinical relevance are less well understood. This may be related to the absence of a systematic approach to measure the increase in sympathetic activity and the lack of a comprehensive approach to assess the underlying mechanisms by which MSNA increases. The nature of sympathoexcitation can be dissected by distinguishing the heart rate increasing properties (heart rate and blood pressure variability) from the vasoconstrictive drive to the peripheral vasculature (measurement of catecholamines and MSNA) (**Graphical Abstract Figure 1**). Invasive assessment of MSNA to the point of single unit recordings with analysis of single postganglionic sympathetic firing, and hence SNA drive to the peripheral vasculature, is the gold standard for quantification of SNA in humans but is only available in a few centres worldwide because it is costly, time consuming and requires a high level of training. A broad picture of the underlying pathophysiological determinants of the increase in sympathetic outflow in COPD can only be determined if a combination of these tools are used. Various factors potentially determine SNA in COPD (**Graphical Abstract Figure 1**): Obstructive sleep apnoea (OSA) is highly prevalent in COPD, and leads to repeated bouts of upper airway obstructions with hypoxemia, causing repetitive arousals. This probably produces ongoing sympathoexcitation in the awake state, likely in the "blue bloater" phenotype, resulting in persistent vasoconstriction. Other variables likely describe a subset of COPD patients with increase of sympathetic drive to the heart, clinically likely in the "pink puffer" phenotype. Pharmacological treatment options of increased SNA in COPD could comprise beta blocker therapy. However, as opposed to systolic heart failure a similar

beneficial effect of beta blocker therapy in COPD patients has not been shown. The point is made that although MSNA is undoubtedly increased in COPD (probably independently from concomitant cardiovascular disease), studies designed to determine clinical improvements during specific treatment will only be successful if they include adequate patient selection and translational state of the art assessment of SNA. This would ideally include intraneural recordings of MSNA and—as a future perspective—vagal nerve activity all of which should ideally be assessed both in the upright and in the supine position to also determine baroreflex function.

Keywords: sympathetic drive, chronic lung disease, cardiovascular stress, autonomic nervous system, vagal activity

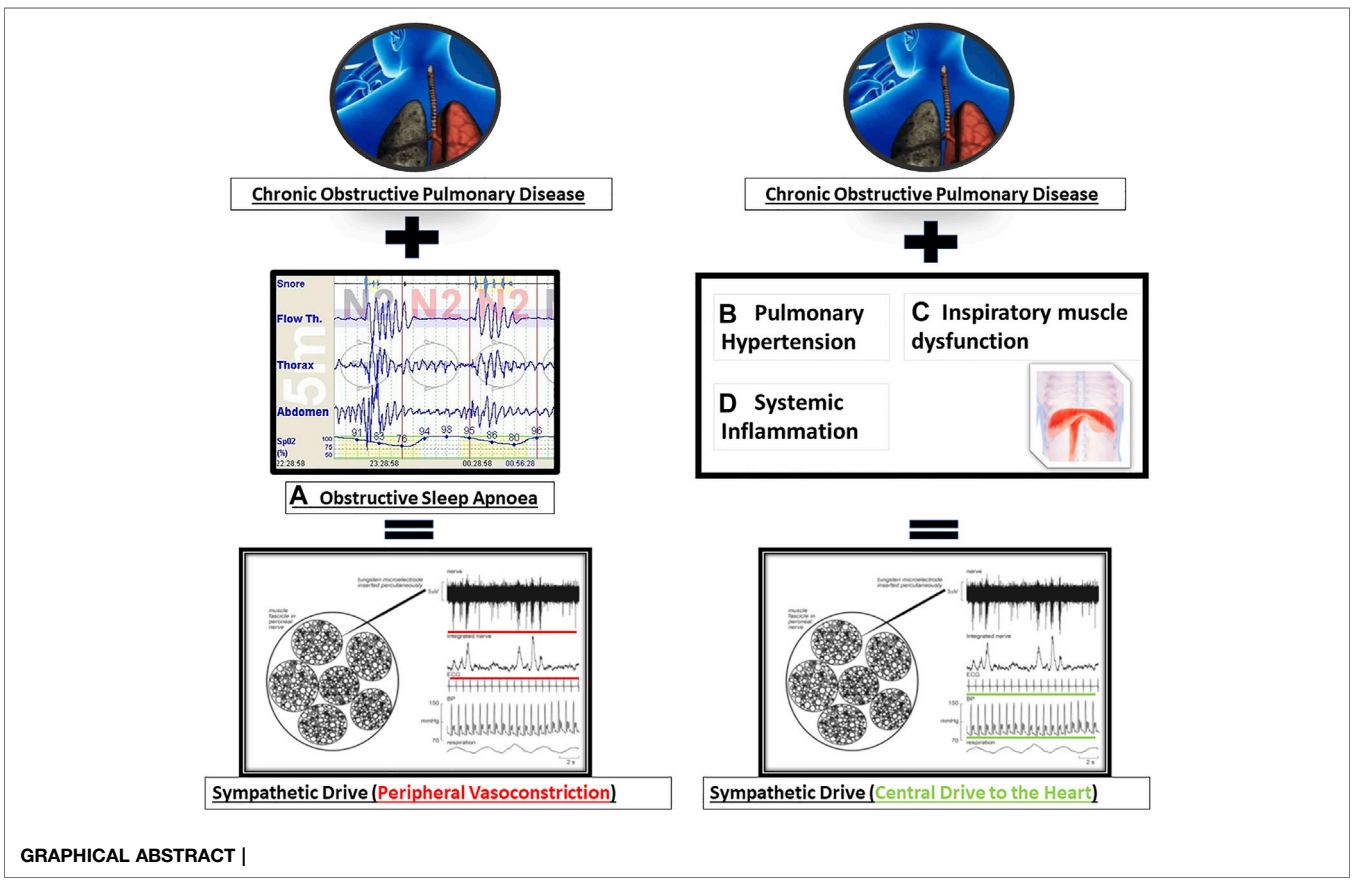

GRAPHICAL ABSTRACT |

1 BACKGROUND TO COPD

Chronic obstructive pulmonary disease (COPD) is a disease characterised by chronic airflow limitation, especially in expiration. Obstruction and hyperinflation alongside systemic inflammation burden the respiratory muscles, especially the diaphragm, which may lead to chronic ventilatory insufficiency with first nocturnal, and later daytime, hypercapnia throughout the disease course (Ntritsos et al., 2018). However, clinically different phenotypes—including hypercapnic variants—of COPD can be encountered, that were traditionally referred to as "pink puffers" with predominantly emphysematous changes to the lung, and "blue bloaters" with predominantly air trapping and hyperinflation (Ntritsos et al., 2018).

According to global prevalence estimates, approximately 9% of men and 6% of women have COPD, making it one of the most prevalent diseases worldwide, and the incidence of COPD is expected to increase further based on population demographics. In both COPD phenotypes, particularly in cases showing overlapping features, the disease has a significant impact and is one of the major causes of death in the developed world (Ntritsos et al., 2018).

Strategies to improve the overall prognosis of patients with COPD are therefore highly desirable. However, although

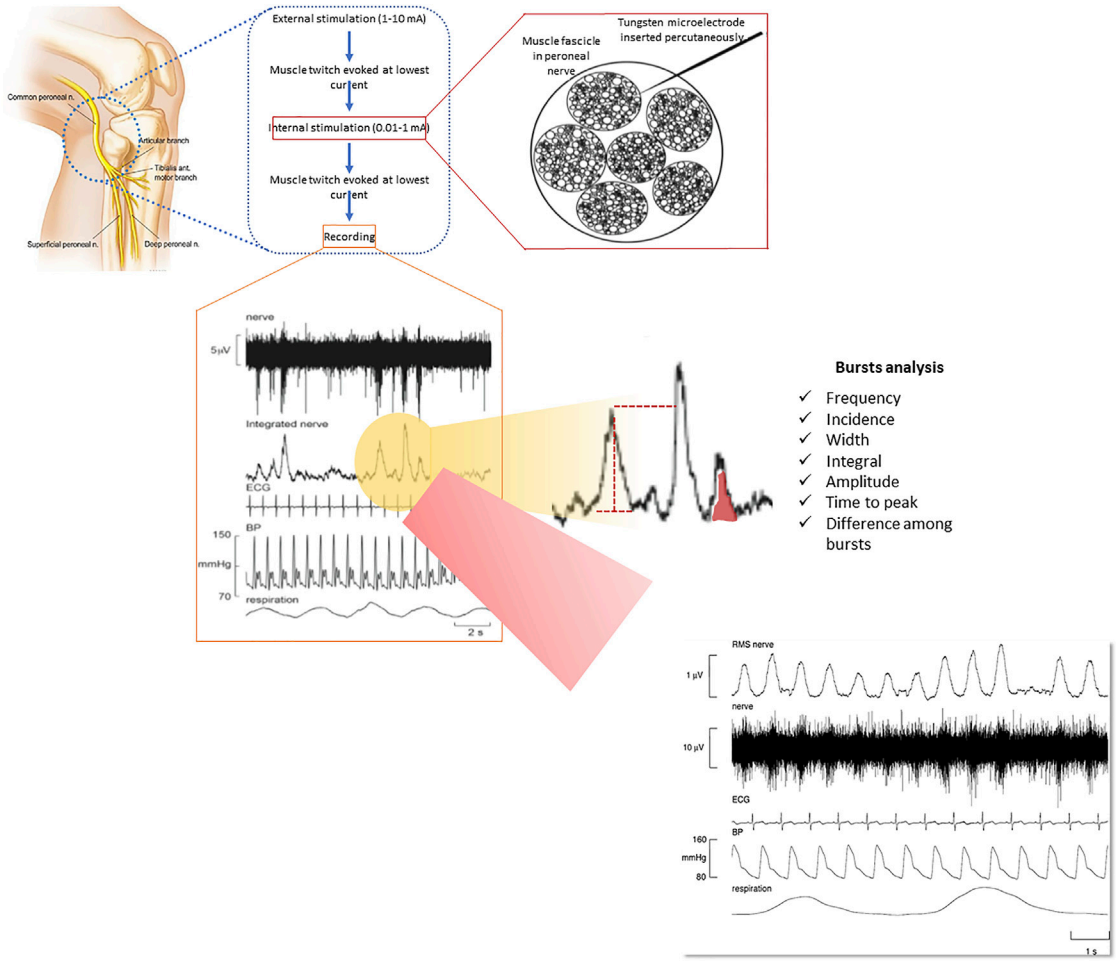

FIGURE 1 | Methodology of recording muscle sympathetic nerve activity (MSNA) through microneurography and its elevation in a patient with COPD. Reproduced, with permission, from Ashley et al. (2010). MSNA is measured via a tungsten microelectrode inserted percutaneously into a muscle fascicle of an accessible peripheral nerve. Various components of the bursts can be measured, providing a comprehensive assessment of muscle vasoconstrictor drive that is put into a broader context of other physiological signals, including heart rate, blood pressure and respiration (see lower part of the figure for representative recordings).

guideline-based therapy with inhaled beta-agonists and anticholinergics improves functional status (and hence the daily symptom burden) in many patients, this pharmacotherapy has not yet been shown to reduce mortality in patients with COPD (Lakshmi et al., 2017; Ntritsos et al., 2018). This makes innovative studies and pathophysiological concepts relating to COPD an extremely important topic.

2 THE SYMPATHETIC NERVE ACTIVITY AXIS AND METHODOLOGY FOR ITS STATE OF THE ART ASSESSMENT

There are several methods for assessing sympathetic nerve activity (SNA). Heart rate (HR) or blood pressure (BP) variability (HRV and BPV, respectively) provide a more general indication of autonomic imbalance and of increases in the heart rate-increasing central drive properties of SNA in particular (Macefield et al., 2010; Karemaker, 2017).

On the other hand catecholamines and MSNA directly reflect the SNA axis and, as such, the peripheral drive to the vasculature (i.e. vasoconstriction) of the SNA axis which also explains lack of clear correlations between HRV, BPV and MSNA (Notarius et al., 1999; Floras, 2009; Macefield et al., 2010; Karemaker, 2017).

In particular, MSNA recordings allow invasive real-time monitoring of the sympathetic burst rate within the efferent peroneal nerve, which provides a direct measure of SNA (Elam et al., 2002; Ashley et al., 2010; Macefield and Wallin, 2018) (**Figure 1**). This methodology represents the gold standard for quantification of SNA in humans (peripheral vasoconstriction in particular) but is only available in few centres worldwide because it is costly, time consuming and requires a high level of training (Heindl et al., 2001; Elam et al., 2002; Macefield et al., 2010). Vaughan Macefield recently developed an approach via which MSNA can be recorded from single neurons rather than

TABLE 1 | Summary of key studies invasively investigating sympathetic nerve activity (SNA) in chronic obstructive pulmonary disease (COPD).

First Author, year (*Journal*)	Cross Sectional	Longitudinal	Intervention (Subjective)	Mortality Endpoint	Key Finding
Heindl, 2001 (*Am J Respir Crit Care Med*)	+	-	-	-	MSNA is increased in COPD
Macefield, 2012 (*Front Physiol*)	+	-	-	-	MSNA is increased in COPD; first in human single unit recording showing that multiple firing is increased in COPD (unlike in systolic heart failure)
Andreas, 2014 (*Lung*)	-	+	-	+	Increased MSNA in COPD is associated with morbidity and mortality
Haarmann, 2015 (*BMC Pulm Med*)	-	+	+	-	Inhaled β-agonist does not modify MSNA in COPD
Haarmann, 2016 (*COPD*)	+	-	-	-	Sympathetic activation is associated with exercise limitation in COPD

from multiple units (Heindl et al., 2001; Elam et al., 2002; Macefield et al., 2010; Macefield and Henderson, 2019). This allows in-depth analysis of MSNA in humans to the point of quantifying the firing frequency, firing probability and the extent of multiple firing of single post ganglionic sympathetic neurons (Heindl et al., 2001; Elam et al., 2002; Macefield et al., 2010; Macefield and Henderson, 2019) (**Figure 1**).

Lack of using a combination of the above mentioned methods in a large enough cohort of patients represents a dilemma because there are methodological limitations if only single metrics of SNA are used. Indeed, using a multimodal approach insights can be generated that facilitate understanding of the nature of increased SNA ("central" heart rate increasing vs peripheral vasoconstriction) in any disease. This also facilitates understanding of the pathophysiological mode of action necessary for any pharmacotherapy to be successful in attacking on increased SNA in various diseases as part of modern precision medicine.

3 COPD: ASSOCIATION WITH INCREASED SYMPATHETIC NERVE ACTIVITY

Increased SNA in COPD has been documented using all the above methods (Keller et al., 1971; Heindl et al., 2001; Elam et al., 2002; Macefield et al., 2010; Chhabra et al., 2015; Mohammed et al., 2015; Goulart et al., 2016; Zangrando et al., 2018). The respiratory and cardiovascular systems are tightly coupled in order to maximise the delivery of oxygen and the removal of carbon dioxide from body tissues. It is therefore not surprising that diseases affecting the respiratory system may have cardiovascular consequences (Macefield, 2012).

Indeed, several studies have documented an increase in MSNA in COPD (Heindl et al., 2001; Raupach et al., 2008; Macefield et al., 2010; Haarmann et al., 2016) (**Table 1**). A Germany based group was the first to prove increased MSNA in COPD in 2001 in 6 hypoxic COPD patients as compared to matched controls. The point was also made that MSNA decreased following oxygen administration (Heindl et al., 2001). In following experiments it was shown by this group that (in 16 normoxic COPD patients) slow breathing reduces MSNA and that there is an association between increased MSNA and limited exercise capacity in patients with COPD (as shown in 16 COPD patients) (Raupach et al., 2008; Haarmann et al., 2016).

However, in COPD the background to increased MSNA likely is multifactorial and therefore deserves a multimodal approach to phenotype (i.e. vasoconstrictive as opposed to central drive to the heart SNA increase) and eventually understand it (**Graphical Abstract Figure 1**).

What is even more striking then is the observation that COPD likely is associated with increased MSNA irrespective of (long before the development of, respectively) concomitant cardiovascular disease (Macefield et al., 2010).

Single-unit recordings, which provide richer information than standard multi-unit recordings of MSNA, have revealed that there is increase in central sympathetic drive in COPD as demonstrated in 18 COPD patients (Macefield et al., 2010). Unlike multi-unit recordings single unit recordings allow for insights into the firing behaviour of single postganglionic muscle vasoconstrictor neurons (Macefield et al., 2010). Compared to healthy subjects with low levels of resting MSNA, single-unit recordings revealed that the augmented MSNA seen in COPD, and systolic heart failure (HF) were each associated with an increase in firing probability and mean firing rates of individual neurons (Macefield et al., 2010). However, unlike patients with heart failure, all patients with COPD exhibited an increase in multiple within-burst firing which, it is argued, reflects an increase in central sympathetic drive (Macefield et al., 2010). These observations emphasize the differences by which the sympathetic nervous system grades its output in health and disease, with an increase in firing probability of active neurons (as seen in COPD) and recruitment of additional neurons (as seen in HF) being the dominant mechanisms (Macefield et al., 2010).

A multi-unit recording (including explanations to its measurement) of MSNA from a patient with COPD is shown in **Figure 1**. In this patient, it can be seen that bursts of MSNA occur with every heartbeat, reflecting a markedly elevated sympathetic outflow. When analyzing MSNA recordings it should be kept in mind that the amplitude of the MSNA bursts is dependent on the position of the needle electrode and it is therefore difficult to obtain comparable inter- and intra-patient recordings (Floras, 2009; Ashley et al., 2010; Macefield et al., 2010; Macefield and Wallin, 2018; Macefield and Henderson, 2019). This can be solved through normalization

procedures or advanced processing of MSNA to obtain calibrated MSNA variability series but it remains an important aspect to consider when applying MSNA recording in large scale pathophysiological studies (Floras, 2009; Ashley et al., 2010; Macefield et al., 2010; Macefield and Wallin, 2018; Macefield and Henderson, 2019).

To the best of our knowledge, the SNA axis has not yet been studied in COPD using a combination of the above mentioned methods in a large enough cohort of patients making it impossible to determine the extent and nature plus the clinical mechanisms and phenotypes responsible for the increase in SNA in COPD to date. In fact, the cohorts of patients in whom MSNA was measured never exceeded 18 COPD patients, a multimodal approach of SNA assessment comprising catecholamines, heart rate and blood pressure variability and MSNA combined has never been applied and MSNA has not yet been put into the context of distinct clinical and physiological phenotypes of COPD patients (obstructive sleep apnea, hypercapnia with inspiratory muscle dysfunction, precapillary pulmonary hypertension (PH), increased levels of systemic inflammation all as reviewed later in this review).

4 LESSONS LEARNED FROM STUDYING SYMPATHETIC NERVE ACTIVITY IN CARDIOVASCULAR DISEASES

Cardiovascular diseases and systolic heart failure (HF) in particular, is a disease in which the relationship between increased sympathetic activity and poor clinical outcomes, and as a therapeutic target, has long been established (Guzzetti et al., 1995; Floras, 2003; Mansfield et al., 2003; Spaak et al., 2005; Floras, 2009; Haarmann et al., 2016). Indeed, elevated levels of MSNA are a better known feature of many diseases affecting the cardiovascular system than of respiratory diseases per se (Grassi et al., 1998; Van De Borne et al., 1998; Elam et al., 2002). This comprises either directly or indirectly HF, essential hypertension, pregnancy-induced hypertension, renovascular hypertension and chronic kidney disease (Elam et al., 2002; Floras, 2009).

Mechanisms for the sympathoexcitation differ in each of these pathophysiological states and are generally still not completely understood, but it is clear that the increase in sympathetic outflow is not limited to the muscle vascular bed but affects many organ systems (Notarius et al., 1999; Floras, 2009; Bruno et al., 2012; Grassi et al., 2019). For example, the sympathoexcitation seen in HF is associated with increases in whole-body (plasma) catecholamines, as well as increases in noradrenaline spillover to the heart and kidneys. Indeed, it is the increase in cardiac sympathetic drive that is deleterious in HF, exacerbating as it does the loss of cardiac function and hence providing the rationale for ß-receptor blockade in HF (Floras, 2009; Grassi et al., 2019). In fact, higher sympathetic outflow has been associated with increased morbidity and mortality in systolic HF (Cohn et al., 1984; Latini et al., 2004; Karasulu et al., 2010).

Therefore, currently recommended therapies for HF target elevated sympathetic outflow (Antman et al., 2016; Jessup et al., 2016; Ponikowski et al., 2016; Seferovic et al., 2019). Many of these guideline-recommended HF treatments (most importantly ß-blockers) have been shown to significantly decrease mortality in patients with HF, something that has not consistently been shown for any COPD treatment to date, despite the fact that COPD is one of the most prevalent diseases worldwide (Lakshmi et al., 2017; Ntritsos et al., 2018).

5 RATIONALE AND AIM TO FOCUS ON SYMPATHETIC NERVE ACTIVITY IN COPD

Despite several previous observations, the underlying mechanisms for the sympathoexcitation seen in COPD and their relationship with concomitant cardiovascular disease are not completely clear. It is known that sustained hypoxaemia (as seen in COPD) causes a long-lasting increase in MSNA and blood pressure, and that this persists even following the return to normoxia (Morgan et al., 1995; Narkiewicz et al., 1999; Tamisier et al., 2005).

Primary lung damage per se, as seen in COPD, also increases plasma catecholamines, irrespective of concomitant cardiovascular disease, suggesting a general increase in sympathetic outflow (Keller et al., 1971). Consecutive inspiratory muscle dysfunction, precapillary PH and systemic inflammation may also be involved, but this has not been investigated or reviewed to date.

Therefore, increased SNA in COPD could explain why patients with COPD are almost three times more likely to die of HF than smokers not diagnosed with COPD (Huiart et al., 2005). Such data suggest that sympathoexcitation may be involved in the pathophysiology of COPD-related mortality, independent of the development of cardiovascular disease in the same COPD patient (Huiart et al., 2005). However, systematic analyses on the mechanisms involved in the sympathoexcitation occurring in patients with COPD are currently lacking, which provides the rationale for this critical review of existing literature. Owing to decisive gaps in knowledge this includes suggestions for future translational research projects that could help elucidate both the precise mechanisms mediating increased SNA and its corresponding clinical phenotypes.

5.1 Obstructive Sleep Apnoea: Overlap With COPD and Impact on Sympathetic Nerve Activity

Obstructive sleep apnoea (OSA) might be one of the most significant determinants of increased MSNA in COPD. Coexisting COPD and OSA is now commonly referred to as "COPD-OSA overlap syndrome" (Kasai et al., 2012; McNicholas, 2018). It is estimated that at least 1 billion people worldwide are affected by OSA, half of whom have moderate to severe (and, therefore, clinically significant) OSA (McNicholas, 2018; Ntritsos et al., 2018; Benjafield et al., 2019). Therefore, the worldwide prevalence of COPD-OSA overlap syndrome in the general population might be as high as 1–2% (McNicholas, 2018).

Despite this, little research has been conducted on the COPD-OSA overlap syndrome (McNicholas, 2018).

The coexistence of COPD and OSA could be associated with particularly high sympathetic outflow, manifested as increased vasoconstriction, that would persist even in the awake state and can be reversed by nocturnal use of continuous positive airway pressure:

This rationale is supported by three arguments.

First, OSA is associated with cyclic oxygen desaturations, and it is known that—as noted above—cyclic hypoxaemia causes a sustained increase in MSNA and BP that persists even after the return to normoxia (Morgan et al., 1995; Tamisier et al., 2005; Macefield, 2012).

Second, it is also known that episodes of airway obstruction during sleep (that can, by definition, be found in OSA patients) cause an increase in MSNA even under normoxic conditions and that this increase also persists in the awake state, leading, in the long term, to the development of arterial hypertension (Morgan et al., 1995; Narkiewicz et al., 1999; Macefield and Elam, 2002; Hansen and Sander, 2003; Tamisier et al., 2005).

Third, OSA is known to have unfavourable effects on sleep architecture, decreasing objective sleep quality and the time spent in deep sleep, all of which adversely impacts on nocturnal MSNA, as recently shown by our group (Spiesshoefer et al., 2019a; Oldenburg and Spiesshoefer, 2020). Alterations in sleep stages with less deep sleep and altered individual chronobiology can potentially cause or promote major cardiovascular diseases through sympathoexcitation, perhaps beyond what might be explained by OSA severity alone (Pagani et al., 1997; Van de Borne et al., 1997; Penzel et al., 2007; Camillo et al., 2011).

Curiously, the clinical phenotype in which such a marked sympathoexcitation with predominantly increased vasoconstriction due to OSA could be encountered, likely corresponds to the phenotype of the "blue bloater" rather than the "pink puffer", a hypothesis that could be investigated in future experiments.

5.2 Lung and Inspiratory Muscle Function as Potential Determinants of Sympathetic Nerve Activity in COPD

Despite being an obstructive lung disease, metrics reflecting inspiratory muscle dysfunction rather than the actual extent of obstruction show the closest association with hypercapnic ventilatory failure in COPD. Inspiratory muscle dysfunction with hypercapnic ventilatory failure in COPD may contribute to an additional increase in sympathetic outflow, but this question has not been addressed to date. In fact, only one recent study showed that maximal inspiratory mouth occlusion pressure (PIMax) is inversely correlated with sympathetic outflow, manifested as a presumed increase in central drive to the heart, as assessed indirectly by heart rate variability, in COPD (Goulart et al., 2016). In line with this, improvements of heart rate variability after exercise training have been documented in COPD patients (Camillo et al., 2011). This makes pulmonary rehabilitation with improvements in muscle strength and exercise capacity a widely available therapeutic approach to reduce increased SNA in COPD.

However, in this study neither inspiratory muscle dysfunction nor MSNA have been directly assessed using gold standard techniques. These would have comprised invasive measurement of the transdiaphragmatic pressure response to supramaximal magnetic cervical phrenic nerve stimulation (CMS) by double balloon catheters and invasive measurement of MSNA by microneurography. Combined application of PIMax, diaphragm ultrasound-derived metrics and cervical phrenic nerve stimulation-derived metrics provides a comprehensive pathophysiological picture of inspiratory muscle function, as evaluated and applied by our group (Spiesshoefer et al., 2019b; Spiesshoefer et al., 2019c; Spiesshoefer et al., 2019d; Spiesshoefer et al., 2020a; Spiesshoefer et al., 2020b).

Clinically, once inspiratory muscle dysfunction is severe enough to result in muscle pump failure, it likely causes nocturnal hypercapnia that then might extend into the awake state in COPD, predisposing to precapillary pulmonary hypertension.

5.3 Pulmonary Hypertension as a Potential Contributor to Sympathetic Nerve Activity in COPD

Precapillary PH might develop in COPD, especially in those with advanced disease and respiratory insufficiency with chronic hypoxemia and/or daytime hypercapnia (Simonneau et al., 2013). PH probably further increases sympathetic outflow in COPD. Indeed, there is evidence that PH and increased right atrial pressure (as a surrogate marker of right heart dysfunction) directly increase sympathetic outflow, occurring as an increase in central drive to the heart, as supported by findings from our group (Velez-Roa et al., 2004; Ciarka et al., 2007; Spiesshoefer et al., 2019e).

This, and additional cardiac function and haemodynamic variables, can be assessed using state-of-the-art comprehensive transthoracic echocardiography, combined with a non-invasive hemodynamic monitor, as recently established by our group (Vahanian et al., 2007; Lang et al., 2015; Oldenburg et al., 2015). However, no study has yet assessed the impact of PH and right HF on MSNA in patients with COPD or COPD-OSA overlap syndrome. Notably, PH may have impact on inspiratory muscle function in COPD, and therefore lung and cardiac insufficiency may influence each other (Kabitz et al., 2008; Spiesshoefer et al., 2019f).

In this context, a comprehensive protocol for ultrasound of the diaphragm (the key inspiratory muscle) has recently been established by our group and applied to patients with precapillary PH levels of differing severity based on the 6-min walking distance (6MWD) (Spiesshoefer et al., 2019f; Spiesshoefer et al., 2020a).

5.4 Inflammation as a Potential Contributor to Sympathetic Nerve Activity in COPD

Systemic inflammation has been reported to be present in COPD, as shown by increased levels of circulating interleukin (IL)-1 beta,

IL-6, tumour necrosis factor-alpha (TNF-α), high-sensitivity C-reactive protein (CRP) and total white blood cell count (Sethi et al., 2012; Barnes, 2013; Chhabra et al., 2015; Okamoto et al., 2015). Levels of these proinflammatory markers most likely increase in response to structural and functional lung function impairment in COPD and impact on inspiratory muscle function as shown by our group in a cohort of patients after lung transplantation (Spiesshoefer et al., 2020c).

Systemic inflammation may have an additive effect on the increase in sympathetic outflow in COPD. Proinflammatory mediators like IL-6 and TNF-α may directly influence inspiratory muscle function, as shown in animal studies (Sethi et al., 2012; Barnes, 2013; Chhabra et al., 2015; Okamoto et al., 2015). Given these proactive effects, these inflammatory markers cannot be considered trivial bystanders of hypoxia, OSA, PH, and inspiratory muscle dysfunction with hypercapnia. Therefore, systemic inflammation, inspiratory muscle function, and potentially sympathetic outflow, may be interrelated in an exponential rather than linear fashion (Spiesshoefer et al., 2019g). Such interrelation has recently been suggested by Chhabra and colleagues, who recently showed a positive correlation between serum IL-6 and the low frequency (0.04–0.15 Hz)/high frequency (0.15–0.40) component ratio of heart rate variability (LF/HF ratio), a marker of sympathetic activation, in patients with COPD (although such an interpretation needs to be made with caution) (Chhabra et al., 2015). Conversely, it has also been shown that inappropriate sympathetic activation may upregulate IL-6 levels (Okamoto et al., 2015).

6 PHARMACOLOGICAL TREATMENT OF INCREASED SYMPATHETIC NERVE ACTIVITY IN COPD

Certainly, given the evidence for an increase in plasma noradrenaline (but not adrenaline), MSNA and "sympathovagal" imbalance in COPD, there is a rationale for pursuing pharmacological means of reducing sympathoexcitation in COPD, such as through the administration of ß1-blockers to protect the heart (Henriksen et al., 1980; Lipworth et al., 2016). However, there have been few systematic studies examining this issue.

The *New England Journal of Medicine* recently reported the results of the first large prospective randomised placebo-controlled trial investigating the effects of a ß-blocker on exacerbations in patients with COPD (Dransfield et al., 2019). In this study, patients aged 40–85 years were randomised to receive either a ß-blocker (extended-release metoprolol, a ß1-antagonist) or placebo (Dransfield et al., 2019). All patients had a clinical history of COPD, with moderate airflow limitation, and were at increased risk of exacerbations, but without an indication for ß-blocker therapy for cardiovascular comorbidities; patients already taking a ß-blocker or with an established indication for these agents were excluded (Dransfield et al., 2019). The trial was designed to address the hypothesis that increased SNA could be linked to COPD-associated lung damage and that reductions in SNA during treatment with a ß-blocker may translate into decreased time to exacerbation and a reduction in exacerbation severity (Dransfield et al., 2019). However, the outcomes of the trial were negative, with a similar time to first COPD exacerbation in the metoprolol and placebo groups (Dransfield et al., 2019).

This result highlights the need for better insights into increased SNA in COPD, allowing identification of a subgroup of COPD patients who might benefit from ß-blocker therapy. Indeed, all patients in this trial were not stratified for factors indicating a potential benefit of ß-blocker therapy, including an increase in sympathetic outflow. In fact, not a single metric of increased sympathetic activity in the COPD patients was specifically assessed at baseline. Clearly, insights into the features and underlying mechanisms, including defining specific clinical phenotypes and measuring a range of physiological variables, are urgently needed to identify patients who may potentially benefit from individualised therapy to reduce sympathoexcitaiton. It therefore likely is the quantification of the single patient cardiovascular and respiratory autonomic profile, possibly obtained by the maximum precision and rigor by using direct recording techniques and the complex analyses of cardiovascular and respiratory coupling, that will maybe help to identify the target COPD population to assess the benefit of beta-blocker therapy in.

Of course, there is also a rationale for locally *increasing* sympathetic outflow in COPD—specifically to the airways—to improve lung function, but would this have adverse effects elsewhere? A recent study showed that inhaled salmeterol, a long-acting $ß_2$-receptor agonist, improved lung function in COPD and caused a small but significant increase in heart rate, but did not affect MSNA (Haarmann et al., 2015).

For successful therapy that targets an increase in cardiac sympathetic drive in COPD, such as the use of a ß-blocker, it would be essential to identify a specific patient phenotype (by physiological and/or clinical variables) characterised by an increase in central drive to the heart, and not just as an increase in MSNA and peripheral vasoconstriction. Curiously, clinically that would likely correspond to the "pink puffer" without OSA and hence predominantly peripheral vasoconstriction, rather than the "blue bloater" phenotype.

Thus, using a comprehensive, multimodal approach and state-of-the-art technology, future research projects must be designed to determine the extent and nature, plus the clinical mechanisms, responsible for the increase in sympathetic outflow in COPD, and their specific targets.

Based on pathophysiological considerations and a small number of previous studies, it can be hypothesised that in COPD patients without an established cardiovascular disease (ideally including age-, sex- and body mass index [BMI]-matched healthy controls) it is concomitant OSA and poor sleep that is independently associated with increased SNA (manifesting as increased drive to the peripheral vasculature with vasoconstriction). Factors including PH, inspiratory muscle dysfunction and systemic inflammation would then likely describe a COPD phenotype characterised by increased SNA manifesting an increased central drive to the heart. It is this subset of COPD patients (presumably without OSA) that needs to be specifically identified and enrolled as part of modern precision medicine trials

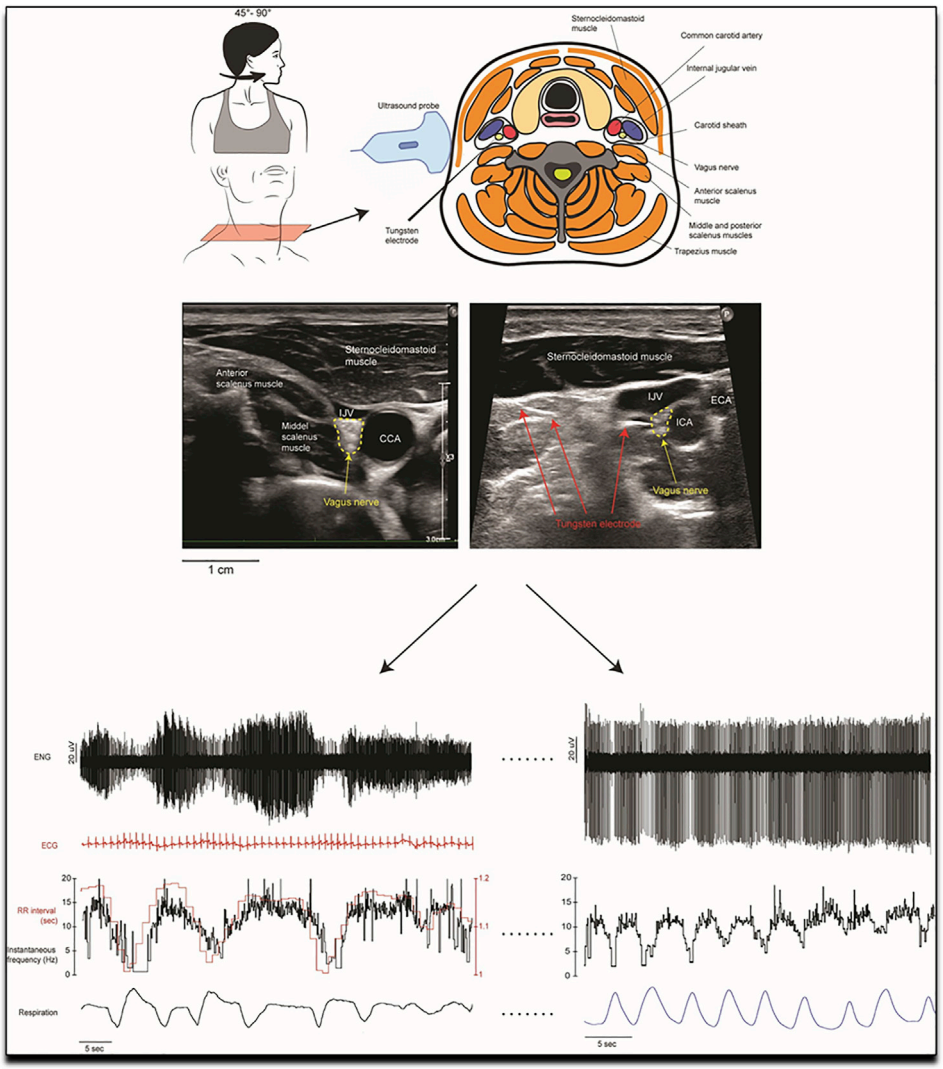

FIGURE 2 | Methodology of the first in human invasive measurement of vagal nerve activity. A tungsten microelectrode is carefully and under ultrasound guidance placed in the vagal nerve, where its activity can then be recorded and analysed. Invasive measurement of vagal nerve activity have not been performed in COPD to date. Reproduced, with permission, from Ottaviani et al. (2020) (Ottaviani et al., 2020). Upper part of the figure: Schematic representation of the orientation of the head, the structures in the neck and the dorsolateral approach of the microelectrode as it is advanced manually towards the right vagus nerve. This approach avoided the carotid artery and jugular vein. The nerve is highlighted in the ultrasound images from two recording sessions which shows the common carotid artery (CCA), internal carotid artery (ICA), external carotid artery (ECA) and the internal jugular vein (IJV) and nearby muscles. The image on the right shows the microelectrode tip as it impales the vagus nerve. Lower part of the figure: Examples of microelectrode recordings from the left cervical vagus nerve in one participant. Lower left recording: The firing of the tonically active unit is covaried with cardiac interval. Variations in spike amplitude reflect slight movements of the microelectrode with neck movements. Superimposed spikes confirm that this was a single-unit recording. Lower right recording: a tonically firing axon, the firing rate of which decreased during inspiration.

in COPD as a crucial step towards achieving a therapeutic benefit of ß-blocker therapy on exacerbations in COPD.

7 THE NOVEL FIELD OF CHANGES IN PARASYMPATHETIC NERVE ACTIVITY IN COPD

While much discussion has been directed towards the sympathoexcitation seen in COPD, we should not forget that the primary neural control of airway diameter is achieved via the parasympathetic nervous system (Stewart et al., 1991; Mohammed et al., 2015; Mohammed et al., 2017; Zangrando et al., 2018). Although circulating hormones and blood gases affect bronchiolar diameter, parasympathetic axons travelling in the vagus nerve supplying the smooth muscle (and glands) of the airways are important in health and disease: bronchomotor neurones are the primary means by which airflow is controlled because there is negligible sympathetic innervation of the airways in humans (van der Beek et al., 2011; Karemaker, 2017).

In COPD a new trial aims to selectively denervate parasympathetic supply to the airways (Slebos et al., 2019). The point should be made

here that selectively denervating parasympathetic supply to the airways is the endpoint here (in an attempt to selectively increase airway diameter, hence decrease the extent of obstruction and hence potentially indirectly decrease SNA overall through improved ventilation and exercise tolerance) and not decreasing parasympathetic drive overall. The background to this is that, clearly, decreased SNA and increased parasympathetic nerve activity should be the pathophysiologically desired endpoints to improve exercise intolerance and potentially mortality in COPD patients. Until recently, the parasympathetic nervous system could only be assessed indirectly in humans, largely through measurement of changes in heart rate variability. However, we now have the means of recording from parasympathetic axons directly, by inserting a microelectrode into the cervical vagus nerve under ultrasound guidance (displayed and explained in greater depth in **Figure 2**) (Ottaviani et al., 2020).

Respiratory and cardiac modulation of multi-unit recordings of vagal activity has recently been quantified (Patros et al., 2022). With few exceptions, the peak of respiratory modulation coincided with the peak of inspiration, whereas the latencies for the peak in cardiac modulation of vagal activity showed a bimodal distribution: some had peak latencies that preceded the synchronising R-wave whereas others had latencies that followed the R-wave (Patros et al., 2022). Unitary recordings from the human vagus nerve will also help us understand how disease affects the behavior of afferents coming from the heart and great vessels, and from the lungs and airways. We propose making parallel recordings from the cervical vagus nerve and from the common peroneal nerve when participants lay on a tilt table, and taking them from the horizontal to near-vertical position; we have success in obtaining stable recordings of muscle sympathetic nerve activity from the leg when tilting participants, and have no doubt about the stability of the vagus nerve recording during this challenge (Ottaviani et al., 2020). However, given the challenges to obtain (mainly in having the needle in the right position) and analyse (see complexity in correlating vagal activity depicted above) these recordings, those measurements will, for now, likely be available in few dedicated expert centres only.

Curiously, inappropriate sympathetic activation was shown to potentially upregulate IL-6 levels and vagal stimulation was suggested as a possible tool to reduce systemic inflammation, in a different pathological population characterized by increased sympathetic modulation—a "positive loop" that hence may also provide a potential novel treatment pathway in COPD (Diedrich et al., 2021).

This will allow us to assess the firing properties of individual preganglionic parasympathetic axons directed to the airways, as well as to the heart, in the same way we have been able to record from single postganglionic sympathetic axons in awake humans (Macefield and Wallin, 2018).

8 TESTING BARORECEPTOR FUNCTION TO OBTAIN A COMPREHENSIVE PICTURE OF SYMPATHETIC AND PARASYMPATHETIC NERVE ACTIVITY IN HUMANS

It is baroreflex-mediated modifications of the sympathetic drive that are responsible for the changes in heart rate, and they partially explain the link between MSNA and heart rate variations (Marchi et al., 2016; Barbic et al., 2019). Indeed, the link between MSNA and arterial pressure (AP) is widely accepted with MSNA burst rate increasing when blood pressure falls and MSNA becoming silent when blood pressure rises as a result of an operating baroreflex that inhibits sympathetic drive (Marchi et al., 2016; Barbic et al., 2019; Furlan et al., 2019). Therefore, to obtain a comprehensive picture of sympathetic nerve activity in humans tilt-table testing is used to unload the low-pressure baroreceptors, emulating the changes on standing. Head-up tilt causes an increase in MSNA to prevent venous pooling and maintain blood pressure (Marchi et al., 2016; Barbic et al., 2019; Furlan et al., 2019). Therefore, such test can determine whether MSNA and heart rate response and hence baroreceptor function is adequate (Marchi et al., 2016; Barbic et al., 2019; Furlan et al., 2019). Until recently only heart rate variability (HRV) has been used, in which spectral analysis separates the signal into a low frequency (0.04–0.15 Hz) and/high frequency (0.15–0.40 Hz) component. The LF/HF ratio has been referred to as sympathovagal balance, with an increase in LF/HF being attributed to an increase in cardiac sympathetic activation drive, although such an interpretation needs to be made with caution (Barbic et al., 2019; Patros et al., 2022). Recently, variability has also been applied to MSNA bursts, with the resulting calibrated MSNA being more suitable in describing sympathetic control in humans than traditional uncalibrated MSNA (Marchi et al., 2016; Barbic et al., 2019). The latter takes into account absolute values for MSNA bursts, which show greater inter- and intra-individual reproducibility, with the LF component of calibrated but not of uncalibrated MSNA being positively related to tilt angle and with the LF power of heart rate and blood pressure (Marchi et al., 2016; Barbic et al., 2019).

As far as heart rate variability analysis is concerned it should be kept in mind that the newer non-linear analyses (symbolic, dynamic and complexity) could be useful in these patients (Serrão et al., 2020).

We propose making parallel recordings from the cervical vagus nerve and from the common peroneal nerve when participants lay on a tilt table, and taking them from the horizontal to near-vertical position; we have success in obtaining stable recordings of muscle sympathetic nerve activity from the leg when tilting participants, and have no doubt about the stability of the vagus nerve recording during this challenge. This will help us, for the first time in humans, to answer the question as to how the firing properties of atrial receptors or baroreceptors from the aortic arch change with changes in gravitational load, how they change in hypertension and systolic heart failure and COPD and how they affect heart rate, blood pressure and sympathetic outflow to the muscle vascular bed.

9 CONCLUSION

Little is currently known about the underlying pathophysiological mechanisms leading to the sympathoexcitation seen in COPD, especially in COPD-OSA overlap syndrome.

Attempts to better understand these mechanisms require a multimodal, systematic approach to assess both the increase in

sympathetic outflow, and to specific target organs, and the presumed underlying clinical mechanisms.

A multimodal, systematic approach should comprise heart rate variability, blood pressure variability, plasma catecholamines and direct recordings of MSNA together to distinguish between differences in sympathetic outflow to the heart and to the muscle vascular bed. Furthermore, the presumed underlying clinical manifestations to assess are OSA and sleep, PH, inspiratory muscle dysfunction and systemic inflammation.

Based on currently available scientific evidence, it likely is OSA with poor sleep that, in the presence of COPD, is independently associated with increased sympathetic Outflow. This is then associated with increased drive to the peripheral vasculature with vasoconstriction. Other clinical variables, namely PH, inspiratory muscle dysfunction and systemic inflammation, may describe additional phenotypes of COPD patients with increased sympathetic outflow to the heart.

By phenotyping COPD patients with regard to the target organs affected by an increase in sympathetic outflow we might define a subgroup that can be enrolled in clinical trials to assess directed pharmacologic treatment. This would be a step towards modern precision medicine in COPD, and a crucial step towards determining the potential therapeutic benefit of ß-blockers on the rate of exacerbations in COPD.

Finally, while much discussion has been directed towards the sympathoexcitation seen in COPD, we should not forget that the primary neural control of airway diameter is achieved via the parasympathetic nervous system. Only now are we invasively assessing the firing properties of individual preganglionic parasympathetic axons directed to the airways, as well as to the heart, in the same way we have been able to record from single postganglionic sympathetic axons in awake humans, more insights into which offer unprecedented future therapeutic potential in COPD.

AUTHOR CONTRIBUTIONS

JS, BR and VM contributed to the conception and design of the present work. JS, BR, and MD contributed to the acquisition, analysis, or interpretation of data for the work. JS, VM, MO, MD, and AG drafted the manuscript, which was critically revised by all authors. All authors gave final approval and agree to be accountable for all aspects of work ensuring integrity and accuracy.

ACKNOWLEDGMENTS

This study was supported in part by the Tuscany Region through the Tuscany Network for Bioelectronic Approaches in Medicine: AI-based predictive algorithms for fine-tuning of electroceutical treatments in neurological, cardiovascular and endocrinological diseases (TUNE-BEAM, H14I20000300002). English language editing assistance was provided by Nicola Ryan, independent medical writer.

REFERENCES

Antman, E. M., Bax, J., Chazal, R. A., Creager, M. A., Filippatos, G., Halperin, J. L., et al. (2016). Updated Clinical Practice Guidelines on Heart Failure: An International Alignment. *Eur. Heart J.* 37, 2096. doi:10.1093/eurheartj/ehw219

Ashley, C., Burton, D., Sverrisdottir, Y. B., Sander, M., McKenzie, D. K., and Macefield, V. G. (2010). Firing Probability and Mean Firing Rates of Human Muscle Vasoconstrictor Neurones Are Elevated during Chronic Asphyxia. *J. Physiol.* 588, 701–712. doi:10.1113/jphysiol.2009.185348

Barbic, F., Heusser, K., Minonzio, M., Shiffer, D., Cairo, B., Tank, J., et al. (2019). Effects of Prolonged Head-Down Bed Rest on Cardiac and Vascular Baroreceptor Modulation and Orthostatic Tolerance in Healthy Individuals. *Front. Physiol.* 10. doi:10.3389/fphys.2019.01061

Barnes, P. J. (2013). New Anti-inflammatory Targets for Chronic Obstructive Pulmonary Disease. *Nat. Rev. Drug Discov.* 12, 543–559. doi:10.1038/nrd4025

Benjafield, A. V., Ayas, N. T., Eastwood, P. R., Heinzer, R., Ip, M. S. M., Morrell, M. J., et al. (2019). Estimation of the Global Prevalence and Burden of Obstructive Sleep Apnoea: a Literature-Based Analysis. *Lancet Respir. Med.* 7, 687–698. doi:10.1016/s2213-2600(19)30198-5

Bruno, R. M., Ghiadoni, L., Seravalle, G., Dell'oro, R., Taddei, S., and Grassi, G. (2012). Sympathetic Regulation of Vascular Function in Health and Disease. *Front. Physiol.* 3, 284. doi:10.3389/fphys.2012.00284

Camillo, C. A., Laburu, V. d. M., Gonçalves, N. S., Cavalheri, V., Tomasi, F. P., Hernandes, N. A., et al. (2011). Improvement of Heart Rate Variability after Exercise Training and its Predictors in COPD. *Respir. Med.* 105, 1054–1062. doi:10.1016/j.rmed.2011.01.014

Chhabra, S. K., Gupta, M., Ramaswamy, S., Dash, D. J., Bansal, V., and Deepak, K. K. (2015). Cardiac Sympathetic Dominance and Systemic Inflammation in COPD. *J. Chronic Obstr. Pulm. Dis.* 12, 552–559. doi:10.3109/15412555.2014.974743

Ciarka, A., Vachièry, J.-L., Houssière, A., Gujic, M., Stoupel, E., Velez-Roa, S., et al. (2007). Atrial Septostomy Decreases Sympathetic Overactivity in Pulmonary Arterial Hypertension. *Chest* 131, 1831–1837. doi:10.1378/chest.06-2903

Cohn, J. N., Levine, T. B., Olivari, M. T., Garberg, V., Lura, D., Francis, G. S., et al. (1984). Plasma Norepinephrine as a Guide to Prognosis in Patients with Chronic Congestive Heart Failure. *N. Engl. J. Med.* 311, 819–823. doi:10.1056/nejm198409273111303

Diedrich, A., Urechie, V., Shiffer, D., Rigo, S., Minonzio, M., Cairo, B., et al. (2021). Transdermal Auricular Vagus Stimulation for the Treatment of Postural Tachycardia Syndrome. *Aut. Neurosci.* 236, 102886. doi:10.1016/j.autneu.2021.102886

Dransfield, M. T., Voelker, H., Bhatt, S. P., Brenner, K., Casaburi, R., Come, C. E., et al. (2019). Metoprolol for the Prevention of Acute Exacerbations of COPD. *N. Engl. J. Med.* 381, 2304–2314. doi:10.1056/nejmoa1908142

Elam, M., McKenzie, D., and Macefield, V. (2002). Mechanisms of Sympathoexcitation: Single-Unit Analysis of Muscle Vasoconstrictor Neurons in Awake OSAS Subjects. *J. Appl. Physiology* 93, 297–303. doi:10.1152/japplphysiol.00899.2001

Floras, J. S. (2003). Sympathetic Activation in Human Heart Failure: Diverse Mechanisms, Therapeutic Opportunities. *Acta Physiol. Scand.* 177, 391–398. doi:10.1046/j.1365-201x.2003.01087.x

Floras, J. S. (2009). Sympathetic Nervous System Activation in Human Heart Failure. *J. Am. Coll. Cardiol.* 54, 375–385. doi:10.1016/j.jacc.2009.03.061

Furlan, R., Heusser, K., Minonzio, M., Shiffer, D., Cairo, B., Tank, J., et al. (2019). Cardiac and Vascular Sympathetic Baroreflex Control during Orthostatic Pre-syncope. *J. Clin. Med.* 8, 1434. doi:10.3390/jcm8091434

Goulart, C. d. l., Cristiano Simon, J., De Borba Schneiders, P., Antunes San Martin, E., Cabiddu, R., Borghi-silva, A., et al. (2016). Respiratory Muscle Strength Effect on Linear and Nonlinear Heart Rate Variability Parameters in COPD Patients. *Int. J. Chron. Obstruct Pulmon Dis.* 11, 1671–1677. doi:10.2147/copd.s108860

Grassi, G., Cattaneo, B. M., Seravalle, G., Lanfranchi, A., and Mancia, G. (1998). Baroreflex Control of Sympathetic Nerve Activity in Essential and Secondary Hypertension. *Hypertension* 31, 68–72. doi:10.1161/01.hyp.31.1.68

Grassi, G., D'Arrigo, G., Pisano, A., Bolignano, D., Mallamaci, F., Dell'Oro, R., et al. (2019). Sympathetic Neural Overdrive in Congestive Heart Failure and its Correlates. *J. Hypertens.* 37, 1746–1756. doi:10.1097/hjh.0000000000002093

Guzzetti, S., Cogliati, C., Turiel, M., Crema, C., Lombardi, F., and Malliani, A. (1995). Sympathetic Predominance Followed by Functional Denervation in the Progression of Chronic Heart Failure. *Eur. Heart J.* 16, 1100–1107. doi:10.1093/oxfordjournals.eurheartj.a061053

Haarmann, H., Mohrlang, C., Tschiesner, U., Rubin, D. B., Bornemann, T., Rüter, K., et al. (2015). Inhaled β-agonist Does Not Modify Sympathetic Activity in Patients with COPD. *BMC Pulm. Med.* 15, 46–10. doi:10.1186/s12890-015-0054-7

Haarmann, H., Folle, J., Nguyen, X. P., Herrmann, P., Heusser, K., Hasenfuß, G., et al. (2016). Sympathetic Activation Is Associated with Exercise Limitation in COPD. *J. Chronic Obstr. Pulm. Dis.* 13, 589–594. doi:10.3109/15412555.2015.1136272

Hansen, J., and Sander, M. (2003). Sympathetic Neural Overactivity in Healthy Humans after Prolonged Exposure to Hypobaric Hypoxia. *J. Physiology* 546, 921–929. doi:10.1113/jphysiol.2002.031765

Heindl, S., Lehnert, M., Criée, C.-P., Hasenfuss, G., and Andreas, S. (2001). Marked Sympathetic Activation in Patients with Chronic Respiratory Failure. *Am. J. Respir. Crit. Care Med.* 164, 597–601. doi:10.1164/ajrccm.164.4.2007085

Henriksen, J. H., Christensen, N. J., Kok-Jensen, A., and Christiansen, I. (1980). Increased Plasma Noradrenaline Concentration in Patients with Chronic Obstructive Lung Disease: Relation to Haemodynamics and Blood Gases. *Scand. J. Clin. Laboratory Investigation* 40, 419–427. doi:10.3109/00365518009101864

Huiart, L., Ernst, P., and Suissa, S. (2005). Cardiovascular Morbidity and Mortality in COPD. *Chest* 128, 2640–2646. doi:10.1378/chest.128.4.2640

Jessup, M., Marwick, T. H., Ponikowski, P., Voors, A. A., and Yancy, C. W. (2016). 2016 ESC and ACC/AHA/HFSA Heart Failure Guideline Update - what Is New and Why Is it Important? *Nat. Rev. Cardiol.* 13, 623–628. doi:10.1038/nrcardio.2016.134

Kabitz, H.-J., Schwoerer, A., Bremer, H.-C., Sonntag, F., Walterspacher, S., Walker, D., et al. (2008). Impairment of Respiratory Muscle Function in Pulmonary Hypertension. *Eur. Respir. J.* 114, 165–171. doi:10.1042/cs20070238

Karasulu, L., Epöztürk, P. Ö., Sökücü, S. N., Dalar, L., and Altın, S. (2010). Improving Heart Rate Variability in Sleep Apnea Patients: Differences in Treatment with Auto-Titrating Positive Airway Pressure (APAP) versus Conventional CPAP. *Lung* 188, 315–320. doi:10.1007/s00408-010-9237-4

Karemaker, J. M. (2017). An Introduction into Autonomic Nervous Function. *Physiol. Meas.* 38, R89–R118. doi:10.1088/1361-6579/aa6782

Kasai, T., Floras, J. S., and Bradley, D. (2012). Sleep Apnea and Cardiovascular Disease: a Bidirectional Relationship. *Circulation* 126, 1495–1510. doi:10.1161/CIRCULATIONAHA.111.070813

Keller, R., Lohmann, F. W., and Schüren, K. P. (1971). Catecholamines in Chronic Respiratory Insufficiency. *Respiration* 28, 273–279. doi:10.1159/000192843

Lakshmi, S., Reddy, A., and Reddy, R. (2017). Emerging Pharmaceutical Therapies for COPD. *Copd* 12, 2141–2156. doi:10.2147/copd.s121416

Lang, R. M., Badano, L. P., Mor-avi, V., Afilalo, J., Armstrong, A., Ernande, L., et al. (2015). Recommendations for Cardiac Chamber Quantification by Echocardiography in Adults: An Update from the American Society of Echocardiography and the European Association of Cardiovascular Imaging. *J. Am. Soc. Echocardiogr.* 28, 1–39. e14. doi:10.1016/j.echo.2014.10.003

Latini, R., Masson, S., Anand, I., Monica, S., Allen, H., Dianne, J., et al. (2004). The Comparative Prognostic Value of Plasma Neurohormones at Baseline in Patients with Heart Failure Enrolled in Val-HeFT. *Eur. Heart J.* 25, 292–299. doi:10.1016/j.ehj.2003.10.030

Lipworth, B., Wedzicha, J., Devereux, G., Vestbo, J., and Dransfield, M. T. (2016). Beta-blockers in COPD: Time for Reappraisal. *Eur. Respir. J.* 48, 880–888. doi:10.1183/13993003.01847-2015

Macefield, V. G., Wallin, B. G., and Haarmann, H. (2010). Firing Patterns of Muscle Vasoconstrictor Neurons in Respiratory Disease. *J. Physiol.* 588, 925–931. doi:10.3389/fphys.2012.00153

Macefield, V. G., and Elam, M. (2002). Prolonged Surges of Baroreflex-Resistant Muscle Sympathetic Drive during Periodic Breathing. *Clin. Aut. Res.* 12, 165–169. doi:10.1007/s10286-002-0032-z

Macefield, V. G. (2012). Firing Patterns of Muscle Vasoconstrictor Neurons in Respiratory Disease. *Front. Physio.* 3, 153–159. doi:10.3389/fphys.2012.00153

Macefield, V. G., and Henderson, L. A. (2019). Identification of the Human Sympathetic Connectome Involved in Blood Pressure Regulation. *Neuroimage* 202, 116119. doi:10.1016/j.neuroimage.2019.116119

Macefield, V. G., and Wallin, B. G. (2018). Physiological and Pathophysiological Firing Properties of Single Postganglionic Sympathetic Neurons in Humans. *J. Neurophysiology* 119, 944–956. doi:10.1152/jn.00004.2017

Mansfield, D., Kaye, D. M., Brunner La Rocca, H., Solin, P., Esler, M. D., and Naughton, M. T. (2003). Raised Sympathetic Nerve Activity in Heart Failure and Central Sleep Apnea Is Due to Heart Failure Severity. *Circulation* 107, 1396–1400. doi:10.1161/01.cir.0000056520.17353.4f

Marchi, A., Bari, V., De Maria, B., Esler, M., Lambert, E., Baumert, M., et al. (2016). Calibrated Variability of Muscle Sympathetic Nerve Activity during Graded Head-Up Tilt in Humans and its Link with Noradrenaline Data and Cardiovascular Rhythms. *Am. J. Physiology-Regulatory, Integr. Comp. Physiology* 310, R1134–R1143. doi:10.1152/ajpregu.00541.2015

McNicholas, W. T. (2018). Comorbid Obstructive Sleep Apnoea and Chronic Obstructive Pulmonary Disease and the Risk of Cardiovascular Disease. *J. Thorac. Dis.* 10, S4253–S4261. doi:10.21037/jtd.2018.10.117

Mohammed, J., Da Silva, H., Van Oosterwijck, J., and Calders, P. (2017). Effect of Respiratory Rehabilitation Techniques on the Autonomic Function in Patients with Chronic Obstructive Pulmonary Disease: A Systematic Review. *Chron. Respir. Dis.* 14, 217–230. doi:10.1177/1479972316680844

Mohammed, J., Meeus, M., Derom, E., Da Silva, H., and Calders, P. (2015). Evidence for Autonomic Function and its Influencing Factors in Subjects with COPD: A Systematic Review. *Respir. Care* 60, 1841–1851. doi:10.4187/respcare.04174

Morgan, B. J., Crabtree, D. C., Palta, M., and Skatrud, J. B. (1995). Combined Hypoxia and Hypercapnia Evokes Long-Lasting Sympathetic Activation in Humans. *J. Appl. Physiology* 79, 205–213. doi:10.1152/jappl.1995.79.1.205

Narkiewicz, K., Kato, M., Phillips, B. G., Pesek, C. A., Davison, D. E., and Somers, V. K. (1999). Nocturnal Continuous Positive Airway Pressure Decreases Daytime Sympathetic Traffic in Obstructive Sleep Apnea. *Circulation* 100, 2332–2335. doi:10.1161/01.cir.100.23.2332

Notarius, C. F., Butler, G. C., Ando, S.-i., Pollard, M. J., Senn, B. L., and Floras, J. S. (1999). Dissociation between Microneurographic and Heart Rate Variability Estimates of Sympathetic Tone in Normal Subjects and Patients with Heart Failure. *Clin. Sci.* 96, 557–565. doi:10.1042/cs19980347

Ntritsos, G., Franek, J., Belbasis, L., Christou, M. A., Markozannes, G., Altman, P., et al. (2018). Gender-specific Estimates of COPD Prevalence: A Systematic Review and Meta-Analysis. *Copd* 13, 1507–1514. doi:10.2147/copd.s146390

Okamoto, L. E., Raj, S. R., Gamboa, A., Shibao, C. A., Arnold, A. C., Garland, E. M., et al. (2015). Sympathetic Activation Is Associated with Increased IL-6, but Not CRP in the Absence of Obesity: Lessons from Postural Tachycardia Syndrome and Obesity. *Am. J. Physiology-Heart Circulatory Physiology* 309, H2098–H2107. doi:10.1152/ajpheart.00409.2015

Oldenburg, O., and Spiesshoefer, J. (2020). Impact of Lifestyle on Sleep. *J. Am. Coll. Cardiol.* 75, 1000–1002. doi:10.1016/j.jacc.2019.12.055

Oldenburg, O., Spießhöfer, J., Fox, H., Bitter, T., and Horstkotte, D. (2015). Cheyne-Stokes Respiration in Heart Failure: Friend or Foe? Hemodynamic Effects of Hyperventilation in Heart Failure Patients and Healthy Volunteers. *Clin. Res. Cardiol.* 104, 328–333. doi:10.1007/s00392-014-0784-1

Ottaviani, M. M., Wright, L., Dawood, T., and Macefield, V. G. (2020). *In Vivo* recordings from the Human Vagus Nerve Using Ultrasound-guided Microneurography. *J. Physiol.* 598, 3569–3576. doi:10.1113/jp280077

Pagani, M., Montano, N., Porta, A., Malliani, A., Abboud, F. M., Birkett, C., et al. (1997). Relationship between Spectral Components of Cardiovascular Variabilities and Direct Measures of Muscle Sympathetic Nerve Activity in Humans. *Circulation* 95, 1441–1448. doi:10.1161/01.cir.95.6.1441

Patros, M., Ottaviani, M. M., Wright, L., Dawood, T., and Macefield, V. G. (2022). Quantification of Cardiac and Respiratory Modulation of Axonal Activity in the Human Vagus Nerve. *J. Physiology*. doi:10.1113/JP282994

Penzel, T., Wessel, N., Riedl, M., Kantelhardt, J. W., Rostig, S., Glos, M., et al. (2007). Cardiovascular and Respiratory Dynamics during Normal and Pathological Sleep. *Chaos* 17, 015116. doi:10.1063/1.2711282

Ponikowski, P., Voors, A. A., Anker, S. D., Bueno, H., Cleland, J. G. F., Coats, A. J. S., et al. (2016). 2016 ESC Guidelines for the Diagnosis and Treatment of Acute and Chronic Heart Failure. *Eur. J. Heart Fail* 18, 891–975. doi:10.1002/ejhf.592

Raupach, T., Bahr, F., Herrmann, P., Luethje, L., Heusser, K., Hasenfuss, G., et al. (2008). Slow Breathing Reduces Sympathoexcitation in COPD. *Eur. Respir. J.* 32, 387–392. doi:10.1183/09031936.00109607

Seferovic, P. M., Ponikowski, P., Anker, S. D., Bauersachs, J., Chioncel, O., Cleland, J. G. F., et al. (2019). Clinical Practice Update on Heart Failure 2019: Pharmacotherapy, Procedures, Devices and Patient Management. An Expert Consensus Meeting Report of the Heart Failure Association of the European Society of Cardiology. *Eur. J. Heart Fail* 21, 1169–1186. doi:10.1002/ejhf.1531

Serrão, N. F., Jr, Porta, A., Minatel, V., Castro, A. A. M., Catai, A. M., Sampaio, L. M. M., et al. (2020). Complexity Analysis of Heart Rate Variability in Chronic Obstructive Pulmonary Disease: Relationship with Severity and Symptoms. *Clin. Auton. Res.* 30, 157–164. doi:10.1007/s10286-019-00659-z

Sethi, S., Mahler, D. A., Marcus, P., Owen, C. A., Yawn, B., and Rennard, S. (2012). Inflammation in COPD: Implications for Management. *Am. J. Med.* 125, 1162–1170. doi:10.1016/j.amjmed.2012.06.024

Simonneau, G., Gatzoulis, M. A., Adatia, I., Celermajer, D., Denton, C., Ghofrani, A., et al. (2013). Updated Clinical Classification of Pulmonary Hypertension. *J. Am. Coll. Cardiol.* 62, D34–D41. doi:10.1016/j.jacc.2013.10.029

Slebos, D. J., Shah, P. L., Herth, F. J. F., Pison, C., Schumann, C., Hübner, R. H., et al. (2019). Safety and Adverse Events after Targeted Lung Denervation for Symptomatic Moderate to Severe Chronic Obstructive Pulmonary Disease (AIRFLOW). A Multicenter Randomized Controlled Clinical Trial. *Am. J. Respir. Crit. Care Med.* 200, 1477–1486. doi:10.1164/rccm.201903-0624OC

Spaak, J., Egri, Z. J., Kubo, T., Yu, E., Ando, S.-I., Kaneko, Y., et al. (2005). Muscle Sympathetic Nerve Activity during Wakefulness in Heart Failure Patients with and without Sleep Apnea. *Hypertension* 46, 1327–1332. doi:10.1161/01.hyp.0000193497.45200.66

Spiesshoefer, J., Boentert, M., Tuleta, I., Giannoni, A., Langer, D., and Kabitz, H. J. (2019). Diaphragm Involvement in Heart Failure: Mere Consequence of Hypoperfusion or Mediated by Hf-Related Pro-inflammatory Cytokine Storms? *Front. Physiol.* 10, 1335–1336. doi:10.3389/fphys.2019.01335

Spiesshoefer, J., Henke, C., Herkenrath, S., Randerath, W., Schneppe, M., Young, P., et al. (2019). Electrophysiological Properties of the Human Diaphragm Assessed by Magnetic Phrenic Nerve Stimulation: Normal Values and Theoretical Considerations in Healthy Adults. *J. Clin. Neurophysiol.* 36, 375–384. doi:10.1097/WNP.0000000000000608

Spiesshoefer, J., Henke, C., Herkenrath, S., Winfried, R., Tobias, B., Peter, Y., et al. (2019). Assessment of Central Drive to the Diaphragm by Twitch Interpolation: Normal Values, Theoretical Considerations, and Future Directions. *Respiration* 98 (4), 283–293. doi:10.1159/000500726

Spiesshoefer, J., Herkenrath, S., Mohr, M., Randerath, W., Tuleta, I., Diller, G. P., et al. (2019). Diaphragm Function Does Not Independently Predict Exercise Intolerance in Patients with Precapillary Pulmonary Hypertension after Adjustment for Right Ventricular Function. *Biosci. Rep.* 39, BSR20190392. doi:10.1042/BSR20190392

Spiesshoefer, J., Becker, S., Tuleta, I., Mohr, M., Diller, G. P., Emdin, M., et al. (2019). Impact of Simulated Hyperventilation and Periodic Breathing on Sympatho-Vagal Balance and Hemodynamics in Patients with and without Heart Failure. *Respiration* 98, 482–494. doi:10.1159/000502155

Spiesshoefer, J., Henke, C., Herkenrath, S., Brix, T., Randerath, W., Young, P., et al. (2019). Transdiapragmatic Pressure and Contractile Properties of the Diaphragm Following Magnetic Stimulation. *Respir. Physiology Neurobiol.* 266, 47–53. doi:10.1016/j.resp.2019.04.011

Spiesshoefer, J., Henke, C., Kabitz, H. J., Nofer, J. R., Mohr, M., Evers, G., et al. (2020). Respiratory Muscle and Lung Function in Lung Allograft Recipients: Association with Exercise Intolerance. *Respiration* 99, 398–408. doi:10.1159/000507264

Spiesshoefer, J., Herkenrath, S., Henke, C., Langenbruch, L., Schneppe, M., Randerath, W., et al. (2020). Evaluation of Respiratory Muscle Strength and Diaphragm Ultrasound: Normative Values, Theoretical Considerations, and Practical Recommendations. *Respiration* 99, 369–381. doi:10.1159/000506016

Spiesshoefer, J., Linz, D., Skobel, E., Arzt, M., Stadler, S., Schoebel, C., et al. (2019). Sleep - the yet Underappreciated Player in Cardiovascular Diseases: A Clinical Review from the German Cardiac Society Working Group on Sleep Disordered Breathing. *Eur. J. Prev. Cardiol.* 28, 189–200. doi:10.1177/2047487319879526

Spiesshoefer, J., Orwat, S., Henke, C., Kabitz, H.-J., Katsianos, S., Borrelli, C., et al. (2020). Inspiratory Muscle Dysfunction and Restrictive Lung Function Impairment in Congenital Heart Disease: Association with Immune Inflammatory Response and Exercise Intolerance. *Int. J. Cardiol.* 318, 45–51. doi:10.1016/j.ijcard.2020.06.055

Stewart, A. G., Waterhouse, J. C., and Howard, P. (1991). Cardiovascular Autonomic Nerve Function in Patients with Hypoxaemic Chronic Obstructive Pulmonary Disease. *Eur. Respir. J.* 4, 1207–1214.

Tamisier, R., Anand, A., Nieto, L. M., Cunnington, D., and Weiss, J. W. (2005). Arterial Pressure and Muscle Sympathetic Nerve Activity Are Increased after Two Hours of Sustained but Not Cyclic Hypoxia in Healthy Humans. *J. Appl. Physiology* 98, 343–349. doi:10.1152/japplphysiol.00495.2004

Vahanian, A., Baumgartner, H., Bax, J., Butchart, E., Dion, R., Filippatos, G., et al. (2007). Guidelines on the Management of Valvular Heart Disease: The Task Force on the Management of Valvular Heart Disease of the European Society of Cardiology. *Eur. Heart J.* 28, 230–268. doi:10.1093/eurheartj/ehl428

Van de Borne, P., Montano, N., Zimmerman, B., Pagani, M., and Somers, V. K. (1997). Relationship between Repeated Measures of Hemodynamics, Muscle Sympathetic Nerve Activity, and Their Spectral Oscillations. *Circulation* 96, 4326–4332. doi:10.1161/01.cir.96.12.4326

Van De Borne, P., Oren, R., Abouassaly, C., Anderson, E., and Somers, V. K. (1998). Effect of Cheyne-Stokes Respiration on Muscle Sympathetic Nerve Activity in Severe Congestive Heart Failure Secondary to Ischemic or Idiopathic Dilated Cardiomyopathy. *Am. J. Cardiol.* 81, 432–436. doi:10.1016/s0002-9149(97)00936-3

van der Beek, N. A. M. E., van Capelle, C. I., van der Velden-van Etten, K. I., Hop, W. C. J., van den Berg, B., Reuser, A. J. J., et al. (2011). Rate of Progression and Predictive Factors for Pulmonary Outcome in Children and Adults with Pompe Disease. *Mol. Genet. Metabolism* 104, 129–136. doi:10.1016/j.ymgme.2011.06.012

Velez-Roa, S., Ciarka, A., Najem, B., Vachiery, J.-L., Naeije, R., and van de Borne, P. (2004). Increased Sympathetic Nerve Activity in Pulmonary Artery Hypertension. *Circulation* 110, 1308–1312. doi:10.1161/01.cir.0000140724.90898.d3

Zangrando, K., Trimer, R., Carvalho Jr, L. C. S., Arêas, G., Caruso, F., Cabiddu, R., et al. (2018). Chronic Obstructive Pulmonary Disease Severity and its Association with Obstructive Sleep Apnea Syndrome: Impact on Cardiac Autonomic Modulation and Functional Capacity. *Copd* 13, 1343–1351. doi:10.2147/copd.s156168

Conflict of Interest: The authors declare that the research was conducted in the absence of any commercial or financial relationships that could be construed as a potential conflict of interest.

Publisher's Note: All claims expressed in this article are solely those of the authors and do not necessarily represent those of their affiliated organizations, or those of the publisher, the editors and the reviewers. Any product that may be evaluated in this article, or claim that may be made by its manufacturer, is not guaranteed or endorsed by the publisher.

frontiers | Frontiers in Neuroscience

ORIGINAL RESEARCH
published: 15 July 2022
doi: 10.3389/fnins.2022.907658

A Temporospatial Study of Sympathetic Skin Response and Electroencephalogram in Oral Mucosa Thermal Perception

Hao Zhang[1†], Shengjing Hu[2†], Zhangang Wang[3], Xiang Li[4], Suogang Wang[2] and Gang Chen[1*]*

[1] Department of Oral and Maxillofacial Surgery, School of Stomatology, Tianjin Medical University, Tianjin, China, [2] School of Biomedical Engineering and Technology, Tianjin Medical University, Tianjin, China, [3] Changzhou Hospital of Traditional Chinese Medicine, Changzhou, China, [4] Department of Oral Surgery, School of Dentistry, University of Birmingham, Birmingham, United Kingdom

OPEN ACCESS

Edited by:
Vaughan G. Macefield, Baker Heart and Diabetes Institute, Australia

Reviewed by:
Songsong Zhu, Sichuan University, China
Ubedullah Kaka, University of Putra Malaysia, Malaysia

***Correspondence:**
Gang Chen
doctorchen@tmu.edu.cn
Suogang Wang
suogangwang@tmu.edu.cn

[†] These authors have contributed equally to this work and share first authorship

Specialty section:
This article was submitted to Autonomic Neuroscience, a section of the journal Frontiers in Neuroscience

Received: *30 March 2022*
Accepted: *23 June 2022*
Published: *15 July 2022*

Citation:
Zhang H, Hu S, Wang Z, Li X, Wang S and Chen G (2022) A Temporospatial Study of Sympathetic Skin Response and Electroencephalogram in Oral Mucosa Thermal Perception. Front. Neurosci. 16:907658. doi: 10.3389/fnins.2022.907658

Objective: To investigate the temporospatial changes in sympathetic skin response (SSR) and electroencephalogram (EEG) under thermal stimuli and to draw a topographic map of SSR threshold temperature of the oral mucosa.

Materials and Methods: A total of 40 healthy volunteers (24 men, 16 women, mean age of 23 ± 3) were enrolled. Thermal stimuli were applied to the 35 partitions of oral mucosa starting from 36°C at the gradience of 1°C and the lowest temperature evoked SSR was defined as SSR threshold temperature. SSR and EEG signals at 45, 48, 51, and 54°C were then recorded synchronously.

Results: The SSR threshold temperature increased from the anterior areas to the posterior areas. No significant difference between bilateral corresponding areas or between genders was observed. The SSR amplitude value increased from 45 to 54°C in the same area, while the highest value was recorded on the tip of the tongue and decreased backwardly from the anterior area. There were significant differences in latency of SSR between the tip of the tongue and the molar areas of the oral cavity ($p < 0.05$). Reduction in the alpha frequency band was observed after thermal stimuli, and there were statistical differences between baseline and thermal stimuli in all four degrees of temperatures ($p < 0.05$).

Conclusion: The result of the experiment revealed that the autonomic and central nervous system (CNS) played important roles in thermal perception of oral mucosa and could be helpful for better understanding of pathological mechanism of burning mouth syndrome (BMS).

Keywords: sympathetic skin response, electroencephalogram, autonomic nervous system, oral mucosa, thermal perception

INTRODUCTION

Thermal perception is one of the essential senses. As the initial part of the digestion system, oral mucosa played a significant role in perception, protection, and secretion by acting as a major barrier (Liu et al., 2015). Thermal stimuli that exceed the threshold of thermal perception of the oral mucosa can lead to unpleasant feelings and even injury (Petrus et al., 2007; Wei et al., 2011; Nakamura et al., 2012). In addition, in our clinical practice, the patient who suffered from burning mouth syndrome (BMS) usually complained about painful heat feeling without real stimuli and obvious mucosal pathology. This could be potentially explained by hypothesis of nerve damage or sensory abnormalities (Forssell et al., 2002; Hagelberg et al., 2003).

The sympathetic skin response (SSR) was referred to as the process of a transient change in skin action potential upon receipt of external or internal stimulation (Vetrugno et al., 2003). Hilz et al. (1999) demonstrated the feasibility of evoking SSR by means of thermal stimuli. Moreover, temperature nociceptors and receptors were involved in the nervous control of sweat glands (Karl et al., 1975). In addition, Koszewicz et al. (2012) revealed significant prolongation of SSR latency in the foot of patients with burning mouth syndrome. However, there were few studies on the difference in the temperature-sensing ability between various areas of the oral mucosa, and studies on the SSR evoked by oral mucosal upon thermal temperature stimuli are limited.

Electroencephalogram (EEG) is a recording of typical physiological signals of the central nervous system (Pachori and Bajaj, 2011), which can be used to detect the response of the brain to temperature sense. The EEG was chosen as a central nervous system (CNS) index due to its importance in measuring and monitoring cerebral cortical activity as well as its sensitivity to arousal fluctuation (Evans, 1993; Makeig and Inlow, 1993). Huber et al. (2006) investigated the effects of tonic heat pain on EEG rhythmic components and found that brain power in the delta band increased in most of the brain regions during tonic heat stimuli, while the theta band power in the frontotemporal diminished. In the meanwhile, the power in the alpha band was reduced, while beta power was increased (Huber et al., 2006).

Sympathetic skin response and EEG were often used as auxiliary methods to detect functional changes in autonomic and central nerves, which were helpful for the diagnosis and prediction of clinical nervous system diseases (Bach et al., 2010; Ellaway et al., 2010; Parisi et al., 2011). However, the roles played by the central nervous system as well as the autonomic nervous system (ANS) in thermal perception of the oral mucosa are unclear. Moreover, to the best of our knowledge, this was the first attempt to associate SSR with EEG to measure thermal perception of the oral mucosa, which could reflect the nerve function of ANS and CNS.

Therefore, the aims of this study were to (1) investigate and map the SSR threshold temperature in the oral mucosa at various sites in healthy young adults, (2) measure the SSR and EEG triggered in different areas of the oral mucosa under various levels of thermal stimuli, (3) explore the potential relationship between SSR and EEG, and (4) provide a theoretical basis for diagnosis and treatment of patients with abnormal temperature perception or BMS.

MATERIALS AND METHODS

Participants

Forty healthy subjects from Tianjin Medical University were included in this study, including 24 men and 16 women, aged 19–28 years old, with a mean age of 23 ± 3 (**Supplementary Table 1**).

The inclusion criteria were as follows: (1) participants who had complete dentition without any mucosal diseases or abnormal temperature sensation in the oral cavity; (2) participants without the intake of psychotropics or drugs inhibiting glandular secretion in the past 2 weeks, such as diazepam and atropine; (3) participants with normal cardiac function, without any heart-related diseases; and (4) participants who did not participate in other medical experiments or clinical trials in the past 2 months. Subjects, with psychiatric or neurologic disorders, or without written informed consent, were excluded from the study. In addition, participants whose waveform could not be obtained were excluded from the final analysis.

This study was approved by the Ethics Committee of Tianjin Medical University (No. TMUhMEC20210201) and has been performed in accordance with the ethical standards laid down in the 1964 Declaration of Helsinki. Informed consent was obtained before the study. Participants were able to withdraw from this study at any time during the period of the study.

Instrumentation of the Experiment

The thermal stimulation instrument worked on the principle of intelligent temperature control (Chinese Patent No. ZL202121087859.2) (**Supplementary Figure 1**). Hot temperature stimuli was imposed on the oral mucosa via a 5 mm × 5 mm Peltier semiconductor chip. Real-time data from the sensor were transmitted to the temperature control computer where fluctuations of ±0.5°C would be recorded (**Supplementary Figure 2**). The stability of real-time temperature was attained by a PT100 sensor (Heraeus, Shanghai, China) temperature control system.

An NDI-92 nerve/electromyogram evoked potential instrument (Shanghai Poseidon Medical Electronic Instrument Co., Ltd., Shanghai, China) was used to test SSR. It was provided by the Stomatological Anatomy and Physiology Laboratory of the Stomatological Hospital of Tianjin Medical University.

EEG signals were collected by a 32-channel Quik-Cap with a NuAmps amplifier (Compumedics Neuroscan, Australia).

Oral Mucosa Partitions

To make the results more representative and reliable, the oral mucosa in the labial area, gingival area, and anterior 2/3 of the tongue were fully measured. The authors distinguished the mucosa at the tip of the tongue and the central areas of the upper lip and lower lip as partitions 1–3, respectively. Then, according to the position of teeth, from the right maxillary third molar, the gingival mucosa was defined as area 4–35, in a clockwise direction (**Figure 1**).

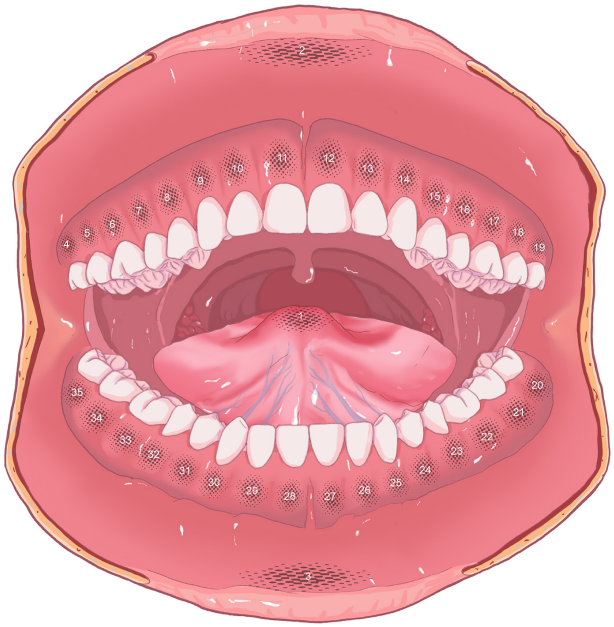

FIGURE 1 | Partitions of oral mucosa (partition 1: tip of the tongue; partition 2: upper lip; partition 3: lower lip; partitions 4–35: gingival areas).

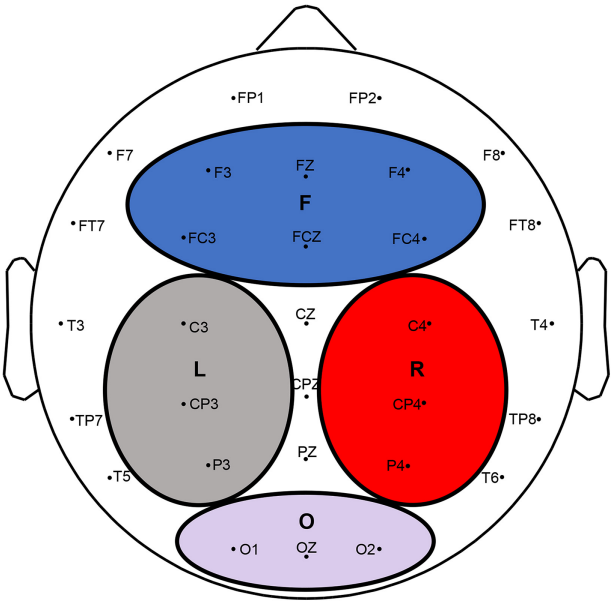

FIGURE 2 | EEG electrodes and four divided regions (F, L, R, and O indicated the frontal, left parietal, right parietal, and occipital lobes, respectively).

Electroencephalogram Electrodes of Scalp Partitions

To compute global frequency changes, electrodes were selected and grouped into four main areas: the frontal, left parietal, right parietal, and occipital areas (Zhang et al., 2016). The frontal region included F3, Fz, F4, Fc3, FCz, and Fc4. The left region included C3, Cp3, and P3, and the right region included C4, Cp4, and P4. The occipital region included O1, Oz, and O2 (**Figure 2**).

Sympathetic Skin Response Threshold Temperature Measurements

Prior to the testing, participants were asked to have a rest in a supine position for 10 min, during which the procedures of testing were introduced, and participants were instructed on how to collaborate with the investigators. The testing was performed in a quiet, properly shaded room with an indoor temperature of 22–25°C between 3 and 5 pm.

Two hydrogel electrodes were attached to the palm and the back of the non-dominant hand of the subjects, whereby the palmar electrode served as the recording electrode and the dorsal electrode as the reference electrode. The grounding wire was placed on the wrist. The bandwidth of the Butterworth bandpass filter was set between 0.5 and 30 Hz, and the sampling frequency of SSR was 120 Hz. The analysis time was 10 s, during which the temperature of the palm skin was above 32°C.

First, participants were asked to gargle with water at 36°C which was the baseline temperature of the stimulus. The Peltier semiconductor chip was then placed on each area for at least 3 s. After that, the chip was removed from the testing area. If SSR could not be recorded, the temperature was set to increase by 1°C and the test was repeated. Then, the SSR threshold temperature was recorded until the SSR waveform was evoked (**Supplementary Figure 3**). The lowest temperature value that satisfied both of the above criteria was defined as SSR threshold temperature.

The value of SSR threshold temperature at each partition was tested twice. If the difference between these two values was significant (more than 10% of the first value), a third test would be performed. Two values that showed the smallest deviation were selected out of three results, and their mean value was defined as the final SSR threshold temperature. All partitions were tested in the same way (**Supplementary Figure 4**). Between two tests, the subject was required to have a short break for 1 min and gargle 36°C water for 10 s. Irregular time intervals and non-adjacent stimulation sites were used to reduce the habituation.

Sympathetic Skin Response and Electroencephalogram Tests

Sympathetic skin response and EEG tests were conducted after the SSR threshold temperature test. Before the testing of SSR and EEG, 5-min EEG signals were recorded as a baseline EEG for each subject in a supine position with eyes closed.

Electroencephalogram electrodes were placed in the testing areas according to the extended international 10–20 system. The sampling frequency of EEG was 1,000 Hz, and the contact resistance between the electrode and scalp was less than 5 kΩ. To simultaneously perform SSR and EEG tests, a trigger device was designed and used by the researchers to synchronize the acquisition of signals. The onset of each thermal stimuli automatically excited the trigger operation, which allowed the synchronized acquisition of the SSR and EEG signals.

There were four different levels of temperature stimuli in SSR and EEG tests. A temperature of 45°C was identified as the initial temperature for the tests, and the temperature gradient was set to 3°C. Therefore, the stimulation temperatures were 45, 48, 51, and 54°C, respectively. Each testing area received four different levels of temperature stimuli.

Considering the physiological nature of the oral cavity, some representative areas were selected for the SSR and EEG tests, including (1) the central areas of incisors, premolars, and molars in maxillary and mandibular dentition, (2) the central area of the inner side of the upper and lower lip, and (3) the tip of the tongue. Since the SSR threshold temperatures were with no significant difference in premolar and molar areas, the authors, therefore, grouped these adjacent areas and irregular time intervals and non-adjacent stimulation areas were used to reduce the habituation. Each stimulation lasted for 3–5 s. Each area was tested three times, and the mean value was taken. All areas were tested in the same way.

Subjective Numerical Pain Ratings

The participants were asked to rate their pain intensity on a visual analog scale (VAS). The scores were summed across categories and can range from 0 to 10. 0 points represented no pain; a score of 1–3 represented mild pain; a score of 4–7 represented moderate pain; and a score of 7–10 represented severe pain. The rating was obtained at the end of each recording in SSR and EEG tests.

Analysis

Data Collection and Management

There were many essential parameters in the analysis of SSR, such as latency, amplitude, and waveform (Gutrecht, 1994). The latency of SSR signified the start of the record as the first deflection from the baseline. The value between the highest negative wave and the highest positive wave was known as the amplitude. In addition, the SSR area (the area under the negative component of the waveform) was also recorded (Bir et al., 2005). In this study, the SSR data were stored by the software in the electromyography (EMG) machine. The amplitude, latency, and area of SSR, in this study, were analyzed by MATLAB.

Electroencephalogram processing and analysis were also performed in MATLAB. The recorded data were bandpass-filtered (0.05–100 Hz). The line noise of 50 Hz was suppressed by a notch filter. The eye movement and muscle artifacts were corrected by independent component analysis (ICA) using EEGLAB (version 13.6.5b). Spectral analysis was performed for each data segment by the periodogram method (Akin and Kiymik, 2000). Next, the average power of the alpha and beta bands of EEG data after each temperature stimuli for all subjects for all 32 channels was calculated. The trend of the average power of the EEG delta, theta, alpha, and beta bands was analyzed and investigated according to the settings of different temperatures and thermal stimuli of different areas within the oral mucosa.

Statistical Analysis

Statistical analysis was performed using SPSS statistics version 25.0 (SPSS, Chicago, IL, United States). All data were tested for normality using the Shapiro–Wilk normality test. The SSR threshold temperature values were analyzed by a one-way ANOVA. The relationship between gender and SSR temperature threshold was analyzed using a generalized estimation equation (GEE), in which SSR temperature threshold was defined as the dependent variable, while partitions and gender were covariables. The SSR and EEG data were analyzed by a two-way repeated-measures ANOVA. The Bonferroni test was used when the variances were homogeneous, while Dunnett's T3 test was used when the variances were not homogeneous. Correlational analysis was performed using Pearson's correlations.

RESULTS

Sympathetic Skin Response Threshold Temperature of the Oral Mucosa

The SSR waveform was successfully evoked in 35 subjects, while the other five subjects failed to evoke the SSR waveform and had no data for further analysis. In terms of oral mucosa in different areas, the SSR threshold temperatures of posterior gingival areas were higher than that in anterior gingival areas. The SSR threshold temperature of partition 6 was the highest (50.18 ± 1.71°C), and the difference between the SSR threshold temperature of partition 6 and that in other areas was significant ($P < 0.001$). In contrast, partition 1 was the most sensitive area to heat stimuli, with an SSR threshold temperature value of 36.13 ± 1.95°C, and there was a significant difference between the SSR threshold temperature of partition 1 and that in other areas ($P < 0.001$). These results reflected that the sensitivity of SSR threshold temperature of oral mucosa gradually decreased from the anterior areas to the posterior areas. However, there was no significant difference between the SSR threshold temperature of symmetrical areas on either side, such as partition 8 (46.20 ± 1.65) and partition 15 (45.88 ± 1.91) ($P = 0.65$). In addition, the sensitivity of the SSR threshold temperature of the oral mucosa showed a tendency to gradually decrease from the midline backward to both sides. The SSR threshold temperature of the oral mucosa was not affected by sex since there was no significant difference between male and female volunteers (men 45.12 ± 3.57°C; women 44.96 ± 3.43°C, OR = 1.17, $P = 0.57$). Finally, the map of the SSR threshold temperature of the oral mucosa was formed by the data obtained from the study (**Figure 3**).

The Parameters of Sympathetic Skin Response

A two-way repeated-measures ANOVA revealed a significant effect of area ($F = 279.30$, $P < 0.001$), temperature ($F = 694.20$, $P < 0.001$), and a significant area × temperature interaction on SSR amplitude ($F = 5.51$, $P < 0.001$) (**Supplementary Table 2**). At stimulation temperatures of 45, 48, and 51°C, the values of SSR amplitude in the anterior area of the oral cavity were significantly higher than those in the posterior area. In particular, the SSR amplitude value in the tip of the tongue, which was the highest value of SSR amplitude, was significantly greater than those in all other areas ($P < 0.001$), while SSR amplitudes recorded in

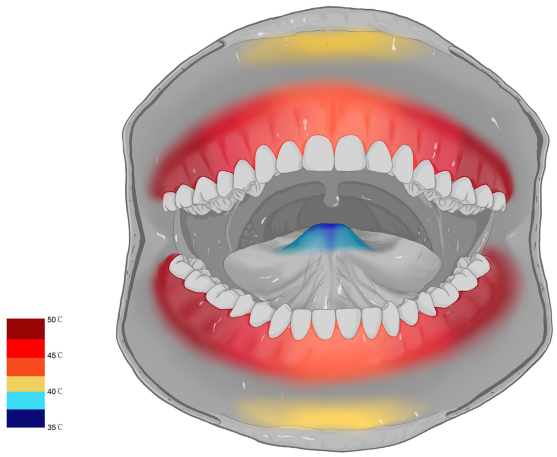

FIGURE 3 | Map of the SSR threshold temperature of the oral mucosa.

premolar and molar areas were lower. In addition, the second and third highest values of SSR amplitude were detected in the region of the upper lip and the lower lip, respectively. In gingival areas, the first highest value of the SSR amplitude was obtained in the maxillary incisor area with significant statistical difference ($P < 0.001$). However, there was no statistical difference between the SSR amplitude obtained in the premolar and molar areas ($P > 0.05$). At the temperature of 54°C, no significant statistical difference was observed between the values of the SSR amplitude in the tip of the tongue, lips area, and the maxillary incisor area. However, compared with SSR amplitudes in the premolar or molar areas, there were significant differences between these areas ($P < 0.001$) (**Figure 4**). The changes in the SSR amplitudes with various areas at four different levels of stimulation temperatures followed the same trend. In addition, the SSR area showed similar trends (**Table 1**).

There were significant differences in the SSR amplitudes obtained at different degrees of thermal stimuli ($P < 0.001$). Comparing the values of the area of SSR at different temperatures, significant differences ($P < 0.001$) were observed except at 45 and 48°C, and at 51 and 54°C. In addition, the statistical results showed that the amplitude and the area of SSR were both positively related to the intensity of temperature stimuli (**Supplementary Tables 3, 4**), and there was a high positive correlation between the SSR amplitude and VAS score (**Supplementary Table 5**).

There were significant differences in the latency of SSR between the tip of the tongue and molar areas of the oral cavity at different degrees of temperatures ($P < 0.001$) (**Table 2**). However, there was no significant difference in the latency of SSR between different degrees of temperatures ($P > 0.05$).

The Average Power of Electroencephalogram

To observe and analyze the changes in the EEG of healthy subjects in two states (rest and thermal stimuli), the average power of the baseline and four degrees of temperatures in each frequency band were calculated in each of the four areas of the brain (**Figure 5**). A two-way repeated-measures ANOVA revealed that temperature greatly affected the average power of delta band ($F = 23.25$, $P < 0.001$), theta band ($F = 46.97$, $P < 0.001$), alpha band ($F = 60.28$, $P = 0.10$), and beta band ($F = 11.19$, $P = 0.02$). However, neither the areas (frontal, left parietal, right parietal, and occipital areas) nor the interaction effect (area × temperature) affected the average power of all four bands ($P > 0.05$) (**Supplementary Table 6**). Delta band: Compared to the baseline, the delta power decreased at each degree of thermal stimuli in all four brain areas. The statistical difference was observed between baseline and 45°C ($P = 0.01$) and 48°C ($P = 0.01$) in the frontal area, while in the left and right parietal area, only between baseline and 45°C ($P < 0.001$). Theta band: Compared to the baseline, the theta power decreased at each degree of thermal stimuli in all four brain areas. In the frontal region, there were statistical differences between baseline and 45°C ($P < 0.001$) and 48°C ($P < 0.001$), while in the occipital area, and left and right parietal area, only between baseline and 45°C ($P < 0.001$). Alpha band: Compared to the baseline, the alpha power also decreased at each degree of thermal stimuli in all four brain areas. There were statistical differences between baseline and thermal stimuli at all four degrees in all four brain areas ($P < 0.001$). Beta band: Compared to the baseline, the beta power also decreased at each degree of thermal stimuli in all four brain areas except 51 and 54°C in the occipital area. Statistical difference was observed in the frontal, left, and right parietal areas between baseline and 45°C ($P < 0.001$).

The results showed that the reduction in the alpha frequency band was most obvious after thermal stimuli, and there were statistical differences between baseline and thermal stimuli in all four degrees of temperatures ($P < 0.001$) (**Figure 5**). To test which part of the brain areas had the most pronounced reduction at the alpha band, power change was calculated at each electrode. The results showed that the reduction in alpha power was in the global brain, and the reduction was mainly concentrated in the right parietal area near electrode P4 (**Figure 6**).

DISCUSSION

Partitions and Sympathetic Skin Response Threshold Temperature of the Oral Mucosa

In terms of innervation, the areas of maxillary labial, buccal, and gingival mucosa were mainly innervated by the maxillary nerve, while the areas of mandibular labial, buccal, and mandibular gingival mucosa were primarily innervated by the mandibular nerve (Yamauchi et al., 2012). The anterior 2/3 area of the dorsal tongue mucosa was mainly innervated by the lingual nerve, and the latter 1/3 by the glossopharyngeal nerve—the ninth pair of the cranial nerve. In addition, Lauria et al. (2005) suggested that neurologic disturbance could act as a potential risk factor for patients with BMS. The patients with BMS were usually suffering

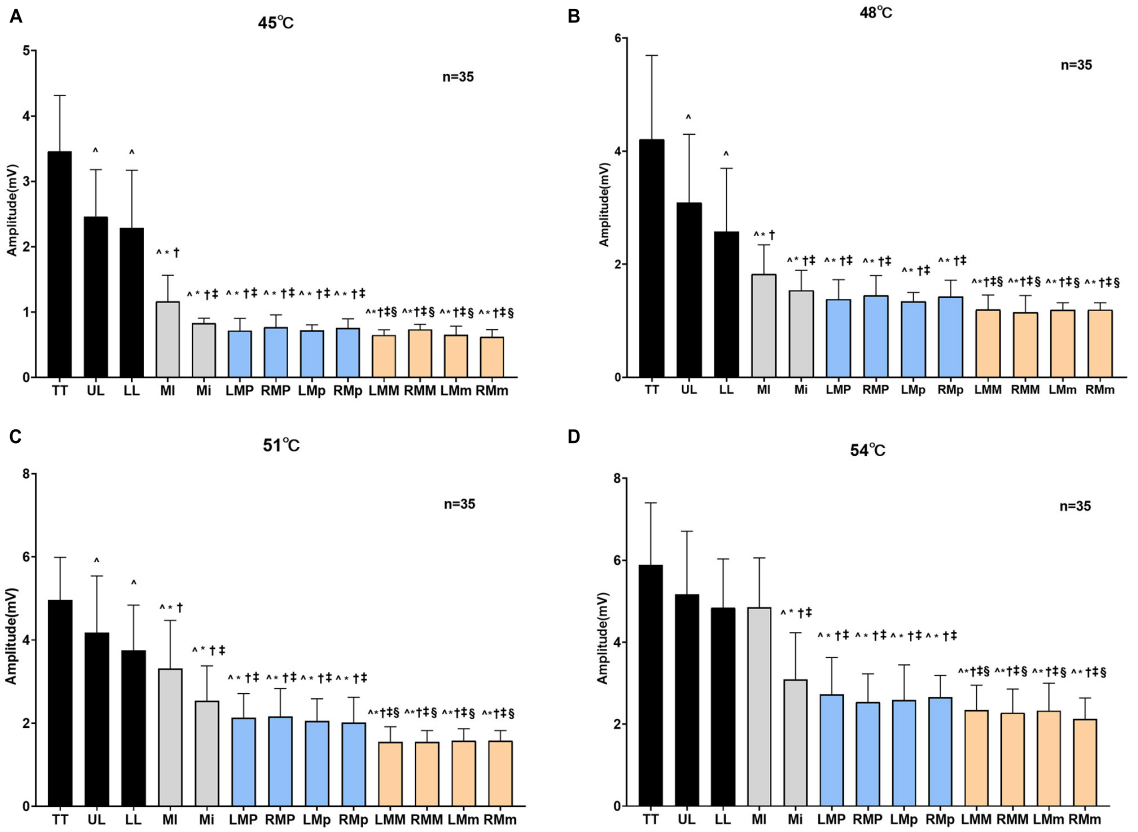

FIGURE 4 | Amplitudes of SSR obtained by stimulating different areas at different degrees of temperatures. The amplitudes of SSR obtained by stimulating different areas when oral mucosa was stimulated at 45°C **(A)**, 48°C **(B)**, 51°C **(C)**, and 54°C **(D)**. TT, tip of the tongue; UL, upper lip; LL, lower lip; MI, maxillary incisor area; Mi, mandibular incisor area; LMP, left maxillary premolar area; RMP, right maxillary premolar area; LMp, left mandibular premolar area; RMp, right mandibular premolar area; LMM, left maxillary molar area; RMM, right maxillary molar area; LMm, left mandibular molar area; RMm, right mandibular molar area.
^$P < 0.05$ vs. TT, *$P < 0.001$ vs. UL, †$P < 0.001$ vs. LL, ‡$P < 0.001$ vs. MI, §$P < 0.001$ vs. Mi.

TABLE 1 | Area of SSR obtained by stimulating different areas at different degrees of temperatures (mean ± SD).

Areas	SSR area (mVS)			
	45°C	48°C	51°C	54°C
Tip of tongue	16.10 ± 0.94	17.01 ± 1.56	19.42 ± 1.87	21.46 ± 1.70
Upper lip	13.59 ± 1.54*	14.29 ± 1.09*	17.46 ± 1.51*	18.67 ± 1.08
Lower lip	11.36 ± 1.06*	13.14 ± 1.03*	14.73 ± 1.01*	17.01 ± 0.65
Maxillary incisor area	9.13 ± 0.97*†	11.18 ± 1.24*†	13.36 ± 1.14*†	16.89 ± 1.63
Mandibular incisor area	7.23 ± 1.07*†‡	9.37 ± 1.31*†‡	12.18 ± 1.01*†‡	15.23 ± 1.17*†‡
Left maxillary premolar area	5.75 ± 0.87*†‡	6.74 ± 0.96*†‡	8.87 ± 0.97*†‡	9.45 ± 0.78*†‡
Right maxillary premolar area	5.10 ± 0.75*†‡	6.05 ± 0.72*†‡	9.63 ± 1.04*†‡	10.97 ± 1.09*†‡
Left mandibular premolar area	5.28 ± 0.80*†‡	6.27 ± 1.03*†‡	8.57 ± 1.21*†‡	10.79 ± 0.92*†‡
Right mandibular premolar area	4.79 ± 0.67*†‡	7.16 ± 0.84*†‡	9.68 ± 0.76*†‡	10.58 ± 1.06*†‡
Left maxillary molar area	2.97 ± 0.32*†‡§	4.26 ± 0.58*†‡§	5.31 ± 0.47*†‡§	6.21 ± 0.45*†‡§
Right maxillary molar area	3.12 ± 0.37*†‡§	4.02 ± 0.50*†‡§	4.70 ± 0.68*†‡§	6.36 ± 0.78*†‡§
Left mandibular molar area	3.10 ± 0.42*†‡§	3.70 ± 0.50*†‡§	5.07 ± 0.46*†‡§	6.16 ± 0.59*†‡§
Right mandibular molar area	3.33 ± 0.36*†‡§	3.94 ± 0.44*†‡§	4.95 ± 0.51*†‡§	6.38 ± 0.58*†‡§

*$P < 0.001$ vs. tip of the tongue.
†$P < 0.001$ vs. upper lip.
‡$P < 0.001$ vs. lower lip.
§$P < 0.001$ vs. maxillary incisor area.

from persistent complex pain and abnormal temperature perception. The areas we measured were more sensitive in sensing temperature compared with the other tissues of the oral cavity, such as the soft palate, and posterior tongue. Specifically, the lip and the tip of the tongue were the prominent areas of patients with BMS. This could provide

TABLE 2 | Latency of SSR was obtained by stimulating different temperatures in different areas (Mean ± SD).

Areas	Latency (s)			
	45°C	48°C	51°C	54°C
Tip of tongue	1.41 ± 0.06	1.38 ± 0.07	1.36 ± 0.07	1.29 ± 0.06
Upper lip	1.51 ± 0.06	1.49 ± 0.06	1.47 ± 0.06	1.40 ± 0.07
Lower lip	1.56 ± 0.06	1.52 ± 0.06	1.48 ± 0.07	1.47 ± 0.03
Maxillary incisor area	1.61 ± 0.05	1.57 ± 0.04	1.55 ± 0.06	1.53 ± 0.07
Mandibular incisor area	1.67 ± 0.05	1.66 ± 0.05	1.63 ± 0.06	1.57 ± 0.06
Left maxillary premolar area	1.70 ± 0.05	1.66 ± 0.08	1.61 ± 0.07	1.60 ± 0.06
Right maxillary premolar area	1.71 ± 0.06	1.63 ± 0.07	1.60 ± 0.06	1.58 ± 0.07
Left mandibular premolar area	1.69 ± 0.07	1.62 ± 0.08	1.61 ± 0.05	1.60 ± 0.04
Right mandibular premolar area	1.68 ± 0.07	1.67 ± 0.07	1.65 ± 0.09	1.60 ± 0.06
Left maxillary molar area	1.79 ± 0.10*	1.76 ± 0.06*	1.75 ± 0.12*	1.71 ± 0.08*
Right maxillary molar area	1.80 ± 0.11*	1.78 ± 0.10*	1.72 ± 0.06*	1.67 ± 0.09*
Left mandibular molar area	1.81 ± 0.10*	1.78 ± 0.08*	1.75 ± 0.10*	1.74 ± 0.08*
Right mandibular molar area	1.81 ± 0.08*	1.79 ± 0.06*	1.76 ± 0.07*	1.73 ± 0.08*

*$P < 0.001$ vs. tip of the tongue.

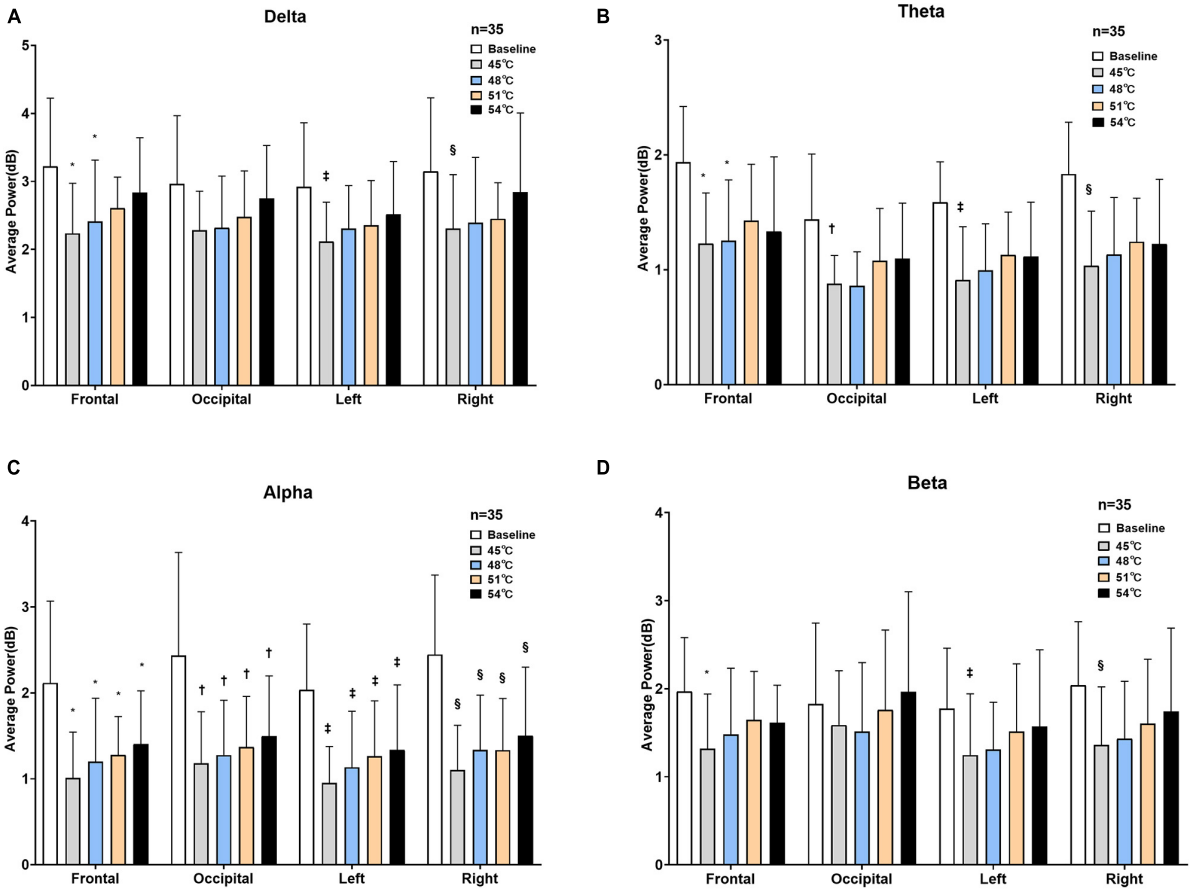

FIGURE 5 | Average power of four brain areas under two states. Delta **(A)**, theta **(B)**, alpha **(C)**, and beta **(D)** power at baseline and four degrees of thermal stimulus in the frontal, occipital, left parietal, and right parietal lobes (*$P < 0.001$ vs. baseline in the frontal lobe, †$P < 0.001$ vs. baseline in the occipital lobe, ‡$P < 0.001$ vs. baseline in the left parietal lobe, §$P < 0.001$ vs. baseline in the right parietal lobe).

a clue for further study in BMS. Based on the complicated nerve innervation and characteristic of oral mucosa disease, the fine partitions were divided by researchers. Furthermore, our results demonstrated that the SSR threshold temperature values were significantly different in different areas of the oral mucosa. The findings and ideas could generate hypotheses for

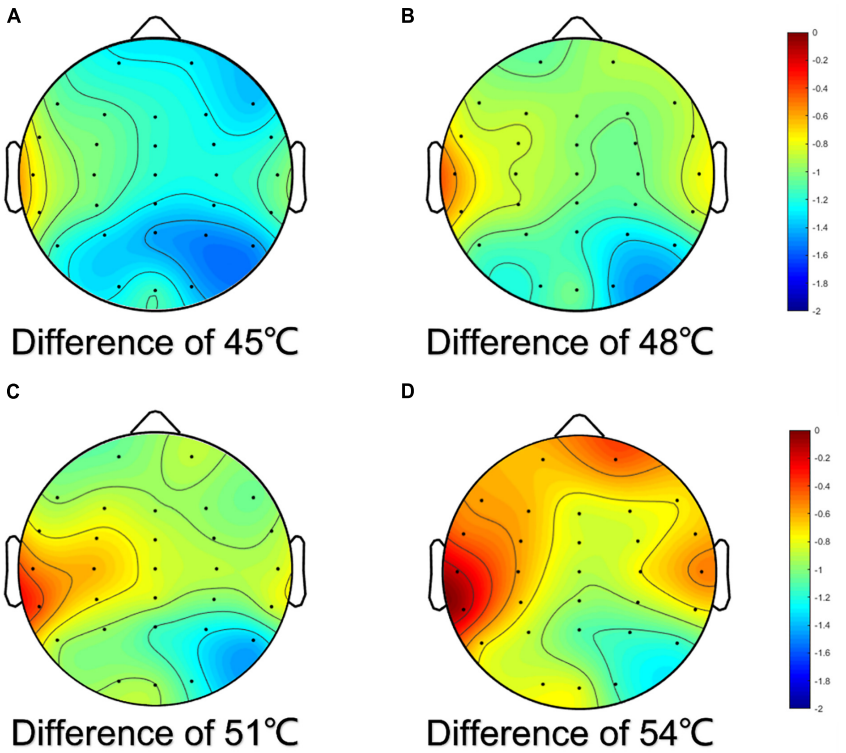

FIGURE 6 | Topographic map of difference of alpha power for EEG electrodes. The difference was the power of baseline minus the power of thermal stimuli at 45°C **(A)**, 48°C **(B)**, 51°C **(C)**, and 54°C **(D)**, respectively.

further exploration of whether the patients with BMS developed autonomic neuropathy.

The differences in the sensitivity to heat among the oral partitions are caused by a series of factors, including differences in receptor location or type within the oral mucosa, diversities in innervation density, and variables related to the thermal conductivity of the oral mucosa (Green, 1984). For instance, the anterior area of the oral cavity contained more nerve endings than the posterior area, which may contribute to the superior sensitivity in the tip of the tongue area compared to the posterior gingival areas (Capra, 1995). Therefore, the sensitivity of the SSR threshold temperature of oral mucosa showed a tendency of gradual decrease backwardly bilaterally from the midline.

In addition, the degree of keratinization and physiological function of the oral mucosa were different. Compared with the lining (lip) and the specialized mucosa (tongue), the masticatory mucosa (gingiva) contacted food more frequently; therefore, its degree of keratinization was higher, leading to a higher SSR threshold. According to the findings in this study, sex had no significant effect on the SSR threshold temperature of the oral mucosa. This may relate to the small sample size, and larger samples for verification will be needed in the future. The SSR threshold temperature of oral mucosa with a high degree of keratinization was also high. Furthermore, we found that people with unilateral chewing habits had a higher tolerance to heat temperature on the preferred side than on the non-preferred side, which was more sensitive to heat. However, in this study, we observed that the SSR could not be evoked in five subjects, which did not result from the equipment, experimental process, or environmental factors, thus requiring further investigation.

Sympathetic Skin Response Evoked by Thermal Stimuli

The tolerance of heat in different areas of oral mucosa was different. In general, the oral cavity mucosa could tolerate higher temperatures than the lip, and a temperature below 60°C will not cause harmful results. Forty-five degrees Celsius was defined as the baseline temperature in the SSR test based on the pre-experiment. In the pre-experiment, the stimulation temperature started at 36°C and increased by 1°C each time. First, it was noted that SSR began to appear frequently only after temperature stimuli of 43°C. However, SSR could not be evoked stably until each temperature stimuli was applied at approximately 45°C. Therefore, a temperature stimuli of 45°C was used to ensure that the SSR could be evoked every time and that the waveform of the SSR was stable. The authors compared the efficacy of temperature gradients of 3 and 1°C. Eventually, the gradient of 3°C was determined as ideal to test the minimum difference of SSR under different stimulation temperatures, and great differences between the amplitudes obtained at different temperatures could be observed and the areas of SSR showed the same trend. Furthermore, this study suggested that the amplitudes and the areas of SSR were positively correlated with

the intensity of stimulation (Toyokura, 2003). At the same time, the SSR amplitudes and the areas obtained by the same degree of thermal temperature in different areas of the oral mucosa were different, which proved that the afferents and efferents of these areas were not innervated by the same nerve. In addition, the correlation between the SSR amplitude and VAS score was positive. Whether a direct, proportional relationship between these two parameters still needs further studies.

However, under 54°C stimulation, the amplitude of the SSR in the tip of the tongue was close to that in the upper and lower lip areas as well as the maxillary incisor area. These results further supported the idea that nociceptors could be activated at higher temperatures and subsequently initiate an extraordinary stress response (Green, 1984). Therefore, it has been hypothesized that the primary protection mechanism of the human body will be aroused when the temperature increases to a certain value. In addition to the innervation and degree of keratinization of the oral mucosa, an appropriate temperature of thermal stimuli should be taken into consideration in future research.

However, there were no significant differences in the latency of SSR between four degrees of temperatures, and the reason for differences in the latency of SSR between areas was that these areas were innervated by different nerves and the nerve conduction rate was different. Although the latency was one of the most essential factors of SSR. However, in this study, the participants were healthy young adults and the differences in latency were not obvious. Moreover, this study focused more on the relationship between SSR and EEG. Therefore, the study of latency was only a small fraction, and we will further study the difference between healthy people and patients with BMS.

Changes in Electroencephalogram

Delta waves (0.5–4 Hz) were the slowest waves. The waveform used in the sleep assessment was the 0.5–2 Hz band. These waves were commonly found in the frontal lobe and have a relatively large amplitude of activity, normally 75 μV or even greater, with no fixed waveform duration, and were more pronounced during deep sleep or coma. Theta waves (4–8 Hz) were often found in the central region, with no fixed amplitude range, mostly in areas of the brain unrelated to hand function, and were easily detected during the shift from relaxation to sleep. Alpha waves (8–13 Hz) often appeared in the parieto-occipital region, and normal alpha waves were synchronized and symmetrical in the cerebral hemispheres and were easily detected in the state of quiet, awake, relaxed, and eyes closed resting. Beta waves (13–30 Hz) were commonly found in the frontal and central regions and were often present in states of positive thinking, concentration, anxiety, tension, and agitation. Beta waves were decreased during deep sleep, reappear during rapid-eye-movement sleep, and vary in amplitude in both hemispheres which should exceed 50% (Chokroverty, 2014).

The observed decrease in alpha power during painful stimulation was a robust finding that previous studies have also repeatedly found. Dowman et al. (2008) revealed that the lower central alpha power during thermal stimuli at the central electrodes might be relevant to pain-related activation in the primary somatosensory cortex (SI) and the somatosensory associated areas located in the parietal operculum and insula. Tension heat pain induced by heat pulses above the pain domain decreased central alpha 1 and alpha 2 activity, and the EEG pattern of lower central alpha power was related to acute human pain (Giehl et al., 2014). Zhang et al. (2016) suggested that the alpha band played a key role in invoking responses in higher hierarchical nodes of the brain such as the anterior cingulate cortex (ACC) and the ACC played an essential role in the emotional and perception aspects of pain processing. Our results showed that thermal stimuli suppressed the alpha rhythm, which was consistent with these previous findings. It has been hypothesized that as the thermal stimuli was applied, the subjects began to feel nervous and more attention was paid to uncomfortable sensations, even pain, and perhaps they acted more tensed (Chang et al., 2001; Huber et al., 2006; Herrmann et al., 2016; Jurewicz et al., 2018). Zhang et al. (2016) found a decrease in theta power in their study of the effects of tonic thermal pain on EEG rhythm, which is consistent with our study, and the change in beta power was most likely related to the presence of more noise in this frequency band (Giehl et al., 2014). However, some other studies in tonic pain stimulation have found that delta power showed an upward trend which was inconsistent with our finding (Ferracuti et al., 1994; Chang et al., 2002; Huber et al., 2006). This may be because, in previous studies, the thermal stimuli was mostly applied to the outer epidermis such as hands or legs, while our stimulation was applied to the oral mucosa, and there were differences in nerve conduction mechanism and receptors between the skin and oral mucosa (Capra, 1995).

Our results showed that the decreasing trend of alpha power in all four brain areas became less obvious as the temperature of thermal stimuli increased. There was no doubt that the psychological state of the subjects at rest was relaxed, as indicated by the maximum alpha power at baseline. However, there were only statistical differences between baseline and certain temperature stimuli, and no statistical differences between temperatures. In addition, previous studies often used much larger differences between thermal stimulus intensities, and the stimulation sites were different from our study (Nickel et al., 2017; Albu and Meagher, 2019). Therefore, different experimental paradigms may result in different results. The stimulation time in our study was shorter than that in continuous stimulation. There were many reasons for the differences between studies such as stimulation protocol, stimulus intensity, and electrode locations (Tripanpitak et al., 2021). In future research, we will make full use of the 32-channel data collected from the perspective of the brain network to analyze the information flow between different nodes in detail, including the characteristics of the brain network, such as the flow gain, clustering coefficient, and characteristic path length, to investigate what difference between different temperature and the EEG brain network connection to thermal stimuli (Bunk et al., 2018).

Physiological studies have confirmed that during the transmission of human oral temperature stimuli from the periphery to the center, the oral cavity received oral internal temperature and cold sensory stimuli through mucosal receptors

and converged to the caudate nucleus of the bilateral trigeminal spinal tract nucleus through the tympanic cord nerve fibers, trigeminal nerve, and lingual nerve fibers. Then, the caudate nucleus of the spinal trigeminal nucleus further transmitted the warm pain information to the ventroposteromedial nucleus and ventroposterolateral nucleus of the thalamus (Adams, 1976) and then transmitted the information to the cerebral cortex after changing neurons (Darian-Smith et al., 1979; Kawahara et al., 1986). Temperature and pain afferent down to the spinal nucleus of the trigeminal nerve, and the ascending conduction pathway of pain and temperature sensation came from the spinal nucleus of the trigeminal nerve. Bromm (2001) reported that pain response in the brain was a complex process which involved multiple cortical brain areas such as the primary and secondary somatosensory cortices, the insular cortex (IC), and the ACC. The temperature receptors in the cerebral cortex were located in the paracentral part of the parietal cortex of the posterior central gyrus, and these areas were referred to as the somatosensory region I which was located in the left and right parietal areas of the scalp electrode (Brownsett and Wise, 2010). Our results revealed that there was a reduction in alpha power in both the left and right parietal areas, with the greatest change in the right parietal areas and contralateral somatosensory regions (SI and SII) near the P4 electrode were most responsive to sensing and relaying pain caused by thermal stimuli. This was the same as the consensus that SI and SII are part of the pain network (Oertel et al., 2012).

The Relationship Between Sympathetic Skin Response and Electroencephalogram

Lim et al. (1996) reported a strong correlation between beta-band activity and skin conductance level, due to these measures were shared reticulo-thalamo-hypothalamo-cortical networks; therefore, a functional link between these measures might be predicted. Belyavin and Wright (1987) reported that beta activity can serve as a good discriminator for worsening the vigilance level. Garcia et al. (2011) suggested an electrophysiological framework with interactions between brain dynamics and autonomic responses elicited by emotional engagement in a working memory task. In addition, the sympathetic changes in the skin conductance level have been related to mental stress and emotion regulation (Crone et al., 2004; Werner et al., 2009). As the temperature stimuli was increased, in this study, the amplitudes and the area of SSR which could represent the intensity of perception of the oral cavity were both gradually increased, below the noxious temperature level. Meanwhile, the average powers of the alpha band that could represent relaxation in the brain cortex also showed an upward trend. According to the results of SSR and EEG, this phenomenon suggested that the oral mucosa was always sensitive to temperature stimuli and could accurately distinguish the difference in stimulation temperature. At the same time, the CNS gradually showed certain habituation as the temperature increased. The oral mucosa, especially the lips and tongue areas at the forefront, could feel the temperature of the food ingested accurately and could determine the appropriate intake time, speed, and capacity of food to avoid damage from temperature. Although the CNS has an adaptive mechanism to temperature stimuli, the oral mucosa could always maintain an accurate perception of temperature stimuli, which was beneficial to avoid injury from ingesting overheated food. However, when this adaptive mechanism upregulated the intake temperature, continuous higher temperature stimuli may damage the oral mucosa, which could cause ulcers and even induce diseases such as esophageal cancer.

These findings, including ours, bear testimony to the fact that the CNS and the ANS are structurally linked. Kenchadze et al. (2011) reported improved BMS patients' condition using the EEG–feedback method; the clinical manifestations of some cases were evened out completely. In the meantime, in our clinical experience, patients who suffered from BMS could benefit from neurotropic medications improving the state of the autonomic nervous system. In the follow-up study, we will use the perspective of the brain network to deeply explore the response of the central nervous system to oral thermal stimuli at different temperatures and further reveal the relationship between the CNS and the ANS.

Limitations

The degree of keratinization of the oral mucosa was related to many influencing factors such as age, dietary type, and chewing habits. There were certain differences in the degree of keratinization of the oral mucosa among people of different ages (Abu Eid et al., 2012). In addition, the distribution density and sensitivity of the receptors and nerve conduction velocity also varied among different participants. It was true that a sense of hypothetically suitable ambient temperature is subjective. It could be, therefore, dramatically various among individuals with potential influence on the tension of the nervous system. SSR was normally present in both palms and soles under the age of 60 years, but in subjects aged 60 and over, it was found in only 50% of feet and 73% of hands (Drory and Korczyn, 1993). In this study, participants were all healthy young adults whose age and level of physiological function were similar, so the data of this experiment did not reflect the trend in the change among the whole population with age. Therefore, middle-aged and older people were necessary for follow-up research.

Sympathetic skin response can be used to assess the activity of the sympathetic nervous system. However, the biggest limitation was the habituation of this procedure. The essence of habituation was unclear. For SSR, with the increase in the number of stimuli at the same stimulation site, the amplitude decreased in a short period and could recover soon (Cariga et al., 2001). The habituation of SSR was difficult to avoid. Therefore, in this study, we used irregular time intervals and non-adjacent stimulation sites to reduce habituation, although the habituation evoked by temperature stimuli was less than that evoked by electrical stimulation. However, as a definite physiological characteristic, this trend still existed. SSR characteristics depended highly on habituation. In particular, the excitability level and the surprise effect of sympathetic neurons are important factors influencing the progressive and irregular variability of the reactions during

long-term experimental assessments. Reducing the influence of SSR habituation will be a focus in future research.

CONCLUSION

The SSR threshold temperature of the oral mucosa varied greatly in different areas. The anterior area of the oral mucosa was the most sensitive to temperature, while the posterior area of the oral mucosa was less sensitive, which was consistent with the pattern of food intaking function of the oral cavity. The topographic map of the oral mucosa SSR threshold temperature summarily elucidated the physiological characteristics of the thermal perception pattern as well as the mechanisms of thermal habituation and protection from harmful stimuli. The action potential of SSR evoked by thermal stimuli was an objective parameter reflecting the activity of the autonomic nervous system; in this study, we hypothesized that thermal stimuli aroused SSR existed extensively over the human body than limited to the oral cavity.

Our study tried to transform the subjective perception of oral mucosa to thermal stimuli into a relatively objective and accurate quantitative description, which was helpful for us to have a deeper understanding of the neurophysiological mechanism of temperature perception of oral mucosa from a new point of view. In this study, through the perception of thermal temperature in oral mucosa, we further explored the activities, mechanisms, and influencing factors of the ANS and CNS, to better understand and diagnose BMS.

Measurement of synchronous activities of the CNS by EEG average power level indicated that both the autonomic and central nervous system played important roles in thermal perception. Further application of multiple channels of electrophysiological parameter analysis could be helpful to better understand the interrelationship between the CNS and ANS.

DATA AVAILABILITY STATEMENT

The original contributions presented in this study are included in the article/**Supplementary Material**, further inquiries can be directed to the corresponding authors.

ETHICS STATEMENT

The studies involving human participants were reviewed and approved by the Ethics Committee of Tianjin Medical University (No. TMUhMEC20210201) and have been performed in accordance with the ethical standards laid down in the 1964 Declaration of Helsinki. The patients/participants provided their written informed consent to participate in this study.

AUTHOR CONTRIBUTIONS

HZ was responsible for study conception and design, device design, and assemble. SH was responsible for volunteer recruitment, data analyses, and drafted the manuscript. ZW contributed to the data interpretation. XL contributed to the data interpretation and critical revision of the manuscript. GC and SW contributed to the study conception and design, data interpretation, critically reviewing the manuscript, and crucial guidance in the study. All authors have given final approval and agreed to be responsible for all aspects of this study to ensure accuracy and integrity.

FUNDING

This work was supported by the National Natural Science Foundation of China (No. 61977050).

ACKNOWLEDGMENTS

We are grateful to the National Natural Science Foundation of China (No. 61977050).

SUPPLEMENTARY MATERIAL

The Supplementary Material for this article can be found online at: https://www.frontiersin.org/articles/10.3389/fnins.2022.907658/full#supplementary-material

REFERENCES

Abu Eid, R., Sawair, F., Landini, G., and Saku, T. (2012). Age and the architecture of oral mucosa. *Age* 34, 651–658. doi: 10.1007/s11357-011-9261-1

Adams, D. (1976). Keratinization of the oral epithelium. *Ann. R. Coll. Surg. Engl.* 58, 351–358.

Akin, M., and Kiymik, M. K. (2000). Application of periodogram and AR spectral analysis to EEG signals. *J. Med. Syst.* 24, 247–256. doi: 10.1023/a:1005553931564

Albu, S., and Meagher, M. W. (2019). Divergent effects of conditioned pain modulation on subjective pain and nociceptive-related brain activity. *Exp. Brain Res.* 237, 1735–1744. doi: 10.1007/s00221-019-05545-8

Bach, D. R., Friston, K. J., and Dolan, R. J. (2010). Analytic measures for quantification of arousal from spontaneous skin conductance fluctuations. *Int. J. Psychophysiol.* 76, 52–55. doi: 10.1016/j.ijpsycho.2010.01.011

Belyavin, A., and Wright, N. A. (1987). Changes in electrical activity of the brain with vigilance. *Electroencephalogr. Clin. Neurophysiol.* 66, 137–144. doi: 10.1016/0013-4694(87)90183-0

Bir, L. S., Ozkurt, S., Daloğlu, G., and Kurt, T. (2005). Impaired sympathetic skin response in chronic obstructive pulmonary disease. *Tohoku J. Exp. Med.* 207, 243–248. doi: 10.1620/tjem.207.243

Bromm, B. (2001). Brain images of pain. *News Physiol. Sci.* 16, 244–249.

Brownsett, S. L., and Wise, R. J. (2010). The contribution of the parietal lobes to speaking and writing. *Cereb. Cortex* 20, 517–523. doi: 10.1093/cercor/bhp120

Bunk, S. F., Lautenbacher, S., Rüsseler, J., Müller, K., Schultz, J., and Kunz, M. (2018). Does EEG activity during painful stimulation mirror more closely the noxious stimulus intensity or the subjective pain sensation? *Somatosens. Mot. Res.* 35, 192–198. doi: 10.1080/08990220.2018.1521790

Capra, N. F. (1995). Mechanisms of oral sensation. *Dysphagia* 10, 235–247. doi: 10.1007/bf00431416

Cariga, P., Catley, M., Mathias, C. J., and Ellaway, P. H. (2001). Characteristics of habituation of the sympathetic skin response to repeated electrical stimuli in man. *Clin. Neurophysiol.* 112, 1875–1880. doi: 10.1016/s1388-2457(01)00647-2

Chang, P. F., Arendt-Nielsen, L., and Chen, A. C. (2002). Dynamic changes and spatial correlation of EEG activities during cold pressor test in man. *Brain Res. Bull.* 57, 667–675. doi: 10.1016/s0361-9230(01)00763-8

Chang, P. F., Arendt-Nielsen, L., Graven-Nielsen, T., Svensson, P., and Chen, A. C. (2001). Topographic effects of tonic cutaneous nociceptive stimulation on human electroencephalograph. *Neurosci. Lett.* 305, 49–52. doi: 10.1016/s0304-3940(01)01802-x

Chokroverty, S. (2014). *Atlas of Sleep Medicine* 2nd Edn. Philadelphia, PA: Elsevier/Saunders.

Crone, E. A., Somsen, R. J., Van Beek, B., and Van Der Molen, M. W. (2004). Heart rate and skin conductance analysis of antecendents and consequences of decision making. *Psychophysiology* 41, 531–540. doi: 10.1111/j.1469-8986.2004.00197.x

Darian-Smith, I., Johnson, K. O., Lamotte, C., Shigenaga, Y., Kenins, P., and Champness, P. (1979). Warm fibers innervating palmar and digital skin of the monkey: responses to thermal stimuli. *J. Neurophysiol.* 42, 1297–1315. doi: 10.1152/jn.1979.42.5.1297

Dowman, R., Rissacher, D., and Schuckers, S. (2008). EEG indices of tonic pain-related activity in the somatosensory cortices. *Clin. Neurophysiol.* 119, 1201–1212. doi: 10.1016/j.clinph.2008.01.019

Drory, V. E., and Korczyn, A. D. (1993). Sympathetic skin response: age effect. *Neurology* 43, 1818–1820. doi: 10.1212/wnl.43.9.1818

Ellaway, P. H., Kuppuswamy, A., Nicotra, A., and Mathias, C. J. (2010). Sweat production and the sympathetic skin response: improving the clinical assessment of autonomic function. *Auton. Neurosci.* 155, 109–114. doi: 10.1016/j.autneu.2010.01.008

Evans, B. M. (1993). Cyclical activity in non-rapid eye movement sleep: a proposed arousal inhibitory mechanism. *Electroencephalogr. Clin. Neurophysiol.* 86, 123–131. doi: 10.1016/0013-4694(93)90084-9

Ferracuti, S., Seri, S., Mattia, D., and Cruccu, G. (1994). Quantitative EEG modifications during the cold water pressor test: hemispheric and hand differences. *Int. J. Psychophysiol.* 17, 261–268. doi: 10.1016/0167-8760(94)90068-x

Forssell, H., Jääskeläinen, S., Tenovuo, O., and Hinkka, S. (2002). Sensory dysfunction in burning mouth syndrome. *Pain* 99, 41–47. doi: 10.1016/s0304-3959(02)00052-0

Garcia, A., Uribe, C. E., Tavares, M. C., and Tomaz, C. (2011). EEG and autonomic responses during performance of matching and non-matching to sample working memory tasks with emotional content. *Front. Behav. Neurosci.* 5:82. doi: 10.3389/fnbeh.2011.00082

Giehl, J., Meyer-Brandis, G., Kunz, M., and Lautenbacher, S. (2014). Responses to tonic heat pain in the ongoing EEG under conditions of controlled attention. *Somatosens. Mot. Res.* 31, 40–48. doi: 10.3109/08990220.2013.837045

Green, B. G. (1984). Thermal perception on lingual and labial skin. *Percept. Psychophys.* 36, 209–220. doi: 10.3758/bf03206361

Gutrecht, J. A. (1994). Sympathetic skin response. *J. Clin. Neurophysiol.* 11, 519–524. doi: 10.1097/00004691-199409000-00006

Hagelberg, N., Forssell, H., Rinne, J. O., Scheinin, H., Taiminen, T., Aalto, S., et al. (2003). Striatal dopamine D1 and D2 receptors in burning mouth syndrome. *Pain* 101, 149–154. doi: 10.1016/s0304-3959(02)00323-8

Herrmann, C. S., Strüber, D., Helfrich, R. F., and Engel, A. K. (2016). EEG oscillations: from correlation to causality. *Int. J. Psychophysiol.* 103, 12–21. doi: 10.1016/j.ijpsycho.2015.02.003

Hilz, M. J., Azelrod, F. B., Schweibold, G., and Kolodny, E. H. (1999). Sympathetic skin response following thermal, electrical, acoustic, and inspiratory gasp stimulation in familial dysautonomia patients and healthy persons. *Clin. Auton. Res.* 9, 165–177. doi: 10.1007/bf02330480

Huber, M. T., Bartling, J., Pachur, D., Woikowsky-Biedau, S., and Lautenbacher, S. (2006). EEG responses to tonic heat pain. *Exp. Brain Res.* 173, 14–24. doi: 10.1007/s00221-006-0366-1

Jurewicz, K., Paluch, K., Kublik, E., Rogala, J., Mikicin, M., and Wróbel, A. (2018). EEG-neurofeedback training of beta band (12-22Hz) affects alpha and beta frequencies - A controlled study of a healthy population. *Neuropsychologia* 108, 13–24. doi: 10.1016/j.neuropsychologia.2017.11.021

Karl, H., Sato, A., and Schmidt, R. F. (1975). Electrodermal reflexes induced by activity in somatic afferent fibers. *Brain Res.* 87, 145–150. doi: 10.1016/0006-8993(75)90410-2

Kawahara, K., Sawada, Y., and Aoki, M. (1986). Dual pathways for thermal afferents from the cat's tongue. *Brain Res.* 378, 61–68. doi: 10.1016/0006-8993(86)90286-6

Kenchadze, R., Iverieli, M., Okribelashvili, N., Geladze, N., and Khachapuridze, N. (2011). The psychological aspects of burning mouth syndrome. *Georgian Med. News* 194, 24–28.

Koszewicz, M., Mendak, M., Konopka, T., Koziorowska-Gawron, E., and Budrewicz, S. (2012). The characteristics of autonomic nervous system disorders in burning mouth syndrome and Parkinson disease. *J. Orofac. Pain* 26, 315–320.

Lauria, G., Majorana, A., Borgna, M., Lombardi, R., Penza, P., Padovani, A., et al. (2005). Trigeminal small-fiber sensory neuropathy causes burning mouth syndrome. *Pain* 115, 332–337. doi: 10.1016/j.pain.2005.03.028

Lim, C. L., Barry, R. J., Gordon, E., Sawant, A., Rennie, C., and Yiannikas, C. (1996). The relationship between quantified EEG and skin conductance level. *Int. J. Psychophysiol.* 21, 151–162. doi: 10.1016/0167-8760(95)00049-6

Liu, H., Zheng, Y. F., Li, C. Y., Zheng, Y. Y., Wang, D. Q., Wu, Z., et al. (2015). Discovery of anti-inflammatory ingredients in Chinese herbal formula kouyanqing granule based on relevance analysis between chemical characters and biological effects. *Sci. Rep.* 5:18080. doi: 10.1038/srep18080

Makeig, S., and Inlow, M. (1993). Lapses in alertness: coherence of fluctuations in performance and EEG spectrum. *Electroencephalogr. Clin. Neurophysiol.* 86, 23–35. doi: 10.1016/0013-4694(93)90064-3

Nakamura, Y., Une, Y., Miyano, K., Abe, H., Hisaoka, K., Morioka, N., et al. (2012). Activation of transient receptor potential ankyrin 1 evokes nociception through substance P release from primary sensory neurons. *J. Neurochem.* 120, 1036–1047. doi: 10.1111/j.1471-4159.2011.07628.x

Nickel, M. M., May, E. S., Tiemann, L., Postorino, M., Ta Dinh, S., and Ploner, M. (2017). Autonomic responses to tonic pain are more closely related to stimulus intensity than to pain intensity. *Pain* 158, 2129–2136. doi: 10.1097/j.pain.0000000000001010

Oertel, B. G., Preibisch, C., Martin, T., Walter, C., Gamer, M., Deichmann, R., et al. (2012). Separating brain processing of pain from that of stimulus intensity. *Hum. Brain Mapp.* 33, 883–894. doi: 10.1002/hbm.21256

Pachori, R. B., and Bajaj, V. (2011). Analysis of normal and epileptic seizure EEG signals using empirical mode decomposition. *Comput. Methods Programs Biomed.* 104, 373–381. doi: 10.1016/j.cmpb.2011.03.009

Parisi, P., Verrotti, A., Paolino, M. C., Castaldo, R., Ianniello, F., Ferretti, A., et al. (2011). "Electro-clinical syndromes" with onset in paediatric age: the highlights of the clinical-EEG, genetic and therapeutic advances. *Ital. J. Pediatr.* 37:58. doi: 10.1186/1824-7288-37-58

Petrus, M., Peier, A. M., Bandell, M., Hwang, S. W., Huynh, T., Olney, N., et al. (2007). A role of TRPA1 in mechanical hyperalgesia is revealed by pharmacological inhibition. *Mol. Pain* 3:40. doi: 10.1186/1744-8069-3-40

Toyokura, M. (2003). Influence of stimulus intensity on waveform of sympathetic skin response evoked by magnetic stimulation. *Clin. Neurophysiol.* 114, 1423–1430. doi: 10.1016/s1388-2457(03)00162-7

Tripanpitak, K., He, S. Y., Sonmezisik, I., Morant, T., Huang, S. Y., and Yu, W. W. (2021). Granger causality-based pain classification using EEG evoked by electrical stimulation targeting nociceptive A delta and C Fibers. *IEEE Access* 9, 10089–10106. doi: 10.1109/access.2021.3050302

Vetrugno, R., Liguori, R., Cortelli, P., and Montagna, P. (2003). Sympathetic skin response: basic mechanisms and clinical applications. *Clin. Auton. Res.* 13, 256–270. doi: 10.1007/s10286-003-0107-5

Wei, H., Koivisto, A., Saarnilehto, M., Chapman, H., Kuokkanen, K., Hao, B., et al. (2011). Spinal transient receptor potential ankyrin 1 channel contributes to central pain hypersensitivity in various pathophysiological conditions in the rat. *Pain* 152, 582–591. doi: 10.1016/j.pain.2010.11.031

Werner, N. S., Duschek, S., and Schandry, R. (2009). Relationships between affective states and decision-making. *Int. J. Psychophysiol.* 74, 259–265. doi: 10.1016/j.ijpsycho.2009.09.010

Yamauchi, K., Takahashi, T., Kaneuji, T., Nogami, S., Yamamoto, N., Miyamoto, I., et al. (2012). Risk factors for neurosensory disturbance after bilateral sagittal split osteotomy based on position of mandibular canal and morphology of mandibular angle. *J. Oral Maxillofac. Surg.* 70, 401–406. doi: 10.1016/j.joms.2011.01.040

Zhang, C. H., Sohrabpour, A., Lu, Y., and He, B. (2016). Spectral and spatial changes of brain rhythmic activity in response to the sustained thermal pain stimulation. *Hum. Brain Mapp.* 37, 2976–2991. doi: 10.1002/hbm.23220

Conflict of Interest: The authors declare that the research was conducted in the absence of any commercial or financial relationships that could be construed as a potential conflict of interest.

Publisher's Note: All claims expressed in this article are solely those of the authors and do not necessarily represent those of their affiliated organizations, or those of the publisher, the editors and the reviewers. Any product that may be evaluated in this article, or claim that may be made by its manufacturer, is not guaranteed or endorsed by the publisher.

frontiers | Frontiers in Neurology

TYPE Review
PUBLISHED 29 July 2022
DOI 10.3389/fneur.2022.911332

OPEN ACCESS

EDITED BY
Joel C. Bornstein,
The University of Melbourne, Australia

REVIEWED BY
Grazia Devigili,
IRCCS Carlo Besta Neurological Institute Foundation, Italy
Nicola Tambasco,
Hospital of Santa Maria della Misericordia in Perugia, Italy
Habip Gedik,
Bakirköy Dr.Sadi Konuk Egitim ve Araştirma Hastanesi, Turkey

*CORRESPONDENCE
Guixia Wang
gwang168@jlu.edu.cn

SPECIALTY SECTION
This article was submitted to Autonomic Neuroscience, a section of the journal Frontiers in Neurology

RECEIVED 02 April 2022
ACCEPTED 06 July 2022
PUBLISHED 29 July 2022

CITATION
Ren L, Gang X, Yang S, Sun M and Wang G (2022) A new perspective of hypothalamic disease: Shapiro's syndrome. *Front. Neurol.* 13:911332. doi: 10.3389/fneur.2022.911332

A new perspective of hypothalamic disease: Shapiro's syndrome

Linan Ren[1], Xiaokun Gang[1], Shuo Yang[2], Meixin Sun[1] and Guixia Wang[1]*

[1]Department of Endocrinology and Metabolism, The First Hospital of Jilin University, Changchun, China, [2]Department of Clinical Nutrition, The First Hospital of Jilin University, Changchun, China

Shapiro's syndrome (SS) is characterized by spontaneous periodic hypothermia. It occurs to patients regardless of age or sex. To date, <60 cases have been reported worldwide. Current knowledge of the disease is limited to clinical feature since the pathogenesis and etiology are still controversial. In this review, the clinical characteristics, pathological mechanism, and possible etiology of the syndrome were reviewed to improve the clinical understanding of the disease.

KEYWORDS

Shapiro's syndrome, hypothermia, hyperhidrosis, agenesis of the corpus callosum, hypothalamic dysfunctional

Introduction

Shapiro's syndrome (SS), traditionally defined as the triad of spontaneous periodic hypothermia, hyperhidrosis, and agenesis of the corpus callosum (ACC), is a rare disease (1). However, spontaneous periodic hypothermia has been reported in recent years as a hallmark of both typical and variant SS (2). To date, <60 cases have been reported worldwide (3). The limited amount of data may be related to a lack of awareness among clinicians about the disease. Most of the publications on this disease were case reports, and only a limited number of reviews were based on observational studies of its clinical manifestations. The pathological mechanism of SS is still unclear, and there are several hypotheses that are hypothalamic dysfunction, neurotransmitter disorder (4–6), endogenous high melatonin, and genetic variation (2). This review summarizes the clinical manifestations and pathological mechanisms of the syndrome in order to improve clinicians' understanding of the disease.

Overview of clinical presentation

SS was first reported in 1969 and was characterized by hypothermia and hyperhidrosis associated with agenesis of the corpus callosum (1). In 1994, patients with SS with an intact corpus callosum were reported and considered to be a variant of SS (7). To date, about 60 cases have been reported worldwide, including adults and children. This paper summarizes the current available cases of SS, with the exception of

some cases where complete patient information is not available (Table 1) (3, 4, 7–12, 14–22, 27–29, 33–37). These results suggest that spontaneous periodic hypothermia is a hallmark of typical and variant SS, and that hyperhidrosis and ACC are supportive features not observed in all cases, consistent with a previous finding (2). Moreover, we found that the clinical manifestations of the syndrome included autonomic nervous dysfunction, complications related to hypothermia, and complications related to agenesis of the corpus callosum, etc. (see Table 2 for details).

The role of the hypothalamus in Shapiro's syndrome

The pathophysiological mechanism of SS is still controversial. Initially, William Shapiro et al. (1) considered the syndrome to be "diencephalic epilepsy," but this hypothesis was contradicted by the variant form of SS and the non-epileptiform focal changes of the EEG (17, 23). At present, there are three hypotheses, which are hypothalamic dysfunction, neurotransmitter dysfunction (2, 5, 9, 20, 27), and endogenous hypermelatonemia (6).

Hypothalamic dysfunction

The hypothalamus is the body's thermo regulatory center. It mainly functions on the anterior preoptic area, the anterior center controls heat dissipation by inducing vasodilatation and sweating, and the posterior center conserves heat by inducing vasoconstriction and shivering. Dysfunction of the anterior center may result in fever, and dysfunction of the posterior center may cause hypothermia. At the same time, the hypothalamus is also the neuroendocrine regulation center. Symptoms of autonomic dysfunction occur when the cortical and hippocampal hypothalamus fibers and afferent fibers from the septum to the hypothalamus are destroyed (24, 30). These theories provide a reasonable explanation for the clinical manifestations of SS. Previously, Noel et al. (17) have found severe neuronal loss and fibroglial proliferation in the infundibular nucleus of hypothalamus, especially in the arcuate nucleus, in the postmortem pathological examination of a patient with SS. Similarly, Pineda et al. (36) reported that moderate spongiosis was found in the anterior and the lateral hypothalamic nuclei in two cases of agenesis of the corpus callosum with hypothermia. These findings confirm that hypothalamic lesions play an important role in SS pathogenesis. However, patients with SS syndrome, especially those with SS variant (SS with intact corpus callosum), showed normal brain structural imaging by magnetic resonance imaging (MRI) and other imaging examinations. In recent years, functional neuroimaging data of SS have been found. Dundar et al. (10) utilized technetium 99 m-labeled hexamethylpropylene amine oxime single-photon emission computed tomography (SPECT) in a patient with SS variant, which found increased perfusion in the right thalamus, basal ganglia, and inferior frontal areas. Pazderska et al. (28) employed (18) F-fluorodeoxyglucose positron emission tomography (FDG-PET) in a patient with SS variant, and reported mild increases in metabolism in the tectal plate regions bilaterally, posterior pons, posterior medulla, and a superior margin of the cerebellar vermis. Clearly, these areas of increased activity have been shown to be involved in thermoregulation, such as the right thalamus posterior pons and the medulla (38, 39). It is plausible that the hyperperfusion and hypermetabolism may be a secondary or compensatory response to hypothermia rather than direct evidence of hypothalamic lesions. Together, the essence of SS is hypothalamic dysfunction; however, there is a lack of reliable examination for the diagnosis of patients with SS.

Hypermelatonemia

Melatonin is a hormone, which is recognized as the regulator of sleep-wake cycles, secreted primarily by the pineal gland. It is reported that melatonin played a role in the modulation of arterial blood pressure, locomotion, and thermoregulation (40). The result of a systematic review demonstrated that hypothermia was one of the adverse events in melatonin-treated sleep disorders (41). In a case of SS with hypermelatonemia, Duman et al. (6) found that the serum melatonin level increased markedly at midnight, and her symptoms were aggravated. It suggested the association between hypermelatonemia and the development of SS. However, this was the only reported case of SS with hypermelatonemia (6). Whether all patients with SS suffer from hypermelatonemia will need further clinical confirmation. Additionally, the rhythmic secretion of melatonin is regulated by the suprachiasmatic nucleus of the hypothalamus (42). Studies have shown that melatonin levels were significantly correlated with hypothalamic gray matter volume and disease severity in Parkinson's disease (PD) (43). Thus, we support the hypothesis of Duman et al. (6) that hypermelatonemia was secondary to hypothalamic dysfunction.

Neurotransmitter dysregulation

Patients with SS had obvious symptoms of autonomic nervous dysfunction. Previous studies have confirmed that neurotransmitter disorders, such as dopamine and serotonin, are associated with the development of SS (19, 31, 44). Based on "threshold temperature for shivering" and the patient response to cyproheptadine, Sheth et al. (7) reported that specific serotonin dysfunction in the extrapyramidal shivering mechanism in the anterior hypothalamus is central to the pathogenesis of paroxysmal spontaneous hypothermia with

TABLE 1 Articles and characteristics of patients with Shapiro's syndrome.

Category	Clinical features		Number ($n = 50$)	References
Basic Features	Age (years)	<20	25 (50%)	(2, 5–13)
		20–50	19 (38%)	(1, 3, 4, 13–26)
		>50	6 (12%)	(27–32)
	Gender	Female	25 (50%)	(1, 5–10, 12–15, 19, 20, 25, 27, 28, 30–32)
		Male	25 (50%)	(2–4, 7, 8, 11, 13, 16–18, 21–24, 26, 29)
	Duration (years)	≤10	33 (66%)	(2, 3, 5–13, 15, 16, 24, 25, 27, 31)
		>10	9 (18%)	(1, 4, 14, 17, 19, 22, 23, 30, 32)
	Attack Time (hours)	<1h	13 (26%)	(1, 7, 8, 11, 13, 19, 20, 26, 29–31)
		1–3h	10 (20%)	(1–3, 5, 7, 9, 12, 13, 21, 22, 32)
		3–6h	14 (28%)	(6, 8, 10)
		>6h	5 (10%)	(7, 15, 17, 24, 27)
Symptoms	Hypothermia		50 (100%)	(1–32)
	Hyperhidrosis		44 (88%)	(1–14, 16, 17, 19–23, 25–32)
	Flush		9 (18%)	(1, 3, 8, 17, 21, 22, 28)
	Pallor		20 (40%)	(2, 5–8, 10–13, 27)
	Chill		20 (40%)	(1, 2, 4–6, 8, 10, 13, 16, 17, 19, 21, 22, 24, 28, 31)
	Feelinghot		4 (8%)	(7, 23, 30, 32)
	Fatigue		8 (16%)	(1, 4, 8, 14)
	Headache		8 (16%)	(8, 21, 27)
	Faint		4 (8%)	(5, 6, 10, 13)
	Unresponsive		5 (10%)	(1, 7, 12, 21, 23)
	Alteredconsciousness		24 (48%)	(1, 4–10, 12, 13, 15–17, 20, 24, 28, 30)
	Cognitive impairment		3 (6%)	(7, 27)
	Urinaryincontinence		3 (6%)	(1, 6, 23)
	Urgency to urinate		2 (4%)	(6, 30)
	Sleep disorder		5 (10%)	(8, 14)
	Hallucinations		3 (6%)	(8)
	Anxietyordepression		3 (6%)	(14, 17, 31)
	Mental disorder		5 (10%)	(13, 16, 18, 28, 32)
	Bradycardia		20 (40%)	(1, 4, 7, 8, 12, 13, 17, 18, 21, 23–25, 28)
	Hypotension		10 (20%)	(1, 8, 15, 17, 23, 25, 29, 31)
	Dyspnea		4 (8%)	(1, 2, 7, 24)
	Abdominalpain		6 (12%)	(6–8, 12)
	Vomiting		4 (8%)	(8, 12, 28)
	Incoordination		4 (8%)	(8, 18, 20, 23)
	Dehydration		3 (6%)	(8, 16, 24)
	Tinnitus		1 (2%)	(1)
Laboratory and imaging features	Anemia		4 (8%)	(1, 15, 23, 24)

(Continued)

TABLE 1 Continued

Category	Clinical features	Number ($n = 50$)	References
	Leucopenia	1 (2%)	(23)
	Thrombocytopenia	3 (6%)	(15, 23, 24)
Laboratory and imaging features	Hypothyroidism	3 (6%)	(1, 11, 30)
	Decreasedsexhormones	3 (6%)	(4, 21, 30)
	Growth hormone deficiency	1 (2%)	(24)
	Hyponatremia	4 (8%)	(15, 23, 25, 31)
	Decrease in HVA and 5-HIAA in CSF	2 (4%)	(5)
	Endogenous hypermelatonemia	1 (2%)	(6)
	ACC	25 (50%)	(1, 3, 4, 8, 13–17, 19, 21–26, 28–32)
	SPECT: increased perfusion in regions near the thalamus	2 (4%)	(6, 10)
	FDG-PET:Increased metabolism in regions near the thalamus	1 (2%)	(28)

Based on the actual number, the percentage is for reference, especially in the symptoms, laboratory, and imaging examination sections. ACC, agenesis of the corpus callosum; HVA, homovanillic acid; 5-HIAA, 5-hydroxyindoleacetic acid; CSF, cerebrospinal fluid; SPECT, single-photon emission computed tomography; FDG-PET,18F-fluorodeoxyglucose positron emission tomography.

TABLE 2 Clinical features of Shapiro's syndrome.

Category	Clinical features
Autonomic nervous dysfunction	Hypothermia, hyperhidrosis, hypotension, dyspnea bradycardia, flush, pallor, abdominal pain, vomiting, headache, sleep disorder, urinary incontinence, urgency to urinate
Complications related to hypothermia	Unresponsive, altered consciousness, chills, shiver, edema, anemia, thrombocytopenia, leukopenia
Complications related to ACC	Epilepsy, cognitive impairment, physical dysplasia, incoordination or ataxia
Undetermined symptoms	Fatigue, tinnitus, depression or anxiety, hallucination, mental disorder, dehydration

hyperhidrosis. Increased plasma levels of norepinephrine have been reported in a patient with SS (31). Rodrigues et al. (5) reported two cases of SS, which showed reduced metabolites of 5-HIAA, HVA, 5-hydroxytryptamine and dopamine in CSF. Recently, drugs-regulating neurotransmitters, such as clonidine, cyproheptadine, pizotifen, and chlorpromazine, have achieved certain efficacy in the treatment of SS (2, 9, 20, 27, 31, 44). These results suggest that neurotransmitter regulation plays a role in SS pathogenesis. However, as mentioning above, the hypothalamus plays an important role in neuroregulation. Moreover, results of Rodrigues et al. were challenged by Duman et al. (45) who reported a case of SS in which 5-HIAA, vanillylmandelic, and HVA were normal in urine at 24 h. Therefore, we hypothesized that neurotransmitter dysregulation plays a secondary role in SS.

In conclusion, hypothalamic dysfunction is considered to be at the heart of SS. Neurochemical abnormalities secondary to hypothalamic dysfunction, such as neurotransmitter dysregulation and hypermelatonemia, play an indispensable role in the onset of SS (Figure 1).

Is Shapiro syndrome a congenital disorder?

SS is a rare disease. As mentioning above, SS is associated with hypothalamic lesions. Therefore, various factors that cause damage or lesions in the hypothalamus region may lead to SS. We hypothesized that genetic factors, infections, immune diseases, neurodegenerative changes, and et al. are the important etiologies or inducements of SS (Figure 1).

Genetic factors

ACC is an important clinical feature of SS. According to the California Birth Defects Surveillance Program, the prevalence of ACC is 1.4 per 10,000 live births, and the prevalence of CC dysplasia is 0.4 per 10,000 live births (46). These data suggest that CC abnormalities may be fairly common congenital abnormalities of the central nervous system. ACC involves the partial or complete loss of the main connectivity

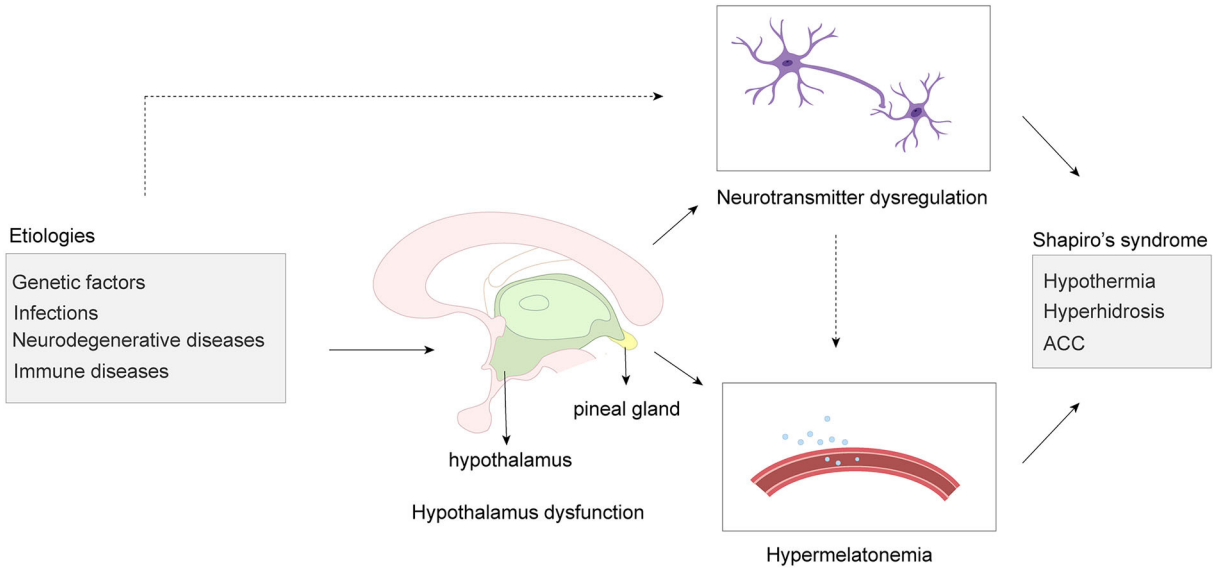

FIGURE 1
Schematic illustration of the etiologies and pathological mechanisms of the Shapiro syndrome. The dashed arrows indicate that more evidence may still be needed in this respect. Neurotransmitter dysregulation and hypermelatonemia are collectively referred to as neurochemical abnormalities. ACC, agenesis of the corpus callosum.

pathway connecting the two brain hemispheres and may be isolated (without other abnormalities) or complex (co-existing with other abnormalities) (47). In the majority of cases, genetic factors contribute to ACC. These factors include single gene mutations, multiple gene changes, and chromosomal aberrations (48). Belcastro et al. (13) reported a familial SS variant and concluded that SS was an autosomal recessive inheritance pattern. Tambasco et al. (2) also showed that SS was a congenital disorder. Additionally, the neurological channelopathies, which are similar manifestations to SS, have been confirmed as a rare monogenic genetic disease, and a variety of mutant genes, such as SCN, KCNQ, KCNA, CHRNA, GABRB, etc., have been reported (49–52). This also supports that SS may be a genetic disease. However, genetic testing is still unable to identify SS mutations or abnormal genes. Moreover, to date, SS has been reported in men and women aged 2 months to 80 years (13, 28), but only two familial cases (36). Therefore, the role of genetic variation in SS still requires further research in the future.

Neurodegenerative diseases

PD is the second most common neurodegenerative disorder, affecting about 315 per 100,000 people (53, 54). Patients often develop non-motor autonomic features, such as sleep disturbances, temperature imbalances, pain, cognitive deficits, depression, etc. (54, 55). Recently, it has been reported that patients with PD developed spontaneous periodic hypothermia, and MRI imaging showed normal brain tissue structure, which is consistent with the clinical symptoms of SS (27, 56). These results indicate that PD may be a potential reason of SS. In PD patients with a higher SCOPA-AUT score (PD Autonomic Nerve Outcome Scale), functional connection between HTH and the striatum (caudate nucleus, putamen) and thalamus was significantly reduced, compared with those with a lower SCOPA-AUT score (57). It indicates that thalamo-striatal artery-hypothalamus functional connection is interrupted in PD patients with autonomic nerve dysfunction symptoms. In addition, Renga et al. (56) observed brain tissue sections of PD patients with spontaneous periodic hypothermia and found α -synuclein deposition in the hypothalamus. These results suggest that clinical features of SS occur when PD involves the hypothalamus, and that variants of SS are more common. Furthermore, evidence of hypothalamic involvement has been found in other neurodegenerative diseases. In animal studies, degeneration of the supraspinal nucleus in mice with Alzheimer's disease was detected by magnetic resonance relaxation measurements and immunohistochemical monitoring (58).

Infections

Nervous system complications caused by infection are common and a hot topic of concern for many researchers. Previous studies have reported a 22-year-old woman who developed encephalopathy after H1N1 influenza, followed by

multiple manifestations of hypothalamic dysfunction, insomnia, and persistent PD (59). Gamboa et al. (60) also found antigenic substances associated with neurotropic influenza strain A0 in some neurons of the hypothalamus and substantia nigra in Parkinson's posterior brain. The coronavirus disease 2019 (COVID-19), caused by severe acute respiratory syndrome coronavirus 2 (SARS-CoV-2), has become a global epidemic in recent years (61). Apart from the lungs, the heart and the brain are the main target organs of SARS-CoV-2 (62, 63). SARS-CoV-2 may travel cross the blood-brain barrier or invade the central nervous system *via* the olfactory tract and infect neurons and glial cells that express ACE2, leading to neuroinflammation and neuropathogenesis in brain regions, including the hypothalamus (62–66). COVID-19 has been reported to worsen preexisting symptoms in patients with Shapiro's syndrome variants (67). Additionally, clinical manifestations of SS have been reported in HIV-infected patients (37, 68, 69). Moulignier et al. (68) have demonstrated coordination and consistency between transient hypothermia processes and high levels of HIV replication. Langford et al. (70) found microglial nodules, multinucleated giant cells, perivascular cuff of inflammatory cells, and the presence of HIV-infected cells in the hypothalamic tissue of HIV-infected patients. Collectively, these pieces of evidence suggest that the virus may invade the hypothalamus through various pathways and may eventually lead to SS.

Immune diseases

Multiple sclerosis (MS) is a chronic, predominantly immune-mediated disease of the central nervous system and one of the most common reasons of neurological disability in young people worldwide (71, 72). The global median prevalence of MS was 33 cases per 100,000 population, with significant differences between countries (71). Prevalence was highest in North America and Europe (140 and 108 cases per 100,000 population, respectively) and lowest in Asia and sub-Saharan Africa (2.2 and 2.1 cases per 100,000 population, respectively) (71, 73). MS usually develops in adults between the ages of 20 and 40 (71). The incidence is about three times higher in women than in men. Paroxysmal hypothermia often occurs in patients with MS (71, 74). Linker et al. (25) reported on a patient with long-term secondary progressive MS and six recurrent episodes of hypothermia as low as 29.9°C with hypotension, bradycardia, coagulopathy, and electrolyte imbalance. MRI showed severe involvement of the CC with associated lesions in the right posterior thalamus (25). These symptoms and MRI findings were consistent with SS syndrome. Toledano et al. (75) demographic analysis of paroxysmal hypothermia in multiple sclerosis found that, among 156 patients, 34 patients had both MS and hypothermia, accounting for 21.8%, but only 4 patients had significant MRI lesions in the hypothalamus. Huitinga et al. (76) found MS lesions in the hypothalamus in 16 out of 17 patients (95%) through the pathological examination of the cadaver, and the overall incidence of active MS lesions was as high as 60%. These data suggest that hypothalamic dysfunction is a potential reason of SS in patients with MS, and lesions in the hypothalamic region are not easily detected by MRI.

Conclusion

SS is a rare disorder characterized by hypothermia and hyperhidrosis, with or without ACC. SS is a disease with autonomic nerve dysfunction as the main clinical manifestation caused by hypothalamic dysfunction. Genetic, neurodegenerative, infectious and immune diseases are important causes or predisposing factors of SS. There are no reliable imaging or laboratory tests to diagnose SS. The diagnosis of SS by testing neurotransmitter levels in cerebrospinal fluid or serum melatonin levels remains controversial. This review encourages clinicians and investigators to explore more reliable diagnostic methods to improve the diagnosis and treatment rate of SS. Meanwhile, this review recommends that hospitals around the world establish SS registration centers so that clinicians may understand more clinical features of the disease, explore more possible causes of SS, and achieve early prevention, early diagnosis, and early treatment.

Author contributions

LR designed the study, searched and careened literature, and wrote the manuscript. SY revised the manuscript. MS searched and careened literature. XG and GW designed the study, obtained the funding, and revised the manuscript. All the authors have read and approved the final version of the manuscript.

Funding

This work was financially supported by grants from the National Natural Science Foundation of China (81972372 to XG) and the Department of Science and Technology of Jilin Province (20190901006JC to GW).

Conflict of interest

The authors declare that the research was conducted in the absence of any commercial or financial relationships that could be construed as a potential conflict of interest.

Publisher's note

References

1. Shapiro WR, Williams GH, Plum F. Spontaneous recurrent hypothermia accompanying agenesis of the corpus callosum. *Brain.* (1969) 92:423–36. doi: 10.1093/brain/92.2.423

2. Tambasco N, Belcastro V, Prontera P, Nigro P, Donti E, Rossi A, et al. Shapiro's syndrome: defining the clinical spectrum of the spontaneous paroxysmal hypothermia syndrome. *Eur J Paediatr Neurol.* (2014) 18:453–7. doi: 10.1016/j.ejpn.2014.02.001

3. Zhao C, Zhang J, Liang B, Zhong Q, Gao W. A Chinese case of Shapiro syndrome: responsive to carbamazepine. *Neurol Sci.* (2016) 37:489–90. doi: 10.1007/s10072-015-2438-0

4. Sadowsky C, Reeves AG. Agenesis of the corpus callosum with hypothermia. *Arch Neurol.* (1975) 32:774–6. doi: 10.1001/archneur.1975.00490530096011

5. Rodrigues Masruha M, Lin J, Arita JH, De Castro Neto EF, Scerni DA, Cavalheiro EA, et al. Spontaneous periodic hypothermia and hyperhidrosis: a possibly novel cerebral neurotransmitter disorder. *Dev Med Child Neurol.* (2011) 53:378–80. doi: 10.1111/j.1469-8749.2010.03854.x

6. Duman O, Durmaz E, Akcurin S, Serteser M, Haspolat S. Spontaneous endogenous hypermelatoninemia: a new disease? *Horm Res Paediatr.* (2010) 74:444–8. doi: 10.1159/000315477

7. Sheth RD, Barron TF, Hartlage PL. Episodic spontaneous hypothermia with hyperhidrosis: implications for pathogenesis. *Pediatr Neurol.* (1994) 10:58–60. doi: 10.1016/0887-8994(94)90069-8

8. Tambasco N, Paoletti FP, Prato G, Mancardi MM, Pronter P, Giordano L, et al. Long-term follow-up in pediatric patients with paroxysmal hypothermia (Shapiro's syndrome). *Eur J Paediatr Neurol.* (2018) 22:1081–6. doi: 10.1016/j.ejpn.2018.08.004

9. Denegri L, Prato G, Mancardi MM, Schiaffino C, Striano P, Baglietto MG. Early-Onset shapiro syndrome variant treated with pizotifen: a case report. *Neurodiagn J.* (2017) 57:139–46. doi: 10.1080/21646821.2017.1309941

10. Dundar NO, Boz A, Duman O, Aydin F, Haspolat S. Spontaneous periodic hypothermia and hyperhidrosis. *Pediatr Neurol.* (2008) 39:438–40. doi: 10.1016/j.pediatrneurol.2008.08.010

11. Arkader R, Takeuchi CA. Shapiro syndrome with hypothalamic hypothyroidism. *Arq Neuropsiquiatr.* (2008) 66:418–9. doi: 10.1590/S0004-282X2008000300029

12. Alves Martins W. do Amaral Cristovam R, Fussiger H, Maria Vedana V, Hemb M. Thermoregulatory instability in childhood: linking the normal brain to hypothalamic storm. *Case Rep Neurol Med.* (2016) 2016:3903854. doi: 10.1155/2016/3903854

13. Belcastro V, Striano P, Pierguidi L, Arnaboldi M, Tambasco N. Recurrent hypothermia with hyperhidrosis in two siblings: familial Shapiro syndrome variant. *J Neurol.* (2012) 259:756–8. doi: 10.1007/s00415-011-6237-0

14. Bozkurt Zincir S, Zincir S, Kabak SG. Remission of episodic sweating attacks and comorbid depression in shapiro syndrome: case report. *Noro psikiyatri arsivi.* (2014) 51:405–7. doi: 10.5152/npa.2014.6996

15. Roeker LE, Gupta V, Gonsalves WI, Wolanskyj AP, Gangat N. Cyclic bicytopenia in a patient with shapiro syndrome. *Case Rep Hematol.* (2013) 2013:231713. doi: 10.1155/2013/231713

16. Shenoy C. Shapiro syndrome. *QJM.* (2008) 101:61–2. doi: 10.1093/qjmed/hcm106

17. Noël P, Hubert JP, Ectors M, Franken L, Flament-Durand J. Agenesis of the corpus callosum associated with relapsing hypothermia. a clinico-pathological report. *Brain.* (1973) 96:359–68. doi: 10.1093/brain/96.2.359

18. Braams NJ, Hendriks ML, van Halm VP. Mode of death in Shapiro syndrome: a case report. *Eur Heart J Case Rep.* (2019) 3:ytz074. doi: 10.1093/ehjcr/ytz074

19. Darku B, Kalra P, Prasad C, Yadav R. Episodic hyperhydrosis with corpus callosum agenesis: a rare case of Shapiro syndrome. *Neurol India.* (2011) 59:130–1. doi: 10.4103/0028-3886.76868

20. Elkoundi A, Mounir K, Atmani W, Balkhi H. Management of a patient with Shapiro syndrome variant during pregnancy. *Int J Obstet Anesth.* (2020) 43:87–8. doi: 10.1016/j.ijoa.2020.03.004

21. Segeren CM, Polderman KH, Lips P. Agenesis of the corpus callosum associated with paroxysmal hypothermia: Shapiro's syndrome. *Neth J Med.* (1997) 50:29–35. doi: 10.1016/S0300-2977(96)00071-X

22. Owen AJ, Backman SB. Perioperative temperature changes in a patient with Shapiro syndrome. *Anesthesiology.* (2001) 95:268–70. doi: 10.1097/00000542-200107000-00042

23. Summers GD, Young AC, Little RA, Stoner HB, Forbes WS, Jones RA. Spontaneous periodic hypothermia with lipoma of the corpus callosum. *J Neurol Neurosurg Psychiatry.* (1981) 44:1094–9. doi: 10.1136/jnnp.44.12.1094

24. Hemelsoet DM, De Bleecker JL. Post-traumatic spontaneous recurrent hypothermia: a variant of Shapiro's syndrome. *Eur J Neurol.* (2007) 14:224–7. doi: 10.1111/j.1468-1331.2006.01609.x

25. Linker RA, Mohr A, Cepek L, Gold R, Prange H. Core hypothermia in multiple sclerosis: case report with magnetic resonance imaging localization of a thalamic lesion. *Mult Scler.* (2006) 12:112–5. doi: 10.1191/135248506ms1268cr

26. Jiang F, Tang Z, Zhong D, Li G. Shapiro syndrome: recurrent hyperhidrosis and hypothermia with corpus callosum agenesis. *Neurology.* (2022) 98:460–1. doi: 10.1212/WNL.0000000000200101

27. Aubignat M, Tir M, Krystkowiak P, Andriuta D. Episodic headache with spontaneous hypothermia reveal Shapiro's syndrome variant with effectiveness of clonidine therapy. *J Headache Pain.* (2021) 22:30. doi: 10.1186/s10194-021-01245-3

28. Pazderska A, O'Connell M, Pender N, Gavin C, Murray B, O'Dowd S. Insights into thermoregulation: a clinico-radiological description of Shapiro syndrome. *J Neurol Sci.* (2013) 329:66–8. doi: 10.1016/j.jns.2013.03.014

29. Kenney DL, Toledano M, Moseley BD. Hypothermia and corpus callosum agenesis in Shapiro syndrome: too cold, even for a Viking. *Neurology.* (2012) 79:e78. doi: 10.1212/WNL.0b013e318266fc66

30. Wright AT. Basal forebrain malformation with hyperhidrosis and hypothermia: variant of Shapiro's syndrome. *Neurology.* (2002) 58:508–9. doi: 10.1212/WNL.58.3.508

31. Sanfield JA, Linares OA, Cahalan DD, Forrester JM, Halter JB, Rosen SG. Altered norepinephrine metabolism in Shapiro's syndrome. *Arch Neurol.* (1989) 46:53–7. doi: 10.1001/archneur.1989.00520370055019

32. Klein CJ, Silber MH, Halliwill JR, Schreiner SA, Suarez GA, Low PA. Basal forebrain malformation with hyperhidrosis and hypothermia: variant of Shapiro's syndrome. *Neurology.* (2001) 56:254–6. doi: 10.1212/WNL.56.2.254

33. Topcu Y, Bayram E, Karaoglu P, Yis U, Kurul SH. The combination of thermal dysregulation and agenesis of corpus callosum: Shapiro's or/and reverse Shapiro's syndrome. *Ann Indian Acad Neurol.* (2013) 16:716–9. doi: 10.4103/0972-2327.120451

34. Bosacki C, Hausfater P, Koenig M, Serratrice J, Piette AM, Cathébras P. [Spontaneous hypothermia: a series of ten cases, place of Shapiro's syndrome]. *Rev Med Interne.* (2005) 26:615–23. doi: 10.1016/j.revmed.2005.05.005

35. Gramont B, Labouré J, Soulier H, Cathébras P. [Spontaneous periodic hypothermia syndrome: a systematic review of the literature]. *Rev Med Interne.* (2021) 42:686–93. doi: 10.1016/j.revmed.2021.04.001

36. Pineda M, Gonzalez A, Fàbregues I, Fernández-Alvarez E, Ferrer I. Familial agenesis of the corpus callosum with hypothermia and apneic spells. *Neuropediatrics.* (1984) 15:63–7. doi: 10.1055/s-2008-1052343

37. Okechukwu CN, Pesanti E. Episodic spontaneous hyperhidrosis hypothermia in human immunodeficiency virus-positive patients. *Clin Infect Dis.* (1999) 29:210. doi: 10.1086/520162

38. Nakamura K, Morrison SF. A thermosensory pathway that controls body temperature. *Nat Neurosci.* (2008) 11:62–71. doi: 10.1038/nn2027

39. Morrison SF. RVLM and raphe differentially regulate sympathetic outflows to splanchnic and brown adipose tissue. *Am J Physiol.* (1999) 276:R962–73. doi: 10.1152/ajpregu.1999.276.4.R962

40. Lin MT, Chuang JI. Melatonin potentiates 5-HT(1A) receptor activation in rat hypothalamus and results in hypothermia. *J Pineal Res.* (2002) 33:14–9. doi: 10.1034/j.1600-079X.2002.01867.x

41. Besag FMC, Vasey MJ, Lao KSJ, Wong ICK. Adverse events associated with melatonin for the treatment of primary or secondary sleep disorders: a systematic review. *CNS Drugs.* (2019) 33:1167–86. doi: 10.1007/s40263-019-00680-w

42. Pfeffer M, Korf HW, Wicht H. Synchronizing effects of melatonin on diurnal and circadian rhythms. *Gen Comp Endocrinol.* (2018) 258:215–21. doi: 10.1016/j.ygcen.2017.05.013

43. Breen DP, Nombela C, Vuono R, Jones PS, Fisher K, Burn DJ, et al. Hypothalamic volume loss is associated with reduced melatonin output in Parkinson's disease. *Mov Disord.* (2016) 31:1062–6. doi: 10.1002/mds.26592

44. Ferguson KM, Fyfe T, Montgomery J. A case of spontaneous hypothermia. *Scott Med J.* (1992) 37:85–6. doi: 10.1177/003693309203700308

45. Duman O, Durmaz E. Spontaneous periodic hypothermia and hyperhidrosis: its relation with spontaneous endogenous hypermelatoninemia. *Dev Med Child Neurol.* (2012) 54:190. doi: 10.1111/j.1469-8749.2011.04145.x

46. Glass HC, Shaw GM, Ma C, Sherr EH. Agenesis of the corpus callosum in California 1983-2003: a population-based study. *Am J Med Genet A.* (2008) 146A:2495-500. doi: 10.1002/ajmg.a.32418

47. Santo S, D'Antonio F, Homfray T, Rich P, Pilu G, Bhide A, et al. Counseling in fetal medicine: agenesis of the corpus callosum. *Ultrasound Obstet Gynecol.* (2012) 40:513–21. doi: 10.1002/uog.12315

48. Palmer EE, Mowat D. Agenesis of the corpus callosum: a clinical approach to diagnosis. *Am J Med Genet C Semin Med Genet.* (2014) 166c:184-97. doi: 10.1002/ajmg.c.31405

49. Ryan DP, Ptácek LJ. Episodic neurological channelopathies. *Neuron.* (2010) 68:282–92. doi: 10.1016/j.neuron.2010.10.008

50. Kullmann DM. Neurological channelopathies. *Annu Rev Neurosci.* (2010) 33:151–72. doi: 10.1146/annurev-neuro-060909-153122

51. Spillane J, Kullmann DM, Hanna MG. Genetic neurological channelopathies: molecular genetics and clinical phenotypes. *J Neurol Neurosurg Psychiatry.* (2016) 87:37–48. doi: 10.1136/jnnp-2015-311233

52. Kessi M, Chen B, Peng J, Yan F, Yang L, Yin F. Calcium channelopathies and intellectual disability: a systematic review. *Orphanet J Rare Dis.* (2021) 16:219. doi: 10.1186/s13023-021-01850-0

53. Broen MP, Narayen NE, Kuijf ML, Dissanayaka NN, Leentjens AF. Prevalence of anxiety in Parkinson's disease: A systematic review and meta-analysis. *Mov Disord.* (2016) 31:1125–33. doi: 10.1002/mds.26643

54. Li S, Wang Y, Wang F, Hu LF, Liu CF. A new perspective for parkinson's disease: circadian rhythm. *Neurosci Bull.* (2017) 33:62–72. doi: 10.1007/s12264-016-0089-7

55. Palma JA, Mano T. Central or peripheral autonomic dysfunction in Parkinson disease: Does it matter? *Neurology.* (2018) 90:1045–6. doi: 10.1212/WNL.0000000000005624

56. Renga V, Hickey WF, JL B. Spontaneous periodic hypothermia in Parkinson disease with hypothalamic involvement. *Neurol Clin Pract.* (2017) 7:538–40. doi: 10.1212/CPJ.0000000000000402

57. Dayan E, Sklerov M, Browner N. Disrupted hypothalamic functional connectivity in patients with PD and autonomic dysfunction. *Neurology.* (2018) 90:e2051–8. doi: 10.1212/WNL.0000000000005641

58. Roy U, Heredia-Muñoz MT, Stute L, Höfling C, Matysik J, Meijer JH, et al. Degeneration of the suprachiasmatic nucleus in an Alzheimer's disease mouse model monitored by in vivo magnetic resonance relaxation measurements and immunohistochemistry. *J Alzheimers Dis.* (2019) 69:363–75. doi: 10.3233/JAD-190037

59. González-Duarte A, Magaña Zamora L, Cantú Brito C, García-Ramos G. Hypothalamic abnormalities and Parkinsonism associated with H1N1 influenza infection. *J Neuroinflammation.* (2010) 7:47. doi: 10.1186/1742-2094-7-47

60. Gamboa ET, Wolf A, Yahr MD, Harter DH, Duffy PE, Barden H, et al. Influenza virus antigen in postencephalitic parkinsonism brain. detection by immunofluorescence. *Arch Neurol.* (1974) 31:228–32. doi: 10.1001/archneur.1974.00490400042003

61. Majumder J, Minko T. Recent developments on therapeutic and diagnostic approaches for COVID-19. *AAPS J.* (2021) 23:14. doi: 10.1208/s12248-020-00532-2

62. Selvaraj K, Ravichandran S, Krishnan S, Radhakrishnan RK, Manickam N, Kandasamy M. Testicular atrophy and hypothalamic pathology in COVID-19: possibility of the incidence of male infertility and HPG axis abnormalities. *Reproduct Sci.* (2021) 28:2735–42. doi: 10.1007/s43032-020-00441-x

63. Wu Y, Xu X, Chen Z, Duan J, Hashimoto K, Yang L, et al. Nervous system involvement after infection with COVID-19 and other coronaviruses. *Brain Behav Immun.* (2020) 87:18–22. doi: 10.1016/j.bbi.2020.03.031

64. Hamming I, Timens W, Bulthuis ML, Lely AT, Navis G, van Goor H. Tissue distribution of ACE2 protein, the functional receptor for SARS coronavirus. a first step in understanding SARS pathogenesis. *J Pathol.* (2004) 203:631–7. doi: 10.1002/path.1570

65. Pascual-Goñi E, Fortea J, Martínez-Domeño A, Rabella N, Tecame M, Gómez-Oliva C, et al. COVID-19-associated ophthalmoparesis and hypothalamic involvement. *Neurol Neuroimmunol Neuroinflamm.* (2020) 7:e823. doi: 10.1212/NXI.0000000000000823

66. Baig AM, Khaleeq A, Ali U, Syeda H. Evidence of the COVID-19 virus targeting the CNS: tissue distribution, host-virus interaction, and proposed neurotropic mechanisms. *ACS Chem Neurosci.* (2020) 11:995–8. doi: 10.1021/acschemneuro.0c00122

67. Lamotte G, Benarroch EE, Coon EA. Paroxysmal hypothermia and hyperhidrosis with exacerbation after COVID-19 Infection. *Clin Auton Res.* (2021) 31:327–9. doi: 10.1007/s10286-021-00783-9

68. Moulignier A, Guiard-Schmid JB, Gbadoe AH, RozenbaumW. HIV-1-related spontaneous episodic hypothermia. *Neurology.* (2003) 61:418–9. doi: 10.1212/01.WNL.0000073539.21469.b7

69. Simpson SJ, Ratnappuli A, Porte ME, McGann H, Lacey CJ. Hypothermia - an unusual initial presentation of human immunodeficiency virus infection. *Int J STD AIDS.* (2020) 31:1219–21. doi: 10.1177/0956462420939409

70. Langford D, Baron D, Joy J, Del Valle L, Shack J. Contributions of HIV infection in the hypothalamus and substance abuse/use to HPT dysregulation. *Psychoneuroendocrinology.* (2011) 36:710–9. doi: 10.1016/j.psyneuen.2010.10.005

71. Oh J, Vidal-Jordana A, Montalban X. Multiple sclerosis: clinical aspects. *Curr Opin Neurol.* (2018) 31:752–9. doi: 10.1097/WCO.0000000000000622

72. Dobson R, Giovannoni G. Multiple sclerosis - a review. *Eur J Neurol.* (2019) 26:27–40. doi: 10.1111/ene.13819

73. Belbasis L, Bellou V, Evangelou E, Ioannidis JP, Tzoulaki I. Environmental risk factors and multiple sclerosis: an umbrella review of systematic reviews and meta-analyses. *Lancet Neurol.* (2015) 14:263–73. doi: 10.1016/S1474-4422(14)70267-4

74. Amato MP, Derfuss T, Hemmer B, Liblau R, Montalban X, Sørensen PS, et al. Environmental modifiable risk factors for multiple sclerosis: report from the 2016 ECTRIMS focused workshop. *Mult Scler.* (2018) 24:590–603. doi: 10.1177/1352458516686847

75. Toledano M, Weinshenker BG, Kaufmann TJ, Parisi JE, Paz Soldán MM. Demographics and clinical characteristics of episodic hypothermia in multiple sclerosis. *Mult Scler.* (2019) 25:709–14. doi: 10.1177/1352458518767045

76. Huitinga I, Erkut ZA, van Beurden D, Swaab DF. The hypothalamo-pituitary-adrenal axis in multiple sclerosis. *Ann N Y Acad Sci.* (2003) 992:118–28. doi: 10.1111/j.1749-6632.2003.tb03143.x

frontiers | Frontiers in Neuroscience

TYPE Original Research
PUBLISHED 01 September 2022
DOI 10.3389/fnins.2022.882602

OPEN ACCESS

EDITED BY
Joel C. Bornstein,
The University of Melbourne, Australia

REVIEWED BY
Jiande Chen,
University of Michigan, United States
Gimiga Nicoleta,
Sfanta Maria Emergency Clinical Hospital for Children, Romania

*CORRESPONDENCE
Jan D. Huizinga
huizinga@mcmaster.ca
Ji-Hong Chen
chen338@mcmaster.ca

SPECIALTY SECTION
This article was submitted to Autonomic Neuroscience, a section of the journal Frontiers in Neuroscience

RECEIVED 03 March 2022
ACCEPTED 04 August 2022
PUBLISHED 01 September 2022

CITATION
Ali MK, Saha S, Milkova N, Liu L, Sharma K, Huizinga JD and Chen J-H (2022) Modulation of the autonomic nervous system by one session of spinal low-level laser therapy in patients with chronic colonic motility dysfunction.
Front. Neurosci. 16:882602.
doi: 10.3389/fnins.2022.882602

Modulation of the autonomic nervous system by one session of spinal low-level laser therapy in patients with chronic colonic motility dysfunction

M. Khawar Ali[1,2], Shrayasee Saha[2], Natalija Milkova[2], Lijun Liu[2], Kartik Sharma[2], Jan D. Huizinga [1,2]* and Ji-Hong Chen [2]*

[1]Faculty of Engineering, School of Biomedical Engineering, McMaster University, Hamilton, ON, Canada, [2]Division of Gastroenterology, Department of Medicine, Faculty of Health Sciences, Farncombe Family Digestive Health Research Institute, Hamilton, ON, Canada

Patients with a defecation disorder may not evoke a normal defecation reflex, or the reflex may be excessive, as a dysfunction of the spinal autonomic nervous system. Treatment with various forms of lumbar and sacral neuromodulation have shown symptom improvement, but potential changes in autonomic functioning are rarely studied. Here we evaluate the effects on autonomic function of a single session of low-level laser therapy (LLLT) on the lumbar and sacral spine in 41 patients with chronic gastrointestinal motor dysfunction. The LLLT protocol used red LED light at a wavelength of 660 nm for 10 min and infrared LED light at a wavelength of 840 nm for 10 min, followed by infrared laser light at a wavelength of 825 nm for 10 min. Effects on the autonomic nervous system were assessed by measuring heart rate variability (HRV) changes. Respiratory Sinus Arrhythmia (RSA) and Root Mean Square of Successive Differences (RMSSD) were used to quantify parasympathetic reactivity; the Baevsky's Stress Index (SI) reflected sympathetic activity while the ratios SI/RSA and SI/RMSSD were used to show shifts in autonomic dominance. The results indicate that lumbar and sacral neuromodulation using light arrays reduced, whereas stimulation by the laser probes significantly increased parasympathetic activity. The light arrays increased whereas the laser probes significantly decreased sympathetic activity (SI). The entire protocol shifted the autonomic balance toward parasympathetic activity. The comparison of actual vs. sham neuromodulation proved that the change in HRV parameters was due to actual light stimulation and not due to the arrays and probe touching the skin. In conclusion, a single session of LLLT markedly affects autonomic nervous system activity reflected

in changes in HRV which is only possible by generating activity in the spinal autonomic nerves. These results warrant a study into the effects of LLLT on restoring autonomic dysfunction in chronic refractory colonic motility disorders.

KEYWORDS

autonomic nervous system, low level laser (light) therapy (LLLT), constipation, respiratory sinus arrhythmia, Baevsky stress index, sacral neuromodulation

Introduction

Sacral neuromodulation is explored as a treatment for motor disorders of the gastrointestinal and urinary tracts (Jones et al., 2016; Goldman et al., 2018; Payne et al., 2019). Short term stimulation of sacral nerves with implanted electrodes decreased fecal incontinence (Vaizey et al., 1999) and a multicenter study showed that chronic stimulation of the spinal cord with implanted electrodes in patients with fecal incontinence is a safe and effective treatment (Wexner et al., 2010).

Neuromodulation for chronic constipation has been explored to a lesser extent compared to fecal incontinence. In a prospective study at 5 European sites, 39 out of 45 patients achieved improvement with stimulation of implanted electrodes, from 2.3 to 6.6 evacuations per week (Kamm et al., 2010). Patients with chronic constipation associated with neurological disease also showed improvement (Khan et al., 2014). In other studies, success for alleviation of constipation was more limited (Thaha et al., 2015; Widmann et al., 2019).

The inference from many studies on chronic stimulation with implanted electrodes is that the sustained effects are caused by neuromodulation in response to repeated stimulation of both sensory and efferent fibers, causing changes in organ function. Kenefick et al. (2003) studying laser Doppler rectal mucosal blood flow, showed that activation of implanted sacral electrodes caused a marked increase in blood flux within seconds, suggesting modulation by extrinsic neural activity. Stimulation with implanted electrodes was also shown to create an electromyography response and contraction of the external anal sphincter *via* a polysynaptic reflex (Fowler et al., 2000). Furthermore, it evokes responses in the sensorimotor learning centers in cortical and subcortical structures, assessed by MRI (Blok et al., 2006).

Sacral neuromodulation using non-invasive methods is also pursued (Chen et al., 2017). Transcutaneous electrical nerve stimulation (TENS) has been shown to improve constipation symptoms in children (Leong et al., 2011; Veiga et al., 2013, 2016; Kim and Yi, 2014). Transabdominal electrical stimulation has also shown promise for lasting improvement of constipation (Leong et al., 2011). A systematic review showed that TENS had a significantly larger effect on stool frequency compared to placebo (Zheng et al., 2019). In rats, it was shown that TENS improved constipation *via* modulation of the autonomic nervous system, increased vagal activity and decreased sympathetic activity, assessed by spectral analysis of heart rate variability (HRV) (Huang et al., 2019).

Neuromodulation can also be achieved by low-level laser therapy (LLLT) or photobiomodulation. LLLT has a photochemical effect, where the application of specific frequencies of light causes chemical changes in the tissue. There is ongoing research about the cellular and molecular mechanisms through which LLLT promotes healing. It is well established that LLLT improves wound healing and reduces pain and inflammation (Mester et al., 1976). Activation of photoreceptor molecules inside the mitochondria results in increased adenosine triphosphate and reactive oxygen species, followed by activation of transcription factors producing anti-apoptotic, anti-oxidant, and pro-proliferation gene products (Hashmi et al., 2010; Chung et al., 2012). Increased ATP production from LLLT also upregulates the production of nitric oxide, which is a potent vasodilator and allows for increased blood flow and, therefore, nutrient delivery to the areas being stimulated (Hashmi et al., 2010; Chung et al., 2012). LLLT was able to enhance neural regeneration in rats following chronic depression of dorsal root ganglia (DRG) and improve their ambulatory behavior (Chen et al., 2014); the neuro-reparative effect through photobiomodulation has thus far been proven in painful diabetic neuropathy and various other neurological conditions (Hashmi et al., 2010; Yamany and Sayed, 2012; Rola et al., 2014; Chen et al., 2014; Andreo et al., 2017).

Our overall objective is to develop new treatments for patients with severe chronic colonic motility disorders, refractory to established treatments (Rao et al., 2016; Camilleri et al., 2017; Chen and Huizinga, 2019). Our specific objective related to neuromodulation is to evaluate if sacral neuromodulation can relieve symptoms and restore autonomic dysfunction in these patients (Liu et al., 2022). Patients with

Abbreviations: LLLT, Low-Level Laser Therapy; HRV, Heart rate Variability; RSA, Respiratory Sinus Arrhythmia; SI, Baevsky's Stress Index or Sympathetic Index; RMSSD, Root Mean Square of Successive Differences.

chronic constipation may not be able to generate spontaneous bowel movements. Constipation is the inability to generate one or more defecation reflexes that are orchestrated by the extrinsic autonomic nervous system involving propulsive motor activity and anal sphincter relaxation (Bharucha et al., 1993; Rao et al., 2016; Camilleri et al., 2017; Callaghan et al., 2018; Milkova et al., 2020; Ali et al., 2021). A propulsive colonic motor pattern may start with triggering of afferent neurons whose cell bodies lie within the DRG of the lumbar and sacral portions of the spinal cord (Brookes et al., 2009). Then, sacral parasympathetic nerves may initiate motor patterns in the descending colon, stimulate the rectum, and relax the internal anal sphincter in preparation for defecation (Brookes et al., 2009; Huizinga et al., 2020, 2021). At the same time, sacral information projects to the Barrington's nucleus and the nucleus tractus solitarius through spinal pathways (Valentino et al., 1999). Barrington's nucleus can then project the information to the vagus nerve through the dorsal motor nucleus of the vagus. The vagus nerve can invoke propulsive motor patterns in the ascending and transverse parts of the colon, thus transporting more colonic content in the anal direction (Valentino et al., 1999; Brookes et al., 2009). Through the neural activity in the brain stem, particularly the NTS, the neural traffic originating in the sacrum can influence autonomic innervation to the heart and hence affect HRV (Yuan et al., 2020; Ali et al., 2021).

HRV analysis is explored to evaluate autonomic functioning and dysfunction (Shields, 2009; Huizinga et al., 2018; Barbier et al., 2022; Liu et al., 2022). We used HRV successfully to show that propulsive motor patterns generated by the human colon are associated with an increase in parasympathetic activity and a decrease in sympathetic activity (Yuan et al., 2020; Ali et al., 2021). HRV is also used to assess success of treatment of autonomic dysfunction in animal models (Ouyang et al., 2020) and human studies (Karpyak et al., 2004; Euteneuer et al., 2022).

The goal of neuromodulation of the spinal cord is to affect the neural circuitries that are underlying the defecation reflexes; to drive them into their homeostatic state. It was, therefore, important to investigate whether or not LLLT can trigger autonomic nerves. The aim of the present study was to examine whether one treatment session of LLLT would show autonomic reactivity, assessed *via* HRV (Thayer et al., 2012; Baevsky and Chernikova, 2017; Ali et al., 2021), which would prove its ability to activate autonomic spinal nerves.

Materials and methods

Participants

Forty-one patients (male = 13, female = 28, age = 37 ± 17 years) with colonic motility disorders took part in this study. Out of 41 patients, 28 had chronic constipation, 5 had fecal incontinence while 8 were suffering from both constipation and fecal incontinence. The study was carried out with ethics approval from the Hamilton Integrated Research Ethics Board and written consent was obtained from all participants. All participants underwent concurrently one session of LLLT, ECG and impedance recording. Six healthy volunteers without any motility and cardiac disorders took part in a sham study.

Heart rate and impedance measurements

ECG signals were recorded using MindWare BioLab Recording Software. MindWare HRV 3.1 software was used for artifact correction and to calculate the values of the beat-to-beat intervals (RR intervals), respiratory sinus arrhythmia (RSA), and root mean square of successive differences (RMSSD) (Thayer et al., 2012; Ali et al., 2021). The sampling frequency was 500 Hz. Baevsky's stress index (Baevsky and Chernikova, 2017) (SI) was calculated using code developed in MATLAB using the RR interval time series. RSA and RMSSD were used as measures of parasympathetic reactivity; SI was used as a measure of sympathetic reactivity. The ratios SI/RSA and SI/RMSSD were used to measure shifts in combined parasympathetic and sympathetic activity. The HRV parameters were calculated for 6 min (baseline) before the LLLT session, during the three stages of the LLLT protocol, as well as 6 min recovery after the one time LLLT session. HRV parameters are obtained by short or 24 h monitoring periods; a 6 min period appears optimal for analysis of short intervention protocols (Shaffer and Ginsberg, 2017).

Low-level laser therapy protocol

Two BioFlex Duo + Professional Systems were used simultaneously to provide light therapy to the lower back; each BioFlex Duo + system included a control unit connected to a computer, an LED array containing 240 LEDs (each LED provided red light with a wavelength of 660 nm and infrared LED light at a wavelength of 840 nm) and a laser probe which provided infrared light with a wavelength of 825 nm.[1] We applied a single session of the LLLT protocol to target the lumbar and sacral area using parameters developed by Dr. Fred Kahn and colleagues (Kahn, 2022). Two arrays were used simultaneously at positions A and C for 10 min and then at positions B and D for 10 min. The array positions are shown in **Figure 1A**, and the LLLT protocol is given in **Table 1**. The LED arrays generated continuous red light for the first 5 min and infrared light pulses at 20 Hz for the next 5 min at each position. The arrays were followed by IR Laser Probe stimulations generating infrared laser light at 825 nm

1 https://bioflexlaser.com

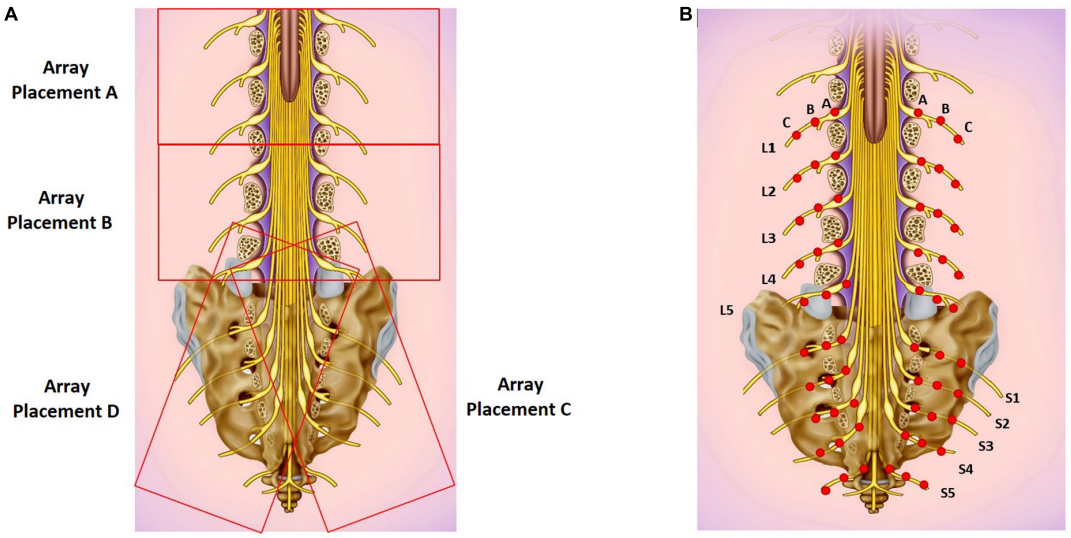

FIGURE 1
(A) LED array placements A, B, C, and D. **(B)** Target areas for laser probe stimulation marked as red dots. Each point is stimulated for 20 seconds. Basic image obtained from dreamstime.com with permission.

for 10 min. The laser probe contains one laser diode with a touch sensor to turn ON only upon touching the skin. Two laser probes were used simultaneously, one on each side of the spinal cord starting from the lumbar spine points L1-A as shown in Figure 1B for 10 s and then moving laterally on both sides by 1 cm marked as point L1-B and again stimulated for 10 s and in the third step, moving further away from the previous point by 1 cm marked as L1-C and stimulated for 10 s (Figure 1B). Similarly, for L2-L5 and S1-S5 to target the sacral sensory, sympathetic and parasympathetic nerves. Stimulating L1-S5 [three points lateral to the spinal cord for each (Figure 1B)] took 5 min using two probes simultaneously, the procedure then was repeated for the second time and the total stimulation time for the IR laser probe was 10 min. The placements of the laser probes are shown in Figure 1B. The technical specifications for LED array and the IR laser probe are given in Table 2.

Sham study

To rule out a placebo effect, the LLLT protocol was repeated twice in six healthy volunteers such that the arrays and probe were not turned ON during the first round while they were turned ON during the second round. The sham protocol included baseline (6 min) followed by simultaneously placed LED arrays at positions A and C (10 min) followed by simultaneous array placement at positions B and D (10 min) and in the next step, two IR laser probes were used to work simultaneously on both sides of the spinal column for 10 min with a 6 min recovery period (Figure 1).

Visual representation of autonomic nervous system activity

The HRV spectrogram of the RR intervals signal was generated as an image for each step of the LLLT protocol. The ECG and impedance signals were imported into ImageJ using Cardio Images plugins.[2] In the Cardio Images plugins, the peak detection and correction of the ECG signal was carried out by the Pan-Tomkins algorithm and a neural networks model generated and trained in TensorFlow with manual checking and editing of wrongly detected/edited R peaks. The tachogram of RR intervals was plotted as a raster image using a sampling frequency of 10 Hz, an image width of 5 s with cubic interpolation in the Intervals plugin. The Frequency Win plugin was used to calculate FFT spectra of the tachogram raster image using a window length of the 60 s and intervals of 10 s. The power spectra were collated into an image with time on the y-axis and frequency on the x-axis with pixel intensity as amplitude. The Win frequency plugin generated the HRV spectrogram from 0 to 5 Hz to study the RSA/HF (0.15–0.5 Hz.) band only, which represents the parasympathetic activity at normal breathing frequencies (Berntson et al., 1997). Lower frequency bands (0–0.15 Hz.), as well as the frequency band above 1 Hz, were removed in MATLAB. The spectrogram with the frequency band of 0.15–1 Hz was plotted as an image. The raster image of RR intervals was also read into MATLAB and was used to calculate RMSSD and SI, which were also plotted as

2 http://www.scepticalphysiologist.com

TABLE 1 Low level laser therapy protocol.

Session	Head used	Position	Light	Pulse frequency	Duty cycle	Duration (min)
1	Baseline					6
2	LED arrays	A and C	Red, 660 nm	Continuous		5
			IR, 840 nm	20 Hz.	50%	5
3	LED arrays	B and D	Red, 660 nm	Continuous		5
			IR, 840 nm	20 Hz.	50%	5
4	Laser probes		IR, 825 nm	Continuous		10
5	Recovery					6

aligned images. RMSSD and SI measured parasympathetic and sympathetic activity, respectively. These images were generated for the whole recording of the patients before the LLLT session—during array at AC—during array at BD—during IR laser probe—during recovery. The same procedure was used for the sham study.

Statistical analysis

The HRV parameters (RSA, RMSSD, SI, SI/RSA, SI/RMSSD) and HR were calculated from the recorded ECG signal for each stage of the LLLT protocol, including baseline and recovery for each patient. The changes in each parameter during each stage were assessed statistically for 41 patients using GraphPad Prism software. The data were first checked for normality (gaussian distribution) using the Shapiro-Wilk Normality test. A dataset was normally distributed if all the columns (before-Array AC-Array BD-Probe-Recovery) passed the Shapiro-Wilk Normality test. In the case of the normally distributed data set One-Way-ANOVA followed by Holm-Sidak, multiple comparison tests were used to see the changes in the HRV parameter during each stage of the LLLT protocol. If data was not normally distributed, the Friedman test followed by Dunn's multiple comparison test was applied to check the changes in that parameter. For subgroup analyses, the patients were divided into their main symptom: chronic constipation, fecal incontinence or both constipation and fecal incontinence. To identify the correlation between the major symptom with the HRV response during LLLT, a change in a HRV variable between baseline and each step of LLLT was assessed for correlation using the Pearson correlation test. A value of r greater than 0.50 or less than −0.50 with p-value of less than 0.05 was used as criteria for correlation. For the Sham protocol, two-way Anova followed by Bonferroni's multiple comparison test was used to compare the changes in HRV parameters during the actual and sham protocol. The significance level was set at $p < 0.05$.

The data are presented as the effect of the light arrays, focusing on the outcome measured during activation of the BD array combination and during laser probe stimulation.

TABLE 2 Specifications for LED array and IR laser probe.

	LED array	IR Laser probe
Average power	1,000 mW	180 mW
Wavelength (λ)	660 nm (Red)/840 nm (IR)	825 nm
Spot size	100 cm^2	0.1 cm^2
Power density	10 mW/cm^2	1,800 mW/cm^2
Time of application	5 min	10 min
Total energy	30,000 J	10,800 J
Energy density	3 J/cm^2	1,080 J/cm^2

Energy density = (energy × time)/spot size; power density = power/spot size.

The figures will show the data from each part of the stimulation protocol.

Results

Parasympathetic reactivity in response to light arrays and laser probe activation

Activation of the light arrays significantly decreases RSA from 5.98 to 5.80 ln (ms^2) (Figure 2A), consistent with a significant decrease in RMSSD (Figure 2B).

Laser probe stimulation increased the RSA significantly to 6.22 ln (ms^2) (Figure 2A). After the infrared laser probe stimulation, the RSA decreased back to 5.99 during recovery. Consistently, the RMSSD significantly increased in the period of laser probe stimulation.

The RSA and RMSSD values at baseline and recovery were not significantly different (Figures 2A,B). The percentage change in RSA due to laser probe stimulation and its subsequent recovery for each patient are shown in Figure 3. Figure 4 shows a continuous assessment of the HRV parameters during the entire LLLT protocol in one patient. Figure 4B represents the HF power band from which the RSA is derived. A dramatic increase in parasympathetic activity occurs, measured by HF power and RMSSD during probe stimulation.

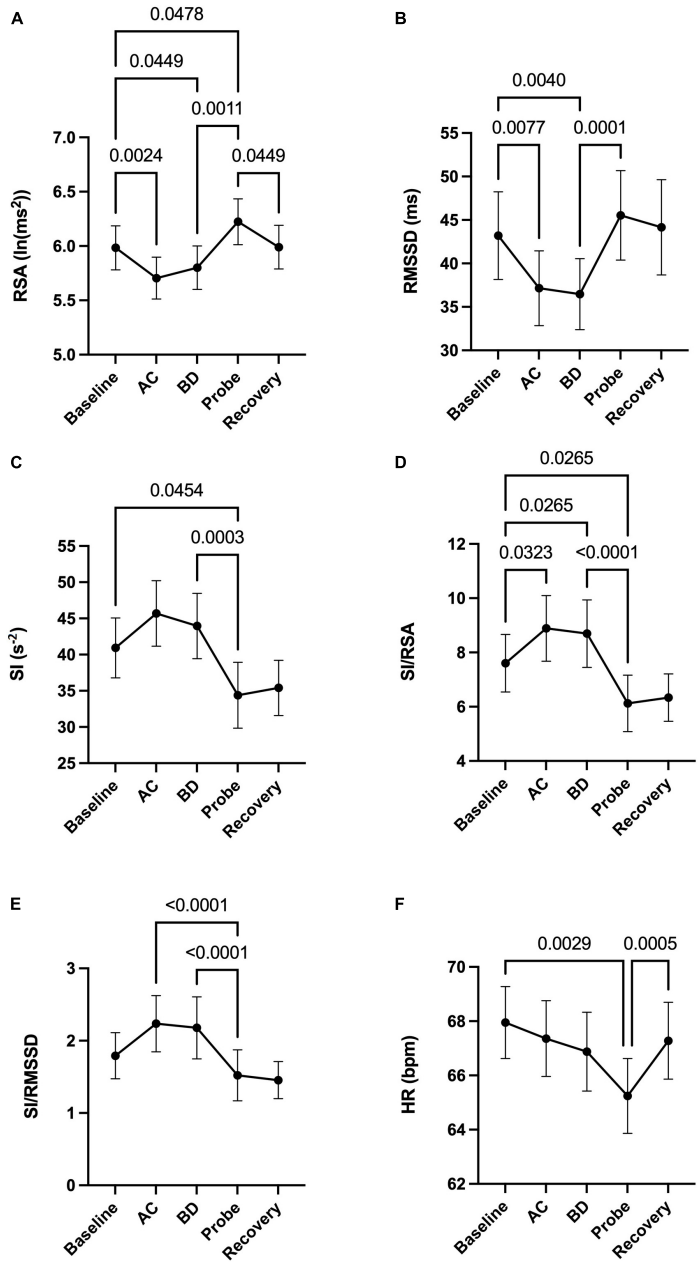

FIGURE 2
Autonomic nervous system modulation as deduced from HRV changes during one session of low-level laser therapy, stimulating the lumbar and sacral spine. **(A)** RSA, **(B)** RMSSD, **(C)** SI, **(D)** SI/RSA, **(E)** SI/RMSSD, **(F)** HR. Average values ± SEM from 41 patients with chronic colonic motility dysfunction.

Sympathetic reactivity in response to light arrays and laser probe activation

Laser probe stimulation decreased sympathetic activity without immediate recovery.

The sympathetic index (SI) measured the sympathetic nervous system response to the LLLT stimulations. The SI value numerically but not significantly increased during light array stimulation but significantly decreased from 41.3 to 34.8 s^{-2} during probe stimulation (Figure 2C). The SI values did not recover within 5 min following laser probe stimulation; stimulation decreased SI 17%, in the recovery period the decrease was still 12%. The percentage change in SI due to laser probe stimulation and the subsequent recovery values for each patient are shown in Figure 3.

	△SI		△RSA		△(SI/RSA)	
Patient#	△SI (IR Probe-Baseline)	△SI (Recovery-IR Probe)	△RSA (IR Probe-Baseline)	△RSA (Recovery-IR Probe)	△(SI/RSA) (IR Probe-Baseline)	△(SI/RSA) (Recovery-IR Probe)
pt1	-7.65%	-28.62%	40.65%	-14.98%	-34.34%	-16.04%
pt2	-53.14%	106.62%	3.17%	9.81%	-54.58%	88.17%
pt3	4.25%	-11.30%	9.26%	8.03%	-4.58%	-17.89%
pt4	50.52%	-37.72%	-9.18%	-1.34%	65.74%	-36.87%
pt5	-39.96%	21.91%	13.10%	-13.79%	-46.91%	41.40%
pt6	-13.89%	-2.11%				
pt7	-75.02%	63.52%	49.36%	-6.65%	-83.28%	74.40%
pt8	-25.05%	104.30%	5.51%	3.11%	-28.97%	97.94%
pt9	-47.12%	136.17%	15.42%	-2.86%	-54.18%	142.92%
pt10	-14.33%	1.70%	-5.64%	9.96%	-9.21%	-8.43%
pt11	13.06%	-12.34%	-33.82%	20.05%	70.82%	-29.91%
pt12	73.11%	-58.13%	-3.64%	0.00%	79.64%	-58.13%
pt13	-28.50%	-17.20%	-5.21%	-1.03%	-24.56%	-16.34%
pt14	-69.74%	22.62%	30.71%	-11.82%	-76.85%	37.12%
pt15	-62.58%	9.86%	-6.02%	5.97%	-60.18%	3.30%
pt16	-40.81%	63.90%	21.13%	-18.42%	-51.14%	94.09%
pt17	-48.36%	15.95%	11.81%	6.05%	-53.81%	8.94%
pt18	106.22%	-35.83%	-0.36%	5.70%	106.98%	-39.49%
pt19	-47.88%	25.46%	3.49%	-3.72%	-49.64%	30.13%
pt20	-56.54%	34.29%	0.17%	1.19%	-56.61%	32.69%
pt21	-22.99%	8.73%	12.58%	-0.29%	-31.60%	9.05%
pt22	54.10%	3.91%	2.07%	-6.50%	50.98%	10.67%
pt23	-65.31%	52.83%	24.09%	-18.04%	-72.05%	80.40%
pt24	-5.09%		-1.07%		-4.06%	-100.00%
pt25	-25.58%	-17.72%	8.02%	-0.43%	-31.11%	-14.69%
pt26	-19.46%	0.96%	1.84%	3.90%	-20.91%	-2.97%
pt27	-44.27%	60.52%	5.05%	-11.07%	-46.95%	181.37%
pt28	60.38%	-20.60%	-1.06%	-4.15%	62.10%	-13.64%
pt29	-44.45%		-0.45%		-44.20%	
pt30	111.85%	-74.04%	-14.64%	-0.52%	148.20%	-42.24%
pt31	-42.34%	29.95%	4.95%	-18.88%	-45.06%	69.69%
pt32	-15.06%	30.66%	3.53%	-0.26%	-17.96%	44.60%
pt33	-1.53%	-145.13%	-3.49%	15.10%	2.04%	-65.36%
pt34	56.11%	-12.17%	-11.46%	7.07%	76.31%	-17.15%
pt35	16.96%	16.46%	-10.13%	1.46%	30.14%	17.95%
pt36	-34.30%		11.43%		-41.04%	
pt37	8.96%	-5.89%	-9.08%	3.18%	19.84%	-8.56%
pt38	-36.22%	40.93%	7.73%	0.35%	-40.80%	68.71%
pt39	-58.43%	48.58%	6.17%	-18.07%	-60.84%	129.60%
pt40	-44.28%	60.77%	0.48%	-4.91%	-44.55%	167.45%
pt41	1.61%	41.89%	-2.77%	-3.32%	4.50%	77.80%

FIGURE 3
Change in RSA, SI, and SI/RSA due to laser probe stimulation and recovery in all 41 patients.

Assessing shifts in parasympathetic or sympathetic dominance

The ratios SI/RSA and SI/RMSSD showed a shift toward parasympathetic activity in response to the one-time LLLT session, dominated by a reduction in sympathetic activity.

During the laser probe stimulation, SI/RSA significantly decreased from a baseline value of 7.60 to 6.12, a 19.5% decrease. SI/RSA significantly decreased from the light arrays' effect at 8.30 to 6.12, a 29.7% decrease (Figure 2D). The value of SI/RSA remained at 6.34 during the recovery period suggesting a sustained effect of the probe. SI/RMSSD showed numerically the same direction of change with a significant effect of the laser probe compared to the effect of the light arrays (Figure 2E).

Figure 3 shows the percentage change in SI/RSA during probe stimulation of all patients, indicating a shift toward parasympathetic activity in 30 out of the 41 patients.

The change in RSA and the change in SI, in response to LLLT were assessed for correlation with either constipation, fecal incontinence or the combination, but no correlation was

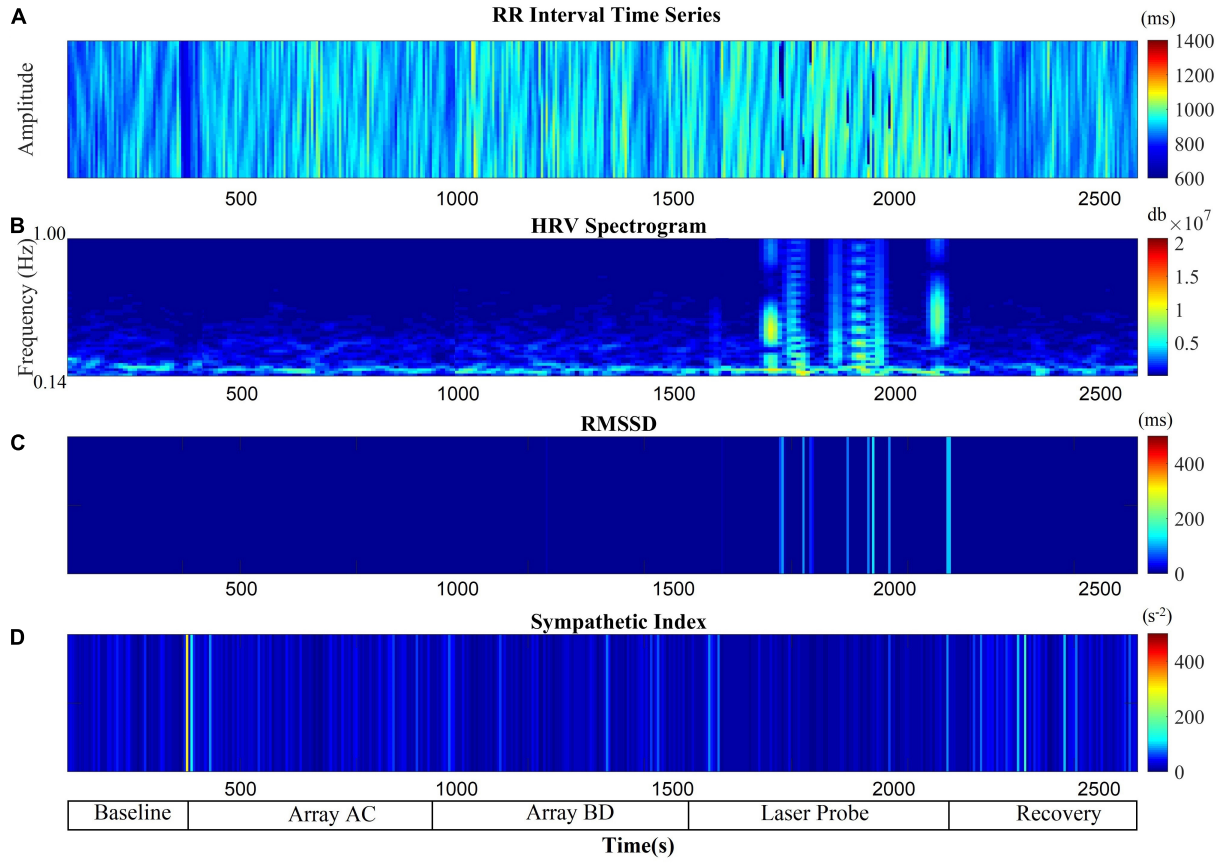

FIGURE 4
Autonomic nervous system modulation as deduced from HRV changes during the entire protocol of one session of low-level laser therapy in one patient. **(A)** RR Intervals time series, **(B)** HF band power, **(C)** RMSSD, **(D)** SI.

observed, hence the changes in the HRV parameters were not specific for any of the symptom groups.

Assessing heart rate changes during a one-time low-level laser therapy session

Comparing before and after the LLLT session, there was no significant change in heart rate. However, the average heart rate decreased by 2.7 beats per minute during laser probe stimulation compared to baseline. It recovered back to its baseline value after laser stimulation (Figure 2F).

Sham neuromodulation on healthy subjects

Sham activation of light arrays and laser probe did not significantly change HRV parameters.

In six healthy volunteers, laser probe stimulation increased RSA significantly from 6.16 during baseline to 7.00 ln (ms^2); this decreased back to 6.20 ln (ms^2) during recovery (Figure 5A). The sham procedure did not show any significant change in RSA during any step (Figure 5A). Similarly, the RMSSD increased significantly to 70.70 ms during laser probe stimulations compared to the baseline value of 59.19 ms (Figure 5B). RMSSD did not show any significant change during the sham protocol (Figure 5B).

The average value SI decreased significantly from 53.27 s^{-2} during baseline to 30.07 s^{-2} during laser probe stimulation (Figure 5C). The sham procedure did not show a significant change in SI during any step (Figure 5C).

During laser probe stimulation, the SI/RSA markedly decreased from its average baseline value of 10.41 to 5.41. This is almost a 50% decrease, which indicates a shift of autonomic dominance toward parasympathetic nervous system activity during laser probe stimulation. The sham procedure did not affect SI/RSA values during any step (Figure 5D). SI/RMSSD decreased numerically from 2.59 to 0.91 (Figure 5E). No change

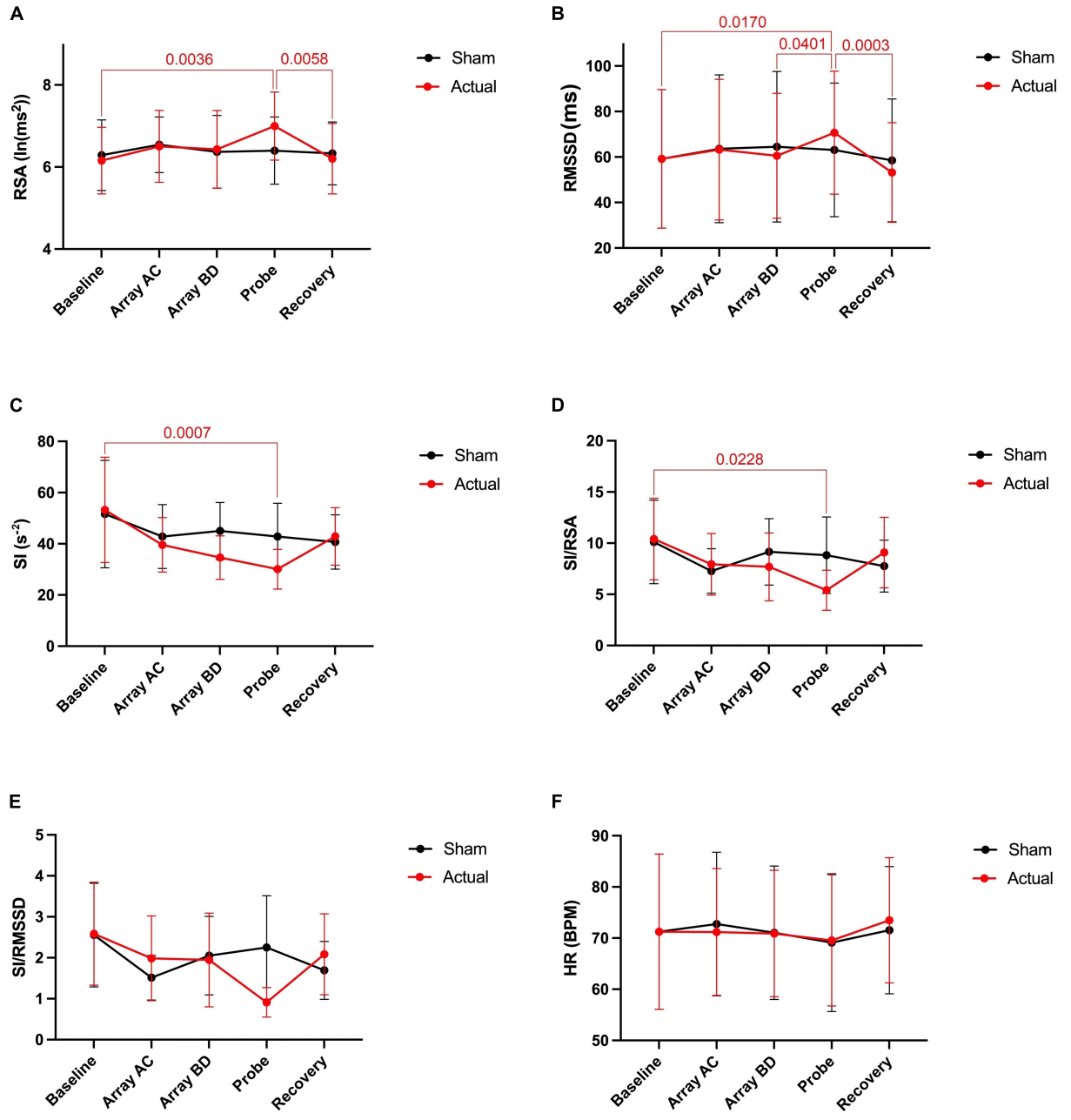

FIGURE 5
Autonomic nervous system modulation as deduced from HRV changes during one session of low-level laser therapy, stimulating the lumbar and sacral spine. **(A)** RSA, **(B)** RMSSD, **(C)** SI, **(D)** SI/RSA, **(E)** SI/RMSSD, **(F)** HR. Average values ± SEM from 6 healthy subjects during sham (placement of arrays and probe but no stimulation) and during actual activation of the arrays and probe.

was observed during the sham procedure (Figure 5E). During actual and sham procedures, the heart rate did not change compared to baseline values (Figure 5F).

Figure 6 shows a continuous assessment of HRV parameters during the sham and laser probe stimulation of a single subject. The high-frequency band power of the RR interval signal indicates that during sham probe stimulation, there was no significant change in HF parasympathetic activity. In contrast, the amplitude of the HF power band increased markedly during actual laser probe stimulation compared to baseline, sham, and recovery (Figure 6B). This was also reflected in an increased RMSSD amplitude during actual laser probe stimulations (Figure 6C). A decrease in SI amplitude during the actual laser probe stimulation

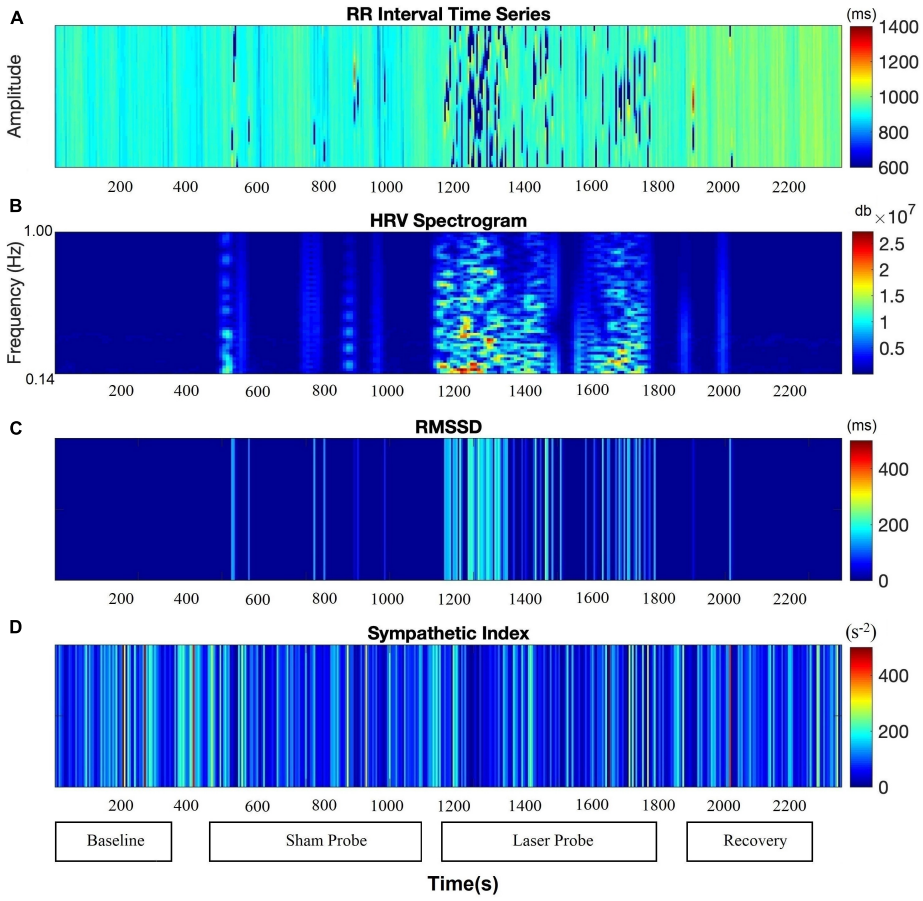

FIGURE 6
Comparison of autonomic nervous system activity during the application of the probe procedure with and without (sham) activating the probe. **(A)** RR Intervals time series, **(B)** HF band power, **(C)** RMSSD, **(D)** SI.

was observed (Figure 6D), compared to sham probe, baseline, and recovery.

Discussion

The overall effect of a single LLLT session was increased parasympathetic activity and decreased sympathetic activity, resulting in a shifting of autonomic activity into the parasympathetic domain. The protocol involved stimulation using light arrays followed by a laser probe, with the arrays, on average, decreasing and the laser probe, on average, increasing parasympathetic activity. The sham study showed that the change in autonomic activity was due to activation by light and not due to touching or pressing the probes onto the skin.

The LLLT protocol used was developed over many years by the Bioflex clinic in Toronto (see text footnote 1) and we adopted the protocol that is used in this clinic for patients with lumbar spine problems. Light is focused on the nerves exiting and entering the spinal cord, including sensory nerves with its DRG. DRG, not being part of the central nervous system, are outside the vertebrae. The pedicles associated with the vertebrae create a foramen for the spinal nerves to enter or exit the intervertebral foramen. DRG can be close to the pedicles and can be obscured by the articular processes of the vertebrae, in particular related to the large lumbar vertebrae. Hence, the laser stimulation is focused on the areas immediately outside the body of the spinal cord.

Our focused objective was to investigate whether a single session of LLLT would demonstrably affect the autonomic nervous system as measured through HRV. The fact that HRV parameters significantly changed shows that the autonomic innervation to the heart was affected; hence a neural signal from the sacral-lumbar area evoked by low-level laser stimulation reached the brain stem. This will happen when nerve action potentials are evoked in the ascending autonomic nerves. The arrays and the probe gave different responses, likely because the probe light has a much higher intensity and will penetrate deeper in the tissue, potentially activating different neuronal circuitries.

Constipation is the inability of physiological stimuli such as eating or rectal filling to evoke effective defecation reflexes. Hence the extrinsic autonomic neural circuitries that facilitate defecation reflexes are not optimally functioning. The goal of LLLT concerning colonic motility disorders is to neuromodulate the circuitry of the autonomic nervous system so that normal reflexes are restored. Stimulation with LLLT may stimulate neurons to fire action potentials with, as a consequence, the strengthening of the functionality of the synapses while also stimulating increased energy production and nutrient delivery through cellular activation and vasodilation (Chung et al., 2012; Rola et al., 2014). This would allow for recovery of the functionality of neuronal circuitries and neural regeneration (Chen et al., 2014) and ultimately help in the restoration of the defecation reflex (Furness et al., 2014; Milkova et al., 2020). The data of the present study do not inform about the likelihood of success of this therapy but give credence to exploring sacral neuromodulation using LLLT as a treatment for chronic colonic motility dysfunction.

Data availability statement

The original contributions presented in the study are included in the article/supplementary material, further inquiries can be directed to the corresponding author/s.

Ethics statement

The studies involving human participants were reviewed and approved by the Hamilton Integrated Research Ethics Board. The patients/participants provided their written informed consent to participate in this study.

Author contributions

MA analyzed all the data, contributed to interpretation, and wrote a manuscript draft. SS made a significant contribution to data analysis and data interpretation at the beginning of the project. NM and LL contributed to patient assessment and data analysis. KS made a substantial contribution to data analysis. JH and J-HC designed the study and contributed to data collection, data analysis, interpretation, and revisions to the manuscript. All authors contributed to the article and approved the submitted version.

Funding

This study was supported by the Natural Sciences and Engineering Research Council (NSERC) (grant no. 386877) to JH. MA was supported by a fellowship from the Farncombe Family Digestive Health Research Institute and NSERC.

Acknowledgments

We gratefully acknowledge that Dr. Sean Parsons provided all ImageJ plug-ins. We are grateful to Dr. Alexander Ball for his anatomical insights. We are grateful for the training provided by the Bioflex laser therapy clinic in Toronto, in particular Dr. Fred Kahn and Slava Kim.

Conflict of interest

The authors declare that the research was conducted in the absence of any commercial or financial relationships that could be construed as a potential conflict of interest.

Publisher's note

References

Ali, M. K., Liu, L., Chen, J. H., and Huizinga, J. D. (2021). Optimizing Autonomic Function Analysis *via* Heart Rate Variability Associated With Motor Activity of the Human Colon. *Front. Physiol.* 12:619722. doi: 10.3389/fphys.2021.619722

Andreo, L., Soldera, C. B., Ribeiro, B. G., de Matos, P. R. V., Bussadori, S. K., Fernandes, K. P. S., et al. (2017). Effects of photobiomodulation on experimental models of peripheral nerve injury. *Lasers Med. Sci.* 32, 2155–2165.

Baevsky, R. M., and Chernikova, A. G. (2017). Heart rate variability analysis: Physiological foundations and main methods. *Cardiometry* 10, 66–76. doi: 10.12710/cardiometry.2017.6676

Barbier, A., Chen, J.-H., and Huizinga, J. D. (2022). Autism Spectrum Disorder in Children Is Not Associated With Abnormal Autonomic Nervous System Function: Hypothesis and Theory. *Front. Psychiatry* 13:830234. doi: 10.3389/fpsyt.2022.830234

Berntson, G. G., Bigger, J. T., Eckberg, D. L., Grossman, P., Kaufmann, P. G., Malik, M., et al. (1997). Heart rate variability: Origins, methods, and interpretive caveats. *Psychophysiology* 34, 623–648. doi: 10.1111/j.1469-8986.1997.tb02140.x

Bharucha, A. E., Camilleri, M., Low, P. A., and Zinsmeister, A. R. (1993). Autonomic dysfunction in gastrointestinal motility disorders. *Gut* 34, 397–401.

Blok, B. F., Groen, J., Bosch, J. L., Veltman, D. J., and Lammertsma, A. A. (2006). Different brain effects during chronic and acute sacral neuromodulation in urge incontinent patients with implanted neurostimulators. *BJU Int.* 98, 1238–1243.

Brookes, S. J., Dinning, P. G., and Gladman, M. A. (2009). Neuroanatomy and physiology of colorectal function and defaecation: From basic science to human clinical studies. *Neurogastroenterol. Motil.* 21, 9–19. doi: 10.1111/j.1365-2982.2009.01400.x

Callaghan, B., Furness, J. B., and Pustovit, R. V. (2018). Neural pathways for colorectal control, relevance to spinal cord injury and treatment: A narrative review. *Spinal Cord* 56, 199–205. doi: 10.1038/s41393-017-0026-2

Camilleri, M., Ford, A. C., Mawe, G. M., Dinning, P. G., Rao, S. S., Chey, W. D., et al. (2017). Chronic constipation. *Nat. Rev. Dis. Primers* 3:17095.

Chen, J. D., Yin, J., and Wei, W. (2017). Electrical therapies for gastrointestinal motility disorders. *Expert Rev. Gastroenterol. Hepatol.* 11, 407–418.

Chen, J.-H., and Huizinga, J. D. (2019). "Pathophysiology of constipation," in *McMaster Textbook of Internal Medicine*, eds R. Jaeschke, P. Gajewski, and P. M. O'Byrne (Krakow: Empendium), 978.

Chen, Y. J., Wang, Y. H., Wang, C. Z., Ho, M. L., Kuo, P. L., Huang, M. H., et al. (2014). Effect of low level laser therapy on chronic compression of the dorsal root ganglion. *PLoS One* 9:e89894. doi: 10.1371/journal.pone.0089894

Chung, H., Dai, T., Sharma, S. K., Huang, Y. Y., Carroll, J. D., and Hamblin, M. R. (2012). The nuts and bolts of low-level laser (light) therapy. *Ann. Biomed. Eng.* 40, 516–533. doi: 10.1007/s10439-011-0454-7

Euteneuer, F., Neuert, M., Salzmann, S., Fischer, S., Ehlert, U., and Rief, W. (2022). Does psychological treatment of major depression reduce cardiac risk biomarkers? An exploratory randomized controlled trial. *Psychol. Med.* [Epub ahead of print]. doi: 10.1017/S0033291722000447

Fowler, C. J., Swinn, M. J., Goodwin, R. J., Oliver, S., and Craggs, M. (2000). Studies of the latency of pelvic floor contraction during peripheral nerve evaluation show that the muscle response is reflexly mediated. *J. Urol.* 163, 881–883.

Furness, J. B., Callaghan, B. P., and Rivera, L. R. (2014). The enteric nervous system and gastrointestinal innervation: Integrated local and central control. *Adv. Exp. Med. Biol.* 817, 39–71.

Goldman, H. B., Lloyd, J. C., Noblett, K. L., Carey, M. P., Castaño Botero, J. C., Gajewski, J. B., et al. (2018). International Continence Society best practice statement for use of sacral neuromodulation. *Neurourol. Urodyn.* 37, 1823–1848.

Hashmi, J. T., Huang, Y. Y., Osmani, B. Z., Sharma, S. K., Naeser, M. A., and Hamblin, M. R. (2010). Role of low-level laser therapy in neurorehabilitation. *Physical Med. Rehabil.* 2:S292–S305.

Huang, Z., Li, S., Foreman, R. D., Yin, J., Dai, N., and Chen, J. D. Z. (2019). Sacral nerve stimulation with appropriate parameters improves constipation in rats by enhancing colon motility mediated *via* the autonomic-cholinergic mechanisms. *Am. J. Physiol. Gastrointest. Liver Physiol.* 317:G609–G617. doi: 10.1152/ajpgi.00150.2018

Huizinga, J. D., Liu, L., Barbier, A., and Chen, J. H. (2021). Distal Colon Motor Coordination: The Role of the Coloanal Reflex and the Rectoanal Inhibitory Reflex in Sampling, Flatulence, and Defecation. *Front. Med.* 8:720558. doi: 10.3389/fmed.2021.720558

Huizinga, J. D., Mathewson, K. J., Yuan, Y., and Chen, J. (2018). Probing heart rate variability to determine parasympathetic dysfunction. *Physiol. Rep.* 6:e13713.

Huizinga, J. D., Milkova, N., and Chen, J. H. (2020). Transient Anal Sphincter Relaxations Are a Normal Phenomenon in Healthy Subjects. *J. Neurogastroenterol. Motil.* 26, 552–553.

Jones, J., Van de Putte, D., De Ridder, D., Knowles, C., O'Connell, R., Nelson, D., et al. (2016). A Joint Mechanism of Action for Sacral Neuromodulation for Bladder and Bowel Dysfunction. *Urology* 97, 13–19. doi: 10.1016/j.urology.2016.05.032

Kahn F (2022). *Reflects on 30 Years as a Leader and Innovator in Laser Therapy*. Available online at: http://fredkahnmd.com/ (accessed Jul 7, 2022).

Kamm, M. A., Dudding, T. C., Melenhorst, J., Jarrett, M., Wang, Z., Buntzen, S., et al. (2010). Sacral nerve stimulation for intractable constipation. *Gut* 59, 333–340.

Karpyak, V. M., Rasmussen, K. G., Hammill, S. C., and Mrazek, D. A. (2004). Changes in heart rate variability in response to treatment with electroconvulsive therapy. *J. ECT* 20, 81–88.

Kenefick, N. J., Emmanuel, A., Nicholls, R. J., and Kamm, M. A. (2003). Effect of sacral nerve stimulation on autonomic nerve function. *Br. J. Surg.* 90, 1256–1260.

Khan, U., Mason, J. M., Mecci, M., and Yiannakou, Y. (2014). A prospective trial of temporary sacral nerve stimulation for constipation associated with neurological disease. *Colorectal Dis.* 16, 1001–1009.

Kim, J. S., and Yi, S. J. (2014). Effects of Low-frequency Current Sacral Dermatome Stimulation on Idiopathic Slow Transit Constipation. *J. Phys. Ther. Sci.* 26, 831–832. doi: 10.1589/jpts.26.831

Leong, L. C., Yik, Y. I., Catto-Smith, A. G., Robertson, V. J., Hutson, J. M., and Southwell, B. R. (2011). Long-term effects of transabdominal electrical stimulation in treating children with slow-transit constipation. *J. Pediatr. Surg.* 46, 2309–2312.

Liu, L., Milkova, N., Nirmalathasan, S., Ali, M. K., Sharma, K., HuizInga, J. D., et al. (2022). Diagnosis of dysmotility associated with autonomic dysfunction in patients with chronic refractory constipation. *Nat. Sci. Rep.* 12:12051. doi: 10.1038/s41598-022-15945-6

Mester, E., Nagylucskay, S., Döklen, A., and Tisza, S. (1976). Laser stimulation of wound healing. *Acta Chir. Acad. Sci. Hung.* 17, 49–55.

Milkova, N., Parsons, S. P., Ratcliffe, E., Huizinga, J. D., and Chen, J. H. (2020). On the nature of high-amplitude propagating pressure waves in the human colon. *Am. J. Physiol. Gastrointest. Liver Physiol.* 318:G646–G660. doi: 10.1152/ajpgi.00386.2019

Ouyang, X., Li, S., Zhou, J., and Chen, J. D. (2020). Electroacupuncture Ameliorates Gastric Hypersensitivity *via* Adrenergic Pathway in a Rat Model of Functional Dyspepsia. *Neuromodulation* 23, 1137–1143. doi: 10.1111/ner.13154

Payne, S. C., Furness, J. B., and Stebbing, M. J. (2019). Bioelectric neuromodulation for gastrointestinal disorders: Effectiveness and mechanisms. *Nat. Rev. Gastroenterol. Hepatol.* 16, 89–105.

Rao, S. S., Rattanakovit, K., and Patcharatrakul, T. (2016). Diagnosis and management of chronic constipation in adults. *Nat. Rev. Gastroenterol. Hepatol.* 13, 295–305.

Rola, P., Doroszko, A., and Derkacz, A. (2014). The use of low-level energy laser radiation in basic and clinical research. *Adv. Clin. Exp. Med.* 23, 835–842.

Shaffer, F., and Ginsberg, J. P. (2017). An Overview of Heart Rate Variability Metrics and Norms. *Front. Public Health* 5:258. doi: 10.3389/fpubh.2017.00258

Shields, R. W. (2009). Heart rate variability with deep breathing as a clinical test of cardiovagal function. *Cleve Clin. J. Med.* 76:S37–S40.

Thaha, M. A., Abukar, A. A., Thin, N. N., Ramsanahie, A., and Knowles, C. H. (2015). Sacral nerve stimulation for faecal incontinence and constipation in adults. *Cochrane Database Syst. Rev.* 2015:CD004464.

Thayer, J. F., Ahs, F., Fredrikson, M., Sollers, J. J., and Wager, T. D. (2012). A meta-analysis of heart rate variability and neuroimaging studies: Implications for heart rate variability as a marker of stress and health. *Neurosci. Biobehav. Rev.* 36, 747–756. doi: 10.1016/j.neubiorev.2011.11.009

Vaizey, C. J., Kamm, M. A., Turner, I. C., Nicholls, R. J., and Woloszko, J. (1999). Effects of short term sacral nerve stimulation on anal and rectal function in patients with anal incontinence. *Gut* 44, 407–412.

Valentino, R. J., Miselis, R. R., and Pavcovich, L. A. (1999). Pontine regulation of pelvic viscera: Pharmacological target for pelvic visceral dysfunctions. *Trends Pharmacol. Sci.* 20, 253–260. doi: 10.1016/s0165-6147(99)01332-2

Veiga, M. L., Costa, E. V., Portella, I., Nacif, A., Martinelli Braga, A. A., and Barroso, U. (2016). Parasacral transcutaneous electrical nerve stimulation for overactive bladder in constipated children: The role of constipation. *J. Pediatr. Urol.* 12, 396.e1–396.e6. doi: 10.1016/j.jpurol.2016.04.047

Veiga, M. L., Lordêlo, P., Farias, T., and Barroso, U. (2013). Evaluation of constipation after parasacral transcutaneous electrical nerve stimulation in children with lower urinary tract dysfunction–a pilot study. *J. Pediatr. Urol.* 9, 622–626. doi: 10.1016/j.jpurol.2012.06.006

Wexner, S. D., Coller, J. A., Devroede, G., Hull, T., McCallum, R., Chan, M., et al. (2010). Sacral nerve stimulation for fecal incontinence: Results of a 120-patient prospective multicenter study. *Ann. Surg.* 251, 441–449. doi: 10.1097/SLA.0b013e3181cf8ed0

Widmann, B., Galata, C., Warschkow, R., Beutner, U., Ögredici, Ö, Hetzer, F. H., et al. (2019). Success and Complication Rates After Sacral Neuromodulation for Fecal Incontinence and Constipation: A Single-center Follow-up Study. *J. Neurogastroenterol. Motil.* 25, 159–170. doi: 10.5056/jnm17106

Yamany, A. A., and Sayed, H. M. (2012). Effect of low level laser therapy on neurovascular function of diabetic peripheral neuropathy. *J. Adv. Res.* 3, 21–28.

Yuan, Y., Ali, M. K., Mathewson, K. J., Sharma, K., Faiyaz, M., Tan, W., et al. (2020). Associations between colonic motor patterns and autonomic nervous system activity assessed by high-resolution manometry and concurrent heart rate variability. *Front. Neurosci.* 13:1447. doi: 10.3389/fnins.2019.01447

Zheng, H., Chen, Q., Chen, M., Wu, X., She, T., Li, J., et al. (2019). Nonpharmacological conservative treatments for chronic functional constipation: A systematic review and network meta-analysis. *Neurogastroenterol. Motil.* 31:e13441.

frontiers | Frontiers in Physiology

TYPE Original Research
PUBLISHED 05 September 2022
DOI 10.3389/fphys.2022.934372

OPEN ACCESS

EDITED BY
Nick Spencer,
Flinders University, Australia

REVIEWED BY
Eugene Nalivaiko,
The University of Newcastle, Australia
Edgar Toschi-Dias,
Methodist University of São Paulo, Brazil

*CORRESPONDENCE
Jens Spiesshoefer,
jspiesshoefer@ukaachen.de

†These authors have contributed equally to this work

SPECIALTY SECTION
This article was submitted to Autonomic Neuroscience,
a section of the journal
Frontiers in Physiology

RECEIVED 02 May 2022
ACCEPTED 10 August 2022
PUBLISHED 05 September 2022

CITATION
Spiesshoefer J, Giannoni A, Borrelli C, Sciarrone P, Husstedt I, Emdin M, Passino C, Kahles F, Dawood T, Regmi B, Naughton M, Dreher M, Boentert M and Macefield VG (2022), Effects of hyperventilation length on muscle sympathetic nerve activity in healthy humans simulating periodic breathing. *Front. Physiol.* 13:934372.
doi: 10.3389/fphys.2022.934372

Effects of hyperventilation length on muscle sympathetic nerve activity in healthy humans simulating periodic breathing

Jens Spiesshoefer[1,2]*, Alberto Giannoni[1,3], Chiara Borrelli[1], Paolo Sciarrone[3], Imke Husstedt[4], Michele Emdin[1,3], Claudio Passino[1,3], Florian Kahles[5], Tye Dawood[6], Binaya Regmi[2], Matthew Naughton[7,8], Michael Dreher[2], Matthias Boentert[3,9†] and Vaughan G. Macefield[6,10†]

[1]Institute of Life Sciences, Scuola Superiore Sant'Anna, Pisa, Italy, [2]Department of Pneumology and Intensive Care Medicine, University Hospital RWTH Aachen, Aachen, Germany, [3]Fondazione Toscana Gabriele Monasterio, Pisa, Italy, [4]Department of Neurology with Institute for Translational Neurology, University of Muenster, Muenster, Germany, [5]Department of Cardiology and Vascular Medicine, University Hospital RWTH Aachen, Aachen, Germany, [6]Human Autonomic Neurophysiology Laboratory, Baker Heart and Diabetes Institute, Melbourne, VIC, Australia, [7]Department of Respiratory Medicine, The Alfred Hospital, Melbourne, VIC, Australia, [8]Department of Medicine, Monash University, Melbourne, VIC, Australia, [9]Department of Medicine, UKM Marienhospital Steinfurt, Steinfurt, Germany, [10]Department of Anatomy & Physiology, University of Melbourne, Melbourne, VIC, Australia

Background: Periodic breathing (PB) is a cyclical breathing pattern composed of alternating periods of hyperventilation (hyperpnea, HP) and central apnea (CA). Differences in PB phenotypes mainly reside in HP length. Given that respiration modulates muscle sympathetic nerve activity (MSNA), which decreases during HP and increases during CA, the net effects of PB on MSNA may critically depend on HP length.

Objectives: We hypothesized that PB with shorter periods of HP is associated with increased MSNA and decreased heart rate variability.

Methods: 10 healthy participants underwent microelectrode recordings of MSNA from the common peroneal nerve along with non-invasive recording of HRV, blood pressure and respiration. Following a 10-min period of tidal breathing, participants were asked to simulate PB for 3 min following a computed respiratory waveform that emulated two PB patterns, comprising a constant CA of 20 s duration and HP of two different lengths: short (20 s) vs long (40 s). Results: Compared to (3 min of) normal breathing, simulated PB with short HP resulted in a marked increase in mean and maximum MSNA amplitude (from 3.2 ± 0.8 to 3.4 ± 0.8 μV, $p = 0.04$; from 3.8 ± 0.9 to 4.3 ± 1.1 μV, $p = 0.04$, respectively). This was paralleled by an increase in LF/HF ratio of heart rate variability (from 0.9 ± 0.5 to 2.0 ± 1.3; $p = 0.04$). In contrast, MSNA response to simulated PB with long HP did not change as compared to normal breathing. Single CA events consistently resulted in markedly increased MSNA (all $p < 0.01$) when compared to the preceding HPs, while periods of HP, regardless of duration, decreased MSNA ($p < 0.05$) when compared to normal breathing.

Conclusion: Overall, the net effects of PB in healthy subjects over time on MSNA are dependent on the relative duration of HP: increased sympathetic outflow is seen during PB with a short but not with a long period of HP.

KEYWORDS

central sleep apnea, physiology, muscle sympathetic nerve activity, risk factor, hyperventilation

1 Introduction

Periodic breathing (PB) is a cyclical pattern of ventilation characterised by alternating phases of hyperventilation (hyperpnea, HP) and transient cessation of respiratory effort and breathing, i. e. central apnea (CA) (Somers et al., 1989a; Hall et al., 1996; Solin et al., 2003; Giannoni et al., 2016; Giannoni et al., 2019a). Beyond occurring at high altitude, PB is frequently found in patients with systolic heart failure (Heart failure with reduced ejection fraction; HFrEF), where phases of hyperventilation alternate with CA in a crescendo-decrescendo pattern that is known as Hunter-Cheyne-Stokes respiration (Somers et al., 1989a; Hall et al., 1996; Solin et al., 2003; Giannoni et al., 2016; Giannoni et al., 2019a).

Apneic events are known to increase sympathetic outflow as measured by intraneural recording of muscle sympathetic nerve activity (MSNA), reflecting chemoreflex stimulation by hypercapnia and hypoxia and (possibly) loss of ventilation-related vagal inputs (Solin et al., 2003; Giannoni et al., 2016; Giannoni et al., 2019a). Chemoreflex hypersensitivity is often observed and usually considered the main mechanism behind Cheyne-Stokes respiration (Somers et al., 1989a; Somers et al., 1989b; Hall et al., 1996; Wedewardt et al., 2010; Seitz et al., 2013) On the contrary, HP is usually accompanied by a decrease in sympathetic outflow, at least in healthy individuals (Oldenburg et al., 2015).

Obstructive apneas have been consistently shown to increase sympathetic outflow, assessed by means of plasma catecholamines, heart rate variability, and MSNA (Fatouleh et al., 2014). In obstructive sleep apnea periodicity is less evident and the HP usually shorter than in PB or Cheyne-Stokes respiration, also due to anatomical factors preventing the reopening of upper airways (Fatouleh et al., 2014; Butler et al., 2019; Hietakoste et al., 2020). On the other hand, the apnea length is more variable and may reflect individual differences in anatomical factors, chemoreflex sensitivity (low or high) or arousability (low or high) (Fatouleh et al., 2014; Butler et al., 2019; Hietakoste et al., 2020). While shorter apneas have been associated with increased mortality (Butler et al., 2019), longer ones have been associated with higher ultra-short term HRV (Hietakoste et al., 2020).

In patients with HFrEF and Cheyne-Stokes respiration apnea duration is usually less heterogenous, while HP length may vary, and this has been mainly attributed to differences in cardiac output and circulation time (Hall et al., 1996; Giannoni et al., 2019b; Gentile et al., 2022). Regarding the impact of CA on sympathetic outflow in the context of CSR the current evidence is contradictory (Lorenzi-Filho et al., 1999; Fatouleh et al., 2014; Oldenburg et al., 2015; Giannoni et al., 2019b). While some authors found CA to increase sympathetic outflow, others have attributed sympathetic outflow to depend solely on background hemodynamics and hence HFrEF severity (Burnum et al., 1954; Somers et al., 1989a; Maze et al., 1989; Hall et al., 1996; Solin et al., 2003; Oldenburg et al., 2007; Bitter et al., 2009; Wedewardt et al., 2010; Yumino et al., 2013; Cowie et al., 2015; Magalang and Pack, 2015; Cagnoni et al., 2016; Eulenburg et al., 2016; Emdin et al., 2017; Perger et al., 2017). Intermittent HP is an integral part of Hunter-Cheyne-Stokes respiration and may counterbalance the effects of CA on sympathetic outflow, possibly by ensuing hypocapnia-hyperoxia, but also by increasing cardiac output (Somers et al., 1989a; Somers et al., 1989b; Hall et al., 1996; Wedewardt et al., 2010; Seitz et al., 2013; Oldenburg et al., 2015). Thus, the overall impact of PB on sympathetic outflow, a major driver of HFrEF progression, may depend on the net effect of CA and HP and particularly by the relative duration of HP within the PB cycle.

This is of major clinical interest as two large multicentric studies using either continuous positive airway pressure or assisted servo-ventilation to treat CA in HFrEF showed neutral or even detrimental impact on survival (Bradley et al., 2005; Cowie et al., 2015; Eulenburg et al., 2016) In patients with HFrEF and Hunter-Cheyne-Stokes respiration apnea duration is usually less heterogenous, while HP length may vary, and this has been mainly attributed to differences in cardiac output and circulation time (Hall et al., 1996; Giannoni et al., 2019b; Gentile et al., 2022). Therefore, to investigate whether the duration of HP may specifically impact on sympathetic outflow, we instructed a group of healthy subjects to simulate two different oscillatory patterns of PB while measuring sympathetic outflow directly by means of intraneural MSNA recordings (Velez-Roa et al., 2004; Macefield, 2012; Macefield and Wallin, 2018; Macefield and Henderson, 2019) and indirectly via non-invasive assessment of heart rate variability (Oldenburg et al., 2015).

2 Methods

2.1 Study participants

Ten healthy participants (36 ± 9 [standard deviation] years, 5 male, 5 female, BMI 25 ± 2 kg/m^2) were recruited. The study protocol conformed with the 1975 Declaration of Helsinki, other than registration in a database, and was approved by the institution's Human Research Ethics Committee. All participants provided informed written consent to the studies, which were conducted in the Human Autonomic Neurophysiology laboratory at The Baker Heart and Diabetes Institute.

2.2 Study design

All participants underwent a thorough physical examination and evaluation of their past medical history to ensure the absence of previous diseases potentially affecting MSNA (Gratze et al., 1998; Maceira et al., 2006; Ponikowski et al., 2016).

2.3 Non-invasive haemodynamic and respiratory monitoring

Participants lay semi-recumbent in a chair with their back at 45° and their legs supported horizontally. Electrocardiographic activity was recorded with Ag-AgCl surface electrodes (BioAmp, PowerLab, ADInstruments, Sydney, Australia) on the chest and sampled at 2 kHz (bandpass 0.3 Hz–1 kHz). Continuous blood pressure was recorded non-invasively by finger pulse plethysmography, sampled at 400 Hz (DC-200 Hz), and calibrated with an integrated sphygmomanometer cuff on the opposite upper arm (NOVA; Finapres Medical System BV, Amsterdam, Netherlands). Respiration was sampled at 100 Hz (DC-100 Hz) using a respiratory belt transducer (ADInstruments). All physiological signals were stored on computer via a data acquisition and analysis system (PowerLab 16SP™ hardware device and LabChart™ for Macintosh, v7.1.2.5 software; ADInstruments).

2.4 Assessment of sympathetic nerve activity

2.4.1 Assessment of autonomic drive to the heart: Heart rate variability

For assessment of sympathovagal balance heart rate variability was analysed using a 3-lead electrocardiogram (sampling rate 200 Hz). HRV (expressed as ms^2 based on continuously recorded variability in RR intervals) reflects sympathovagal balance and heart-brain interactions. Data were computed by frequency domain analysis and presented as the high frequency component (HF; 0.15–0.40 Hz), the low frequency component (LF; 0.04–0.15 Hz) and their relative ratio (LF/HF) (ESC Guidelines, 1996; Davies et al., 1999; Karemaker, 2017; Woehrle et al., 2017; Spiesshoefer et al., 2020; Spiesshoefer et al., 2021).

2.4.2 Assessment of autonomic drive to the vasculature: Muscle sympathetic nerve activity

Figure 1 displays the methodology to obtain and analyse MSNA measurements. Participants lay semi-recumbent in a chair with their back at 45° and their legs supported horizontally. Electrical pulses (2–10 mA; Stimulus Isolator, ADInstruments, Sydney, Australia) were delivered via a 2 mm surface probe to locate the course of the right common peroneal nerve at the level of the fibular head. After identifying the optimal stimulation site, a sterile insulated tungsten microelectrode (Frederick Haer and Co., Bowdoin, United States) was inserted into the skin; an electrode with a larger uninsulated tip inserted at 1 cm distance served as the reference electrode. Weak electrical stimulation delivered through the active microelectrode (0.2 ms, 1 Hz, 0.01–1.0 mA) was used to guide manipulation of its tip into the nerve; evoked muscle twitches at 0.01–0.02 mA, without radiating paraesthesia, indicated that the tip had penetrated a muscle fascicle of the nerve.

Neural activity was amplified (gain 2 × 10^4, bandpass 0.3–5.0 kHz) via an isolated amplifier and headstage (NeuroAmpEX, ADInstruments) and stored on computer (10 kHz sampling). Spontaneous or stretch-evoked activity of muscle spindle afferents, without afferent activity produced by light stroking of the leg or foot, confirmed the identity of the muscle fascicle of the nerve. The microelectrode was further manipulated until spontaneous bursts of muscle sympathetic nerve activity (MSNA) with clear cardiac rhythmicity, increasing during a maximal inspiratory apnoea, were observed.

A mean voltage neurogram of the filtered nerve signal was displayed from the root-mean square processed signal (200 ms moving average).

MSNA was analysed from the root mean square-processed nerve signal using the "Cyclic Measurements" and "Peak Parameters" features of the LabChart™ software: burst frequency (bursts per minute), burst incidence (bursts per 100 heart beats), burst width, burst area and time to peak (Figure 1) (Bradley et al., 2005; Macefield, 2012; Macefield and Henderson, 2019). In addition, amplitude distribution was determined: burst amplitudes were normalized to the highest burst amplitude seen during 1 minute of normal breathing (Bradley et al., 2005; Macefield, 2012; Macefield and Henderson, 2019).

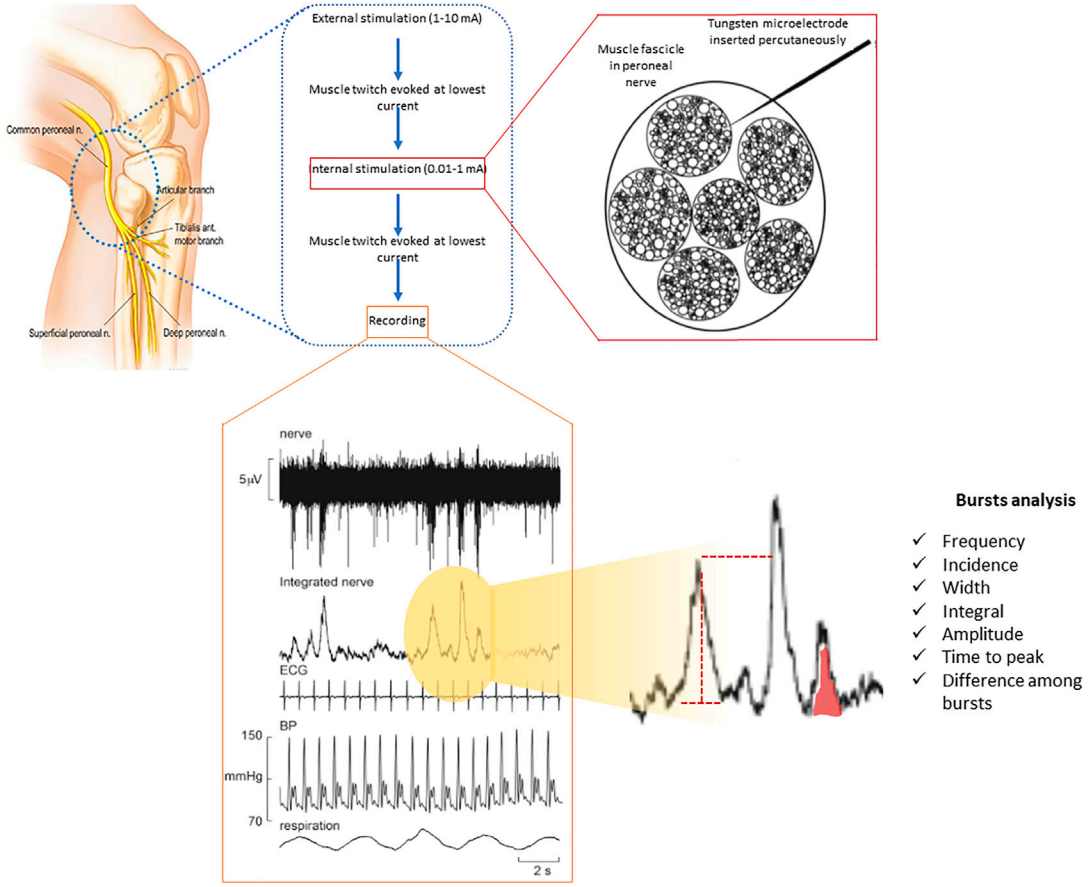

FIGURE 1
Multi-unit recording of muscle SNA from a healthy participant via a tungsten microelectrode inserted percutaneously into a muscle fascicle of the peroneal nerve, shown schematically on the left. Muscle SNA occurs as bursts with a clear cardiac rhythmicity. Heart rate and diastolic blood pressure variability can be derived from the setup used through ECG and continuous (finger) blood pressure all being recorded simultaneously.

2.5 Breathing maneuvers

After recording MSNA and cardiorespiratory signals during 10 min of normal breathing, participants were asked to follow different patterns of respiration displayed on a computer monitor in front of them. Each pattern was composed of sinusoidal waveforms of either constant amplitude and frequency (control) or two different types of PB as described below. These ventilatory patterns were generated in the LabChart™ software and displayed in the computer monitor so that participants could follow them in real time. Simulation of short and long HP cycle length were randomized in order. The patterns are shown in Figure 1. During the experiments participants' own respiratory excursions were displayed below the emulated patterns. The different ventilatory manoeuvres were separated by 3 min of spontaneous breathing until MSNA, heart rate and blood pressure had returned to baseline.

2.5.1 Simulation of periodic breathing

Subjects were instructed to alternate HPs with CAs, thus simulating the typical crescendo-decrescendo pattern of PB. PB was simulated with 2 different HP lengths (20 and 40 s) while keeping the CA phase constant at 20 s duration, as in spontaneous PB in HFrEF, where PB cycle length depends on variable duration of the HP phase rather than apnea length (Solin et al., 2003; Magalang and Pack, 2015; Cagnoni et al., 2016; Perger et al., 2017). In addition, the simulated breathing patterns were specifically designed in such a way that apneas always started at end-expiration (referred to as a "negative PB breathing pattern" below), subsequently causing lung volume to fall below functional residual capacity during the hyperventilation phase. Participants were trained to practice several PB cycles by means of visual feedback before actual recordings were started (Figure 2).

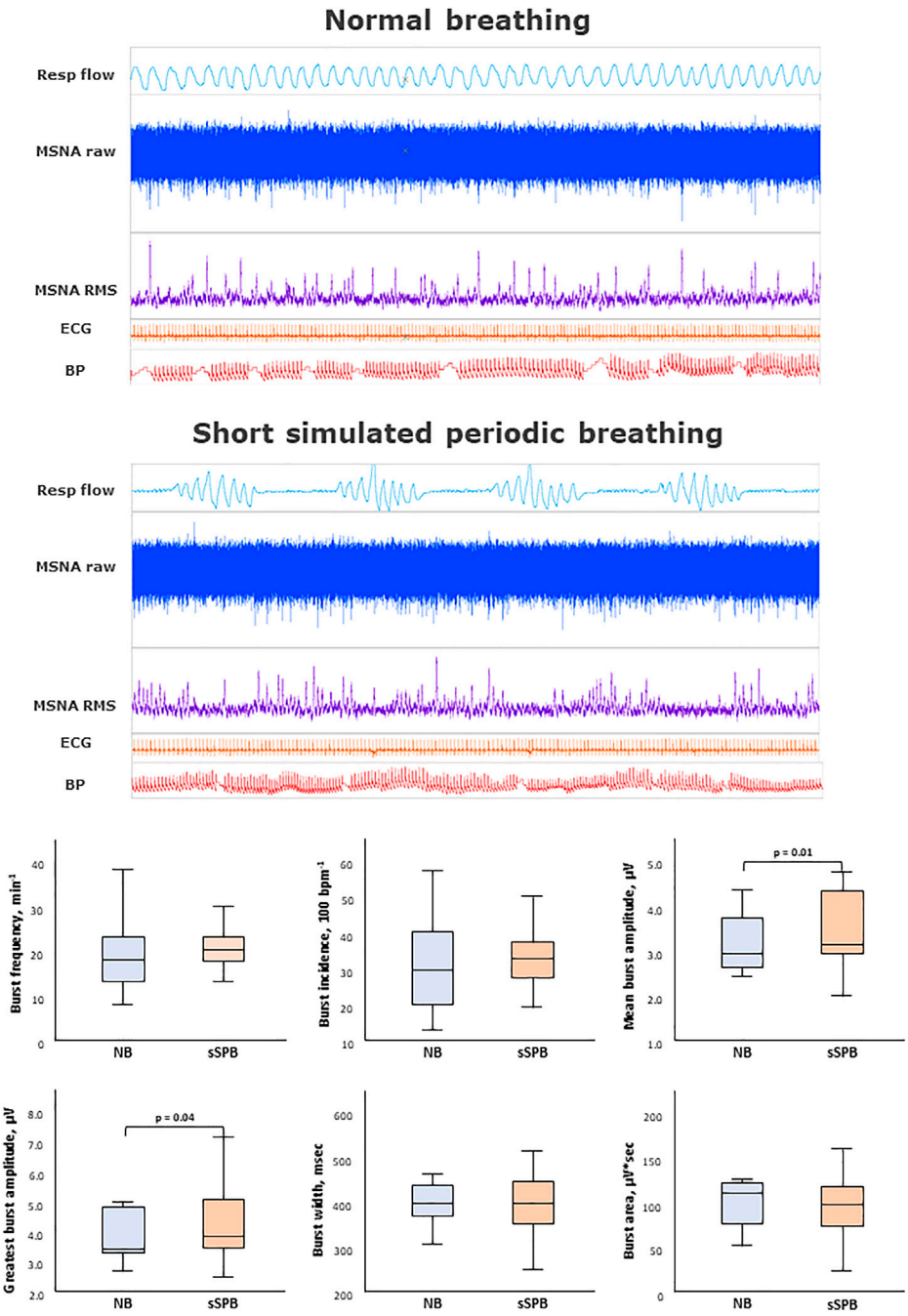

FIGURE 2
Impact of short simulated periodic breathing on muscle sympathetic nerve activity. Multi-unit recording of muscle SNA. RMS, root mean square, BP, blood pressure; Resp flow, respiratory flow.

2.6 Statistical analysis

Assuming a two-sided significance level of 0.05 (alpha) and 80% power (beta), a sample size of at least 10 patients was calculated for detection of a 10% change in MSNA burst rate and amplitude, respectively (mean values and standard deviations of MSNA burst rate and amplitudes for power calculations were derived from preliminary data). Secondary endpoints comprised the MSNA burst amplitude distribution (% amplitude as a ratio of the greatest MSNA burst seen in 1 min of normal breathing), burst width, integral, time to peak, time distance from the R wave and time distance among one

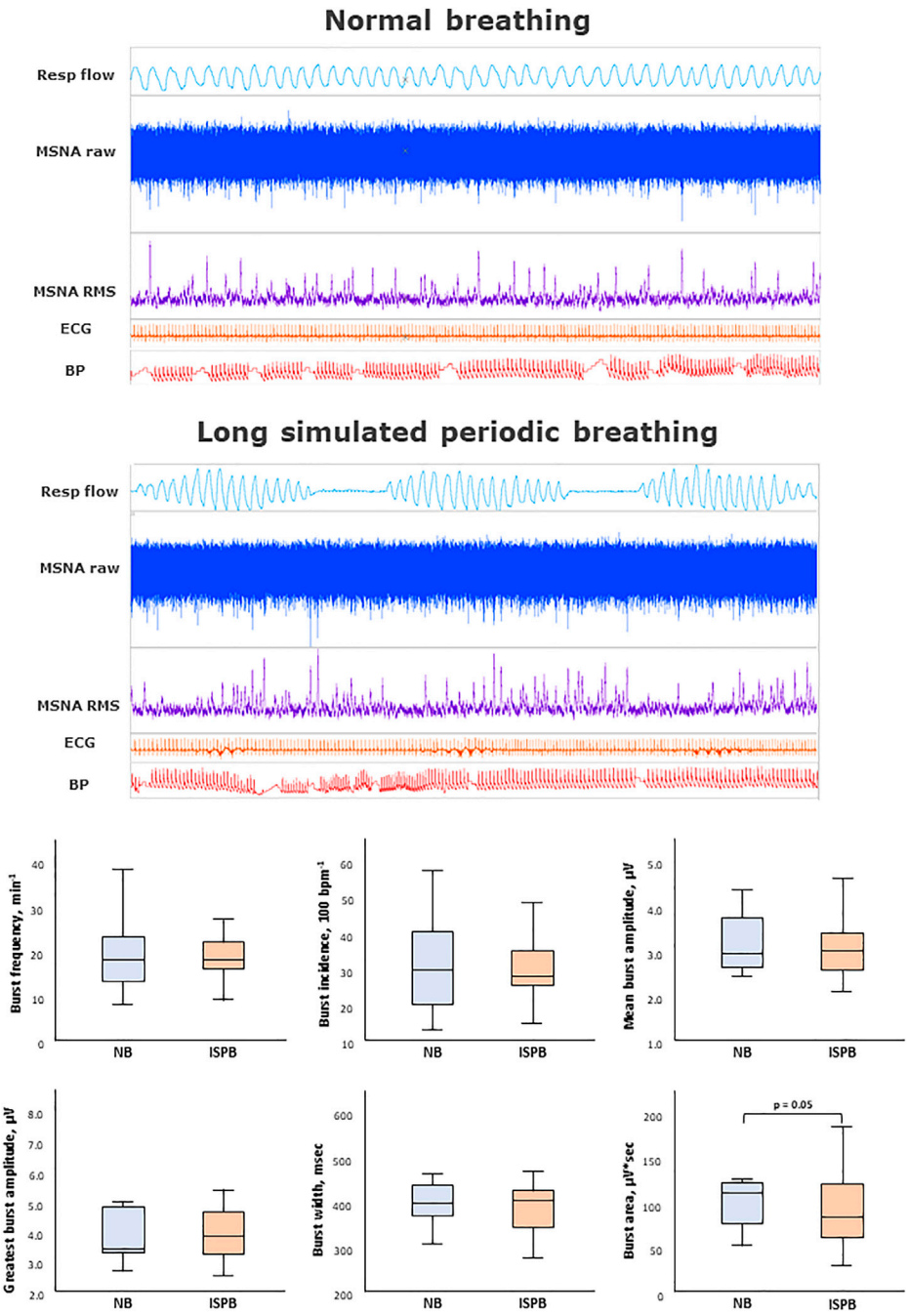

FIGURE 3
Impact of long simulated periodic breathing on muscle sympathetic nerve activity. Multi-unit recording of muscle SNA. RMS, root mean square, BP, blood pressure; Resp flow, respiratory flow.

another. Other secondary endpoints comprised systolic, diastolic and mean arterial blood pressure, heart rate and heart rate variability frequency domain metrics, and oxygen saturation.

All analyses were performed using Sigma Plot software (Version 13.0, Systat Software GmbH, Erkrath, Germany), PASS 14 Power Analysis and Sample Size Software 2015, respectively (NCSS, LLC. Kaysville, Utah, United States). Results were expressed as mean and standard deviation for continuous variables with a normal distribution, and median and interquartile range for continuous variables with a skewed distribution.

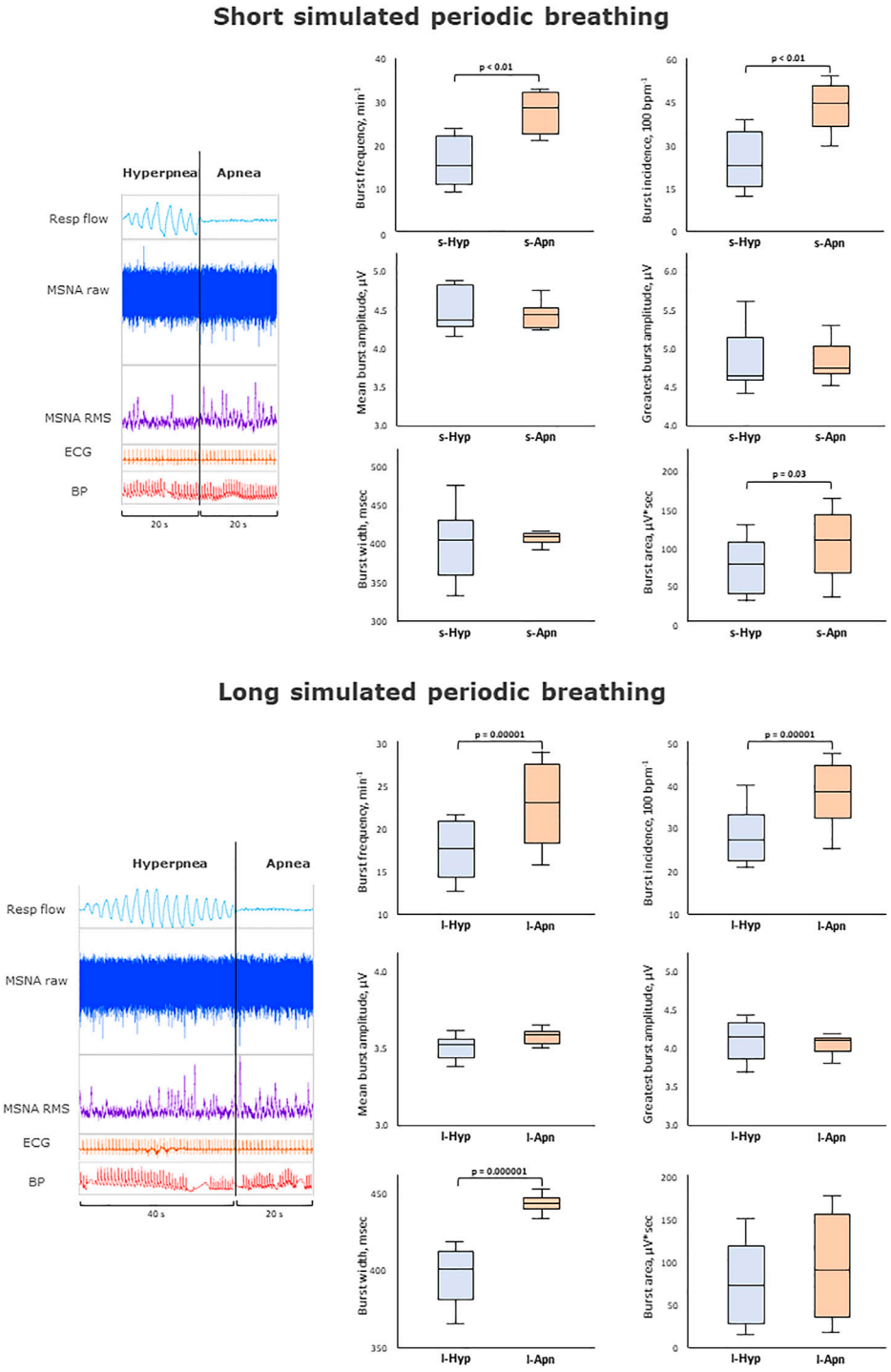

FIGURE 4
Impact of apneas compared to hyperpneas on muscle sympathetic nerve activity. Multi-unit recording of muscle SNA. RMS, root mean square, BP, blood pressure; Resp flow, respiratory flow.

TABLE 1 Comparison of sympathetic outflow, hemodynamic and respiratory data between normal breathing and periodic breathing with a short hyperpnea length.

	Baseline Normal breathing (average of 3 Min)	Periodic breathing with short HP (average of 3 Min)	*p*-value
Sympathetic Outflow parameters (MSNA)			
Burst frequency, min-1	19.2 ± 9.1	20.5 ± 4.8	0.32
Burst incidence, 100 bpm-1	32.0 ± 14.5	32.6 ± 8.1	0.78
Mean Burst Amplitude, μV	3.2 ± 0.8	3.4 ± 0.8	**0.02**
Greatest Burst Amplitude, μV	3.8 ± 0.9	4.3 ± 1.1	**0.01**
Burst Amplitude Distribution, %	84.2 ± 14.6	83.5 ± 14.5	0.84
Burst Width, msec	395.2 (368.2–437.6)	394.8 (327.9–445.0)	0.73
Burst Area, μV*msec	109.8 (76.2–122.0)	97.5 (72.2–118.3)	0.17
Burst time to Peak, msec	387.2 ± 180.5	345.8 ± 190.1	0.25
Burst difference among one another, sec	3.2 ± 1.0	3.1 ± 0.6	0.91
SD Burst difference among one another, sec	2.2 ± 0.9	2.6 ± 0.8	0.51
Sympathovagal balance parameters (HRV)			
HF RRI, ms^2	647.8 ± 593.9	1081.9 ± 809.1	**0.01**
HFnuRRI, %	54 ± 22	44 ± 21	**0.02**
LF RRI, ms^2	553.4 ± 570.5	1354.7 ± 1357.2	**0.0008**
LFnuRRI, %	46 ± 31	56 ± 41	**0.01**
LF/HF RRI	0.9 ± 0.5	1.7 ± 1.7	**0.03**
Haemodynamic parameters			
Heart rate, min-1	61.0 ± 5.8	63.7 ± 7.9	**0.0008**
Systolic BP, mmHg	126.0 ± 13.2	131.4 ± 25.4	0.30
Diastolic BP, mmHg	78.4 ± 26.3	61.7 ± 19.7	0.51
Respiratory parameters			
Respiratory rate, min-1	17.7 ± 2.3	30.5 ± 6.6	**0.0000001**
Oxygen saturation, %	98.9 ± 0.9	99.4 ± 0.7	**0.0004**

Values are mean ± standard deviation for data with a normal distribution, median (interquartile range) for data with a non-normal distribution, respectively. *p* values <0.05 displayed bold. HP, hyperpnea; MSNA; muscle sympathetic nerve activity; HRV; heart rate variability; SD, standard deviation; HF RRI, high frequency component of heart rate variability (nu; expressed as normalized units); LF RRI, low frequency component of heart rate variability (nu; expressed as normalized units); LF/HF RRI, relative ratio of low frequency and high frequency component of heart rate variability; BP, blood pressure.

MSNA and cardiorespiratory parameters were compared using paired *t*-test or Wilcoxon Rank Sum Test, as appropriate. Before comparison, data were averaged across the 3-min intervals of the different PB (either short or long HP) manoeuvres, and the last 3 min of normal breathing that preceded the first respiratory task. When comparing the effects of CAs against HPs, data were again averaged including all phases of CAs, and all phases of HPs during the simulation task. Heart rate variability-derived metrics were also compared with MSNA-derived metrics employing Pearson correlation and Bland-Altman graphs. For all tests, a *p*-value ≤0.05 was considered statistically significant.

3 Results

The main results are shown in Figures 2–4 as graphical summaries.

3.1 Participants

All participants were normotensive, in sinus rhythm and without ectopic beats during all the recordings. No subject was taking any kind of medication possibly influencing sympathetic drive.

3.2 Baseline sympathetic outflow during normal breathing

In all participants and across all breathing manoeuvres a total of 1570 MSNA bursts were analysed. MSNA data, as well as heart rate variability-derived metrics, are shown in Table 1. Notably, during normal breathing, no correlations were found between spectral indices of heart rate variability and any of the MSNA-derived metrics.

TABLE 2 Comparison of sympathetic outflow, hemodynamic and respiratory data between normal breathing and periodic breathing with a long hyperpnea length.

	Baseline Normal breathing (average of 3 Min)	Periodic breathing with long HP (average of 3 Min)	*p*-value
Sympathetic Outflow parameters (MSNA)			
Burst frequency, min-1	19.2 ± 9.1	18.9 ± 4.3	0.81
Burst incidence, 100 bpm-1	32.0 ± 14.5	29.7 ± 7.5	0.36
Mean Burst Amplitude, μV	3.2 ± 0.8	3.1 ± 0.7	0.23
Greatest Burst Amplitude, μV	3.8 ± 0.9	3.9 ± 1.2	0.73
Burst Amplitude Distribution, %	84.2 ± 14.6	84.9 ± 9.9	0.69
Burst Width, msec	395.2 (368.2–437.6)	400.4 (339.0–423.9)	0.83
Burst Area, μV*msec	109.8 (76.2–122.0)	82.9 (55.5–122.6)	**0.05**
Burst time to Peak, msec	387.2 ± 180.5	375.5 ± 150.5	0.53
Burst difference among one another, sec	3.2 ± 1.0	3.2 ± 0.9	0.69
SD Burst difference among one another, sec	2.2 ± 0.9	2.5 ± 1.2	0.55
Sympathovagal balance parameters (HRV)			
HF RRI, ms^2	647.8 ± 593.9	1605.1 ± 1746.7	**0.002**
HFnuRRI, %	54 ± 25	62 ± 30	**0.01**
LF RRI, ms^2	553.4 ± 570.5	1016.9 ± 1265.1	0.08
LFnuRRI, %	46 ± 22	38 ± 21	0.07
LF/HF RRI	0.9 ± 0.5	1.2 ± 2.0	0.54
Haemodynamic parameters			
Heart rate, min-1	61.0 ± 5.8	64.3 ± 7.0	**0.00082**
Systolic BP, mmHg	126.0 ± 13.2	147.8 ± 35.8	0.46
Diastolic BP, mmHg	78.4 ± 26.3	84.2 ± 35.7	0.39
Respiratory parameters			
Respiratory rate, min-1	17.7 ± 2.3	25.9 ± 4.9	**0.000001**
Oxygen saturation, %	98.9 ± 0.9	99.5 ± 0.8	**0.0004**

Values are mean ± standard deviation for data with a normal distribution, median (interquartile range) for data with a non-normal distribution, respectively. *p* values ≤0.05 displayed bold. HP, hyperpnea; MSNA; muscle sympathetic nerve activity; HRV; heart rate variability; SD, standard deviation; HF RRI, high frequency component of heart rate variability (nu; expressed as normalized units); LF RRI, low frequency component of heart rate variability (nu; expressed as normalized units); LF/HF RRI, relative ratio of low frequency and high frequency component of heart rate variability; BP, blood pressure.

3.3 Effects of short HP length on sympathetic outflow during simulated periodic breathing

Table 1 and Figure 2 provides an analysis of sympathetic outflow during simulation of PB with a short (20 s) HP length. An increase in both the mean and the highest burst amplitude was observed between the phases of normal breathing and simulated PB.

Other than this no differences were found in other MSNA parameters between normal breathing and simulated PB with short HP length, including burst frequency, incidence, width, integral, time to peak, or variability.

Despite the increase in respiratory rate and depth, there was no effect on blood pressure. On the contrary, an increase in heart rate, HF, LF, and LF/HF ratio was observed during PB with a short HP length. Likewise, respiratory rate, and oxygen saturation increased significantly during simulated PB ($p < 0.01$).

3.4 Effects of long HP length on sympathetic outflow during simulated periodic breathing

Table 2 and Figure 3 provides an analysis of sympathetic outflow response to simulation of PB with a long (40 s) HP length. Simulated PB with a long HP length decreased mean burst area as well as its standard deviation but otherwise had no effects on other MSNA or heart rate variability parameters. Heart rate and HF component of heart rate variability, respiratory rate and oxygen saturation increased significantly, while there was no change in blood pressure when comparing normal breathing to PB with long HP length.

TABLE 3 Comparison of sympathetic outflow and hemodynamic data between central apneas and hyperpnea phases during periodic breathing with a short and a long hyperpnea length.

	Normal breathing	Periodic breathing with short HP			Periodic breathing with long HP		
		Hyperpnoea	Apnoea	*p*-value	Hyperpnoea	Apnoea	*p*-value
Sympathetic Outflow (MSNA)							
Burst rate, min^{-1}	19.2 ± 9.1	16.5 ± 5.6	27.5 ± 4.8	**>0.01**	17.6 ± 3.3	23.0 ± 4.6	**0.00001**
Burst incidence, 100 bpm^{-1}	32.0 ± 14.5	25.9 ± 9.1	44.0 ± 6.9	**>0.01**	27.8 ± 5.4	38.4 ± 7.6	**0.00001**
Mean Burst Amplitude, μV	3.2 ± 0.8	4.5 ± 0.3	4.6 ± 0.3	0.60	3.6 ± 0.8	3.7 ± 0.4	0.14
Greatest Burst Amplitude, μV	3.8 ± 0.9	4.8 ± 0.5	4.78 ± 0.3	0.45	4.1 ± 0.3	4.0 ± 0.2	0.32
Burst Amplitude Distribution, %	84.2 ± 14.6	91.7 ± 9.2	90.4 ± 9.8	0.53	87.4 ± 8.3	88.8 ± 9.9	0.47
Burst Width, msec	395.2 (368.2–437.6)	402.5 ± 52.9 *	414.6 ± 22.9	0.15	399.8 ± 23.2 *	444.8 ± 10.8	**0.000001**
Burst Area, μV*msec	109.8 (76.2–122.0)	74.3 ± 45.8 *	104.8 ± 68.9	**0.03**	73.6 ± 45.2 *	95.6 ± 60.4	0.05
Burst time to Peak, msec	387.2 ± 180.5	282.6 ± 100.5	316.6 ± 100.8 *	0.13	291.0 ± 81.9 *	317.5 ± 109.2 *	0.06
Standard deviation of Burst difference among one another, sec	3.2 ± 1.0	5.4 ± 14.9	4.1 ± 13.9	0.67	10.2 ± 45.7	3.2 ± 5.8	0.49
Haemodynamic parameters							
Heart rate, min^{-1}	—	63.4 ± 7.6	62.3 ± 7.6	0.39	66.5 ± 7.9 *	65.5 ± 8.9	0.12
Systolic BP, mmHg	—	151.7 ± 18.9	145.1 ± 20.2	0.16	162.2 ± 35.9	160.9 ± 35.1	0.58
Diastolic BP, mmHg	—	78.2 ± 14.9 *	73.4 ± 15.4 *	0.19	95.7 ± 34.1	95.7 ± 35.1	0.49

Values are mean ± standard deviation. *p* values (for paired *t* test hyperpneas vs central apneas) < 0.05 displayed bold. HPhyperpnea, HP, hyperpnea; MSNA; muscle sympathetic nerve activity; SD, standard deviation; BP, blood pressure. *Paired *t*-test or Wilcoxon for comparison versus baseline (normal breathing).

3.5 Effects of central apneas on sympathetic outflow during simulated periodic breathing

Table 3 and Figure 4 provides an analysis of MSNA changes between CAs and HPs during simulated PB. MSNA increased significantly during the apneic phase irrespective of HP length: bursts during apneas had a higher frequency and incidence and an increased burst area compared to the preceding hyperpneas.

4 Discussion

This is the first study to determine the impact of simulated PB of different hyperpnea lengths as well as the immediate effects of CAs on sympathetic outflow in healthy subjects using MSNA, the gold standard technique for sympathetic outflow assessment. We demonstrated that end-expiratory CAs are associated with increased sympathetic outflow compared to HP, and that shorter PB cycles, in contrast to longer ones, are associated with an increase of sympathetic outflow, too. This seems to involve mainly the mean and the highest burst amplitude, at least in healthy individuals. Thus, the net effect of PB, measured over the entire respiratory cycle, derives from the equilibrium between the excitatory drive provided by CAs and the inhibitory effect provided by HPs: when the HP duration is short the relative balance of excitation vs. inhibition shift towards the first one.

This is of importance as PB is a highly prevalent phenomenon with a presumed incremental effect on sympathetic drive in HFrEF, as well as in conditions in the absence of HFrEF, with detrimental effects if left untreated (Burnum et al., 1954; Maze et al., 1989; Yumino et al., 2013; Magalang and Pack, 2015; Eulenburg et al., 2016; Perger et al., 2017). However, a previous study combining polysomnography and right heart catheterisation showed that the increase of sympathetic drive was related to the severity of HFrEF rather than to that of Cheyne-Stokes respiration (as reflected by the apnea-hypopnea index) (Mansfield et al., 2003a; Berry RB Gamaldo et al., 2012). Moreover, the unexpected results of the SERVE-HF trial suggested that treatment of CAs with adaptive servo-ventilation is associated with *increased* rather than decreased mortality in HFrEF patients with CAs, especially in those with severe HFrEF, namely with left ventricular ejection fraction lower than 30% (Cowie et al., 2015; Woehrle et al., 2017). This group of patients is likely to have also a decreased cardiac output and a longer circulatory time.

This has given rise to the hypothesis that CAs and PB potentially exert compensatory rather than detrimental effects in patients with HFrEF. Indeed, during hyperventilation, venous return and thus cardiac output are increased, and sympathetic drive is known to be inhibited by phasic (but not static) changes in lung volume and by hypocapnia (Burnum et al., 1954; Somers et al., 1989b; Hall et al., 1996; Wedewardt et al., 2010; Seitz et al., 2013; Oldenburg et al., 2015). Conversely, apneas are presumed

to lead to increased sympathetic drive mainly in response to apnea-related hypoxemia and hypercapnia (Solin et al., 2003; Giannoni et al., 2016), but also to a lack of inhibitory drive from the stretch receptors located in the airways, lungs and chest wall.

In HFrEF, prolonged circulatory time *per se* prolongs both CA and HP duration (Macefield, 2012). Notably, patients with HFrEF and PB/Cheyne-Stokes respiration show longer HP and cycle length but similar apnea duration when compared with patients with HFrEF and obstructive sleep apnea (Macefield and Henderson, 2019), who usually have a less compromised heamodynamic profile (Hall et al., 1996; Wedewardt et al., 2010; Perger et al., 2017).

The present work suggests that in PB, HP duration may contribute to the net effect of sympathetic outflow.

Simulation of PB (in contrast to assessing its effects when it occurs spontaneously) has the advantage that the length and composition of PB cycles can be standardized, differently from the rather erratic and variable composition observed during spontaneous PB (central and obstructive apneas, mixed apneas, and variable cycle length). Thus, it is possible to precisely predefine the duration of the hyperventilation phase, while keeping CA constant in length. Second, the net effects of PB could be studied having phases of normal breathing as a reliable comparator. Our findings therefore, based on this approach, confirm that CA likely impacts negatively while HP likely impacts positively on sympathetic outflow. It is therefore, that a long cycle length of PB where CAs can be found embedded in long HP impacts neutral on sympathetic outflow, whereas this all results in increased sympathetic outflow should the same CAs be embedded into shorter HP. Furthermore, the present study also directly proved that CAs per se increase sympathetic outflow when compared directly against HP.

Indeed, CA may cause an increase in sympathetic outflow by several mechanisms: by deactivating pulmonary stretch receptors and stimulating peripheral and central chemoreceptors by hypoxia and hypercapnia (Floras, 2009). Furthermore, cortical activation following apneas may further rise central sympathetic outflow plus vagal withdrawal (Floras, 2009). The pathophysiological concept of CAs further increasing SNA is further supported by findings showing that patients with CAs are characterized by increased SNA as reflected by increased HR (Szollosi et al., 2007), decreased heart rate and blood pressure variability (Szollosi et al., 2007), enhanced serum and urinary catecholamine levels (Solin et al., 2003), as well as with increased MSNA (Solin et al., 2003) compared to patients without CAs. This theory is also further supported by studies linking the presence of CAs to worse prognosis in HFrEF with the presumed mechanism being increased SNA through CAs causing arrhythmias and HFrEF related death (Poletti et al., 2009). This has been shown for daytime CA and in HFrEF in particular (Emdin et al., 2017). Another exploratory approach to this key pathophysiological issue is to evaluate the effects of CA treatment on SNA. Indeed, reducing CA through administration of oxygen is also associated with SNA decrease (Staniforth et al., 1998). As for mask-based therapies based on positive pressure ventilation, despite their positive effect on CA in HF, there have been conflicting evidences on their impact on SNA too. While it was shown that cPAP and ASV lead to decreases in SNA as reflected by increased heart rate and blood pressure variability (Iwaya et al., 2014), decreased serum and urinary catecholamine levels (Hetzenecker et al., 2016; Toyama et al., 2017), as well as decreased MSNA (Koyama et al., 2010) other authors as well as a large scale RCT challenged these hypotheses (Cowie et al., 2015; Woehrle et al., 2017).

Nonetheless, the real impact of hyperpnea length may vary in patients with HFrEF, in whom several different pathophysiological mechanisms (chemoreflex gain, plant gain, circulation time, other sources of sympathetic outflow related to HFrEF itself or other altered circuits) may drive to different results. Therefore, an effort to study MSNA and other sympathetic outflow metrics should be attempted also in this relevant clinical setting before exporting our results to improve patients selection and referral to specific PB treatment. Ultimately, it should be noted that also conflicting evidence by other authors has been provided showing that CAs per se may not always result in increased sympathetic outflow (Mansfield et al., 2003b; Grimm et al., 2015).

4.1 Study limitations

Our study has several limitations. MSNA was obtained in 10 healthy participants with no cardiovascular or respiratory disease. Nevertheless, despite it being an invasive technique, one of the advantages of MSNA is undoubtedly its stability over time, requiring smaller sample size (Macefield, 2012; Macefield and Wallin, 2018; Macefield and Henderson, 2019) especially when studying the same participants in different experimental conditions.

Secondly, in our study PB was simulated. As noted above, PB cycle length is rather irregular in various pathologies and might therefore have a different impact on sympathetic outflow. Similarly, cortical influences secondary to simulation cannot be excluded. Studies focusing on spontaneous PB are therefore needed for more definite conclusions.

Third, the duration of each ventilatory manoeuvre was limited to 3 min. Therefore, we cannot exclude the possibility that longer periods of PB may exert different effects on the variables evaluated in this study, and that a drift in the average value of each haemodynamic measure may occur. Longer recordings are needed to clarify this point.

Fourth, considering that increasing the respiratory rate, the HF component may have been moved towards higher frequencies (>0.40 Hz underestimating HF component, by using the same frequency for everybody). Therefore a potential future study might use a wavelet analysis or a Wigner-Ville that may correct for non-stationarity of the signals (considering the respiratory maneuvers performed).

5 Conclusion

Apneas per se consistently resulted in markedly increased sympathetic outflow compared to phases of hyperventilation. However, at least in healthy subject simulating PB, the overall net effects of PB on on sympathetic outflow depend on hyperpnea length, with shorter duration of the hyperpneic phase resulting in increased sympathoexcitation. Future research should focus on the differential impact of longer recordings and focusing on patients with spontaneous PB during either wakefulness or sleep, considering at the same time the impact of several covariates including background haemodynamics, pulmonary mechanics, and the degree of feedback resetting.

Data availability statement

The original contributions presented in the study are included in the article/Supplementary Material, further inquiries can be directed to the corresponding author.

Ethics statement

The study protocol has been approved by the Human Research Ethics Committee of the Alfred Hospital and Governance of the Baker Heart and Diabetes Institute. The participants provided their written informed consent to participate in this study.

Author contributions

JS, AG and MB designed the study. JS, TD and VM were responsible for data collection. IH and JS performed the statistical analyses, and JS, AG and VM prepared the manuscript which was critically revised and amended by all other authors.

Funding

This work was supported by a travel grant awarded by the German Heart Foundation (Deutsche Herzstiftung e.V.). Mit Fördermitteln der Deutschen Herzstiftung e.V". The funders had no role in study design, data collection and analysis, preparation of the manuscript, or the submission process. This study was supported in part by the the Tuscany Region through the Tuscany Network for Bioelectronic Approaches in Medicine: AI-based predictive algorithms for fine-tuning of electroceutical treatments in neurological, cardiovascular and endocrinological diseases (TUNE-BEAM, H14I20000300002).

Acknowledgments

We gratefully acknowledge Gerold Kiersteins, Kevin Evans and Stefan Bornscheins (all AD Instruments, Oxford, United Kingdom) kind technical help in collecting, analysing and interpreting our data. Language editing assistance was provided by Nicola Ryan, independent medical writer.

Conflict of interest

The authors declare that the research was conducted in the absence of any commercial or financial relationships that could be construed as a potential conflict of interest.

Publisher's note

All claims expressed in this article are solely those of the authors and do not necessarily represent those of their affiliated organizations, or those of the publisher, the editors and the reviewers. Any product that may be evaluated in this article, or claim that may be made by its manufacturer, is not guaranteed or endorsed by the publisher.

References

Berry Rb Gamaldo, C. E., Harding, S. M., Lloyd, R. M., and Marcus, C. L.Vaughn BV for the American Academy of Sleep Medicine BR (2012). The AASM manual for the scoring of sleep and associated events. *J Clin Sleep Med* 8, 597–619.

Bitter, T., Faber, L., Hering, D., Langer, C., Horstkotte, D., and Oldenburg, O. (2009). Sleep-disordered breathing in heart failure with normal left ventricular ejection fraction. *Eur. J. Heart Fail.* 11, 602–608. doi:10.1093/eurjhf/hfp057

Bradley, T. D., Logan, A. G., Kimoff, R. J., Series, F., Morrison, D., Ferguson, K., et al. (2005). CANPAP InvestigatorsContinuous positive airway pressure for central sleep apnea and heart failure. *N. Engl. J. Med.* 353, 2025–2033. doi:10.1056/NEJMoa051001

Burnum, J. F., Hickam, J. B., and McIntosh, H. D. (1954). The effect of hypocapnia on arterial blood pressure. *Circulation* 9, 89–95. doi:10.1161/01.cir.9.1.89

Butler, M. P., Emch, J. T., Rueschman, M., Sands, S. A., Shea, S. A., Wellman, A., et al. (2019). Apnea-hypopnea event duration predicts mortality in men and women in the sleep heart health study. *Am. J. Respir. Crit. Care Med.* 199, 903–912. doi:10.1164/rccm.201804-0758OC

Cagnoni, F., Destro, M., Bontempelli, E., Locatelli, G., Gering, D., and Schlaich, M. (2016). Central sympathetic inhibition: a neglegted approach for treatment of cardiac arrhythmias. *Curr. Hypertens. Rep.* 18, 13. doi:10.1007/s11906-015-0619-0

Cowie, M. R., Woehrle, H., Wegscheider, K., Angermann, C., d'Ortho, M. P., Erdmann, E., et al. (2015). Adaptive servo-ventilation for central sleep apnea in systolic heart failure. *N. Engl. J. Med.* 373, 1095–1105. doi:10.1056/NEJMoa1506459

Davies, L. C., Francis, D., Jurák, P., Kara, T., PiepoliM., and Coats, A. J. (1999). Reproducibility of methods for assessing baroreflex sensitivity in normal controls and in patients with chronic heart failure. *Clin. Sci. (Lond).* 97, 515–522. doi:10.1042/cs19990135

Emdin, M., Mirizzi, G., Giannoni, A., Poletti, R., Iudice, G., Bramanti, F., et al. (2017). Prognostic significance of central apneas throughout a 24-hour period in

patients with heart failure. *J. Am. Coll. Cardiol.* 70, 1351–1364. doi:10.1016/j.jacc.2017.07.740

ESC Guidelines (1996). Guidelines Heart rate variability. *Eur. Heart J.* 17, 354–381.

Eulenburg, C., Wegscheider, K., Woehrle, H., Angermann, C., d'Ortho, M. P., Erdmann, E., et al. (2016). Mechanisms underlying increased mortality risk in patients with heart failure and reduced ejection fraction randomly assigned to adaptive servoventilation in the SERVE-HF study: Results of a secondary multistate modelling analysis. *Lancet. Respir. Med.* 4, 873–881. doi:10.1016/S2213-2600(16)30244-2

Fatouleh, R., Mckenzie, D. K., and Macefield, V. G. (2014). Respiratory modulation of muscle sympathetic nerve activity in obstructive sleep apnoea. *Exp. Physiol.* 99 (10), 1288–1298. PMID: 24887112. doi:10.1113/expphysiol.2013.077511

Floras, J. S. (2009). Sympathetic nervous system Activation in human heart failure. Clinical implications of an updated model. *J. Am. Coll. Cardiol.* 54, 375–385. doi:10.1016/j.jacc.2009.03.061

Gentile, F., Borrelli, C., Sciarrone, P., Buoncristiani, F., Spiesshoefer, J., Bramanti, F., et al. (2022). Central apneas are more detrimental in female than in male patients with heart failure. *J. Am. Heart Assoc.* 11, e024103. doi:10.1161/JAHA.121.024103

Giannoni, A., Gentile, F., Navari, A., Borrelli, C., Mirizzi, G., Catapano, G., et al. (2019). Contribution of the lung to the genesis of Cheyne-Stokes respiration in heart failure: Plant gain beyond chemoreflex gain and circulation time. *J. Am. Heart Assoc.* 8, e012419. doi:10.1161/JAHA.119.012419

Giannoni, A., Raglianti, V., Mirizzi, G., Taddei, C., Del Franco, A., Iudice, G., et al. (2016). Influence of central apneas and chemo reflex activation on pulmonary artery pressure in chronic heart failure. *Int. J. Cardiol.* 202, 200–206. doi:10.1016/j.ijcard.2015.09.007

Giannoni, A., Raglianti, V., Taddei, C., Borrelli, C., Chubuchny, V., Vergaro, G., et al. (2019). Cheyne-Stokes respiration related oscillations in cardiopulmonary hemodynamics in patients with heart failure. *Int. J. Cardiol.* 289, 76–82. doi:10.1016/j.ijcard.2019.03.033

Gratze, G., Fortin, J., Holler, A., Pfurtscheller, G., and Wach, P. (1998). A software package for non-invasive, real-time beat-to-beat monitoring of stroke volume, blood pressure, total peripheral resistance and for assessment of autonomic function. *Comput. Biol. Med.* 28, 121–142. doi:10.1016/s0010-4825(98)00005-5

Grimm, W., Sosnovskaya, A., Timmesfeld, N., Hildebrandt, O., and Koehler, U. (2015). Prognostic impact of central sleep apnea in patients with heart failure. *J. Card. Fail.* 21, 126–133. doi:10.1016/j.cardfail.2014.10.017

Hall, M. J., Xie, A., Rutherford, R., Ando, S., Floras, J. S., and Bradley, T. D. (1996). Cycle length of periodic breathing in patients with and without heart failure. *Am. J. Respir. Crit. Care Med.* 154, 376–381. doi:10.1164/ajrccm.154.2.8756809

Hetzenecker, A., Roth, T., Birner, C., Maier, L., Pfeifer, M., and Arzt, M. (2016). Adaptive servo-ventilation therapy of central sleep apnoea and its effect on sleep quality. *Clin. Res. Cardiol.* 105, 189–195. doi:10.1007/s00392-015-0904-6

Hietakoste, S., Korkalainen, H., Kainulainen, S., Sillanmaki, S., Nikkonen, S., Myllymaa, S., et al. (2020). Longer apneas and hypopneas are associated with greater ultra-short-term HRV in obstructive sleep apnea. *Sci. Rep.* 10, 21556. doi:10.1038/s41598-020-77780-x

Iwaya, S., Yoshihisa, A., Nodera, M., Owada, T., Yamada, S., Sato, T., et al. (2014). Suppressive effects of adaptive servo-ventilation on ventricular premature complexes with attenuation of sympathetic nervous activity in heart failure patients with sleep-disordered breathing. *Heart Vessels* 29, 470–477. doi:10.1007/s00380-013-0394-2

Karemaker, J. M. (2017). An introduction into autonomic nervous function. *Physiol. Meas.* 38, R89–R118. doi:10.1088/1361-6579/aa6782

Koyama, T., Watanabe, H., Yusuke, K., Makabe, S., Munehisa, Y., Iino, K., et al. (2010). Beneficial effects of adaptive servo ventilation in patients with chronic heart failure. *Circ. J.* 74, 2118–2124. doi:10.1253/circj.cj-10-0082

Lorenzi-Filho, G., Dajani, H. R., Leung, R. S., Floras, J. S., and Bradley, T. D. (1999). Entrainment of blood pressure and heart rate oscillations by periodic breathing. *Am. J. Respir. Crit. Care Med.* 159, 1147–1154. doi:10.1164/ajrccm.159.4.9806081

Macefield, V. G. (2012). Firing patterns of muscle vasoconstrictor neurons in respiratory disease. *Front. Physiology* 3, 153. PMID: 22654767. doi:10.3389/fphys.2012.00153

Macefield, V. G., and Henderson, L. A. (2019). Identification of the human sympathetic connectome involved in blood pressure regulation. *NeuroImage* 202, 116119. PMID: 31446130. doi:10.1016/j.neuroimage.2019.116119

Macefield, V. G., and Wallin, B. G. (2018). Physiological and pathophysiological firing properties of single postganglionic sympathetic neurons in humans. *J. Neurophysiol.* 119, 944–956. PMID: 29142091. doi:10.1152/jn.00004.2017

Maceira, A. M., Prasad, S. K., Khan, M., and Pennell, D. J. (2006). Reference right ventricular systolic and diastolic function normalized to age, gender and body surface area from steady-state free precession cardiovascular magnetic resonance. *Eur. Heart J.* 27, 2879–2888. doi:10.1093/eurheartj/ehl336

Magalang, U. J., and Pack, A. I. (2015). Heart failure and sleep-disordered breathing—the Plot thickens. *N. Engl. J. Med.* 373, 1166–1167. doi:10.1056/NEJMe1510397

Mansfield, D., Kaye, D., La, R., Solin, P., Esler, M. D., and Naughton, M. T. (2003). Raised sympathetic nerve activity in heart failure and central sleep apnea is due to heart failure severity. *Circulation* 107, 1396–1400. doi:10.1161/01.cir.0000056520.17353.4f

Mansfield, D., Kaye, D. M., La Rocca, H. B., Solin, P., Esler, M. D., and Naughton, M. T. (2003). Raised sympathetic nerve activity in heart failure and central sleep apnea is due to heart failure severity. *Circulation* 107, 1396–1400. doi:10.1161/01.cir.0000056520.17353.4f

Maze, S. S., Kotler, M. N., and Parry, W. R. (1989). Doppler evaluation of changing cardiac dynamics during Cheyne-Stokes respiration. *Chest* 95, 525–529. doi:10.1378/chest.95.3.525

Oldenburg, O., Lamp, B., Faber, L., Teschler, H., Horstkotte, D., and Topfer, V. (2007). Sleep-disordered breathing in patients with symptomatic heart failure. A contemporary study of prevalence in and characteristics of 700 patients. *Eur. J. Heart Fail.* 9, 251–257. doi:10.1016/j.ejheart.2006.08.003

Oldenburg, O., Spießhöfer, J., Fox, H., Bitter, T., and Horstkotte, D. (2015). Cheyne-Stokes respiration in heart failure: friend or foe? Hemodynamic effects of hyperventilation in heart failure patients and healthy volunteers. *Clin. Res. Cardiol.* 104, 328–333. doi:10.1007/s00392-014-0784-1

Perger, E., Inami, T., Lyons, O. D., Alshaer, H., Smith, S., Floras, J. S., et al. (2017). Distinct patterns of hyperpnea during cheyne-stokes respiration: Implication for cardiac function in patients with heart failure. *J. Clin. Sleep. Med.* 13, 1235–1241. doi:10.5664/jcsm.6788

Poletti, R., Passino, C., Giannoni, A., Zyw, L., Prontera, C., Bramanti, F., et al. (2009). Risk factors and prognostic value of daytime Cheyne – Stokes respiration in chronic heart failure patients. *Int. J. Cardiol.* 137, 47–53. doi:10.1016/j.ijcard.2008.06.028

Ponikowski, P., Voors, A. A., Anker, S. D., Bueno, H., Cleland, J. G. F., Coats, A. J. S., et al. (2016). 2016 ESC Guidelines for the diagnosis and treatment of acute and chronic heart failure: The Task Force for the diagnosis and treatment of acute and chronic heart failure of the European Society of Cardiology (ESC)Developed with the special contribution of the Heart Failure Association (HFA) of the ESC. *Eur. Heart J.* 37, 2129–2200. doi:10.1093/eurheartj/ehw128

Seitz, M. J., Brown, R., and Macefield, V. G. (2013). Inhibition of augmented muscle vasoconstrictor drive following asphyxic apnoea in awake human subjects is not affected by relief of chemical drive. *Exp. Physiol.* 98, 405–414. doi:10.1113/expphysiol.2012.067421

Solin, P., Kaye, D. M., Little, P. J., Bergin, P., Richardson, M., and Naughton, M. T. (2003). Impact of sleep apnea on sympathetic nervous system activity in heart failure. *Chest* 123, 1119–1126. doi:10.1378/chest.123.4.1119

Somers, V. K., Mark, A. L., Zavala, D. C., and Aboud, F. M. (1989). Contrasting effects of hypoxia and hypercapnia on ventilation and sympathetic activity in humans. *J. Appl. Physiol.* 67, 2101–2106. doi:10.1152/jappl.1989.67.5.2101

Somers, V. K., Mark, A. L., Zavala, D. C., and Aboud, F. M. (1989). Influence of ventilation and hypocapnia on sympathetic nerve responses to hypoxia in normal humans. *J. Appl. Physiol.* 67, 2095–2100. doi:10.1152/jappl.1989.67.5.2095

Spiesshoefer, J., Bannwitz, B., Mohr, M., Simon, H., Winfried, R., Paolo, S., et al. (2020). Effects of nasal high flow on sympathovagal balance, sleep, and sleep-related breathing in patients with precapillary pulmonary hypertension. *Sleep. Breath.* 25, 705–717. PMID: 32827122. doi:10.1007/s11325-020-02159-1

Spiesshoefer, J., Hegerfeld, N., Gerdes, M. F., Sören, K., Martha, G., Robert, R., et al. (2021). Effects of central apneas on sympathovagal balance and hemodynamics at night: impact of underlying systolic heart failure. *Sleep. Breath.* 25 (2), 965–977. PMID: 32700287. doi:10.1007/s11325-020-02144-8

Staniforth, A. D., Kinnear, W. J. M., Starling, R., Hetmanski, D. J., and Cowley, A. J. (1998). Effect of oxygen on sleep quality, cognitive function and sympathetic activity in patients with chronic heart failure and Cheyne-Stokes respiration. *Eur. Heart J.* 19, 922–928. doi:10.1053/euhj.1997.0861

Szollosi, I., Krum, H., Kaye, D., and Naughton, M. T. (2007). Sleep apnea in heart failure increases heart rate variability and sympathetic dominance. *Sleep* 30, 1509–1514. doi:10.1093/sleep/30.11.1509

Toyama, T., Hoshizaki, H., and Kasama, S. (2017). Adaptive servo-ventilation therapy improves cardiac sympathetic nerve activity , cardiac function , exercise capacity , and symptom in patients with chronic heart failure and Cheyne-Stokes respiration. *J. Nucl. Cardiol.* 24 (6), 1926–1937. doi:10.1007/s12350-016-0529-9

Velez-Roa, S., Ciarka, A., Najem, B., Vachiery, J. L., Naeije, R., and van de Borne, P. (2004). Increased sympathetic nerve activity in pulmonary artery hypertension. *Circulation* 110, 1308–1312. doi:10.1161/01.CIR.0000140724.90898.D3

Wedewardt, J., Bitter, T., Prinz, C., Faber, L., Horstkotte, D., and Oldenburg, O. (2010). Cheyne-Stokes respiration in heart failure: Cycle length is dependent on left ventricular ejection fraction. *Sleep. Med.* 11, 137–142. doi:10.1016/j.sleep.2009.09.004

Woehrle, H., Cowie, M. R., Eulenburg, C., Suling, A., Angermann, C., d'Ortho, M. P., et al. (2017). Adaptive servo ventilation for central sleep apnoea in heart failure: SERVE-HF on-treatment analysis. *Eur. Respir. J.* 50, 1601692. doi:10.1183/13993003.01692-2016

Yumino, D., Kasai, T., Kimmerly, D., Amirthalingam, V., Floras, J. S., and Bradley, T. D. (2013). Differing effects of obstructive and central sleep apneas on stroke volume in patients with heart failure. *Am. J. Respir. Crit. Care Med.* 187, 433–438. doi:10.1164/rccm.201205-0894OC

frontiers | Frontiers in Neuroscience

TYPE Original Research
PUBLISHED 04 October 2022
DOI 10.3389/fnins.2022.869753

OPEN ACCESS

EDITED BY
Joel C. Bornstein,
The University of Melbourne, Australia

REVIEWED BY
Maxim Volgushev,
University of Connecticut,
United States
Xiangping Chu,
University of Missouri–Kansas City,
United States

*CORRESPONDENCE
John P. Horn
jph@pitt.edu

SPECIALTY SECTION
This article was submitted to Autonomic Neuroscience, a section of the journal Frontiers in Neuroscience

RECEIVED 04 February 2022
ACCEPTED 16 September 2022
PUBLISHED 04 October 2022

CITATION
Kullmann PHM and Horn JP (2022) Patch-clamp analysis of nicotinic synapses whose strength straddles the firing threshold of rat sympathetic neurons.
Front. Neurosci. 16:869753.
doi: 10.3389/fnins.2022.869753

Patch-clamp analysis of nicotinic synapses whose strength straddles the firing threshold of rat sympathetic neurons

Paul H. M. Kullmann and John P. Horn*

Department of Neurobiology, School of Medicine, University of Pittsburgh, Pittsburgh, PA, United States

Neurons in paravertebral sympathetic ganglia are innervated by converging nicotinic synapses of varying strength. Based upon intracellular recordings of excitatory postsynaptic potentials (EPSPs) with sharp microelectrodes these synapses were classified in the past as either primary (strong) or secondary (weak) by their ability to trigger postsynaptic action potentials. Here we present an analysis of 22 synapses whose strength straddled threshold, thereby distinguishing them from the original classification scheme for primary and secondary synapses. Recordings at 36°C were made from intact superior cervical ganglia isolated from 13 male and 3 female Sprague-Dawley rats and from 4 male spontaneously hypertensive (SHR) rats. Ganglia were pretreated with collagenase to permit patch recording. By dissecting a 1 cm length of the presynaptic cervical sympathetic nerve as part of the preparation and through use of graded presynaptic stimulation it was possible to fractionate synaptic inputs by their distinct latencies and magnitudes, and by the presynaptic stimulus threshold for each component. Comparison of cell-attached extracellular recordings with intracellular recordings of synaptic potentials and synaptic currents indicated that straddling EPSPs are not an artifact of shunting damage caused by intracellular recording. The results also showed that in cells where a single presynaptic shock elicits multiple action potentials, the response is driven by multiple synapses and not by repetitive postsynaptic firing. The conductance of straddling synapses also provides a direct estimate of the threshold synaptic conductance (9.8 nS ± 7.6 nS, n = 22, mean ± SD). The results are discussed in terms of their implications for ganglionic integration and an existing model of synaptic amplification.

KEYWORDS

sympathetic ganglia, EPSP, EPSC, synaptic integration, synaptic gain

Introduction

The strengths of individual nicotinic synapses that converge on sympathetic neurons shape ganglionic integration. Intracellular recordings from isolated paravertebral sympathetic ganglia using sharp microelectrodes provided the original evidence for a dichotomy in which individual inputs to ganglionic neurons produced either very large nicotinic excitatory postsynaptic potentials (EPSPs) that invariably triggered action potentials or small nicotinic EPSPs that were subthreshold in strength (Dodd and Horn, 1983; Skok and Ivanov, 1983; Hirst and McLachlan, 1984; McLachlan, 2003). Strong suprathreshold EPSPs and weak subthreshold EPSPs were also evident in intracellular microelectrode recordings of natural activity from living animals (Skok and Ivanov, 1983; Ivanov and Skok, 1992; Ivanoff and Smith, 1995; McLachlan et al., 1997, 1998; Bratton et al., 2010). An analysis of B-type secretomotor sympathetic neurons in bullfrog sympathetic ganglia led to the naming of strong synapses as primary and of weak synapses as secondary (Karila and Horn, 2000). These authors then proposed an $n + 1$ rule based on the bullfrog data and on the literature describing mammalian paravertebral ganglia. The rule posited that sympathetic neurons in paravertebral ganglia receive one primary synapse and a variable number, n, of secondary synapses. Models incorporating $n + 1$ convergence make the interesting prediction that ganglionic integration can produce use-dependent amplification of preganglionic activity (Karila and Horn, 2000; Wheeler et al., 2004; Kullmann and Horn, 2006, 2010a; Kullmann et al., 2016).

Possible difficulties with existing models of synaptic amplification are raised by exceptions to the $n + 1$ rule found in mammalian sympathetic ganglia. In some neurons fluctuations in EPSP amplitudes during repetitive stimulation can straddle threshold and single presynaptic shocks sometimes elicit double spikes [cf. Figure 5 in Rimmer and Horn (2010)]. It remains unclear whether straddling synapses are physiological in origin or reflect damage caused by microelectrode impalement. Recording damage may also explain why several authors have interpreted microelectrode recordings as evidence that secondary EPSPs are too small to exert significant effect on ganglionic integration (Maslov et al., 1996; McLachlan, 2003; Janig, 2006). Evidence showing the consequences of a damage artifact comes from dynamic clamp experiments on dissociated rat sympathetic neurons using patch electrodes (Springer et al., 2015). Introducing a virtual non-depolarizing shunt conductance comparable to the damage associated with microelectrode impalement acts to lower the strength of virtual nicotinic EPSPs and can alter postsynaptic repetitive firing dynamics. Nonetheless, it remains unclear whether double spiking reflects repetitive firing or the impact of two or more converging synapses. To circumvent problems introduced by sharp microelectrodes, the present experiments exploit a technical advance that permits patch electrode recording from the isolated intact rat superior cervical ganglion (SCG). After establishing a giga-Ohm seal, one can record extracellularly without impalement damage and then intracellularly from the same neuron in the current-clamp and voltage-clamp modes. This approach permits the unambiguous identification of straddling synapses, and of synapses that can drive double spiking. It also provides the first direct estimate of the synaptic conductance required to reach the postsynaptic action potential threshold.

Materials and methods

Animals

All animal procedures were approved by the Institutional Animal Care and Use Committee (IACUC) at the University of Pittsburgh. Male and female Sprague Dawley (CD) rats and male SHR rats, aged 7–23 weeks, were obtained from Charles River (Wilmington, MA, United States). After killing rats by CO_2 inhalation, superior cervical ganglia were rapidly dissected along with the adjacent carotid artery and transferred to a 60 mm Petri dish coated with Sylgard 184 (Dow Corning, Midland, MI, United States) and filled with Ringer solution for further preparation.

Preparation of ganglia

This study extends previous methods for recording from the isolated intact SCG with microelectrodes (Li and Horn, 2006; Rimmer and Horn, 2010) and with patch electrodes (Springer et al., 2015). The SCG is situated in the neck at the rostral end of the paravertebral sympathetic chain, adjacent to the bifurcation of the carotid artery into its external and internal branches. By virtue of this anatomy (**Figure 1A**), presynaptic axons enter the ganglion through the cervical sympathetic trunk (CST) and postsynaptic axons exit through the external carotid nerve (ECN) and the internal carotid nerve (ICN). This fortuitous separation of inputs and outputs facilitates presynaptic stimulation and postsynaptic recording through separate extracellular suction electrodes (**Figures 1A,B**). When dissecting the ganglion, special care is taken to maximize the length of the associated nerves. In the rat, one can routinely dissect preparations where the CST is 1 cm or longer (**Figure 1B**) and the ECN and ICN are several mm long. To avoid injury during initial stages of the dissection, the preparation is handled by the attached carotid artery and connective tissue sheath. Maximizing the presynaptic conduction distance allows for greater temporal dispersion of postsynaptic events so they can be identified as arising from different synapses. Preservation of the postsynaptic nerves is required for extracellular recording

of compound postsynaptic responses with suction electrodes. The compound postganglionic responses enable one to monitor the efficacy of graded presynaptic stimulation [c.f. Figure 4 in Springer et al. (2015)]. In earlier work, some recordings were made at room temperature in order to slow axonal conduction velocities and assess subsets of preganglionic axons (Li and Horn, 2006). The limitation of this approach is that it also perturbs synaptic transmission. For this reason, the present experiments were all done at 36°C to approximate normal body temperature. Another important aspect of preparing ganglia for patch recording is the dissection of connective tissue. For microelectrode recordings, one splits the connective tissue sheath surrounding the ganglion and tightly pins it out, like the head of a drum. This is essential for piercing remaining barriers with a sharp electrode. Patch recording requires an entirely different approach. After isolating the ganglion, the connective tissue is carefully nicked with fine scissors and then entirely stripped away, like removing a glove. The isolated ganglion is then placed in a recording chamber and fitted with suction electrodes (**Figure 1B**). At this stage, the ganglion is treated with collagenase, allowed to rest, and then used for recording. Installing the tight-fitting suction electrodes before adding the collagenase is essential because it protects the integrity of the nerves, which become very delicate after enzyme digestion. The ganglion is mechanically stabilized for recording by the suction electrodes and by anchoring it with one or two stainless minutien pins (Fine Science Tools, Foster City, CA, United States) (**Figure 1B**). The pins are cut to shorten them, bent into L- or J-like hooks and placed gently beside and over the main body of the ganglion prior to enzyme treatment.

Recording techniques and solutions

Ringer solution for dissection and recording contained (in mM): 146 NaCl, 4.7 KCl, 20 HEPES, 0.6 $MgSO_4$, 1.6 $NaHCO_3$, 0.13 NaH_2PO_4, 2.5 $CaCl_2$, 7.8 glucose, pH adjusted to 7.4 with NaOH, osmolality adjusted to 314 mOsm with dH_2O and bubbled with 100% O_2. For enzyme digestion Ringer was replaced by a solution consisting of Leibovitz's L15 medium (Gibco/Fisher Scientific, Pittsburgh, PA, United States) supplemented with 14 mM $NaHCO_3$ and 10 mg/ml collagenase Type 3 (Worthington, Lakewood, NJ, United States). The recording chamber and ganglion with enzyme solution was then placed uncovered for 60–90 min into a humidified tissue culture incubator (37°C, 5% CO_2). After mounting the recording chamber on a fixed stage upright microscope (Zeiss Axioskop), the enzyme solution was washed away with oxygenated Ringer and the preparation was allowed to rest for 30 min before recording.

Patch electrodes were fabricated from thick-walled borosilicate capillaries (1.5 mm OD, 0.86 mm ID, #1B150F-4, World Precision Instruments (WPI), Sarasota, FL, United States) on a P-87 puller (Sutter Instrument, Novato, CA, United States). Pipettes resistances were 2.8–3.3 MΩ when filled with internal solution (in mM: 94 K^+-gluconate, 30 KCl, 10 HEPES, 0.2 EGTA, 10 phosphocreatine di tris salt, 4 Mg_2ATP, 0.3 Na_2GTP, pH adjusted to 7.3 with KOH and osmolality adjusted to 300 mOsm with sucrose). Data was corrected after experiments to account for a calculated tip potential of + 14 mV.

Extracellular stimulation and recording with suction electrodes fabricated from polyethylene catheter tubing was as previously described (Li and Horn, 2006). Presynaptic stimuli consisting of 30–100 μs unipolar rectangular current pulses were delivered through an isolator (A360; WPI) gated by a pulse train generator (A300; WPI). Differential recordings of extracellular compound action potentials were made with Grass AC preamplifiers (Model P55, Astro-Med, West Warwick, RI, United States) with gain set to 1,000 or 10,000 and bandpass filters at 0.1 Hz and 3 kHz.

Patch recordings were made under visual guidance (**Figure 1C**) through a 40× water immersion objective (Zeiss Achroplan 40×/0.75 W #44 00 90) and TillVision imaging system with IMAGO charge-coupled device (CCD) camera. Signals were fed through a CV-7B head stage to a MultiClamp 700B amplifier (Molecular Devices, San Jose, CA, United States). The electrode and head stage assembly was mounted on a Luigs & Neumann Mini 25 manipulator (Ratingen, Germany). Resistances were 1–3 giga-Ohms during seal formation. In cell-attached and whole-cell voltage-clamp recordings the holding potential was set to −51 mV. In whole-cell voltage clamp mode, series resistance (R_{series}) was monitored throughout the recording and R_{series} compensation was set to 85%. Recordings in which R_{series} exceeded 25 meg-Ohms were excluded from analysis. Experimental control and data logging used a Digidata 1440A interface together with pClamp 10 and MultiClamp Commander software (Molecular Devices). While monitoring R_{series} during voltage clamp recordings, measurements of membrane capacitance (C_m) and input resistance (R_{input}) were obtained using the cell membrane monitoring routine built into pClamp.

Data analysis

Data analysis utilized pClamp 10, Igor Pro 7 (WaveMetrics, Lake Oswego, OR, United States) and Prism 9 (GraphPad Software, La Jolla, CA, United States). Amplitudes of synaptic currents were measured from the baseline to the peak. In cases of temporal overlap between excitatory postsynaptic currents (EPSCs) with different latencies, baselines were extrapolated by fitting an exponential function to the decay of the first EPSC. Peak synaptic conductance (g_{syn}) was calculated from synaptic currents using Ohm's law with a corrected membrane holding potential of −65 mV and a reversal potential of −11 mV. When calculating means and standard deviations of EPSCs, the rare

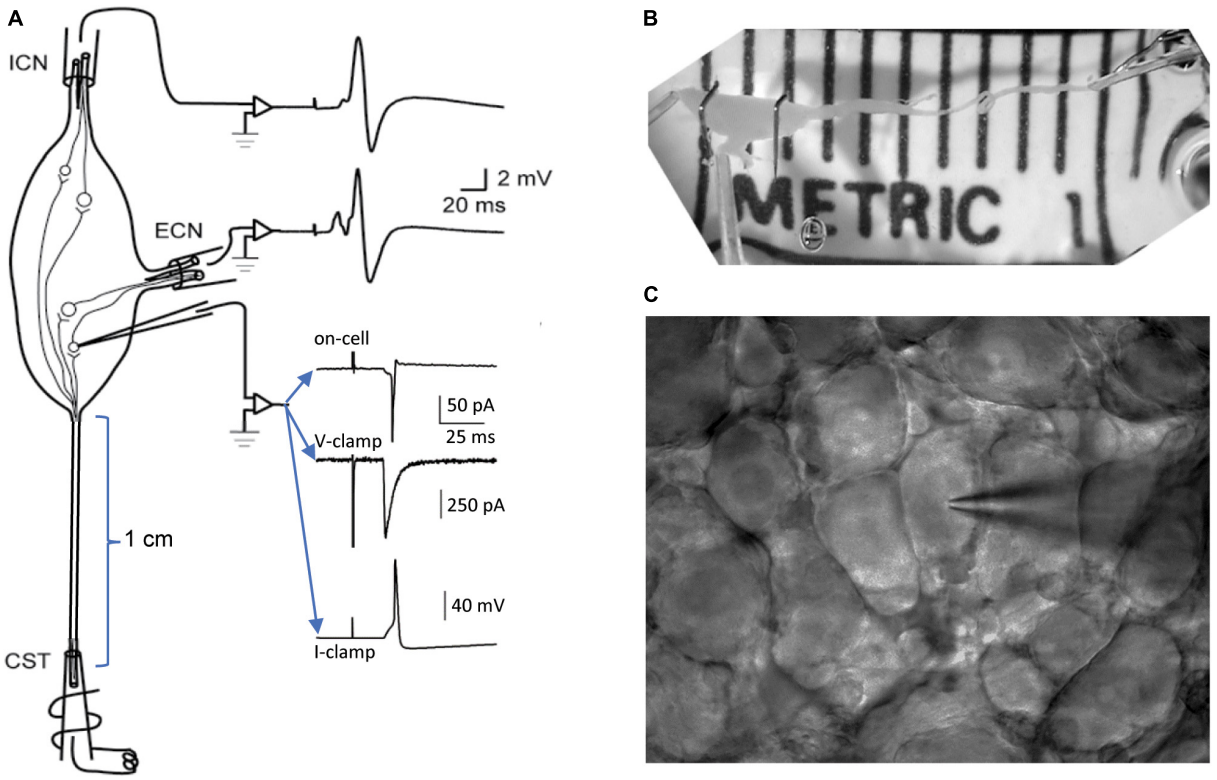

FIGURE 1
Methods for patch recording from the isolated superior cervical ganglion (SCG). **(A)** Schematic organization of the experimental preparation. Tight-fitting extracellular suction electrodes are applied to the preganglionic cervical sympathetic trunk (CST) and to the postganglionic internal carotid nerve (ICN) and external carotid nerve (ECN). Graded presynaptic stimulation is used to recruit and resolve converging synapses. The efficacy of presynaptic stimulation is monitored by recording compound extracellular responses from the ICN and ECN. A patch electrode is used to record extracellular and intracellular responses from individual neurons. Examples of recordings show an on-cell extracellular response, an intracellular synaptic current and an intracellular EPSP that triggers an action potential. **(B)** Photograph of a dissected rat SCG in the recording chamber after removal of the connective tissue sheath and application of suction electrodes. Note the long CST, which allows synaptic components to be separated by variations in axonal conduction velocities. Note also the two stainless pins gently holding down the ganglion. At this stage of preparation the ganglion is ready for collagenase treatment. **(C)** A field of sympathetic neurons and a patch electrode visualized through a 40× water immersion objective and charge-coupled device (CCD) camera, ready for recording.

trials that failed to elicit a response were excluded. Normality tests and Spearman correlation calculations were done with Prism 9. Grouped data are expressed as the mean ± standard deviation except where noted.

Results

This paper presents data from 20 neurons from 20 rats where straddling synapses were initially detected in extracellular on-cell recordings and then characterized further with intracellular whole cell recordings in the voltage-clamp and current-clamp modes. Patch recording in these configurations has not to our knowledge been used before to study the physiology of converging synapses in paravertebral sympathetic neurons. These experiments were part of a larger series, unpublished at present, whose goal was to assess with intracellular recording the properties of individual nicotinic synapses on sympathetic SCG neurons. In all experiments, temperature was held at 36°C and the presynaptic nerve was stimulated repetitively at 1 Hz. The slow rate of stimulation was chosen to minimize possible confounding effects introduced by facilitation, depression, and non-nicotinic synaptic mechanisms. As in previous microelectrode studies of paravertebral sympathetic ganglia, individual converging synaptic inputs were distinguished by their distinct presynaptic stimulus thresholds and their latencies (Dodd and Horn, 1983; Hirst and McLachlan, 1984; Karila and Horn, 2000; McLachlan, 2003; Rimmer and Horn, 2010; Springer et al., 2015). The modest extent of convergence in sympathetic ganglia makes this approach feasible. It has been estimated that an average of 8.7 nicotinic synapses converge on rat SCG neurons, based on sharp microelectrode recordings of membrane potential together with ventral root stimulation (Purves and Lichtman, 1985).

The extracellular cell-attached recordings in **Figure 2** illustrate responses from 2 nicotinic synapses with distinct

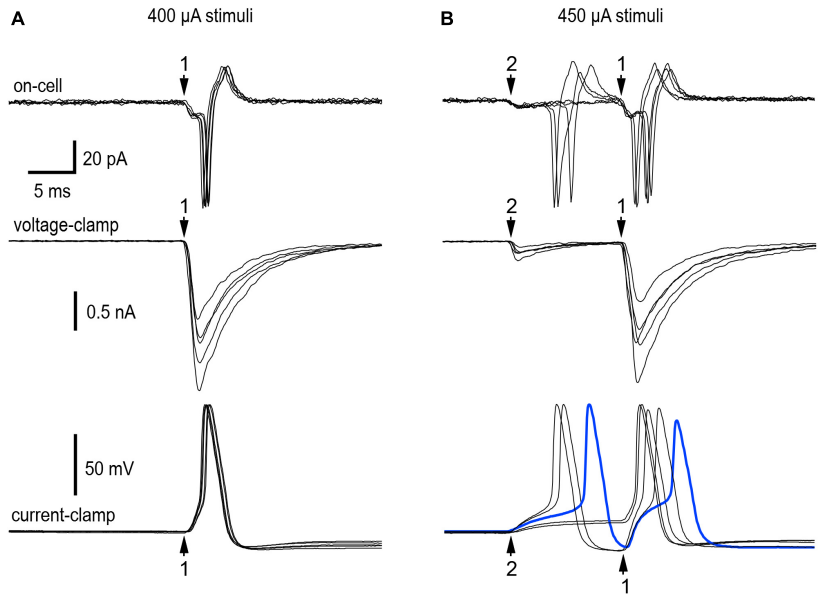

FIGURE 2
Resolution of convergence between a primary synapse and a straddling synapse. Extracellular on-cell recordings (top panels) and intracellular whole-cell recordings under voltage-clamp (middle panels) and current-clamp (bottom panels) made while stimulating the preganglionic cervical sympathetic trunk (CST) at two different shock intensities. **(A)** 400 μA shocks selectively recruited synapse 1–a strong primary synapse that never failed during repetitive stimulation at 1 Hz. **(B)** Raising the stimulus strength to 450 μA recruited synapse 2, a much weaker synapse that straddled threshold during repeated trials at 1 Hz. At 450 μA, single shocks could elicit double spikes resulting from convergence. Each panel contains five traces chosen to reflect variability in responses. See text for additional details about all the responses. In the on-cell recordings (top panels) one sees evidence of excitatory postsynaptic potentials (EPSPs) and the action potentials they trigger. The voltage-clamp recordings of excitatory postsynaptic currents (EPSCs) (middle panels) show the temporal correspondence with extracellular recordings and the markedly different EPSC amplitudes at synapses 1 and 2. Under current-clamp (bottom panels) there was little variation in the onset of action potentials driven by synapse 1. This contrasted with the smaller EPSPs at synapse 2, where the onset of action potentials was more variable. Note the heavy blue trace showing an action potential evoked by synapse 2 very shortly before the activation of synapse 1. This resulted in the second action potential having a slower upstroke and lower amplitude. Experiment 11/9/18 cell 2.

presynaptic stimulus thresholds and latencies (experiment 11/9/18 cell 2). In cell-attached recordings, the currents recorded at the patch reflect unclamped intracellular EPSPs and action potentials. We therefore refer to these extracellular current recordings as on-cell or extracellular EPSPs and action potentials. Five sets of 30 stimuli at 1 Hz were used to find the minimal stimulus intensity needed to recruit synapse 1 and then synapse 2. In response to 400 μA stimuli, 30 of 30 shocks elicited suprathreshold on-cell EPSPs at synapse 1 (**Figure 2A**, top). Finding that all EPSPs at synapse 1 were suprathreshold in strength conforms to the definition of a primary nicotinic synapse (Karila and Horn, 2000). Each postsynaptic response began with a small downward extracellular EPSP that led to a much larger current associated with an action potential. The latency from the stimulus to onset of the extracellular EPSP was 29.5 ms. When the stimulus was reduced slightly, only 36 of 60 stimuli evoked suprathreshold EPSPs and the remaining 24 stimuli failed to evoke any response. We interpret this as the intermittent failure of axonal stimulation to initiate a presynaptic action potential. These observations indicate that 400 μA was the minimum stimulus required for reliable activation of synapse 1. Raising the stimulus to 450 μA recruited synapse 2, whose latency was 17.0 ms. Under these conditions, 29 of 30 stimuli evoked extracellular EPSPs at synapse 2 with 1 failure. Fourteen of the 29 EPSPs (48%) triggered action potentials and the other 15 EPSPs (52%) were subthreshold in strength. Because the latency of synapse 2 was less than that of synapse 1, the properties of synapse 2 were not influenced by synapse 1. The extracellular responses elicited by selective activation of synapse 2 indicate that the ability of a synapse to straddle threshold is not an artifact of intracellular recording. The data from this neuron also shows that a single shock can elicit double spiking by activating 2 synapses. Increasing the stimulus above 450 μA recruited a third synapse that was not included in the analysis.

After going from the on-cell to the whole-cell recording configuration, we assessed EPSCs and EPSPs produced by synapses 1 and 2 (**Figure 2**, middle and bottom traces). Under voltage-clamp the mean EPSC amplitudes were -1272 ± 260 pA (n = 95) at synapse 1 and -232 ± 123 pA (n = 55) at synapse 2. Under current-clamp EPSPs evoked by minimal stimulation (400 μA) to selectively activate synapse 1 triggered action potentials in 30 of 30 trials, consistent with the extracellular observations. Raising the stimulus strength to 450 μA evoked

suprathreshold EPSPs at synapse 2 in 20 of 30 trials (67%) and subthreshold EPSPS in 10 trials (33%), with no failures of stimulation. This provides intracellular confirmation that a single shock can evoke two action potentials by activating two converging synapses. When activated in isolation synapse 1 never failed to evoke an action potential, and the spikes were nearly superimposable (Figure 2A). This contrasts with synapse 2, where EPSPs straddled threshold and the timing of action potential initiation was quite variable (Figure 2B). As a result of this variable timing, action potentials triggered by synapse 2 sometimes occurred within 2–5 ms of the EPSP at synapse 2 (see heavy blue trace in Figure 2B, bottom). In 6 of 11 trials where this happened, the spike at synapse 2 occluded generation of the second spike at synapse 1. This is not surprising given that action potentials undergo a refractory period caused by Na^+ channel inactivation. Signs of inactivation can be seen in Figure 2B (blue trace) where the spike at synapse 1 is reduced in amplitude and upstroke velocity. Nonetheless the difference in synaptic strength at the two synapses was very large. EPSCs were 5.5 times larger and 8.4 standard deviations greater at synapse 1 than 2.

Taking the intracellular and extracellular data into account, how then would one categorize synapse 1 and 2 in terms of the primary-secondary nomenclature that originally defined synapses as being either subthreshold or suprathreshold in strength (Karila and Horn, 2000)? Synapse 2 does not fit into either of the original categories because it straddles threshold when stimulated in isolation. This is distinct from synapse 1 which was much stronger than synapse 2 and always suprathreshold when stimulated in isolation. These criteria indicate synapse 1 should be classified as a primary synapse and synapse 2 as a straddling synapse.

Next, we consider a neuron where 7 converging nicotinic synapses were resolved by their distinct presynaptic stimulus thresholds and latencies (experiment 6/2/16 cell 4). This cell provides another example where a single shock could lead to double spiking driven by converging nicotinic synapses. Initial extracellular on-cell recording from this neuron revealed 2 synapses that both straddled threshold (Figure 3). Synapse 1 had a lower presynaptic stimulus threshold and a latency of 16.5 ms. The traces in Figure 3A illustrate extracellular examples of stimulus failures, subthreshold EPSPs, and suprathreshold EPSPs. In 37 trials, there were 9 failures. In the 28 trials that evoked EPSPs, 20 (71%) were suprathreshold while 8 (29%) were subthreshold. Increasing the stimulus strength recruited synapse 2 (Figure 3B), which had a latency of 23 ms. With the stronger stimuli used to recruit synapse 2 the failures at synapse 1 were eliminated, thereby showing that they arose from failures of stimulation and not failures of transmitter release. In 19 trials, 11 responses (57%) at synapse 2 were suprathreshold in strength and 8 (43%) were subthreshold. Although both synapses straddled threshold, only synapse 1 could be observed in isolation (Figure 3A). One might therefore question whether

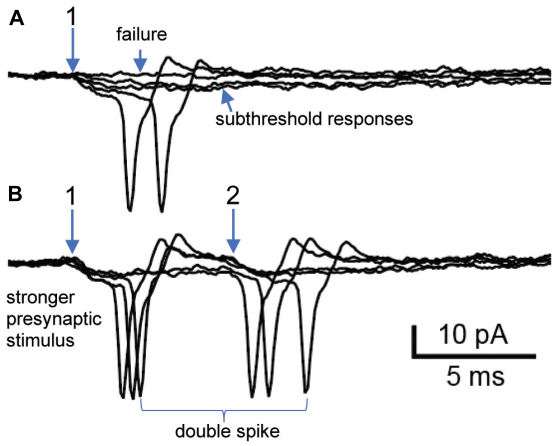

FIGURE 3
Extracellular recording of double spiking driven by two straddling synapses. **(A)** Selective activation of synapse 1. Five responses at synapse 1 include 2 subthreshold responses, 2 suprathreshold responses and 1 stimulus failure. Traces taken from a larger trial at 1 Hz (see text for description of all responses). **(B)** Raising the presynaptic stimulus strength recruited synapse 2 and eliminated failures at synapse 1. Note that synapse 2 also straddled threshold by generating subthreshold and suprathreshold responses. Experiment 6/2/16 cell 4.

the efficacy of synapse 2 was altered by its temporal interaction with synapse 1. Resolving this question required intracellular measurements (Figure 4).

After breaking into the cell under voltage-clamp (Figure 4B) while maintaining the same presynaptic stimulus strength, a total of 3 synapses became evident. The latencies of extracellular EPSPs at synapses 1 and 2 (Figure 4A) correspond to the latencies of the intracellular EPSCs labeled 1 and 2 (Figure 4B). Peak synaptic current amplitudes were -1391 ± 236 pA at synapse 1 and -1520 ± 252 pA at synapse 2. Given that the mean currents for each synapse are within 1 standard deviation of each other and that synapse 1 straddles threshold when stimulated in isolation (Figure 3A), it seems highly likely that synapse 2 would also straddle threshold if it could be stimulated in isolation.

After increasing the presynaptic stimulus strength (Figure 4C) a total of 7 synaptic components were identified. The family of EPSCs at each synapse had a distinct latency and distinct average amplitude (Table 1). Given complexity of waveforms arising from seven converging synapses, one might ask whether trial to trial fluctuations in the latencies of responses obscure additional synaptic inputs. Although impossible to rule out this concern with complete certainty, this problem seems unlikely to confound the results because fluctuations in latency were small. As seen in Figures 4A–C, fluctuations in the latency of individual synaptic components were less than 0.5 ms, while the conduction delays of individual synaptic components ranged from 11 to 23 ms. Due to the

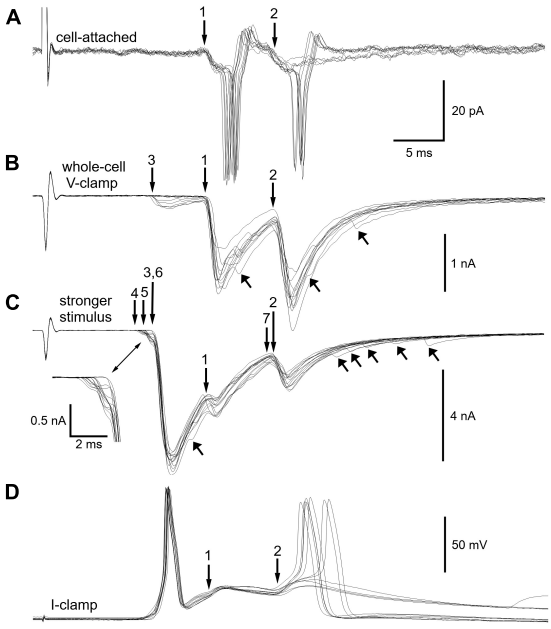

FIGURE 4
Fractionation of 7 synapses that converge on a sympathetic neuron. **(A)** Additional extracellular on-cell recordings from the same neuron illustrated in **Figure 3**. **(B)** Intracellular voltage-clamp recordings of synaptic currents after breaking into the cell. Presynaptic stimulus strength unchanged from panel **(A)**. The records show families of excitatory postsynaptic currents (EPSCs) whose latencies match those of responses 1 and 2 in panel **(A)**. The smaller EPSCs at synapse 3 were not detected in the on-cell recording. Upward arrows point to examples of asynchronous EPSCs present in some trials. **(C)** After increasing the presynaptic stimulus strength, a total of 7 synaptic components were resolved based on the latencies and magnitudes of EPSCs. Inset shows the small EPSCs at the foot of the large EPSCs associated with synapse 6. Upward arrows point to additional asynchronous EPSCs. **(D)** Switching the amplifier to current-clamp mode reveals EPSPs that drive pairs of action potentials. Note that the larger synaptic events (6, 1, 2) obscure the smaller ones. Note also that the double spiking differs from that in panel **(A)**. Synapses 6 and 2 rather than synapses 1 and 2 now trigger action potentials. See text for additional detail.

length of presynaptic CST (**Figure 1B**) and the slow conduction velocities (<1 m/s) of preganglionic axons (Li and Horn, 2006), which are unmyelinated C fibers, the jitter in postsynaptic responses accounts for less than 5% of the total synaptic latency.

The strength of synapse 6 in **Figure 4C** is notable because it produced EPSCs that were >3.5 times larger (>15 standard deviations) than those at synapses 1 and 2, which straddled threshold. Thus, the safety factor for suprathreshold transmission at synapse 6 is very high, consistent with the example shown in **Figure 2** and with the original definition of a primary synapse (Karila and Horn, 2000). Asynchronous EPSCs having low amplitudes were also evident in this neuron (**Figures 4B,C**).

At this point we examined the membrane potential response to strong stimuli that activated all 7 synapses by switching from whole cell voltage-clamp to the current-clamp mode (**Figure 4D**). In these recordings evidence of the weaker synapses is obscured by the larger responses at synapses 1, 2, and 6. Interestingly, the cell double-spiked, just as in the initial extracellular recording. However, now the paired spiking was driven by synapses 6 and 2 rather than by synapses 1 and 2. This shows that the action potentials evoked by suprathreshold EPSPs at synapse 6 had the effect of completely occluding action potentials at synapse 1. The occlusion likely results from reduced excitability due to Na^+ channel inactivation during the refractory period and from increased K^+ conductance during the spike afterpotential (McAfee and Yarowsky, 1979; Galvan and Sedlmeir, 1984; Wheeler et al., 2004).

Table 1 summarizes the average magnitude and variability of each synaptic input to the cell illustrated in **Figure 4** in terms of its underlying peak EPSC amplitude, standard deviation, and the associated synaptic conductance (g_{syn}). Given that the extracellular responses evoked at synapses 1 and 2 straddle threshold, the associated synaptic currents provide a useful index of synaptic strength. Converting the mean peak current to a nicotinic conductance is convenient because it is independent of the holding membrane potential where currents are measured and is often used as an input parameter for computational models and dynamic clamp experiments. Threshold synaptic conductance (threshold-g_{syn}) defines synaptic strength as the minimum nicotinic synaptic conductance required to reach firing threshold for an action potential (Schobesberger et al., 2000; Kullmann et al., 2004; Wheeler et al., 2004). Earlier work estimated threshold-g_{syn} using computational models and a virtual nicotinic synapse whose strength was systematically varied to find threshold. The straddling synapses described here enable one to estimate threshold-g_{syn} independent of simulations and dynamic clamp methods. By using the average synaptic conductance of a straddling synapse as an estimate of threshold-g_{syn} one can then calculate the relative strengths of the other synapses (**Table 1**) and then classify them as primary, straddling, or secondary. This approach indicates that synapse 6 was a primary synapse whose strength was nearly four times threshold-g_{syn}, that synapses 1 and 2 were straddling synapses and that synapses 3, 4, 5, and 7 were secondary synapses whose strengths were <30% threshold-g_{syn}. Unlike straddling EPSPs, secondary EPSPs never trigger action potentials unless they summate with other EPSPs.

The average g_{syn} of 22 straddling synapses was 9.8 ± 7.5 nS (mean ± SD). **Table 2** summarizes the properties of these straddling synapses and the 20 neurons from 20 animals where they were studied. They were identified as straddling through extracellular on-cell recording and then assessed by intracellular voltage-clamp and current-clamp measurements. Synapse 2 in **Figure 2** corresponds to cell 5 in **Table 2**. Synapses 1 and 2 in **Figures 3**, **4** and in **Table 1** correspond to synapses 13 and 14 in **Table 2**. Although we did not set out to study differences between sexes and strains, the data demonstrate that straddling

TABLE 1 Strength classification of synapses converging on one cell.

Synapse number	Peak EPSC (pA) mean ± SD (*n*)	Peak g_{syn} (nS)	Synapse strength% threshold-g_{syn}	Strength classification
1	−1391 ± 236 (37)	25.8	100	Straddling
2	−1520 ± 252 (13)	28.2	109	Straddling
3	−156 ± 57 (14)	2.9	11	Secondary
4	−148 ± 36 (7)	2.7	10	Secondary
5	−381 ± 99 (6)	7.0	27	Secondary
6	−5355 ± 448 (20)	99.2	384	Primary
7	Not resolved	–	–	Secondary

Data in this table are from the neuron illustrated in Figure 4. All currents were measured at a corrected holding potential of −65 mV. Synapses 1 and 2 correspond to synapses 13 and 14 in Table 2. Excitatory postsynaptic currents (EPSCs) at synapse 7 were too small to permit a reliable estimate of their amplitude.

synapses were evident in 3 female CD rats, 13 male CD rats, and 3 male SHR rats.

In light of the trial-to-trial fluctuations in response amplitudes one might expect that the mean g_{syn} of a straddling synapse could underestimate or overestimate threshold-g_{syn} and that this would be reflected in the synaptic efficacy in triggering action potentials. For example, the mean g_{syn} of a synapse that triggers action potentials in 90% of trials would overestimate threshold-g_{syn}. Conversely, the mean g_{syn} of a synapse that triggers action potentials in 10% of trials would underestimate threshold-g_{syn}. To assess this possibility, we counted subthreshold and suprathreshold responses in extracellular and intracellular recordings. In extracellular on-cell recordings, 57.7 ± 27.5% of trials elicited spikes (Table 2, n = 22 synapses, range 9.5–95.2%). In intracellular current-clamp recordings, 61.0 ± 27.0% of trials elicited spikes (n = 17 synapses, range 16.7–96.6%). These data indicate that the overall average g_{syn} of 9.8 nS (Table 2) is a slight overestimate of threshold-g_{syn} that ideally would elicit spikes in 50% of trials.

Age and cell size are factors that could account for some of the cell-to-cell variability in the g_{syn} of straddling synapses, input resistance (R_{input}) and resting potential (V_{rest}). For example, cells might grow over time and larger cells would have lower R_{input} and thus require stronger EPSPs to reach threshold. One might also expect that cells with lower resting potentials would require larger synaptic currents to reach threshold. To examine these possibilities, we examined the data distributions of C_m, R_{input}, V_{rest}, and peak EPSC amplitude, and then looked for correlations between them. The D'Agostino-Pearson normality test indicated that R_{input} measurements were compatible with the null hypothesis (H_0) of a normal distribution, but that measurements of C_m, EPSC amplitude and V_{rest} were incompatible with this H_0. We therefore calculated correlation coefficients (r) using the non-parametric Spearman method, together with 2-tailed P-values and 95% confidence intervals for evaluating the null hypothesis that r = 0. Taking whole cell capacitance (C_m) as an index of cell size, the data were incompatible with correlations between age and either C_m (r = −0.071, P = 0.765), EPSC amplitude (r = 0.086, P = 0.717), R_{input} (r = 0.275, P = 0.239), or V_{rest} (r = 0.007, P = 0.974). By contrast, there were negative correlations between C_m and R_{input} (Figure 5A), C_m and EPSC amplitude (Figure 5B), and C_m and V_{rest} (Figure 5C). These results are consistent with the expectation that larger cells would have more open channels at rest and therefore a lower R_{input}. They also conform to the idea that larger synaptic currents would be required to depolarize cells with lower R_{input} to reach threshold. The correlation between C_m and V_{rest} under current clamp may reflect the possibility that smaller neurons are more susceptible to recording damage. In addition, positive correlations incompatible with H_0 were also seen between R_{input} and EPSC amplitude (Figure 5D) and between V_{rest} and EPSC amplitude (Figure 5E). This supports the idea that cells with higher R_{input} or lower V_{rest} require larger EPSCs to reach threshold.

Discussion

Several years ago, high resolution patch recording of synaptic transmission became possible in the isolated intact SCG (Springer et al., 2015). Using this approach (Figure 1), we set out to explore the properties of individual synapses that converge on individual sympathetic neurons. Along the way, it became evident that on-cell recordings established before breaking into the whole-cell configuration revealed important information about the strength of synapses.

The detection in on-cell extracellular recordings of nicotinic synapses whose strength straddles threshold during repetitive 1 Hz stimulation demonstrates that such straddling is not an artifact of intracellular recording (Figures 2–4 and Table 2). In addition, the present results replicate double spike responses to single presynaptic stimuli seen previously in microelectrode recordings (Rimmer and Horn, 2010). In the earlier work it was unclear whether double spiking reflected converging synapses or repetitive firing. The present results show that double spiking arises from converging synapses with different

TABLE 2 Summary of straddling synapses.

Synapse number	Date	Cell	Sex	Strain	Age (days)	On-cell straddling [% suprathreshold (in *n* trials)]	V_{rest} (mV)	R_{input} (meg-Ω)	R_{series} (meg-Ω)	C_m (pF)	I_{syn} (pA) mean ± SD (*n*)	g_{syn} (nS) mean
1	1/25/2018	c2	M	CD	87	83.3 (6)	−61	258	6.2	127	−779 ± 180 (13)	14.4
2	4/13/2018	c1	M	CD	60	83.3 (6)	−56	234	7.1	74	−564 ± 158 (26)	10.4
3	4/30/2018	c5	M	CD	63	73.3 (30)	−56	577	7.9	61	−252 ± 36 (5)	4.7
4		c5				87.5 (8)					−253 ± 90 (29)	4.7
5	11/9/2018	c2	M	CD	109	37.9 (29)	−57	662	6.9	51	−232 ± 123 (55)	4.3
6	1/11/2017	c2	F	CD	65	9.5 (42)	−57	857	5.3	69	−295 ± 126 (34)	5.5
7	1/13/2017	c3	F	CD	67	95.2 (21)	−68	551	4.6	81	−694 ± 190 (37)	12.9
8	1/27/2017	c2	F	CD	63	41.9 (31)	−51	602	4.9	61	−215 ± 84 (52)	4.0
9	12/21/2017	c2	M	SHR	73	5.3 (57)	−59	703	9.0	65	−328 ± 125 (48)	6.1
10	1/28/2016	c2	M	CD	66	64.3 (28)	−60	312	12.4	95	−1339 ± 295 (65)	24.8
11	2/19/2016	c1	M	SHR	67	74.1 (54)	−65	346	6.5	77	−493 ± 119 (120)	9.1
12	2/19/2016	c5	M	SHR	67	33.3 (12)	−52	721	7.4	34	−196 ± 90 (80)	3.6
13	6/2/2016	c4	M	CD	66	80.4 (51)	−78	393	6.5	80	−1391 ± 236 (37)	25.8
14		c4				57.9 (19)					−1520 ± 252 (13)	28.2
15	6/6/2016	c5	M	SHR	161	20.0 (10)	−58	664	4.9	76	−182 ± 100 (17)	3.4
16	6/8/2016	c1	M	CD	65	62.5 (32)	−59	645	9.9	51	−244 ± 100 (47)	4.5
17	8/24/2016	c1	M	CD	65	10.7 (28)	−62	498	6.6	67	−231 ± 107 (29)	4.3
18	9/13/2016	c4	M	CD	64	59.4 (32)	−62	390	4.9	79	−593 ± 193 (61)	11.0
19	9/16/2016	c2	M	CD	67	69.2 (13)	−59	703	9.5	60	−398 ± 144 (33)	7.4
20	9/30/2016	c4	M	CD	69	90.0 (30)	−58	1200	4.6	46	−205 ± 35 (23)	3.8
21	10/13/2016	c3	M	CD	73	67.9 (53)	−57	263	7.4	77	−739 ± 208 (90)	13.7
22	7/28/2015	c1	M	CD	49	62.1 (29)	−68	293	10.2	88	−449 ± 127 (70)	8.3
				Mean	73.3	57.7	−60.2	544	7.1	71.0	−527	9.8
				SD	23.7	27.5	6.1	242	2.1	19.9	407	7.6

10.3389/fnins.2022.869753

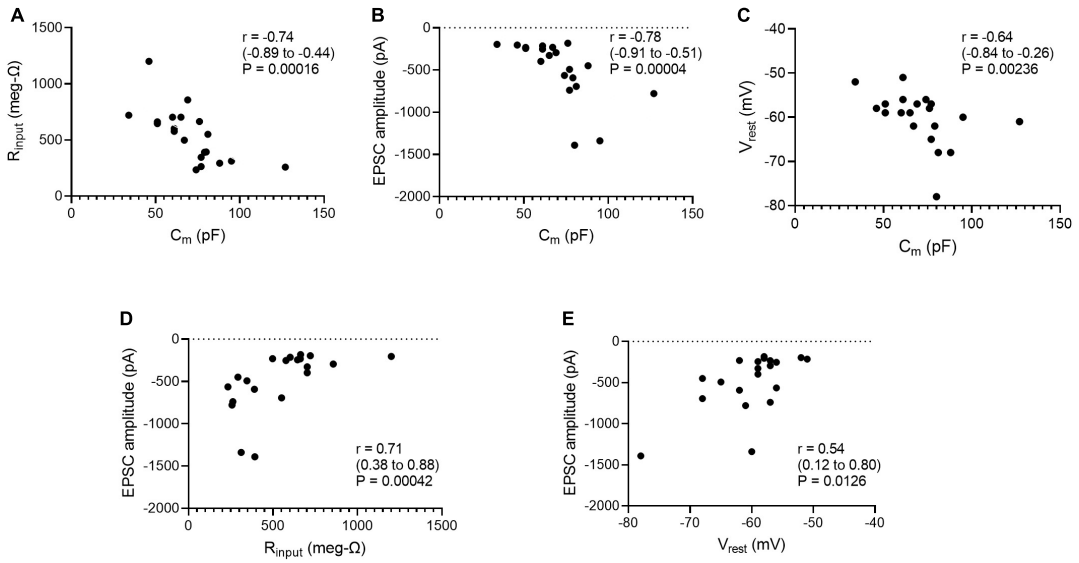

FIGURE 5
Whole cell capacitance correlates with **(A)** input resistance, **(B)** peak excitatory postsynaptic current (EPSC) amplitudes at straddling synapses, and **(C)** resting membrane potential. Peak EPSC amplitudes at straddling synapses correlate with **(D)** input resistance and **(E)** resting membrane potential. C_m was taken as a measure of cell size. Spearman correlation coefficients (r) were calculated for each scatter plot along with 95% confidence intervals and 2-tailed *P*-values. C_m, R_{input}, and EPSCs were measured under voltage-clamp. V_{rest} was measured under-current clamp. All data are from **Table 2**.

latencies (**Figures 2B**, **3B**, **4A,D**) and not to repetitive firing during sustained depolarization or from intracellular recording damage (**Figures 2B**, **3B**, **4A**). In current-clamp recordings, repetitive firing was never seen in response to EPSPs evoked at one synapse, regardless of their strength.

At synapses where nicotinic EPSPs straddle threshold, the underlying synaptic currents provide an estimate of threshold-g_{syn}. Using this approach, threshold-g_{syn} in the intact SCG was 9.8 ± 1.6 nS (mean ± standard error, range 3.4–28.2 nS, n = 22). This closely resembles previous estimates based on a computational model and on dynamic clamp experiments from dissociated sympathetic neurons. In a conductance-based model tuned to replicate properties of bullfrog sympathetic B neurons, threshold-g_{syn} = 10.1 nS (Schobesberger et al., 2000). When dynamic clamp was used to produce virtual nicotinic EPSPs in recordings from dissociated bullfrog sympathetic neurons, threshold-g_{syn} = 14.7 ± 1.7 nS (mean ± standard error) (Wheeler et al., 2004). Other dynamic clamp experiments with dissociated bullfrog sympathetic neurons revealed phenotypic differences in threshold-g_{syn} measurements from identified secretomotor B neurons [17.1 ± 1.2 nS, (mean ± standard error)] and vasomotor C neurons (3.3 ± 0.3 nS, mean ± standard error) (Kullmann and Horn, 2010b). This is interesting because it suggests that phenotypic specialization may explain some of the variability seen in our analysis of straddling synapses in the rat SCG. In dynamic clamp experiments using dissociated rat SCG neurons threshold-g_{syn} = 7.0 ± 0.9 nS (mean ± standard error) (Kullmann et al., 2016). Other experiments on rat SCG neurons suggest that cell specific differences in repetitive firing dynamics may also be associated with variability seen in threshold-g_{syn} (Springer et al., 2015).

Normalizing synaptic conductance measurements to threshold-g_{syn} enables one to appreciate the range of synaptic strength expressed by converging synapses and between different neurons. Whether expressed in terms of size as synaptic current or synaptic conductance, or in terms of strength as %-threshold-g_{syn}, the 6 converging synapses in **Table 1** produced responses whose magnitude spanned a 38-fold range. In moving beyond the original primary-secondary synapse dichotomy (Karila and Horn, 2000), straddling synapses must now be considered. This conclusion supports an earlier idea by Bratton et al. (2010). They devised an ingenious method to estimate the strength of EPSPs recorded *in vivo* from lumbar chain ganglia in the rat with intracellular current-clamp methods. By injecting hyperpolarizing currents, they estimated the extent to which suprathreshold EPSPs could be disrupted. Although indirect, this approach led them to conclude that the synapses that drive firing in different neurons varied in their strength. They also proposed that the distribution of synaptic strength was continuous rather than lumped into two discrete groups. Although this concept is consistent with our data, more work will be required to fully delineate the strength distribution of converging synapses.

Our interest in primary and secondary nicotinic synapses began with an analysis of convergence in bullfrog secretomotor neurons using microelectrode recordings (Karila and Horn, 2000). Given the tools of the time, it was simplest to ask

whether a synapse was very strong with a high safety factor and thus a primary synapse that never failed to elicit an action potential–or whether it was weaker and thus secondary. Now with the advantage of hindsight one can see that straddling synapses also exist in bullfrog sympathetic ganglia. Figure 1 in Karila and Horn (2000) illustrates a bullfrog B-type neuron with 2 converging synapses. The primary synapse invariably evokes an action potential and is strong enough to deform the spike afterhyperpolarization. The weaker synapse is generally subthreshold in strength and does not deform the spike afterhyperpolarization, indicating its underlying synaptic conductance is much smaller than that of the primary synapse. However, fluctuations in EPSPs at the weaker synapse enable it to trigger spikes in some trials! We would therefore now label it as a straddling synapse and not a secondary synapse. Weaker secondary synapses are evident in other data shown in the Karila and Horn's (2000) paper.

Understanding the strength of converging nicotinic synapses in sympathetic ganglia has important implications for ganglionic integration. Postulating that convergence follows an $n + 1$ rule and that summation of secondary EPSPs can drive firing enabled the construction of computational models (Karila and Horn, 2000; Wheeler et al., 2004; Kullmann and Horn, 2006, 2010a; Kullmann et al., 2016). The models predicted that paravertebral sympathetic ganglia function as use-dependent amplifiers of preganglionic activity. Simply stated, more action potentials leave the ganglion than enter it, because of synaptic amplification. Ganglionic gain could be important in normal cardiovascular physiology and in hypertension (Guyenet, 2006; Fadel, 2008; Joyner et al., 2008; Esler, 2010, 2014; Malpas, 2010). In baroreceptor coupled sympathetic circuits that control blood pressure, functional gain is important. Variable synaptic gain in ganglia could play a role. Hypertension in many individuals is associated with sympathetic hyperactivity. What, if any, role does a remodeling of ganglionic gain play in generating sympathetic hyperactivity?

In closing, the identification of straddling synapses demonstrates that previous models of ganglionic integration are no longer sufficient. However, this does not disprove the synaptic gain hypothesis or show that ganglia behave as simple relays rather than as integrative centers. It means that more nuanced models incorporating synapses of different strengths will be required to elucidate ganglionic computation and its contribution to normal physiology and pathophysiology.

Data availability statement

The original contributions presented in this study are included in the article/supplementary material, further inquiries can be directed to the corresponding author.

Ethics statement

The animal study was reviewed and approved by IACUC, University of Pittsburgh.

Author contributions

PK was primarily responsible for conducting the experiments. Both authors contributed to the design of experiments, analysis, and writing the manuscript.

Funding

This work was supported by development funds from the University of Pittsburgh School of Medicine.

Conflict of interest

The authors declare that the research was conducted in the absence of any commercial or financial relationships that could be construed as a potential conflict of interest.

Publisher's note

All claims expressed in this article are solely those of the authors and do not necessarily represent those of their affiliated organizations, or those of the publisher, the editors and the reviewers. Any product that may be evaluated in this article, or claim that may be made by its manufacturer, is not guaranteed or endorsed by the publisher.

References

Bratton, B., Davies, P., Janig, W., and McAllen, R. (2010). Ganglionic transmission in a vasomotor pathway studied in vivo. *J. Physiol.* 588(Pt 9), 1647–1659. doi: 10.1113/jphysiol.2009.185025

Dodd, J., and Horn, J. P. (1983). A reclassification of B and C neurones in the ninth and tenth paravertebral sympathetic ganglia of the bullfrog. *J. Physiol.* 334, 255–269. doi: 10.1113/jphysiol.1983.sp014493

Esler, M. (2010). Sympathetic nervous activation in essential hypertension: Commonly neglected as a therapeutic target, usually ignored as a drug side effect. *Hypertension* 55, 1090–1091. doi: 10.1161/HYPERTENSIONAHA.110.151506

Esler, M. (2014). Sympathetic nervous system moves toward center stage in cardiovascular medicine: From Thomas Willis to resistant hypertension. *Hypertension* 63, e25–e32. doi: 10.1161/HYPERTENSIONAHA.113.02439

Fadel, P. J. (2008). Arterial baroreflex control of the peripheral vasculature in humans: Rest and exercise. *Med. Sci. Sports Exerc.* 40, 2055–2062. doi: 10.1249/MSS.0b013e318180bc80

Galvan, M., and Sedlmeir, C. (1984). Outward currents in voltage-clamped rat sympathetic neurones. *J. Physiol.* 356, 115–133. doi: 10.1113/jphysiol.1984.sp015456

Guyenet, P. G. (2006). The sympathetic control of blood pressure. *Nat. Rev. Neurosci.* 7, 335–346. doi: 10.1038/nrn1902

Hirst, G. D., and McLachlan, E. M. (1984). Post-natal development of ganglia in the lower lumbar sympathetic chain of the rat. *J. Physiol.* 349, 119–134. doi: 10.1113/jphysiol.1984.sp015147

Ivanoff, A. Y., and Smith, P. A. (1995). In vivo activity of B- and C-neurones in the paravertebral sympathetic ganglia of the bullfrog. *J. Physiol.* 485(Pt 3), 797–815. doi: 10.1113/jphysiol.1995.sp020770

Ivanov, A., and Skok, V. I. (1992). Neuronal mechanisms responsible for ongoing activity of rabbit superior cervical ganglion neurons. *J. Auton. Nerv. Syst.* 41, 61–66. doi: 10.1016/0165-1838(92)90127-3

Janig, W. (2006). *The integrative action of the autonomic nervous system*. Cambridge: Cambridge University Press.

Joyner, M. J., Charkoudian, N., and Wallin, B. G. (2008). A sympathetic view of the sympathetic nervous system and human blood pressure regulation. *Exp. Physiol.* 93, 715–724. doi: 10.1113/expphysiol.2007.039545

Karila, P., and Horn, J. P. (2000). Secondary nicotinic synapses on sympathetic B neurons and their putative role in ganglionic amplification of activity. *J. Neurosci.* 20, 908–918. doi: 10.1523/JNEUROSCI.20-03-00908.2000

Kullmann, P. H., and Horn, J. P. (2006). Excitatory muscarinic modulation strengthens virtual nicotinic synapses on sympathetic neurons and thereby enhances synaptic gain. *J. Neurophysiol.* 96, 3104–3113. doi: 10.1152/jn.00589.2006

Kullmann, P. H., and Horn, J. P. (2010a). Homeostatic regulation of M-current modulates synaptic integration in secretomotor, but not vasomotor, sympathetic neurons in the bullfrog. *J. Physiol.* 588(Pt 6), 923–938. doi: 10.1113/jphysiol.2009.182873

Kullmann, P. H., and Horn, J. P. (2010b). Vasomotor sympathetic neurons are more excitable than secretomotor sympathetic neurons in bullfrog paravertebral ganglia. *Auton. Neurosci.* 155, 19–24. doi: 10.1016/j.autneu.2009.12.009

Kullmann, P. H., Sikora, K. M., Clark, K. L., Arduini, I., Springer, M. G., and Horn, J. P. (2016). HCN hyperpolarization-activated cation channels strengthen virtual nicotinic EPSPs and thereby elevate synaptic amplification in rat sympathetic neurons. *J. Neurophysiol.* 116, 438–447. doi: 10.1152/jn.00223.2016

Kullmann, P. H., Wheeler, D. W., Beacom, J., and Horn, J. P. (2004). Implementation of a fast 16-Bit dynamic clamp using LabVIEW-RT. *J. Neurophysiol.* 91, 542–554. doi: 10.1152/jn.00559.2003

Li, C., and Horn, J. P. (2006). Physiological classification of sympathetic neurons in the rat superior cervical ganglion. *J. Neurophysiol.* 95, 187–195. doi: 10.1152/jn.00779.2005

Malpas, S. C. (2010). Sympathetic nervous system overactivity and its role in the development of cardiovascular disease. *Physiol. Rev.* 90, 513–557. doi: 10.1152/physrev.00007.2009

Maslov, V. Y., Ivanov, A. Y., and Skok, V. I. (1996). Background activity of the rabbit superior cervical ganglion neurons: Soundness of random hypothesis of its formation. *Neurofiziologiia* 39, 486–492.

McAfee, D. A., and Yarowsky, P. J. (1979). Calcium-dependent potentials in the mammalian sympathetic neurone. *J. Physiol.* 290, 507–523. doi: 10.1113/jphysiol.1979.sp012787

McLachlan, E. M. (2003). Transmission of signals through sympathetic ganglia–modulation, integration or simply distribution? *Acta Physiol. Scand.* 177, 227–235. doi: 10.1046/j.1365-201X.2003.01075.x

McLachlan, E. M., Davies, P. J., Habler, H. J., and Jamieson, J. (1997). On-going and reflex synaptic events in rat superior cervical ganglion cells. *J. Physiol.* 501(Pt 1), 165–181. doi: 10.1111/j.1469-7793.1997.165bo.x

McLachlan, E. M., Habler, H. J., Jamieson, J., and Davies, P. J. (1998). Analysis of the periodicity of synaptic events in neurones in the superior cervical ganglion of anaesthetized rats. *J. Physiol.* 511(Pt 2), 461–478. doi: 10.1111/j.1469-7793.1998.461bh.x

Purves, D., and Lichtman, J. W. (1985). Geometrical differences among homologous neurons in mammals. *Science* 228, 298–302. doi: 10.1126/science.3983631

Rimmer, K., and Horn, J. P. (2010). Weak and straddling secondary nicotinic synapses can drive firing in rat sympathetic neurons and thereby contribute to ganglionic amplification. *Front. Neurol.* 1:130. doi: 10.3389/fneur.2010.00130

Schobesberger, H., Wheeler, D. W., and Horn, J. P. (2000). A model for pleiotropic muscarinic potentiation of fast synaptic transmission. *J. Neurophysiol.* 83, 1912–1923. doi: 10.1152/jn.2000.83.4.1912

Skok, V. I., and Ivanov, A. Y. (1983). What is the ongoing activity of sympathetic neurons? *J. Auton. Nerv. Syst.* 7, 263–270. doi: 10.1016/0165-1838(83)90079-6

Springer, M. G., Kullmann, P. H., and Horn, J. P. (2015). Virtual leak channels modulate firing dynamics and synaptic integration in rat sympathetic neurons: Implications for ganglionic transmission in vivo. *J. Physiol.* 593, 803–823. doi: 10.1113/jphysiol.2014.284125

Wheeler, D. W., Kullmann, P. H., and Horn, J. P. (2004). Estimating use-dependent synaptic gain in autonomic ganglia by computational simulation and dynamic-clamp analysis. *J. Neurophysiol.* 92, 2659–2671. doi: 10.1152/jn.00470.2004

frontiers | Frontiers in Physiology

TYPE Original Research
PUBLISHED 23 December 2022
DOI 10.3389/fphys.2022.946613

OPEN ACCESS

EDITED BY
Vaughan G. Macefield,
Baker Heart and Diabetes Institute, Australia

REVIEWED BY
Marco Mongillo,
University of Padua, Italy
Thomas E. Dick,
Case Western Reserve University, United States
Beatrice Cairo,
University of Milan, Italy

*CORRESPONDENCE
Zoran Matić,
z.matic157@yahoo.com

†These authors have contributed equally to this work

SPECIALTY SECTION
This article was submitted to Autonomic Neuroscience, a section of the journal Frontiers in Physiology

RECEIVED 17 May 2022
ACCEPTED 09 November 2022
PUBLISHED 23 December 2022

CITATION
Matić Z, Kalauzi A, Moser M, Platiša MM, Lazarević M and Bojić T (2022), Pulse respiration quotient as a measure sensitive to changes in dynamic behavior of cardiorespiratory coupling such as body posture and breathing regime.
Front. Physiol. 13:946613.
doi: 10.3389/fphys.2022.946613

Pulse respiration quotient as a measure sensitive to changes in dynamic behavior of cardiorespiratory coupling such as body posture and breathing regime

Zoran Matić[1]*, Aleksandar Kalauzi[2†], Maximilian Moser[3], Mirjana M. Platiša[4], Mihailo Lazarević[5] and Tijana Bojić[6†]

[1]Biomedical Engineering and Technologies, University of Belgrade, Belgrade, Serbia, [2]Department for Life Sciences, Institute for Multidisciplinary Research, University of Belgrade, Belgrade, Serbia, [3]Chair of Physiology, Medical University of Graz, Graz, Austria; Human Research Institute, Weiz, Austria, [4]Institute of Biophysics, Faculty of Medicine, University of Belgrade, Belgrade, Serbia, [5]Department for Mechanics, Faculty for Mechanical Engineering, University of Belgrade, Belgrade, Serbia, [6]Department of Radiation Chemistry and Physics, "VINČA" Institute of Nuclear Sciences - National Institute of The Republic of Serbia, University of Belgrade, Belgrade, Serbia

Objective: In this research we explored the (homeo)dynamic character of cardiorespiratory coupling (CRC) under the influence of different body posture and breathing regimes. Our tool for it was the pulse respiration quotient (PRQ), representing the number of heartbeat intervals per breathing cycle. We obtained non-integer PRQ values using our advanced Matlab® algorithm and applied it on the signals of 20 healthy subjects in four conditions: supine position with spontaneous breathing (Supin), standing with spontaneous breathing (Stand), supine position with slow (0.1 Hz) breathing (Supin01) and standing with slow (0.1 Hz) breathing (Stand01).

Main results: Linear features of CRC (in PRQ signals) were dynamically very sensitive to posture and breathing rhythm perturbations. There are obvious increases in PRQ mean level and variability under the separated and joined influence of orthostasis and slow (0.1 Hz) breathing. This increase was most pronounced in Stand01 as the state of joint influences. Importantly, PRQ dynamic modification showed greater sensitivity to body posture and breathing regime changes than mean value and standard deviation of heart rhythm and breathing rhythm. In addition, as a consequence of prolonged supine position, we noticed the tendency to integer quantization of PRQ (especially after 14 min), in which the most common quantization number was 4:1 (demonstrated in other research reports as well). In orthostasis and slow breathing, quantization can also be observed, but shifted to other values. We postulate that these results manifest resonance effects induced by coupling patterns from sympathetic and parasympathetic adjustments (with the second as dominant factor).

Significance: Our research confirms that cardiorespiratory coupling adaptability could be profoundly explored by precisely calculated PRQ parameter since cardiorespiratory regulation in healthy subjects is characterized by a high level of autonomic adaptability (responsiveness) to posture and breathing regime, although comparisons with pathological states has yet to be performed. We found Stand01 to be the most provoking state for the dynamic modification of PRQ (cardiorespiratory inducement). As such, Stand01 has the potential of using for PRQ tuning by conditioning the cardiorespiratory autonomic neural networks, e.g., in the cases where PRQ is disturbed by environmental (i.e., microgravity) or pathologic conditions.

KEYWORDS

heart rate, autonomic nervous system, homeodynamics, pulse-respiratory quantization, vagal activity, sympathetic, respiratory sinus arrhythmia

Introduction

During physiological regulation, the heart and the lung produce specific rhythms that, recorded by biomedical instrumentation, can be viewed as signals of biological oscillations (fluctuations). Modern research has observed that biological oscillations are characterized by high temporal variability and mutual interaction (coupling). Also, it turned out that these characteristics, especially as found in heart rhythm and breathing are of fundamental importance for health (Moser et al., 2006 a; b, 2008) and that, in a sense, they are very sensitive to changes in physical and physiological conditions. Body posture and breathing regime changes are a kind of perturbations that induce different physical and physiological conditions of cardiorespiratory functioning in the human organism which has adapted to these perturbations through subtle adjustments of the mean values of internal biorhythms (homeostasis) and its variability and complexity characteristics (homeodynamics) (Ernst 2014, 2017; Matić et al., 2020) mostly by mediation of the autonomic nervous system (ANS). Studies of the influence of orthostasis and especially slow breathing on the ANS regulation have become very relevant in recent years, both in fundamental biomedical research and in clinical practice. From scientific evidence, it has been concluded that the heart rhythm in supine position is characterized by a slight predominance of parasympathetic (vagal) activity (Levy and Martin 1996; Malliani 2005; Mclachlan et al., 2010). Conversely, in the standing position, sympathetic predominance is manifested (Levy & Martin, 1996; Srinivasan et al., 2002; Srinivasan et al., 2002; Maggioni et al., 2020). Slow breathing at the rate of 0.1 Hz (6 breaths per min) has been shown to produce resonant effect on different physiological rhythmicity (brain activity (Hinterberger et al., 2019), mental functions (Schwerdtfeger et al., 2020), heart rate variability (Russo, Santarelli and O'Rourke 2017), blood pressure (Russo, Santarelli and O'Rourke 2017; Brenner et al., 2020), etc) and even hematocrit (Schneditz et al., 1990). Mainly, the resonant effect of slow breathing refers to increase in temporal variability which is usually reflected in the rise of standard deviation (variance or total power of spectral density) (Force of The European Society of Cardiology & North American Society of Pacing, 1996). Overall, coupling and resonance that partake in between physiological rhythms increase variability of rhythms themselves (Dick et al., 2014). Evidence for significant increase of heart rate *variability* (HRV) induced by slow breathing near 0.1 Hz frequency is given in many recent studies (Zautra et al., 2010; Lin et al., 2014; Steffen et al., 2017; Blum et al., 2019; Lehrer et al., 2020). This phenomenon of rise in HRV through slow breathing is also called 'cardiac coherence' (West, 2010; Shaffer et al., 2014; McCraty, 2017), and the technique itself "HRV biofeedback" (Lehrer et al., 2013). Regarding previous research on this topic, it has been generalized that slow (controlled) breathing can be used for conscious regulation enhancement of emotional, cognitive and physiological performances (Boyadzhieva and Kayhan, 2021).

Besides homeodynamics, breathing and heart rhythm interact mutually in a very dynamic manner, forming an integrated physiological behavior called "cardiorespiratory coupling" (CRC) (Kralemann et al., 2013; Dick et al., 2014). Both CRC and homeodynamics might be enhanced by the vagal activity increase induced by slow breathing (Russo, Santarelli and O'Rourke 2017; Matić et al., 2020).

There are various techniques for exploration of CRC. Among them, pulse respiration quotient (PRQ) was reaffirmed as a very elegant and powerful tool by which useful information on ANS regulation patterns can be obtained (Moser et al., 1995; Edelhäuser et al., 2013; Scholkmann et al., 2019; Scholkmann and Wolf 2019; Grote et al., 2021). In earlier research (at the beginning of the 20th century), PRQ was calculated approximately, as integer values (Coleman, 1920). Except for the investigation of Edelhäuser et al. in which temporal phase coordination between heart beats and breathing was calculated (Edelhäuser et al., 2013), due to the lack of greater precision in the automatic calculation of PRQ, the temporal variability of PRQ remained less researched and interpreted compared to the heart rate (temporal) variability (HRV). Claims that the PRQ can

capture reactivity and adaptability of cardiovascular and cardiorespiratory systems to internal and external situations and requirements, that it contains information on "cardio-respiratory adaptability due to change of state" and "the overall current state of human physiology in general" (Scholkmann and Wolf 2019) were based on changes in mean PRQ and should be supplemented by an assessment of PRQ temporal variability. To achieve this, instead of "determining PRQ by averaging HR and BR (breathing rate) measurements" (Scholkmann and Wolf 2019), it is necessary to perform PRQ determination using an algorithm for continuous calculation of heart beat intervals (RRI) per each real-time respiratory cycle. In this paper we focused our analysis on the HR:RR = HR:1 relation, due to the robustness of this type of synchronization (Kotani et al., 2002; Bartsch et al., 2007). In this way, a PRQ signal with high time resolution is obtained. Fluctuations in PRQ signals could be shown to be sensitive to changes in physiological states such as body posture (supine *versus* standing position) and breathing regime (spontaneous *versus* controlled slow breathing). Slow breathing (0.07–0.16 Hz, i.e., 4-10 breaths per minute) influences the PRQ not only by increasing its average value due to the direct effect on the ratio (quotient) of heart and breathing rates, but also by the effect on respiratory sinus arrythmia (Kotani et al., 2002; Russo, Santarelli and O'Rourke 2017).

The basic idea of this research was to examine separate and joint (synergetic) influences of body posture (supine position and standing) and breathing regime (spontaneous and slow-paced 0.1 Hz) on the temporal variability patterns of PRQ. We hypothesized that ANS regulation is responsible for the primary features of PRQ oscillations. Confirmation of this hypothesis was obtained through linear statistic parameters of PRQ. Our aim was to extract information on the state of responsiveness and adaptability of the ANS by dynamic analysis of PRQ in four physiological conditions.

Methods

Our research included, in detail, reproducible conditions and procedures (maneuvers) in which signal acquisition, application of advanced algorithms for calculating linear characterizing parameters, statistic comparison of results and their systematic physical and physiological interpretation were performed. So, this protocol of simultaneous recording of ECG and breathing signal was applied on 20 healthy subjects in four physiological states (supine position with spontaneous breathing, standing with spontaneous breathing, supine position with 0.1 Hz breathing and standing with 0.1 breathing) and performed under controlled laboratory conditions by means of the Biopac MP100 system (Biopac System, Inc., Santa Barbara, CA, United States; AcqKnowledge 3.91 software). For further details of the study protocol please refer to Matić et al., 2020.

Data processing

In order to obtain RR intervals (RRI) and breath-to-breath intervals (BBI) it is necessary to detect the R peaks in the ECG recording and the onset of the breathing cycles in the breathing signal. We did that automatically by using the Pick Peak tool of Origin software (Microcal, Northampton, MA, United States). After that we calculated BB and RR intervals as difference between successive time coordinates of R peaks or the onset of the breathing cycle B (minima) according to the expression:

X (i) = Pk (i + 1) − Pk (i), where

Pk (i) - time coordinates of detected RR peaks or B minima Pk (i + 1) - time coordinates of subsequently detected RR peaks or B minima

X (i) stands for either of two intervals, i.e., RRI (i) or BBI (i), with respect to the type of the signal (ECG or breathing).

Pulse-respiration quotient (PRQ; RRI: BBI = m: 1) might be obtained in two ways: the first is a simple manual technique of palpation the pulse (or by visual follow up) and counting how many heart beats correspond to each breathing cycle (Coleman, 1920). This is not sufficiently precise for modern scientific evaluations. The second approach is by recording both the ECG and the breathing signals, automatic calculation of RR intervals (RRI) and breath-to-breath intervals (BBI), and calculating the number of RRI per BBI. Next, if RRI and BBI are expressed as counts per minute, we get instantaneous heart rate (HR) and breathing rate (BR) according to the following expressions:

$$HR = \frac{60}{RRI}\ [heartbeats/\min]$$

$$BR = \frac{60}{BBI}\ [(inspiration + expiration)/\min]$$

Then, the instantaneous PRQ is derived as the ratio between HR and BR, or reciprocally BBI and RRI:

$$PRQ = \frac{HR}{BR} = \frac{BBI}{RRI}$$

The principle of average PRQ (RRI:BBI = *m*:1) determination is simple: by dividing HR with BR its average value across the whole signal is obtained. However, if we want to explore, as mentioned, its dynamical behavior, precise counting of all RRI that appear within each breathing cycle is needed. Figure 1 illustrates this general principle of PRQ calculation.

In order to automatically calculate (count) the number of RR intervals per respiratory cycle, it is necessary to use an algorithm according to the following procedure (explained for one breathing interval as an example). Suppose that i and e denote the time occurrences (beginnings) of inspiriums and expiriums, respectively, while r marks the occurrences of ECG R-peaks and that they were arranged in the following order:

Respiration e . . . . . i1 . . . . . e . . . .i2 . . . . . .

R peaks r0 . . . . . r1 . . . r2 . . . . . .r3 . . . .r4. . . . ..r5 . . . .r6

Sequential number of 1 2 3 4

Sequential number of RR intervals

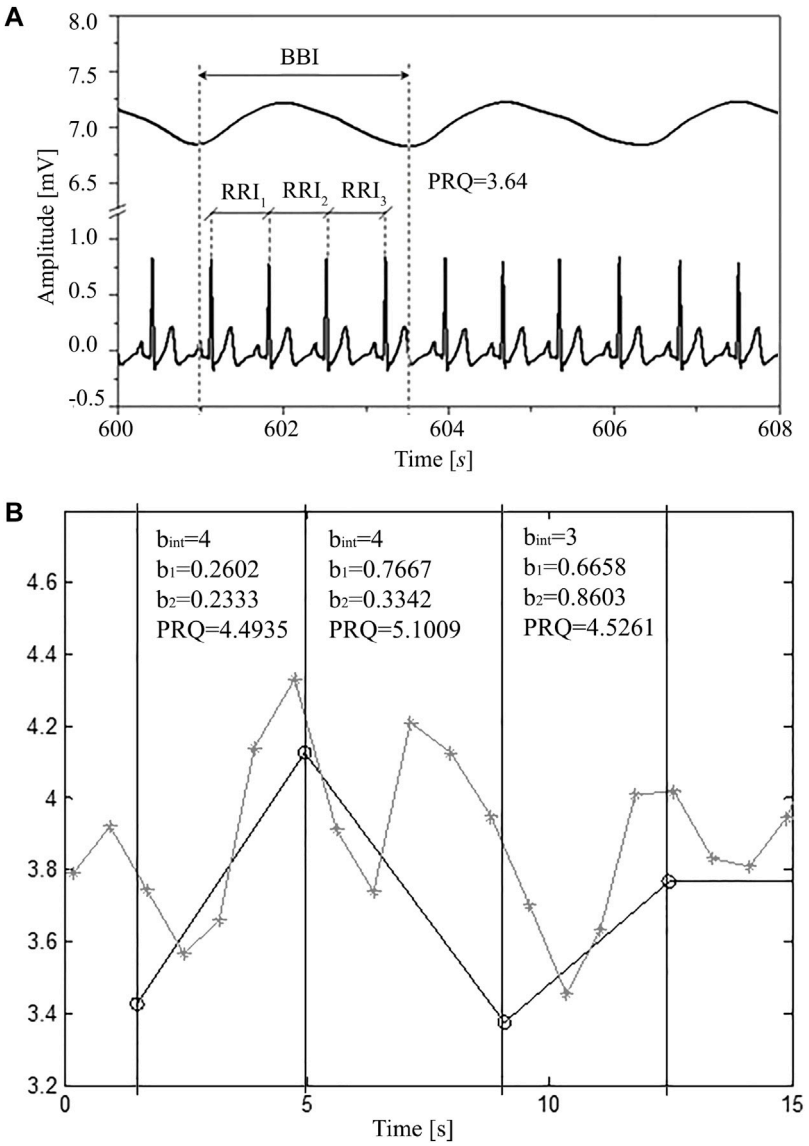

FIGURE 1
(A) A segment of simultaneously recorded signals (8 s selected from a total of 1200 s): breathing and ECG in one subject in a supine position with spontaneous breathing; where: RRI—time interval between two adjacent R peaks of the ECG signal, BBI—breathing interval, calculated as the time difference between onsets of two successive inspirations (respiratory cycle), PRQ—pulse respiration quotient (number of heartbeats per respiratory cycle). **(B)** Obtaining PRQ from signals derived as rr and intervals. Gray line with crosses: rr intervals (ordinates) vs. rr onset time (abscissa). Black line with circles: BB intervals (ordinate) vs. BB onset time (abscissa). Black vertical lines and text boxes with parameter values are added for better explaining the principle behind obtaining PRQ from rr (RRI) and BB (BBI) intervals. Each PRQ value is a sum of the integer number of whole rr intervals (b_{int}) and the non-integer parts of rr intervals (b_1 and b_2) that fall within one BBinterval (breathing cycle). Thus, PRQ = $b_{int} + b_1 + b_2$.

First, we count the integer number of whole RR intervals (b_{int}) that fall between i1 and i2. In this case there are three: r2 – r1, r3 – r2, r4 – r3.

Then we add parts of the boundary RR intervals that belong to (i1, i2) breathing interval, as non-integer parts of the PRQ:

$$b1 = (r1 - i1)/(r1 - r0), \text{and } b2 = (i2 - r4)/(r5 - r4)$$

So, the total instantaneous PRQ value, belonging to (i1, i2) breathing interval, would be

$$PRQ(i1, i2) = bint + b1 + b2 = 3 + b1 + b2$$

In this way we obtain an exact non-integer count, without any averaging.

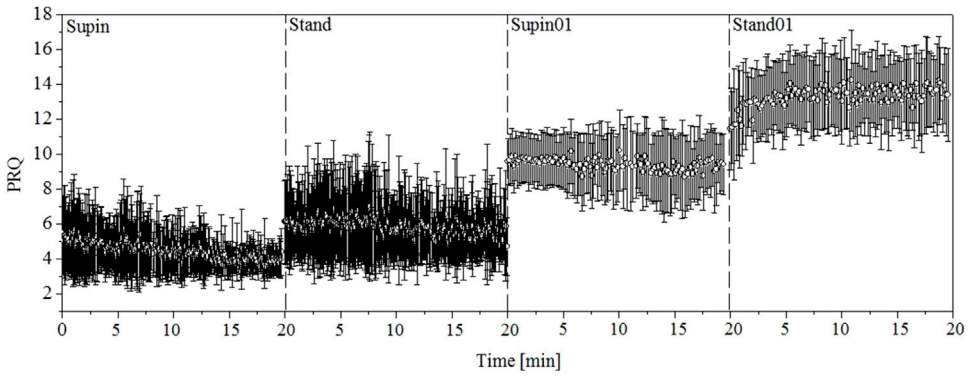

FIGURE 2
One-minute PRQ mean values and variabilities for 20 subjects. Supin—supine position with spontaneous breathing, Stand—standing with spontaneous breathing, Supin01—supine position with slow (0.1 Hz) breathing, Stand01—standing with slow (0.1 Hz) breathing.

As well, with this approach no information is wasted, as the total number of RR intervals is conserved throughout the recording and boundary RR intervals are precisely shared between adjacent breathing intervals. For instance, in this particular case, "b2" part of (i1, i2) and "b1" part of (i2, i3) add up to form the whole r4, r5 interval, *etc.*

An example of this procedure applied for obtaining a few quotients from RRI and BBI signals is given in Figure 1.

When we apply this algorithm to the whole signals of RRI and BBI, we get a new PRQ signal with continuous precise calculation of its values. After visual presentation of PRQ in the four investigated states (Figure 2), it is clear that PRQ has its own variability, the new information calculated from the variability of RRI and BBI.

In order to obtain additional information about a possible quantization of the values in whole number ratios, we plotted the distributions of PRQ variability data by the means of the histograms and probability density estimation (PDE) profiles. Histograms were calculated using Origin program and PDE profiles by an algorithm created in Matlab 2010a (MathWorks Inc., Natick, MA01760–2098, United States). For a more detailed procedure about the generation of PDE profiles please consult the reference Kalauzi et al. (2012). Comparison of PDE profiles was done by means of Kullback-Leibler divergence (D_{KL}) (Kullback and Leibler, 1951). We performed calculation of D_{KL} using Matlab (2010a). In general, D_{KL} (familiar also as relative entropy) is a measure that starts from one distribution, q(x), and calculates how much the new distribution, p(x), is unexpectedly different from the old one, i.e., how much new information it brought in relation to expectations:

$$D_{KL}(p\|q) = \int_{-\infty}^{\infty} \mathcal{P}(x) \log\left(\frac{\mathcal{P}(x)}{q(x)}\right) dx$$

We used this relative entropy measure to compare PRQ ensembles in the states of body posture and breathing regime changes and we used supine position as a reference state.

Statistics

The obtained results were collected and saved in databases created using SPSS 19 (Statistical Package for the Social Sciences 19, IBM, New York, United States). Statistical analysis was then performed using the SPSS 19 tools. Initially, we checked the normality (Gaussian) distribution of the obtained results for each parameter by visual methods (histograms (frequency distribution, tree-leaf plot, stem plot, box plot), PP graph (probability-probability plot) and KK (quantile-quantile graph)) and Shapiro-Wilk normality test. Both visual inspection and Shapiro-Wilk normality test of the PRQ parameters in 20 subjects confirmed that our data did not have a normal (Gaussian) distribution, so we applied the non-parametric Kruskal Wallis test and the post-hoc Man Whitney test with Bonferroni's correction for multiple measurements to compare all samples (Table 2).

Results

Using the previously explained method we obtained the PRQ signals in our four investigated states and performed statistical tests for comparison. Figure 2 gives a visual impression of these signals. From the results calculated for 20 subjects, we made a 1-min horizontal mean values estimation of the PRQ parameter in each state. After that, we plotted these mean values with their standard deviations as

TABLE 1 RRI, BBI and PRQ (mean ± SD) for 20 healthy subjects in four physiological states; Supin—supine position with spontaneous breathing, Stand—standing with spontaneous breathing, Supin01—supine position with slow (0.1 Hz) breathing, Stand01—standing with slow (0.1 Hz) breathing (adopted from Matić et al., 2020 and completed by PRQ data for comprehensive analysis).

Parameter	Supin	Stand	Supin01	Stand01
mRRI [s]	0.9937 ± 0.1377	0.7263 ± 0.1021	1.0592 ± 0.1257	0.7480 ± 0.0867
sdRRI [s]	0.0621 ± 0.0237	0.0465 ± 0.0175	0.0905 ± 0.0347	0.0702 ± 0.0225
mBBI [s]	4.55 ± 1.45	4.56 ± 1.78	10.0605 ± 0.1942	9.9676 ± 0.1466
sdBBI [s]	0.89 ± 0.61	1.09 ± 1.35	1.4235 ± 0.9437	1.0313 ± 0.4060
mPRQ	4.8118 ± 1.6659	6.3854 ± 2.4308	9.4144 ± 1.2062	13.4761 ± 1.6591
sdPRQ	1.1438 ± 0.6673	1.9374 ± 1.7321	1.3932 ± 0.7117	1.5369 ± 0.5344

TABLE 2 Change of RRI, BBI and PRQ under different conditions (Post hoc Mann-Whitney test for independent samples with Bonferroni corrected *p*-value (*p*-value · m < 0.5, for m = 3, where m is the number of comparisons) after Kruskal–Wallis test for multiple comparisons for 20 healthy subjects; direction of change: ↓ - decrease; ↑ - increase); Bold font indicates statistically significant changes (p value less than 0.05); gray color of font indicate a value close to 0.5 which could be regarded as a statistically significant change. (Adopted from Matić et al., 2020 and completed by PRQ data for comprehensive analysis).

Parameter	Supin-Stand	Supin-Supin01	Supin-Stand01
mRRI [s]	**0.001**↓	0.306	**0.001**↓
sdRRI [s]	0.072↓	**0.021**↑	0.831
mBBI [s]	>0.99	-	-
sdBBI [s]	>0.99	-	-
PRQ	**0.000**↑	**0.000**↑	**0.000**↑
sdPRQ	0.141	0.204	**0.039**↑

TABLE 3 Minute values of PRQ parameters (mean ± standard deviation), averaged for 20 subjects in four states. Supin—supine position with spontaneous breathing, Stand—standing with spontaneous breathing, Supin01—supine position with slow (0.1 Hz) breathing, Stand01—standing with slow (0.1 Hz) breathing.

Time (min)	PRQ_{Supin} (–)	PRQ_{Stand} (–)	$PRQ_{Supin01}$ (–)	$PRQ_{Stand01}$ (–)
1	5.26383 ± 2.31472	5.95709 ± 2.20978	9.63582 ± 1.46697	11.79866 ± 2.49239
2	5.013 ± 2.29122	5.98738 ± 2.18034	9.71613 ± 1.4695	12.69322 ± 1.97467
3	4.94698 ± 2.09833	6.15654 ± 2.59441	9.58971 ± 1.40561	12.705 ± 2.0336
4	4.78723 ± 1.64101	6.16053 ± 2.71091	9.68669 ± 1.58039	13.05603 ± 2.15277
5	4.65407 ± 1.58092	6.21829 ± 2.75615	9.62924 ± 1.50201	13.18461 ± 2.10297
6	4.97842 ± 2.18362	6.1176 ± 2.57549	9.58766 ± 1.74327	13.57818 ± 2.10853
7	4.78919 ± 2.17825	6.19114 ± 2.61454	9.17507 ± 1.90426	13.49438 ± 2.32806
8	4.72043 ± 1.93314	6.32685 ± 2.93612	9.42092 ± 1.84727	13.3066 ± 2.15415
9	4.51035 ± 1.60624	5.96568 ± 2.59158	9.37971 ± 1.92135	13.57922 ± 2.25175
10	4.40756 ± 1.51257	5.87847 ± 2.20089	9.35339 ± 1.98915	13.62667 ± 2.2694
11	4.41325 ± 1.60696	5.74063 ± 2.02265	9.56773 ± 2.30129	13.4747 ± 2.36701
12	4.34052 ± 1.2613	5.60282 ± 1.99261	9.46898 ± 1.92909	13.35791 ± 2.21631
13	4.41653 ± 1.54333	5.82723 ± 2.04347	9.18351 ± 2.05129	13.40357 ± 2.06937
14	4.11025 ± 0.97724	5.52863 ± 1.87425	9.1031 ± 2.43961	13.55143 ± 2.27799
15	4.00185 ± 1.04793	5.59959 ± 1.8856	9.08627 ± 2.03071	13.40078 ± 2.24055
16	3.96592 ± 0.92141	5.58987 ± 2.01121	8.97489 ± 2.29802	13.51484 ± 2.053
17	4.07595 ± 0.98849	5.529331.74282	9.32683 ± 1.88533	13.42076 ± 2.21723
18	4.0416 ± 0.88411	5.5067 ± 1.74678	9.47288 ± 1.80233	13.45431 ± 2.49363
19	3.83594 ± 0.95124	5.81484 ± 2.26019	9.33528 ± 1.77989	13.71134 ± 2.24221
20	3.94859 ± 0.90775	5.50322 ± 1.82887	9.24888 ± 2.03297	13.57815 ± 2.227

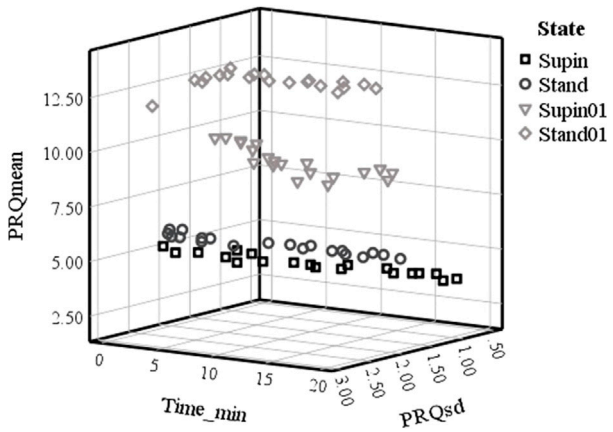

FIGURE 3
Plot of PRQmean versus PRQsd minute values in time in four physiological states in 20 subjects. Supin—supine position with spontaneous breathing, Stand—standing with spontaneous breathing, Supin01—supine position with slow (0.1 Hz) breathing, Stand01—standing with slow (0.1 Hz) breathing.

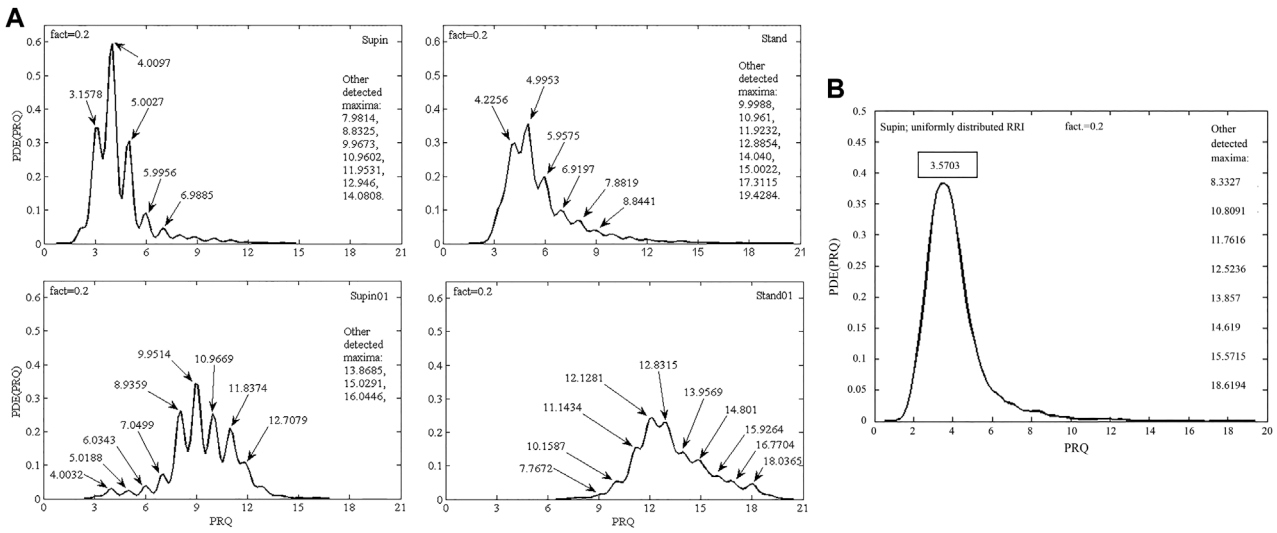

FIGURE 4
(A) PDE distribution profiles of the PRQ parameter for 20 subjects in four physiological states: Supin—supine position with spontaneous breathing, Stand—standing with spontaneous breathing, Supin01—supine position with slow (0.1 Hz) breathing, Stand01—standing with slow (0.1 Hz) breathing; fact—fineness factor. Quantization around integer PRQ values is visible in most local maxima; **(B)** PDE distribution of PRQ parameter for 20 subjects that was calculated from artificial RR intervals (RRI) with uniform distribution (random values within the physiological limits of the RRI parameter) and real BB intervals.

error bars. In signals plotted in this way, the influence of body posture and breathing regime is notable.

Beside visual presentation, mean and standard deviation values of RRI, BBI and PRQ signal are reported in Table 1. Results for RRI and BBI are given here in order to be compared with PRQ as a new quantity.

In Table 2 we present the results of statistical analysis of the quantities presented in Table 1, for the 20 subjects. Because the data did not display Gaussian distribution (which was confirmed by visual inspection and Shapiro-Wilk normality test), we chose to apply the non-parametric Kruskal Wallis test for comparison of the results. We found a significant state dependent change compared to supine position values (as the baseline) by Mann-Whitney test with a Bonferroni correction of significance for multiple permuted measurements ($p^*m < 0.05$, for $m = 3$, where m

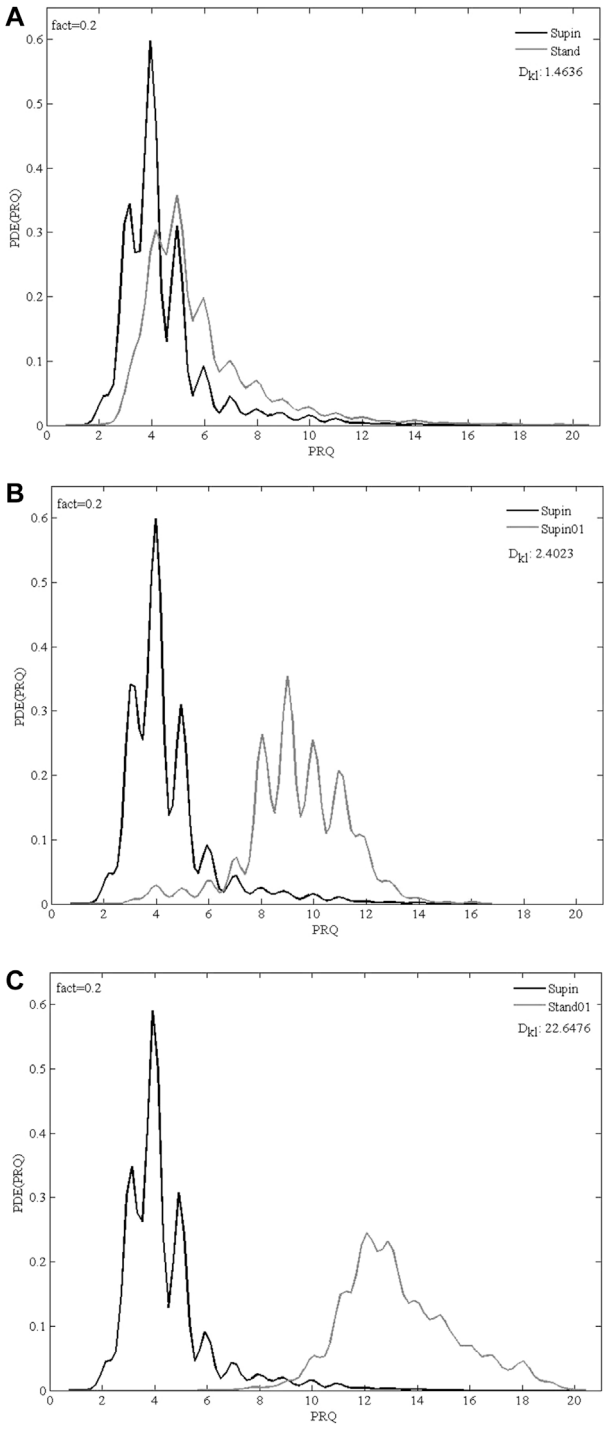

FIGURE 5
Overlapping PDE distribution profiles of PRQ parameter for 20 subjects in 3 comparison of physiological states: **(A)** Supin-Stand, **(B)** Supin-Supin01, **(C)** Supin-Stand01; Supin—supine position with spontaneous breathing, Stand—standing with spontaneous breathing, Supin01—supine position with slow (0.1 Hz) breathing, Stand01—standing with slow (0.1 Hz) breathing; fact—fineness factor; DKL—Kullback-Leibler divergence (relative entropy).

is the number of comparisons)[1]. From Table 2, we can see that orthostasis and slow breathing produce significant changes in RRI, BBI and PRQ.

Table 3 is given for a more detailed view on temporal behavior of PRQ under the influence of body posture and breathing regime. It was obtained by calculation of minute values of PRQ for each subject. Then, its horizontal mean value with corresponding standard deviations was estimated for the whole set of 20 subjects. Thus, temporal changes of all 20 PRQ minute values could be observed in each of the four states.

Based on Table 3, we plotted minute mean values *versus* standard deviation of PRQ (PRQmean, PRQsd, respectively), which is shown on Figure 3. Figure 3 data allows the discrimination of physiological states. It is obvious that mean vs. std dev points create specific clusters of values from which Supin, Stand, Supin01, Stand01 could be recognized as separate, well defined states.

Clustering of PRQmean *versus* PRQsd minute values *in time* (Figure 3) was as distinctive as the clustering of PRQmean *versus* the average PRQsd minute values. These data support the conclusion that PRQ is regulated constantly and in a stable way during the whole course of all 20-min session but in a state-specific manner. The PRQ state dependent regulation is not, though, robustly regulated, but constantly on at least a 1 min (resolution of our analysis) regular basis. This conclusion, evident from Figure 3, is supported by the minute-by-minute PRQmean *versus* PRQsd Supin and Stand relations. These relations, mutually similar, follows quasi-linear, 3D "cigarette-shaped" regimes of quasi-constant PRQmean coupled to very variable PRQsd. The more dynamical states like Supin01 and Stand01 are mutually similar in shape, 3D "boomerang shaped" PRQmean *versus* PRQsd relation, that represent coupled quasi-constant values of PRQmean with quasi-constant values of PRQsd. (Figure 3). On the basis of the 3D shapes of PRQmean vs. PRQsd relation it is clear that Supine and Stand belong to the one "family", while Supine01 and Stand01 belong to another "family" of the PRQ regulating regimes. We can reasonably assume that, in our experimental design, the shift from one "family" to another "family" of regulating regimes determines the breathing regime.

Finally, we plotted state-specific probability density estimation (PDE) profiles of PRQ values which demonstrate that different states have specific distributions and accumulation of PRQ values.

To check, if the quantization (observed in Supin, Stand, Supin01 in Figure 4A) occurs as a consequence of physiological mechanisms (cardiorespiratory coupling) rather than it is an artifact or bias, we used artificial RR intervals with a uniform probability distribution within the same limits as physiological RRI to calculate the supine PRQ parameter. If our assumption is valid, the quantization of PRQ parameter values should not occur in the PDE distribution under these conditions. The result of this procedure is shown in Figure 4B and supports our choice of methods. Similar results were obtained with reshuffled physiological RR intervals (not shown). Figure 5 displays the size of divergence of PDE distributions in Stand, Supin01, Stand01 in respect to the one in Supin (referent state).

Discussion

The scope of this work is based on the representation of methodological and interpretative advancements (with respect to Matić et al., 2020) in analysis of cardiorespiratory adaptability in different physiological states. Its outputs are novel insights which have translational component from basic science to applied telemedicine. In general, PRQ quantification has great research potential. The insights regarding our results related to PRQ can be summarized as follows:

- Physiological and clinical significance of PRQ variability indices: results obtained by our new quantification method demonstrated that PRQ variables have greater sensitivity to influence of orthostasis and slow breathing than mean and standard deviation of heart rate and breathing. This indicates that such PRQ quantification could be used for the detection of physiological state changes;
- The main advantage of our approach compared to earlier ways of obtaining PRQ is the continuous and precise calculation of its values, which enabled us to perform a more accurate analysis of PRQ variability;
- New calculation method potentiated insights into fine temporal PRQ variability patterns that are state dependent and that thereby reflect "the state of cardiorespiratory adaptability" (Scholkmann and Wolf, 2019);
- When displayed in minute resolution scale, PRQ mean vs. standard deviation form state specific clusters of values; we hypothesize that these clusters could represent state specific ventilation-perfusion regimes;
- The main highlight of this research is related to PRQ quantization (appearance of integer values in ratio quotient between heart rate and breathing rate); our method of calculation and analysis of probability density estimation (PDE) distributions gave more evident and precise determination of PRQ quants than classical distribution views used in previous research. In fact, by calculating only integer PRQ values, construction of PDE profiles would not be possible. Beside characterization of state dependence of mean and st dev of PRQ (reported for the first time in the states of combination of slow

1 https://www.ibm.com/support/pages/post-hoc-comparisons-kruskal-wallis-test.

breathing with supination and slow breathing with standing), the PDE distribution of PRQ for the first time registered integer values and the presence of PRQ quantization mechanism in physiological states metabolically and homeodynamicaly different from supine position. Our results show for the first time (to the best of our knowledge) that PRQ quantization exists in variable proportion to "non-integer" PRQ mechanisms even under the influence of slow breathing and orthostasis. Therefore, novel method revealed that PRQ quantization mechanisms make a ubiquitous, constitutive part of cardiorespiratory coupling in supination and in (potentially other) physiological states. It would be of utmost importance to see if PRQ quantization mechanisms remain present (lost or emphasized?) in different cardiorespiratory pathologies and what would be their profile difference with respect to healthy state.

Here we introduce a new method for the precise calculation of both integer and non-integer parts of the RR intervals within a respiratory cycle to accurately and continuously determine instantaneous pulse respiration quotient (PRQ). With our approach, by summing all integer and non-integer parts of RR intervals within a recorded series, the total number of RR intervals is conserved over the whole signal. This is possible because our method preserves each integer and each non-integer part b1and b2 within each respiratory cycle, defined from one inspiration to the next. Although in mathematical terms these PRQ values are rational numbers, we found an accumulation of integer PRQ values, the local maximum appearing over integer PRQ values could be interpreted as PRQ aggregating around that integer.

The results indicate that cardio-respiratory coupling has a certain dynamic that is dependent on specific physiological conditions such as body position and breathing regime and is probably regulated by the activity of the ANS. It is clear from Table 1 and Figure 2 that the supine state is characterized by low values of PRQ. Supine state also is related to increased vagal activity. Our result of mean value of PRQ (=4.8, Table 1) is above the other references specific for supine resting position with spontaneous breathing: 4.1 (Edelhäuser et al., 2013; van Bonin et al., 2014) and 4.2 (Zohdi; Scholkmann and Wolf 2020). It turns out that in our sample interindividual variability elevates the mean value of PRQ, because there are subjects with an average PRQ significantly higher than in the majority of the sample. However, our result of PRQ mean value is below 5.03 and 5.29 that were obtained by Grote et al. (2021). With the duration of the supine state, this decrease becomes more expressed; mean and std dev are significantly lowered (Table 1) which is visually notable in Figure 2 as *narrowing and drop of the PRQ values*. On the other hand, orthostasis (which is usually more sympathetically modulated) and slow breathing induce elevation of PRQ. With respect to Supin, PRQ in prolonged Stand01 increases noticeably. Regarding the results presented in Table 2, it is important to note that the new quantity PRQ appeared to be more sensitive to condition changes (Supin-Stand, Supin-Supin01 and Supin-Stand01) than all the other tested quantities (mRRI, sdRRI, mBBI and sdBBI) (Matić et al., 2020). This qualifies this new measure also for the detection of physiological state changes. The accurate calculation of PRQ, which has been used in medicine earlier (Hildebrandt et al., 1998, 2013) but not continuously calculated, could be of interest for the preparation and performance of space flights with human crew, of sportsmen and non-professional athletes, and of patients with various pathologies *etc.* This is in line with the research of Armañac-;Julián et al. (2021) which pointed out that compared to HRV indices, values of cardiorespiratory coupling (CRC) were more significantly altered in patients with failed weaning, which enabled the authors to differentiate such patients as risky from those that had successful weaning (Armañac-Julián et al., 2021). Superiority of PRQ vs. HRV for the detection of the severity of cardiac pathologies was already described by Weckenmann in 1975 (Weckenmann 1975).

In Figure 3 we report specific forms of clustering of PRQ mean values vs. PRQ standard deviation, the position and shape of which are dependent on the physiological state. Following the sequence Supin-Stand-Supin01-Stand01 we report an opposite tendency of PRQ mean value (increase) and PRQ standard deviation (decrease). Regarding oxygen transport efficiency of cardiorespiratory system, these clusters could represent state specific ventilation-perfusion regimes, closely correlated to increasing metabolic demands of the Supin-Stand-Supin01-Stand01 sequence (Bojić et al., 2020). Regarding the adaptability of the cardiorespiratory system, in our previous study (Matić et al., 2020) we identified the physiological state Stand01 as the state with the most specific CRC in nonlinear domain. PRQ finding supports our hypothesis that Stand01 is the state with the highest potential for cardiorespiratory adaptability (Papaioannou et al., 2011; Matić et al., 2020). In the light of dynamic characteristic of PRQ during this state we could conclude that cardiorespiratory adaptability is most efficient in the state of a highly regulated BBI vs. RRI relation, expressed as a (high) mean value and standard deviation of PRQ (Bojić T et al., 2021). It might be plausible that such graded and a state specific average PRQ value vs. PRQ standard deviation (Figure 3) are necessary preconditions for the state specific cardiorespiratory network adaptability and learning processes initiation and action. In our previous research Stand01 was behaviorally and metabolically the most complex state. It showed the most specific pattern of CR nonlinear coupling, critically important for the adaptability of the cardiorespiratory system (Matić et al., 2020). So, specific results for both nonlinear (Matić et al., 2020) and linear indices in Stan01 indicate that standing and slow breathing in

combination generate unique physiological circumstances, a new and unusual situation for the organism's regulatory system. The peculiarity of this state is that, unlike when lying down, it is unexpected for a subject to breathe slowly while standing. In this sense, it is possible that such a combination of body position and breathing rhythm represents *a provoking (unexpected) stimuli* which induces sympathetic and parasympathetic amplified activity and that as such it could be used as an activation trigger and conditioning excersise of ANS in condtions followed by autonomic disregulation. These results are output from altered (novel) interaction between cardiac (heart rate and blood pressure rate variability), respiratory (0.1 Hz resonant oscillations) and posture (balance and upright meintance) control systems (Siedlecki et al., 2022). Novel, unexpected stimuli are sometimes needed for reactivation of faltered neural feedback systems. Stable, state specific (Figure 3) continuous PRQ regulation could be the prerequisite, a sort of sublime temporal frame of the body's oxygenation regime for the activation of the specific cardiorespiratory adaptability patterns (Matić et al., 2020). Further studies of PRQ relation with CRC nonlinear parameters with learning paradigms (i.e., characterization of memory patterns after daily exercise of standing with slow 0.1 Hz breathing during a certain time period vs. standing with spontaneous breathing) are necessary for the evaluation of this hypothesis. Quantization with a preference for integer values is noticeable on the histogram representations (in supine position) published in different independent studies (Moser et al., 1995; Kotani et al., 2002; Bartsch et al., 2007; Scholkmann and Wolf, 2019; Scholkmann, Zohdi, and Wolf, 2019). Their PRQ histograms indicate a pronounced accumulation of PRQ integer values HR:RR = m:1 (Moser et al., 1995; Kotani et al., 2002; Bartsch et al., 2007; Scholkmann and Wolf, 2019) and especially during sleep (Grote et al., 2021). We also noticed the same accumulations in the supine condition (Supin) with an affinity towards the integer ratio 4:1. In other states (Stand, Supin01, Stand01) a shift towards higher values was observed. Also, it can be seen that different states result in specific forms of PRQ value distributions. This is in line with the research of Scholkmann et al. in which the emphasis was on the analysis of histogram shapes (F. Scholkmann, Zohdi and Wolf 2019). The novelty of our research is that, by the calculation of PRQ non-integer values and its PDE distribution, we obtained PRQ state specific quantization behavior, not only for rest (Supin), but also under the influence of changes in body position and slow breathing. Appearance of PRQ quantization over a broad range of integers is most probably the result of inter-individual variability within the group. Physiological origin of integer peaks of PDE distributions was confirmed by the PDE analysis using synthetic RRI per real BBI, from which we obtained a "smooth" distribution over all values of PRQ, and where local maxima of integer PRQ values did not show (Figure 4). Thus, the physiological regulation responsible for PRQ quantization is not an on-off phenomenon and not an exclusive property of the supine condition (Moser et al., 1995; Scholkmann and Wolf, 2019). Among all four studied states, in Supin state, corresponding to a high vagal activity, the relation of PRQ quantization vs. the PRQ non-integer generating mechanisms is most emphasized. In other states PRQ mean value is shifted towards higher values (Stand, Supin01, Stand01), but quantization is less pronounced. Visual inspection shows that PRQ quantization is more determined by body posture (Supin vs. Stand) than by the change of the breathing regime (Supin vs. Supin01). PRQ quantization is least visible in Stand01, where slow paced breathing regime and standing position manifest synergetic suppression. PRQ quantization seems to be an ubiquitous phenomenon for all four tested physiological states, with a state dependent relative contribution of regulation to the respective amount of quantization. One of the mechanisms proposed in the literature as opponent to PRQ quantization mechanism(s) is respiratory sinus arrhythmia, maximally expressed during physiological quiescence of parasympathetic *modulation* predominance with sympathetic *modulation* withdrawal on HR (Kotani et al., 2002; Bartsch et al., 2007). Our results are not in line with this observation. However, by our approach, the influence of respiratory sinus arrhythmia on PRQ is effectively removed, because all RR variations within each BB interval are averaged out. PDE analysis of PRQ values shows that orthostasis (sympathetic predominance with parasympathetic withdrawal on HR regulation) has a suppressive effect on PRQ quantization. Joined sympathetic and parasympathetic activity (Stand01) has, apparently, additive suppressant effect on PRQ quantization mechanism. It is reasonable to hypothesize that sympatho-vagal relation, specific for the resting state and sleep (vagal dominance, sympathetic withdrawal, Levy, et al., 1996) allows the emergence of emphasized PRQ quantization. With regards to this, our results reflect the ubiquitous presence of adaptive effect of ANS towards the integer harmonization of heart rhythm and respiration. This effect can be especially noticed on the summary diagram of PRQ dynamics in Figure 2 and in Table 3, which contains the minute mean values of PRQ. Namely, after approximately 14 min at supine position with spontaneous breathing (Supin), a very pronounced accumulation of PRQ values around number four is notable—*the drop and narrowing of PRQ flow*, as we mentioned. Apparently, there is an enhancement of quantization by staying in a supine position for a longer time. Scholkman and Wolf (2019) and Grote et al. (2021) mention something similar during sleep - a decrease in PRQ variability and fixation to the whole-number ratio 4:1 (Scholkmann and Wolf 2019). Main factor of this result in sleep is transition from standing to supine position and prolonged staying in supine position in which decrease of heart rate takes place, whereas decrease of respiration rate originates from transition from wakefulness to sleep (von

Bonin et al., 2014). This behavior can be characterized as a homeostatic amplification (mean value steady regulation) that overcomes the homeodynamic principle; or in other words, this is the energetically optimal coupling pattern between heart rhythm and respiration, an effect of activating the physiological mechanisms of the organism's recovery during the rest (prolonged stay in a supine position). It is plausible that PRQ quantization, as an intrinsic property of the cardiorespiratory regulatory network (Kotani et al., 2002; Bartsch et al., 2007) represents a safe, low energy cost state for CPC and maintains the ventilation/perfusion ratio especially while the higher order autonomic networks perform reparatory and regenerative processes as in sleep (Bojic, 2003; Grote et al., 2021), rest (Moser et al., 1995) or recovery after surgery in which increased vagal activity has great significance, due to its immune-modulating properties (Grote et al., 2019). Thus, prolonged stay in supine position (up to 30 min) during day might be beneficial for well-being, e.g., alertness and learning ability (van Bonin et al., 2014).

A breathing regime of 0.1 Hz drives PRQ relation towards the value of 10:1 (Table 1. Supin01–9.41 ± 1.21, Stand01–13.48 ± 1.66; Figure 2. Main (highest) quantization peak in Supin01–9.9514). It should be clear that 10:1 value of PRQ mostly result from experimental setting in which the breathing cycle is 10 s, while average RRI take values close to 1 s (Table 1). *Therefore, the 10:1 PRQ relation of slow breathing is not completely analogous to 4:1 PRQ relation of spontaneous breathing, since the latter is present without conscious adjustments of the breathing rate*. What is evident as a physiological result is that 0.1 Hz slow breathing induce an increase of RRI variability (for 45.7% in respect to spontaneous breathing regime, sdRRI, Table 1). It could also be the manifestation of a resonance effect (synchronization) achieved by respiratory induced increase of vagal modulation (Gerritsen and Band 2018; Sevoz-Couche & Laborde 2022). This regime results with phase synchronization between heart rate and breathing (just as with baroreceptor resonant frequency (increased baroreflex sensitivity, Zautra et el 2010; Steffen et al., 2017; Pagaduan et al., 2019; Sevoz-Couche and Laborde 2022) which is paired with a maximal gas exchange (Lehrer et al., 2020) and higher values of arterial blood oxygenation (Bilo et al., 2012) but with higher metabolic cost due to extensive activation of the "respiratory pump". Hypothetically, if 0.1 Hz training of breathing regime stimulates neural network learning and positioning of PRQ around 10:1, we presume, in accordance with the literature (Bernardi et al., 1998; 351; Russo et al., 2017) that this state would be characterized by higher arterial blood oxygen saturation, higher oxygen consumption, and therefore with positive consequences on overall oxidative metabolic processes.

The study of Bernardi et al. (1998) of the effect of breathing rate on oxygen saturation and exercise performance has confirmed this by measuring arterial oxygen saturation during spontaneous breathing and paced at 15, 6 and 3 breaths per min, in rest and exercise, in healthy subjects and in chronic heart failure patients. Slow breathing at 6 breaths per min (0.1 Hz) was found to be optimal for improving alveolar ventilation and reducing functional dead space in both investigated groups, in terms of increased arterial oxygen saturation and low respiratory effort. Follow-up of chronic heart failure patients who continued the practice of slow breathing, showed increased exercise performance and motivation (Bernardi et al., 1998). Long term beneficial influence of slow breathing on oxygen saturation, perfusion index and PRQ and their inter-relatedness was indicated in study of Xia (2022).

Therefore, analogous to the value of four that appears in Supin, one characteristic (resonant) value of PRQ could have reinforcing influence on synchronization in supine position with slow breathing as well (Supin01). So far, we detected several quantization values in Stand and Supin01 states, but we do not know is their effect similar to value four of Supin state. It seems that slow breathing enhances the tendency towards more integer values, which can be attributed to different resonance effects of slow breathing (Sevoz-Couche and Laborde 2022), as well as the simple fact that BB intervals are artificially extended to 10 s.

Recent research showed that vagal activity is more pronounced during autoregulative periods than sympathetic drive. In Stand, a vagal withdrawal occurs that enables sympathetic drive to be more dominant (Maggioni et al., 2020). Therefore, general cardiorespiratory autonomic responsiveness (adaptability) (Malik et al., 2019) is mostly based on vagal reactivity (Grant et al., 2012; Maggioni et al., 2020). Our observations agree with the statement that "parasympathetic withdrawal reactive to orthostatic challenge", represent "an essential marker of healthy autonomic reactivity" (Maggioni et al., 2020).

In contrast to the supine-induced relative homeostasis, in Stand, Supin01, Stand01 a homeodynamic regulation (an increase of variability, Table 1) is more pronounced.

In the Stand01 state a marked increase in the mean value and standard deviation of PRQ occurs, but without a prominent integer quantization, so we could talk about the combined inhibitory effect of slowed breathing (vagal amplification) and standing (sympathetic amplification) on PRQ quantization. Stand01 was the only state in which variability of PRQ increased significantly (Table 2: sdPRQ rising by 34.4% in respect to Supin). The influence of slow breathing on the rise of RRI variability (sdRRI) in Stand01 was significant (for 13.04% in respect to Supin), but not as pronounced as in Supin01 (by 45.7% in respect to Supin).

In our PDE profiles (Figure 4) the quantization may assume all values of natural numbers up to some maximum value. Using a surrogate signal with uniformly distributed or reshuffled (not shown) RR intervals we could show that this is not a technical artifact: All local maxima either disappear, or acquire non-integer PRQ values, except the one close to PRQ ≈4:1, under these conditions. As PDE (PRQ) and PDE (BBI) are similar in shape, PDE (RRI) appears as a sharp peak positioned over RRI ≈1:1 (not

shown). PRQ quantization therefore is additional mark of CRC synchronization, because if heart beat and respiration were completely desynchronized, i.e., uncorrelated, then the inspirium nadir of a BB interval would partition the corresponding RR interval at a random location, making non-integer PRQ values as probable as integers, and quantization peaks would not occur, which is not the case according to our study. The reason for this could be that the systolic and diastolic phases are the times of feed-back for the higher regulatory networks (i.e., instantaneous systemic arterial pressure and oxygenation monitoring in systole, or cardiac chamber filling, venous pressure regulation, cardiac humoral regulation of body fluids in diastole, *etc.*). The integration of such complex information, for example, obtained during systole, mediated by baro- and chemo-receptors up to higher cardiorespiratory regulatory centers, would be disturbed by concomitant chemo-neuro-mechanical effects of the inspirium. This hypothesis is further supported by the fact that CRC is bidirectional and that cardiac impact on respiration is prevalently mediated by baroreceptors (i.e., on beat-to-beat basis; Dove and Katona, 1985; Jung R and Katona, 1990; Kotani et al., 2002).

It is also likely, that the coupling of the inspiratory onset to the cardiac cycle (Moser et al., 1995) improves the oxygenation of blood in the lung: Just 150 msec after the electric systole (R-peak), most inspirations in a healthy subject start. This is approximately the delay that the heart needs to start the mechanical systole (electromechanical coupling) which than moves the blood. Blood from the right ventricle starts to perfuse the lung tissue and at the same time inspiration starts and the lung is filled with air. Thoracal pressure is reduced due to the inspiration which helps to perfuse the lung with air and blood. Due to the cardio-inspiratory coupling the likeliness of whole number ratios between heart beat and respiration is increased, which makes a whole number PRQ an interesting indicator of good efficiency of blood oxygenation.

Regarding the reference value of minimal relative entropy ($D_{KL} = 0$) which indicates that the two distributions have the same quantity of information (Kullback and Leibler, 1951), the results obtained in our research (Figure 5) indicate that standing and slow breathing produces a significant divergence in PDE distributions ($D_{KLSupin\text{-}Stand} = 1.4636$, $D_{KLSupin\text{-}Supin01} = 2.4023$), while their joint influence exerts much greater change of PDE distribution ($D_{KLSupin\text{-}Stand01} = 22.6476$). This joint influence of slow breathing and orthostasis is not a simply linear additive effect, since D_{KL} as a measure does not fulfill requirements for a metric distance, as it does not adhere to the triangle inequality rule. Thus, it is likely that the combined orthostatic and respiratory stimuli of Stand01 produce a certain nonlinear amplifying effect which should be further explored in context of different demanding cardiorespiratory regimes.

Data availability statement

The raw data supporting the conclusions of this article will be made available by the authors, without undue reservation.

Ethics statement

The studies involving human participants were reviewed and approved by Ethical Committee of Faculty of Medicine, University of Belgrade (No. 2650/IV-24). The patients/participants provided their written informed consent to participate in this study.

Author contributions

TB and MP designed the experimental protocol. TB, MP, and ZM recruited research subjects. ZM performed the experiments and data acquisition. MP supervised the experiments. ZM performed data analysis under MP, AK, and TB supervision. AK devised the method and programmed the algorithms. AK and ZM addressed the major computational tasks. ZM and TB did scientific writing. TB gave physiological interpretation of the data. ML provided consulting in data analysis. MM provided consulting in data interpretation. TB and AK equally contributed to the scientific concept of the paper. All the authors approved the final content of the manuscript.

Funding

This work was supported by Ministry for Education, Science and Technological Development of the Republic of Serbia T0302203 and Project Proof of Concept 5537, Innovation Fund of the Republic of Serbia.

Acknowledgments

We are especially thankful to Mihajlo Stojković, student of the fourth grade of Third Belgrade Lyceum, who volunteered and participated actively in data analysis. We express our gratitude to the volunteers from the Institute of Nuclear Sciences Vinča and Faculty of Medicine University of Belgrade, as well to the friends and colleagues who supported our study by volunteering as the research subjects.

Conflict of interest

The authors declare that the research was conducted in the absence of any commercial or financial relationships that could be construed as a potential conflict of interest.

Publisher's note

All claims expressed in this article are solely those of the authors and do not necessarily represent those of their

affiliated organizations, or those of the publisher, the editors and the reviewers. Any product that may be evaluated in this article, or claim that may be made by its manufacturer, is not guaranteed or endorsed by the publisher.

References

Armañac-Julián, P., Hernando, D., Lázaro, J., de Haro, C., Magrans, R., Morales, J., et al. (2021). Cardiopulmonary coupling indices to assess weaning readiness from mechanical ventilation. *Sci. Rep.* 11 (1), 16014. doi:10.1038/s41598-021-95282-2

Bartsch, R., Kantelhardt, J. W., Penzel, T., and Havlin, S. (2007). Experimental evidence for phase synchronization transitions in the human cardiorespiratory system. *Phys. Rev. Lett.* 98 (5), 054102. doi:10.1103/PhysRevLett.98.054102

Bernardi, L., Spadacini, G., Bellwon, J., HajRic, R., Roskamm, H., and Frey, A. W. (1998). Effect of breathing rate on oxygen saturation and exercise performance in chronic heart failure. *Lancet* 351, 1308–1311. doi:10.1016/S0140-6736(97)10341-5

Bilo, G., Revera, M., Bussotti, M., Bonacina, D., Styczkiewicz, K., Caldara, G., et al. (2012). Effects of slow deep breathing at high altitude on oxygen saturation, pulmonary and systemic hemodynamics. *PloS one* 7, e49074. doi:10.1371/journal.pone.0049074

Bojić, T., Matić, Z., Stojković, M., Platiša, M., Kalauzi, A., Lazarević, M., et al. (2020). Cardiorespiratory coupling is influenced by body position and slow paced 0 1Hz breathing in a state specific manner. *FENS 2020 Virtual Forum Fed Eur Neurosci Soc (FENS) Br Neurosci Assoc (BNA).* https://cslide.ctimeetingtech.com/fens2020/attendee/eposter/poster/5958?r=snm%7E571.

Bojić, T. (2003). Mechanisms of neural control and effects of acoustic stimulation on cardiovascular system during the wake-sleep cycle. PhD dissertation. Bologna, Italy: Alma Mater Università di Bologna.

Bojić, T., Matić, Z., Platiša, M., and Kalauzi, A. (2021). Breathing modulation of cardiopulmonary coupling-a potential way out of autonomic deconditioning after prolonged microgravity exposure. *SEE UNIVERSE, South East Eur. Space Conf. 2020 Proc. Belgr. Serbia* 101, 57–67. doi:10.5281/zenodo.5643545

Boyadzhieva, A., and Kayhan, E. (2021). Keeping the breath in mind: Respiration, neural oscillations, and the free energy principle. *Front. Neurosci.* 15, 647579. doi:10.3389/fnins.2021.647579

Brenner, J., LeBlang, S., Lizotte-Waniewski, M., Schmidt, B., Espinosa, P. S., DeMets, D. L., et al. (2020). Mindfulness with paced breathing reduces blood pressure. *Med. Hypotheses* 142, 109780. doi:10.1016/j.mehy.2020.109780

Coleman, W M. (1920). On the correlation of the rate of heart beat, breathing, bodily movement and sensory stimuli. *J. Physiol.* 54 (4), 213–217. doi:10.1113/jphysiol.1920.sp001920

Dick, T. E., Yee Hsee Hsieh, R. R., Dhingra, D. B, RobertoGalán Erica, M. F. W., Morris, K. F., Galan, R. F., Wehrwein, E., et al. (2014). Cardiorespiratory coupling: Common rhythms in cardiac, sympathetic, and respiratory activities. *Prog. Brain Res.* 209, 191–205. doi:10.1016/B978-0-444-63274-6.00010-2

Dove, E. L., and Katona, P. G. (1985). Respiratory effects of brief baroreceptor stimuli in the anesthetized dog. *J. Appl. Physiol.* 59 (4), 1258–1265. doi:10.1152/jappl.1985.59.4.1258

Edelhäuser, F., Hak, F., Kleinrath, U., Lühr, B., Matthiessen, P. F., Weinzirl, J., et al. (2013). Impact of colored light on cardiorespiratory coordination. *Evid. Based. Complement. Altern. Med.* 2013, 810876. doi:10.1155/2013/810876

Ernst, G. (2014). *Heart rate variability*. London, England: Springer. doi:10.1007/978-1-4471-4309-3

Ernst, G. (2017). Heart-rate variability—more than heart beats? *Front. Public Health* 5, 240. doi:10.3389/fpubh.2017.00240

Gerritsen, R. J. S., and Band, G. P. H. (2018). Breath of life: The respiratory vagal stimulation model of contemplative activity. *Front. Hum. Neurosci.* 12, 397. doi:10.3389/fnhum.2018.00397

Grant, C. C., Margaretha Viljoen, D. C. J, van, R., and Wood, P. S., (2012). Heart rate variability assessment of the effect of physical training on autonomic cardiac control. *Ann. Noninvasive Electrocardiol.* 17 (3), 219–229. doi:10.1111/j.1542-474X.2012.00511.x

Grote, V., Frühwirth, M., Lackner, H. K., Goswami, N., Köstenberger, M., Likar, R., et al. (2021). Cardiorespiratory interaction and autonomic sleep quality improve during sleep in beds made from pinus cembra (stone pine) solid wood. *Int. J. Environ. Res. Public Health* 18 (18), 9749. doi:10.3390/ijerph18189749

Grote, V., Levnajić, Z., Henry, P., Ohland, T., Goswami, N., Frühwirth, M., et al. (2019). Dynamics of vagal activity due to surgery and subsequent rehabilitation. *Front. Neurosci.* 13, 1116. doi:10.3389/fnins.2019.01116

Hildebrandt, G., Moser, M., and Lehofer, M. (1998). *Chronobiologie und Chronomedizin*. Kopais, Boeotia: Hippokrates.

Hinterberger, T., Walter, N., Doliwa, C., and Loew, T. (2019). The brain's resonance with breathing - decelerated breathing synchronizes heart rate and slow cortical potentials. *J. Breath. Res.* 13 (4), 046003. doi:10.1088/1752-7163/ab20b2

Jung, R., and Katona, P. G. (1990). Cardiovascular and respiratory responses to slow ramp carotid sinus pressures in the dog. *J. Appl. Physiol.* 68 (4), 1465–1474. doi:10.1152/jappl.1990.68.4.1465

Kalauzi, A. R, Vuckovic, A, and Bojić, T. (2012). EEG alpha phase shifts during transition from wakefulness to drowsiness. *Int. J. Psychophysiol.* 86 (3), 195–205. doi:10.1016/j.ijpsycho.2012.04.012

Kotani, K., Takamasu, K., Ashkenazy, Y., Stanley, H. E., and Yamamoto, Y. (2002). Model for cardiorespiratory synchronization in humans. *Phys. Rev. E Stat. Nonlin. Soft Matter Phys.* 65 (5), 051923. doi:10.1103/PhysRevE.65.051923

Kralemann, B., Fruhwirth, M., Pikovsky, A., Rosenblum, M., Kenner, T., Schaefer, J., et al. (2013). *In vivo* cardiac phase response curve elucidates human respiratory heart rate variability. *Nat. Commun.* 4 (2418), 2418. doi:10.1038/ncomms3418

Kullback, S., and Leibler, R. A. (1951). On information and sufficiency. *Ann. Math. Stat.* 22 (1), 79–86. doi:10.1214/aoms/1177729694

Lehrer, P., Kaur, K., Sharma, A., Shah, K., Huseby, R., Bhavsar, J., et al. (2020). Heart rate variability biofeedback improves emotional and physical health and performance: A systematic review and meta analysis. *Appl. Psychophysiol. Biofeedback* 45 (3), 109–129. doi:10.1007/s10484-020-09466-z

Levy, M. N., and Martin, P. J. (1996). "Autonomic control of cardiac conduction and automaticity," in *Nervous control of the heart* (Amsterdan, Netherlands: Harwood Academic Publishers), 88, 201–223.3

Maggioni, M. A., Rundfeldt, L. C., Gunga, H. C., Joerres, M., Merati, G., and Steinach, M. (2020). The advantage of supine and standing heart rate variability analysis to assess training status and performance in a walking ultramarathon. *Front. Physiol.* 11, 731. doi:10.3389/fphys.2020.00731

Malik, M., Hnatkova, K., Huikuri, H. V., Lombardi, F., Schmidt, G., and Zabel, M. (2019). CrossTalk proposal: Heart rate variability is a valid measure of cardiac autonomic responsiveness. *J. Physiol.* 597 (10), 2595–2598. doi:10.1113/JP277500

Malliani, A. (2005). Heart rate variability: From bench to bedside. *Eur. J. Intern. Med.* 16 (1), 12–20. doi:10.1016/j.ejim.2004.06.016

Matić, Z., Platiša, M. M., Kalauzi, A., and Bojić, T. (2020). Slow 0.1 Hz breathing and body posture induced perturbations of RRI and respiratory signal complexity and cardiorespiratory coupling. *Front. Physiol.* 11, 24. doi:10.3389/fphys.2020.00024

Mclachlan, C. S., Ocsan, R., Spence, I., Hambly, B., Matthews, S., Wang, L., et al. (2010). Increased total heart rate variability and enhanced cardiac vagal autonomic activity in healthy humans with sinus bradycardia. *Proc.* 23 (4), 368–370. doi:10.1080/08998280.2010.11928655

Moser, M., Fruehwirth, M., and Kenner, T. (2008). The symphony of life - importance, interaction and visualization of biological rhythms. *IEEE Eng. Med. Biol. Mag.* 27, 29–37. doi:10.1109/MEMB.2007.907365

Moser, M., Fruehwirth, M., Penter, R., and Kenner, T. (2006b). Why life oscillates--biological rhythms and health. *Conf. Proc. IEEE Eng. Med. Biol. Soc.* 2006, 424–428. doi:10.1109/IEMBS.2006.259562

Moser, M., Fruehwirth, M., Penter, R., and Winker, R. (2006a). Why Life Oscillates - from a topographical towards a functional chronobiology. *Cancer Causes Control* 17, 591–599. doi:10.1007/s10552-006-0015-9

Moser, M., Voica, M., Kenner, T., Lehofer, M., Egner, S., and Hildebrandt, G. (1995). Phase- and frequency coordination of cardiac and respiratory function. *Biol. Rhythm Res.* 26 (1), 100–111. doi:10.1080/09291019509360328

Pagaduan, J., Wu, S. S. X., Kameneva, T., and Lambert, E. (2019). Acute effects of resonance frequency breathing on cardiovascular regulation. *Physiol. Rep.* 7 (22), e14295. doi:10.14814/phy2.14295

Papaioannou, V. E., Chouvarda, I. G., Maglaveras, N. K., and Pneumatikos, I. A. (2011). Study of multiparameter respiratory pattern complexity in surgical critically ill patients during weaning trials. *BMC Physiol.* 11 (1), 2. doi:10.1186/1472-6793-11-2

Russo, M. A., Santarelli, D. M., and Dean, O'R. (2017). The physiological effects of slow breathing in the healthy human. *Breathe* 13, 298–309. doi:10.1183/20734735.009817

Schneditz, D., Moser, M., SmolJe-Jüttner, F., Dörp, E., Pogglitsch, H., and Kenner, T. (1990). Methods in clinical hemorheology: The continuous measurement of arterial blood density and blood sound speed in man. *Biorheology* 27, 895–902. doi:10.3233/bir-1990-27610

Scholkmann, F., and Wolf, U. (2019). The pulse-respiration quotient: A powerful but untapped parameter for modern studies about human physiology and pathophysiology. *Front. Physiol.* 10, 371. doi:10.3389/fphys.2019.00371

Scholkmann, F., Zohdi, H., and Wolf, U. (2019). The resting-state pulse-respiration quotient of humans: Lognormally distributed and centered around a value of four. *Physiol. Res.* 68 (6), 1027–1032. doi:10.33549/physiolres.934232

Schwerdtfeger, A. R., Schwarz, G., Pfurtscheller, K., Thayer, J. F., Jarczok, M. N., and Pfurtscheller, G. (2020). Heart rate variability (HRV): From brain death to resonance breathing at 6 breaths per minute. *Clin. Neurophysiol.* 131 (3), 676–693. doi:10.1016/j.clinph.2019.11.013

Sevoz-Couche, C., and Laborde, S. (2022). Heart rate variability and slow-paced breathing:when coherence meets resonance. *Neurosci. Biobehav. Rev.* 135, 104576. doi:10.1016/j.neubiorev.2022.104576

Siedlecki, P., Ivanova, T. D., Shoemaker, J. K., and Garland, S. J. (2022). The effects of slow breathing on postural muscles during standing perturbations in young adults. *Exp. Brain Res.* 240, 2623–2631. doi:10.1007/s00221-022-06437-0

Srinivasan, K., Sucharita, S., Vaz, M., and Srinivasan, D. K. (2002). Effect of standing on short term heart rate variability across age. *Clin. Physiol. Funct. Imaging* 22 (6), 404–408. doi:10.1046/j.1475-097x.2002.00450.x

Steffen, P. R., Austin, T., DeBarros, A., and Brown, T. (2017). The impact of resonance frequency breathing on measures of heart rate variability, blood pressure, and mood. *Front. Public Health* 5, 222. doi:10.3389/fpubh.2017.00222

von Bonin, D., Grote, V., Buri, C., Cysarz, D., Heusser, P., Moser, M., et al. (2014). Adaption of cardio-respiratory balance during day-rest compared to deep sleep--an indicator for quality of life? *Psychiatry Res.* 219 (3), 638–644. doi:10.1016/j.psychres.2014.06.004

Weckenmann, M. (1975). The pulse-respiratory quotient of persons with stable and instable postural circulation while standing (author's trans. *Basic Res. Cardiol.* 70, 339–349. doi:10.1007/BF01905516

Xia, A. (2022). Potential benefits of qi gong meditation in quantifiable physiology: A five-year longitudinal observation. *J. Traditional Chin. Med. Sci.* 9, 340–348. doi:10.1016/j.jtcms.2022.06.005

Zautra, A. J., Fasman, R., Davis, M. C., and Craig, A. D., (2010). The effects of slow breathing on affective responses to pain stimuli: An experimental study. *Pain* 149 (1), 12–18. doi:10.1016/j.pain.2009.10.001

Zohdi, H., Scholkmann, F., and Wolf, U. (2020). Frontal cerebral oxygenation asymmetry: Intersubject variability and dependence on systemic physiology, season, and time of day. *Neurophotonics* 7 (02), 025006. doi:10.1117/1.nph.7.2.025006

Frontiers in Neuroscience

Provides a holistic understanding of brain function from genes to behavior

Part of the most cited neuroscience journal series which explores the brain - from the new eras of causation and anatomical neurosciences to neuroeconomics and neuroenergetics.

Discover the latest Research Topics

See more →

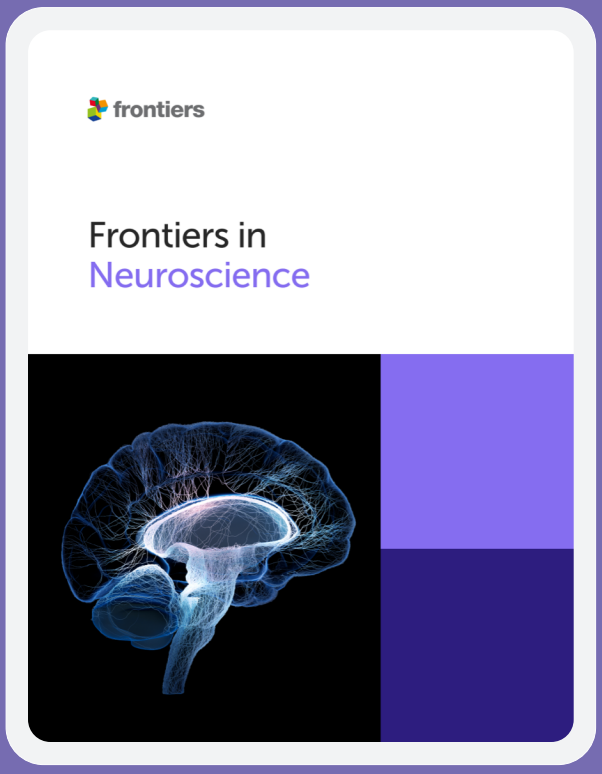

Frontiers

Avenue du Tribunal-Fédéral 34
1005 Lausanne, Switzerland
frontiersin.org

Contact us

+41 (0)21 510 17 00
frontiersin.org/about/contact